Design and Utilization of NADH Sensors in Bacterial Cells, Specifically to Monitor Activity of the Soluble Hydrogenase of *Ralstonia eutropha*

vorgelegt von

M.Sc.

Svea Kristina Wilkening

an der Fakultät II – Mathematik und Naturwissenschaften

der Technischen Universität Berlin

zur Erlangung des akademischen Grades

Doktor der Naturwissenschaften

–Dr. rer. nat. –

genehmigte Dissertation

Promotionsausschuss:

Vorsitzender: Prof. Dr. Thomas

Gutachter: Prof. Dr. Friedrich

Gutachter: Dr. Schmitt

Gutachter: Prof. Dr. Budiša

Tag der wissenschaftlichen Aussprache: 25. März 2021

Berlin 2021

Abstract

The soluble hydrogenase (SH) of *R. eutropha* is a potential candidate for application in clean energy generation in a post-fossil age. In order to elucidate its mode of action, and possibly deduce general parameters for a biotechnological implementation, it is desirable to monitor the protein *in vivo*. The hydrogenase couples the oxidation of H_2 to the reduction of NAD^+ to NADH, offering the possibility of observing the SH activity by fluorescent NADH sensors. Many different fluorescent NADH sensors have been designed the past years. Frex is a prototypical NADH sensor, consisting of a bacterial NADH-sensing repressor protein and a circularly permuted yellow fluorescent protein. The utilization of fluorescence spectroscopy offers the opportunity to observe whole cells with low perturbation and without disruption. By expressing the Frex biosensor in various strains of *R. eutropha*, either containing or devoid of SH, the sensor gives information of the intracellular NADH pool, and the alterations due to the SH activity. The experiments indicated a correlation between the activity of the SH and the duration of elevated Frex fluorescence in *R. eutropha* cells, making the sensor a suitable tool to examine SH activity *in vivo*.

Since NADH is a paramount cofactor for many reactions in cells, the readout of its intracellular concentration is of great interest. However, so far designs of NADH biosensors have been limited by the fact that these were created for an application in mammalian cells. In consequence, transfer of these sensors to bacterial cells is not easily achieved, considering their different, generally higher, NADH and NAD^+ levels. The infrared fluorescent protein (iRFP713) was investigated regarding its behavior in presence of NADH. In these experiments, an excitation energy transfer was detected, in which the protein's tryptophan residue(s) transmit excitation energy towards the biliverdin chromophore. This EET process was impeded by the presence of NADH, effectively exhibiting a promising detection mode for a far-red fluorescent NADH sensor. Since iRFP713 cannot discriminate between NADH and its analogues, an experimental strategy to attach iRFP713 to NADH-sensing Rex subunits was constructed. The resulting Bili-Sense sensor also exhibited the EET process, which was disruptable by NADH, and time-resolved fluorescence spectroscopy revealed that the quenching of the sensor by NADH was of both dynamic and static nature.

Zusammenfassung

Die NAD^+-reduzierende Hydrogenase aus *R. eutropha* ist ein potentieller Kandidat für die Generierung von Wasserstoff als alternativen Energieträger in einem postfossilen Zeitalter. Die SH kombiniert die Oxidation von H_2 mit der Reduktion von NAD^+ zu NADH, welches die Möglichkeit eröffnet, die Aktivität des Enzyms über fluoreszierende NADH-Sensoren zu verfolgen. Frex ist ein NADH-Reporter, der aus einer bakteriellen NADH-sensitiven Einheit eines bakteriellen Repressorproteins und einem zyklisch permutierten gelb-fluoreszierenden Protein besteht. Die Fluoreszenzspektroskopie ermöglicht die Beobachtung ganzer Zellen unter minimal-invasiven Bedingungen. Durch das Einbringen des Frex Sensors in einen *R. eutropha* Stamm, welcher fähig ist die SH zu exprimieren, und dem Vergleich der Fluoreszenzantwort mit einem Stamm, dem dies nicht möglich ist, kann der Sensor Informationen über den intrazellulären NADH Speicher liefern, und folglich lässt die Analyse dieser Daten Rückschlüsse bezüglich der Aktivität der SH zu. Die so gestalteten Experimente zeigten eine Korrelation der Aktivität der SH und der Dauer der erhöhten Fluoreszenz des Reporters auf. Frex ist somit ein geeignetes Hilfsmittel, um die SH-Aktivität *in vivo* zu untersuchen.

NADH ist ein fundamentaler Cofaktor, der an einer Vielzahl von Prozessen und Reaktionen in biologischen Zellen beteiligt ist. Die Bestimmung der intrazellulären Konzentration dieses Stoffes ist daher von größtem Interesse. Bisher wurden NADH-Sensoren ausschließlich für die Anwendung in Säugerzellen generiert. Aufgrund der stark abweichende NAD^+ und NADH Konzentrationen ist die Anwendung dieser Sensoren in Bakterien nicht trivial. Das Infrarot-fluoreszierende Protein iRFP713 wurde hinsichtlich seiner Interaktion mit NADH untersucht, wobei festgestellt wurde, dass ein Anregungsenergietransferprozess (EET) zwischen einem oder mehreren Tryptophanen und dem Chromophor des Proteins auftritt. Dieser EET wird durch NADH konzentrationsabhängig gestört. Da iRFP713 selbst keine Möglichkeit hat, zwischen NADH und anderen verwandten Molekülen zu selektieren, wurde die Fluoreszenzsonde mit den Rex-Untereinheiten aus *B. subtilis* versehen. Spektroskopische Untersuchungen des so entstandenen Sensors Bili-Sense zeigten, dass der EET in dem Protein konserviert ist. Zudem wurde mittels zeitaufgelöster Fluoreszenzspektroskopie ermittelt, dass der Prozess der Fluoreszenzlöschung durch NADH sowohl statische wie auch dynamische Komponenten enthält.

Publications

(1) **Wilkening, S.**; Schmitt, F.-J.; Horch, M.; Zebger, I.; Lenz, O.; Friedrich, T *Photosynth. Res.* **2017**, *133*, 305-315

(2) **Wilkening, S.**; Schmitt, F.-J.; Lenz, O.; Zebger, I.; Horch, M.; Friedrich, T. *Biochim. Biophys. Acta Bioenerg*. **2019**, *1860*(10)

(3) Buhrke, D; Velazquez Escobar, F.; Sauthof, L; **Wilkening, S.**; Herder, N.; Tavraz, N.; Willoweit, M.; Keidel, A.; Utesch, T.; Mroginski, A.; Schmit, F.-J.; Hildebrandt, P.; Friedrich, T. *Sci. Rep.* **2016**, *6*, 1-12

(4) Velazquez Escobar, F.; Buhrke, D.; Michael, N.; Sauthof, L.; **Wilkening, S.**; Tavraz,N.; Salewski, J.; Frankenberg-Dinkel, N.; Mroginski, A.; Scheerer, P.; Friedrich, T.; Siebert, F.; Hildebrandt, P. *Phtotchem. Photobiol.* **2017**, *93*, 724-732

(5) Tejwani, V.; Schmitt, F.-J.; **Wilkening, S.**; Zebger, I.; Horch, M.; Lenz, O.; Friedrich, T. *Biochim. Biophys. Acta Bioenerg.* **2017**, *1858*, 86-94

Table of Content

List of Abbreviations

% w/v	volume percentage
% w/w	weight percentage
ADP	adenosine diphosphate
AH	actinobacterial hydrogenase
ATP	adenosine triphosphate
Aut	autotrophic growth medium
BSA	bovine serum albumin
B. subtilis	*Bacillus subtilis*
CFP	cyan fluorescent protein
cpFP	circularly permuted fluorescent protein
cpT-Sapphire	circularly permuted T-Sapphire
cpTS	circularly permuted T-Sapphire
CTAB	cetyltrimethylammonium bromide
cpYFP	circularly permuted YFP
DAS	decay-associated spectra
ddH_2O	doubly distilled water
ε_x	extinction coefficient at wavelength x
em.	Emission
EPR	electron paramagnetic resonance
EET	excitation energy transfer
exc.	excitation

FGN	fructose glycerol minimal medium
FMN	flavin mononucleotide
FN	fructose minimal medium
FRET	fluorescence resonance energy transfer
Frex	fluorescent Rex
FrexH	Frex of high affinity
GAF	named after the occurrence of such domains in cGMP-specific phosphodiesterases, adenylyl cyclases and FhlA
GFP	green fluorescent protein
GN	glycerol minimal medium
hHOX	human heme oxygenase
IPTG	isopropyl-β-D-1-thiogalactopyranoside
kDa	kilodalton
Lac	lactose
LB	Luria Bertani growth medium
LDH	lactate dehydrogenase
MBH	membrane-bound hydrogenase
NA	nicotinic acid
NAD	nicotinamide dinucleotide phosphate
NAD^+	oxidized nicotinamide dinucleotide
NADH	reduced nicotinamide dinucleotide phosphate
NADK	NAD kinase
NADP	nicotinamide dinucleotide phosphate
$NADP^+$	oxidized nicotinamide dinucleotide phosphate
NADPH	reduced nicotinamide dinucleotide phosphate

NADS	NAD^+ synthase
Nam	nicotinamide
NamMN	nicotinamide mononucleotide
NAMN	nicotinic acid mononucleotide
NAMNAT	nicotinic acid mononucleotide adenosyl transferase
NamPRT	nicotinamide phosphoribosyl transferase
NAPRT	nicotinic acid phosphoribosyl transferase
NIR	near infrared
NMNAT	nicotinamide mononucleotide adenosyl transferase
OD_x	optical density at wavelength x
PAS	Per/Arnt/Sim module
PBS	phosphate buffered saline
PCR	polymerase chain reaction
psi	pounds per square inch
QAPRT	quinolinic acid phosphoribosyl transferase
R. eutropha	*Ralstonia eutropha*
RET	resonance energy transfer
RIPA buffer	radio immunoprecipitation assay buffer
rpm	revolutions per minute
rt	room temperature
SDS	sodium dodecyl sulfate
SDS-PAGE	sodium dodecyl sulfate polyacrylamide gel electrophoresis
SFP	single fluorescent protein
SH	soluble hydrogenase
SoNar	Sensor of NAD(H) redox

T. aquaticus	*Thermus aquaticus*
TB	terrific broth
UV	ultraviolet
Vis	visible
YFP	yellow fluorescent protein

I Introduction

1 Metabolism

Metabolism defines any life-sustaining process or reaction of an organism. In these processes free enthalpy is either generated from high-energy compounds, or free enthalpy is utilized to drive the build-up of complex structures. In catabolic processes, food or cellular components are harvested in turn to generate free enthalpy. In anabolic processes, free enthalpy is used for the biosynthesis of biomolecules such as proteins or hormones from simple building units. The exergonic nature of catabolic processes makes it necessary to couple these to the endergonic processes of the anabolic pathways. The junction between anabolic and catabolic processes is realized via the generation of high-energy intermediates such as ATP. While ATP is commonly known as the "energy currency" of the cell, various other molecules are tasked with the transduction of energy, a particular important group manifests as reducing equivalents, such as the nicotinamides. Nicotinamide adenine dinucleotide (NAD^+) and the reduced version NADH, broadly speaking, are involved in catabolic processes, where energy is generated from the breakdown of high-molecular compounds such as sugars or fats. Nicotinamide adenine dinucleotide phosphate ($NADP^+$) and its reduced counterpart NADPH offer or receive reducing equivalents in the anabolic processes of cells, or partake in mitigating oxidative stress (Blacker & Duchen, 2016). The NAD pool (NAD^+ and NADH) is, in most cells, larger than the NADP pool ($NADP^+$ and NADPH) (Pollak, Dölle, & Ziegler, 2007). While the [NADH]/[NAD^+] pool is kept rather oxidized (Sun, Dai, Xie, & Hu, 2012), due to their primary function as electron acceptors in catabolic pathways, the [NADPH]/[$NADP^+$] pool is kept rather reduced (Pollak et al., 2007), in order to provide the reducing power needed for anabolic pathways. So, while the NAD pool might be larger in total than the NADP pool, the NADH and NADPH concentrations are generally of the same order of magnitude.

The phosphorylated nicotinamides differ merely by an additional phosphate group at the C_2' atom on the adenosine ribose moiety (**Figure 1**). This additional phosphate group only alters the characteristics of the molecule pairs marginally, since they exhibit very similar redox potentials (Agledal, Niere, & Ziegler, 2010) and the respective reduced and oxidized species are spectrally indistinguishable (De Ruyck et al., 2007; Patterson, Knobel, Arkhammar, Thastrup, & Piston, 2000).

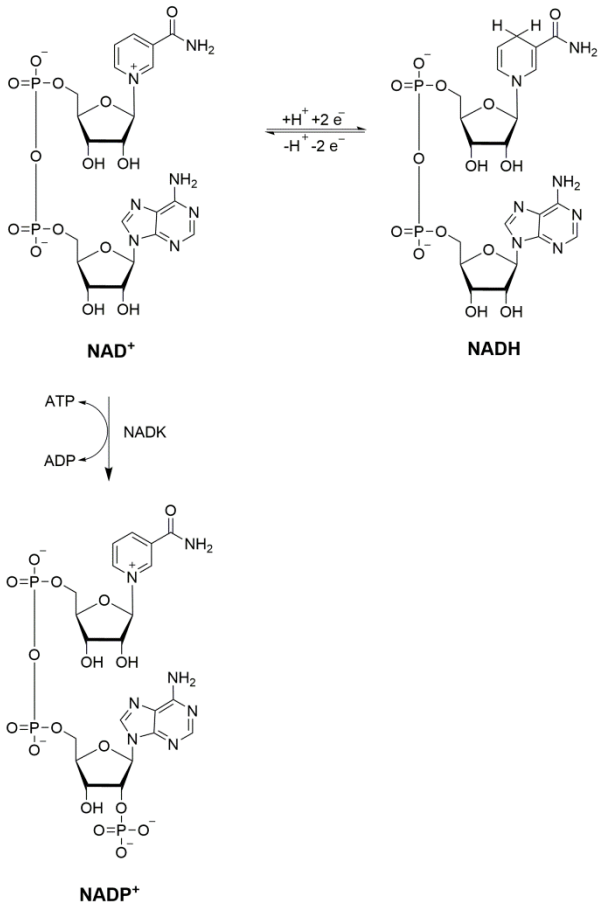

Figure 1 Structural formulas of the oxidized nicotinamide adenine dinucleotide (**NAD⁺**) and the reduced form (**NADH**). NADH formally acts as a hydride transfer reagent ($H^+ + 2\ e^-$). The phosphorylated congener (**NADP⁺**) is synthesized mainly by the NAD^+ kinase (NADK) by phosphorylation of the C_2' position while using a molecule of ATP (Love et al., 2015).

While the role of these molecules as electron carriers has been known for quite some time, in recent years, the capability of nicotinamides acting as signaling molecules, effectively regulating multiple intracellular processes, have been

investigated (Agledal et al., 2010; Belenky, Bogan, & Brenner, 2006; Berger, Ramirez-Hernandez, & Ziegler, 2004; Pollak et al., 2007; Ying, 2006, 2007, 2008), offering a more in-depth view of the various interactions these molecules are partaking in. Particularly the oxidized species have been found to serve as precursors for messenger molecules. NAD^+ has been investigated as a signal transducer in processes such as aging (Blasco, 2005), oxidative cell death (Virag & Szabo, 2002) and calcium homeostasis (Lee, 2001) to name a few. While the interest in $NADP^+$ as signaling molecule has arisen only recently, it has been found to be the precursor of calcium-regulating molecules (Berger et al., 2004; Clapper, Walseth, Dargie, & Hon Cheung Lee, 1987). These regulatory functions, in contrast to the functions as reduction/oxidation agents, often lead to the breakdown of the compounds, rendering the renewed synthesis necessary.

2 NAD Biosynthesis

The synthesis of NAD follows two general pathways, which are shown in **Figure 2**. NAD can be synthesized from L-tryptophan in some bacteria and animals, while L-aspartate is used as precursor in some bacteria and plants, in the so-called *de novo* pathway (Katoh, Uenohara, Akita, & Hashimoto, 2006). Another synthesis pathway utilizes breakdown products such as nicotinic acid (NA) and nicotinamide (Nam), with the preference of the precursor being dependent on the organism, and salvages these for NAD synthesis, therefore aptly named the salvage pathway (for reviews see (Magni et al., 2004; Magni, Amici, Emanuelli, & Raffaelli, 1999)). In the first step in this pathway, NA and Nam are transferred onto a phosphoribosyl pyrophosphate by phosphoribosyl transferases (NAPRT and NamPRT), effectively generating nicotinic acid mononucleotide (NAMN) or nicotinamide mononucleotide (NamMN), respectively. The NAMN is also the intermediate at which the *de novo*- and salvage pathway merge. In the *de novo* pathway, the respective amino acid (in this case L-tryptophan is used exemplarily) is converted into quinolinic acid in a multiple step process. This intermediate is then in turn transferred onto phosphoribosyl pyrophosphate by the dedicated quinolinic acid phosphoribosyl transferase (QAPRT), generating the aforementioned (NANM). The

mononucleotides (NANM and NamNM) are then further functionalized by the enzyme group of the mononucleotide adenosyl transferases (N(A)MNAT) to the nicotinic acid adenine dinucleotide (NAAD) and nicotinamide adenine dinucleotide (NAD^+). In order to convert the nicotinic acid derivate of the dinucleotide to NAD^+, the substrate is amidated by NAD^+ synthase (NADS).

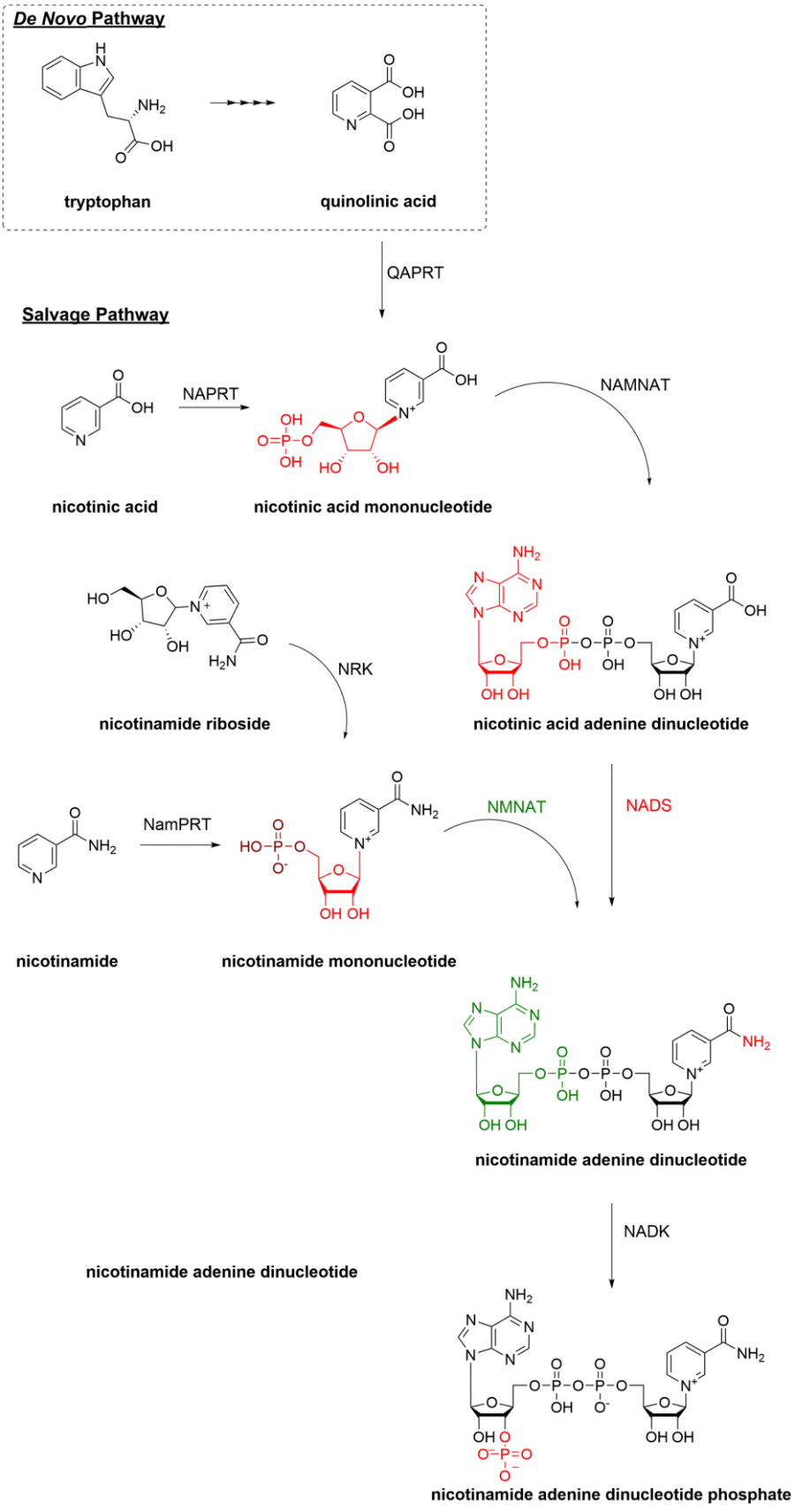

Figure 2 Scheme for the *de novo* and salvage pathway of NAD biosynthesis. Newly introduced moieties by the respective enzymes are highlighted in red or in the respective colors of the active enzymes.

While there are also multiple different pathways for the biosynthesis of $NADP^+$ and NADPH, effectively dependent on organism and organelle, a major contributor is the phosphorylation of NAD^+ by the NAD^+ kinase (NADK) (Love et al., 2015). The reduced congener NADH is formed from NAD^+ during numerous metabolic reactions as has been previously mentioned. Due to the involvement of the nicotinamides in various important cellular processes, there has been a strong desire to monitor these metabolites *in vivo*.

4 Methods to Determine NAD

Nicotinamides are, as cofactors and substrates of many different intracellular processes, valuable parameters in order to infer information about the cellular status. The [NADH]/[NAD^+] pool is influenced by many important metabolic reaction pathways such as the tricyclic acid cycle, glycolysis or cell respiration (J. M. Berg, Tymoczko, Gatto, & Stryer, 2015) and thus, any illness that interferes with these pathways might be detectible by a pathological [NADH]/[NAD^+] ratio, such as cancer (Hasmann & Schemainda, 2003), diabetes (Bordone et al., 2006), neurodegenerative disease (Winkler & Hirrlinger, 2015; Ying, 2006), or even the process of aging itself (Johnson & Imai, 2018; Lin, Ford, Haigis, Liszt, & Guarente, 2004; Sohal & Weindruch, 1996). Not only are many reactions dependent on the respective [NADH]/[NAD^+] pool (Q. Zhang, Piston, & Goodman, 2002), but the ratio of these molecules is a direct marker of the cellular redox status. Furthermore, the oxidized molecules NAD^+ and $NADP^+$ have been recently found to be of great importance in signal transduction and regulation (vide supra) (Anderson, Madsen, Olsen, & Hirschey, 2017; Belenky et al., 2006; Berger et al., 2004; Houtkooper, Cantó, Wanders, & Auwerx, 2010; Johnson & Imai, 2018; Lin & Guarente, 2003; N. Xie et al., 2020; Ying, 2008).

Since NADH is itself a fluorescent molecule, first efforts to quantify the NADH concentration were made by measuring the autofluorescence of the molecule. This method, however, cannot discriminate NADH and its phosphorylated congener

NADPH, and the recorded fluorescence is always a total of NAD(P)H fluorescence. NADPH, in contrast to NADH, is involved in very different reactions intracellularly (J. M. Berg et al., 2015), and thus it is desirable to determine these cofactors independently. Also, other intracellular components such as flavins and lipids are demonstrating fluorescence in this spectral region (Croce, Bottiroli, & Unit, 2014), impeding the ability to distinguish the NAD(P)H signals from cellular autofluorescence. Furthermore, while the reduced nicotinamide is itself fluorescent, the oxidized molecule is not. Since the cellular redox status is dependent on the ratio of reduced to oxidized nicotinamide, the autofluorescence cannot portray this crucial parameter. NAD^+ itself also is a key factor in regulating cellular processes such as the energy metabolism (Rodgers et al., 2005; Starai, Celic, Cole, Boeke, & Escalante-Semerena, 2002; Z. Zhang, Chen, Zhao, & Yang, 2018) or gene expression (D'Amours, Desnoyers, D'Silva, & Poirier, 1999; Z. Q. Wang et al., 1997) and, hence, knowledge of this parameter offers great insight into the cellular status.

Fluorescence spectroscopy performed on whole cells in order to determine the NAD(P)H concentration has the additional drawback of being unable to discriminate between protein-bound or free NADH. However, only the free NADH is relevant for the cellular redox status (Kelly et al., 2018). For a more sophisticated approach, the fluorescence lifetime or the fluorescence anisotropy of NADH can be measured. This allows for discrimination between bound and free NAD(P)H in whole cells (J. R. Lakowicz, Szmacinski, Nowaczyk, & Johnson, 1992; Vishwasrao, Heikal, Kasischke, & Webb, 2005; Zheng, Li, & Qu, 2010), as well as between NADH and NADPH (Blacker et al., 2014). Unfortunately, this method requires an elaborate experimental setup and extensive data processing. Due to the excitation of general cellular autofluorescence with UV-to-blue light, these methods are lacking specificity, and since UV-to-blue light does not sufficiently penetrate into cells, the ability to report on deep tissue events is limited, while the high photon energy of the light could also potentially photodamage the observed tissue. The risk of photodamage can be partially circumvented or at least reduced by employing two-photon excitation of the sample.

The $[NAD^+]/[NADH]$ content of cells can also be estimated by various biochemical methods, such as enzyme cycling assays (Lowry, Passonneau, Schulz, & Rock,

1961), capillary electrophoresis (W. Xie, Xu, & Yeung, 2009), chromatography (Klaidmann, Leung, & Adams Jr., 1995) and mass spectrometry (Trammell & Brenner, 2013; H. Yang et al., 2007). However, all of these methods share the circumstance of being only applicable on lysates or disrupted cells and, therefore, the observation of dynamic changes is cumbersome, if possible at all. In contrast to the autofluorescence methods, the biochemical approaches do not only allow for the determination of the reduced species, but also of the oxidized species. This enables the measurement of the ratio of the respective oxidized and reduced nicotinamides, a valuable readout as a marker for the cellular redox status. The determined [NAD^+]/[NADH] ratios all fall within a certain range for different cell types , when the total pool (protein-bound and free NAD(H)) is considered, where values ranging from 4 – 10 have been reported for *E. coli* (Leonardo, Dailly, & Clark, 1996; Wimpenny & Firth, 1972) and 3 – 10 for mammalian cells (Lin & Guarente, 2003; Oewierczyñski, Somiñska, Smoleñski, & Mayer, 2001). Since the NADH pool is known to be buffered by cellular proteins by about 95 % (Q. Zhang et al., 2002), the determination of the total [NAD^+]/[NADH] ratio does not carry much significance, and the ratios of the free nicotinamides can be drastically different from the values obtained for the total nicotinamide pool (Lin & Guarente, 2003).

A potential workaround to estimate the free [NAD^+]/[NADH] ratio is the indirect measurement via the concentration of related redox couples such as lactate and pyruvate, which are directly linked to the NAD(H) pool by the enzyme lactate dehydrogenase (Williamson, Lund, & Krebs, 1967). The obtained values for the free [NAD^+]/[NADH] ratios vary considerably, where values as low as 0.03 were reported for the [NAD^+]/[NADH] ratio in blood of mice (Sanni, Rae, Maitland, Stocker, & Hunt, 2001), while a ratio of 4 was reported for mice liver cells (Gaikwad, Long, Stringer, & Jaiswal, 2001). For metabolically very active tissue such as heart or liver cells, highly reduced [NAD^+]/[NADH] ratios of 0.05 and 0.07 have been reported, respectively (MacDonald & Marshall, 2000; Mongan et al., 2002). In another study, however, a very oxidized ratio of 644 was reported in monkey Cos7 cells (Q. Zhang et al., 2002), indicating that this parameter is highly specific for the chosen species and the function of the cells investigated. However, these measurements should be treated with caution, since the assumptions made for this method (enzyme-catalyzed reaction near equilibrium, direct connection

between [lactate]/[pyruvate] and [NAD^+]/[NADH] ratio) are not always fulfilled, and the application can lead to errors by one order of magnitude (Sun et al., 2012).

The established methods, hence, display several serious drawbacks, and none is capable of dynamic monitoring the free [NADH], [NAD^+] or their ratio *in vivo*. The advent of genetically encoded fluorescent sensors, thus, is a promising opportunity to alleviate these problems stemming from more traditional biochemical procedures.

5 Genetically Encoded Sensors

Genetically encoded fluorescent sensors are constructs consisting of a sensing unit specific for a certain parameter, combined with a fluorescent protein, which generates an output in form of a light signal. The ever-growing popularity of genetically encoded sensors is reflected in the various publications describing newly designed sensors and their application for detection of, for example, metabolites like NADH (Zhao et al., 2011) or the NADH/NAD^+ ratio (Hung, Albeck, Tantama, & Yellen, 2011; Zhao et al., 2015), NADPH (Tao et al., 2017), $NADP^+$ (Cameron et al., 2016) or the NADPH/$NADP^+$ ratio (Sallin et al., 2018), ATP (Conley, Radhakrishnan, Valentino, & Tantama, 2017; Yoshida, Kakizuka, & Imamura, 2016), the ATP/ADP ratio (J. Berg, Hung, & Yellen, 2009), or ions like calcium (Mank et al., 2008; Miyawaki et al., 1997; Nagai, Sawano, Park, & Miyawaki, 2001), protons (Esposito, Gralle, Dani, Lange, & Wouters, 2008; Miesenböck, De Angelis, & Rothman, 1998; Olsen, Budde, Siegumfeldt, & Bjo, 2002; Robey et al., 1998; Wilks & Slonczewski, 2007), even receptor-substrate interaction (van Unen et al., 2016) or the redox status (Hanson et al., 2004) intracellularly. Their popularity in the majority stems from their ability to resolve intracellular processes spatially and temporally (Chalfie, Tu, Euskirchen, Ward, & Prasher, 1994; Haggie & Verkman, 2005; Lippincott-Schwartz & Patterson, 2003; Möller & Denicola, 2002; Morris & Blondel, 2014). The comparably low disturbance of intracellular processes in this approach allows the scientist to spy on cells under physiological conditions (J. Zhang, Campbell, Ting, & Tsien, 2002).

5.1 Design of a Genetically Encoded Fluorescent Sensor

In a fluorescent sensor, the combination of a sensing entity and a fluorescent protein generates a dynamic output, reflecting the state of the studied analyte. These sensors are expressed, exploiting the cells' intrinsic transcriptional and translational machinery.

The sensing unit is supposed to confer a high specificity for the target analyte, therefore avoiding crosstalk and concomitantly false positives. The affinity of the sensor needs to be carefully designed, being in the order of the magnitude of the intracellular concentration of the analyte, which is desired to be observed, therefore fully exploiting the sensors dynamic range, while not sequestering the analyte pool and interfering with natural cell processes. A perfect sensor would dynamically report back the analyte's concentration in the same manner as if the sensor was not present. This, naturally, presents a paradox (known as the observer effect), since the sensor binds the target analyte and therefore extracts it from the cellular pool and effectively masks it from other enzymes, or binding partners (Teruel & Meyer, 2000; Várnai & Balla, 2006). To limit perturbations of the cellular processes by the sensor, it is favorable to only have low amounts of sensor present. However, a given small sensor concentration, would impede detection of the sensor signal, since the fluorescence signal itself would be of minor intensity (Haugh, 2012). While it is preferable for a good signal-to-noise ratio to have a high amount of sensor present, this would concomitantly disturb the cells pool of the analyte and take up space in an already crowded cell compartment (Beg et al., 2007; Direnberger et al., 2012; Várnai & Balla, 2006). Hence, there needs to be a compromise between high expression of the sensor protein, which would allow a large output signal, but also concomitantly sequestering the analyte pool, and low expression levels, which would diminish the signal. For an adequate and strong signal of the sensor already at lower sensor concentrations, the fluorescence unit should be sufficiently bright, stably fluorescent, have robust folding even when fused to another protein or domain, have short maturation time, and show no

deviation regarding its excitation and emission profile due to other variables, like, for example, pH or ionic strength.

The opportunity of spying on cells in their physiological state with given spatial and temporal resolution, targeting anything from ions to metabolites, has sparked great interest in this non-invasive approach. A wide variety of sensors have been conceptualized and applied *in vivo* (for good reviews see (Ibraheem & Campbell, 2010; Sanford & Palmer, 2017)). These sensors can be subcategorized into three basic sensor models. The first model utilizes the occurrence of fluorescence resonance energy transfer (FRET) between two fluorophores within the sensor, the second model relies on the complementation of a fluorescent unit upon binding of the substrate and the third model depends on the readout of a single fluorescent protein.

5.2 FRET-based Genetically Encoded Fluorescent Sensors

FRET is a process, in which excitation energy is transferred between a donor fluorophore and a spectrally overlapping acceptor fluorophore in a nonradiative "resonant" manner, given close enough proximity between the probes. The concept of FRET was established by Theodor Förster in 1948 (Förster, 1948) and has since been successfully employed to measure distances in the nanometer range, and has therefore been termed "molecular" or "spectroscopic ruler" (Joseph R. Lakowicz, 2006; Stryer, 1978) .

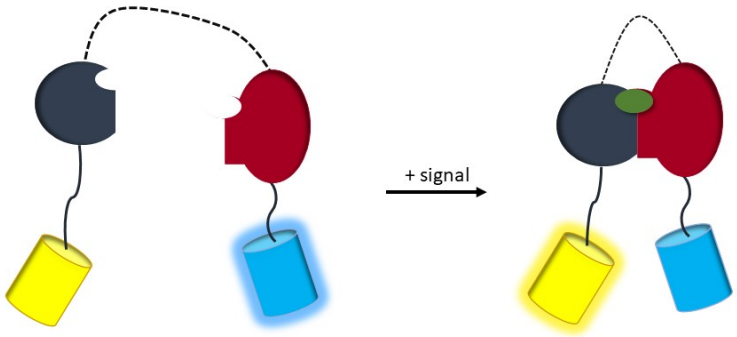

Figure 3 Scheme of FRET-based biosensors. Sensing units are depicted in dark red and dark blue, while the fluorescent proteins are depicted in yellow (yellow fluroescent protein, YFP) and blue (cyan fluroescent protein, CFP). For unimolecular conformational FRET sensors, two sensing subunits, which are connected by a linker (dashed line), are linked to one fluorescent probe of a FRET probe pair. Upon a given signal the distance between the fluorophores is altered and thus a concomitant change in fluroescence occurs. In this particular case the binding of the signal analyte leads to a closer connection of the cyan and yellow fluorescent proteins. While in the unbound state under CFP exctitation the sensor's fluroescence is dominated by the cyan probe, in the bound state FRET is occuring from the CFP donor to the YFP acceptor, effectively altering the fluroescence emission profile of the probe towards YFP fluorescence. For bimolecular FRET based sensors, the linker (dashed line) would be omitted.

This distance dependency of the resonance energy transfer efficiency can also be exploited in biosensors. Upon excitation of the donor fluorophore, the fluorescence readout is predominantly characterized by the donor emission when the fluorophores are sufficiently apart, but upon spatially converging fluorophores, the emission profile will be more and more characterized by the one from the acceptor. Conventional readout schemes mostly determine the ratio of the fluorescence intensity of donor and acceptor, but the FRET signal (or signature) can also be determined by detecting the donor's fluorescence lifetime(s). There are different architectures exploiting the same basic concept, one of the most widely used are the unimolecular conformational FRET sensors.

5.2.1 Unimolecular Conformational FRET Sensors

Sensors of this class share the same basic topology, possessing two spectrally overlapping fluorescent probes, belonging to a FRET pair, flanking a sensing unit, that either changes the state of the probe from open (low FRET efficiency) to closed (high FRET efficiency) or vice versa upon binding the substrate in one polypeptide chain (**Figure 3**). In these sensors, the sensing unit undergoes conformational changes upon binding of the substrate, which in turn translates to the fluorophores of the FRET pair, effectively altering their distance. FRET sensors are ratiometric and the signal is quantified by evaluating the ratio of donor and acceptor fluorescence. The signals of donor and acceptor are, due to the donor acceptor ratio of 1:1 in the sensor, stoichiometrically coupled. Unimolecular FRET-based biosensor constructs always demonstrate basal background fluorescence, because of some FRET efficiency even in the "off" state or unavoidable spectral crosstalk, leading to a limited dynamic range, meaning that the maximum difference between the "on" and "off" state of the probe can never be truly exploited. Another drawback for their application is the fact that these constructs are rather large in size, spanning two full fluorescent probes (~30 kDa each) and a sensing protein, which can interfere with the localization of the probe. Even though, some of the first fluorescent biosensors were based on this concept, like the calcium indicators cameleon from the 1990s (Miyawaki et al., 1997). Also, in recent examples, the protease activity of different enzymes was monitored by FRET biosensors. The designed probes for these experiments would consist of two fluorophores making up the FRET pair and a polypeptide linker, containing the recognition sequence of the protease determined to be investigated. Hence, before cleavage, the fluorescence would be made up primarily of the acceptor fluorescence, while upon proteolysis, the donor fluorescence would be predominant. These constructs have been used for assays to determine the activity of the proteases $3C^{pro}$ of human enterovirus (HEV) (Tsai et al., 2009), NS3-4A of hepatitis C virus (HCV) (Sabariegos et al., 2009) and Caspase-3, which is activated during apoptosis (Zlobovskaya et al., 2016). In further studies, these real-time assays would allow for high-throughput screenings for potential inhibitors of the respective proteases.

5.2.2 Bimolecular FRET

In bimolecular FRET, a sensing unit or protein is fused to one fluorophore of a FRET pair, while another sensing unit or protein is fused to the complementing fluorophore of the FRET pair (**Figure 3**). This procedure greatly diminishes background fluorescence and, therefore, enhances the dynamic range of the sensor, while conserving the ratiometric signal detection as in unimolecular FRET, as well as the reversibility. However, an important drawback is the necessity to express the two subunits separately from two different expression plasmids, mostly leading to different expression levels of the subunits. (Sanford & Palmer, 2017; Tsien, 2005) This approach has been widely applied for the study of fast substrate-receptor interactions, and to derive their activation kinetics in recent examples for a glutamate receptor (mGluRI) (Marcaggi, Mutoh, Dimitrov, Beato, & Knopfel, 2009) and a G-protein coupled receptor (van Unen et al., 2016).

5.3 Single Fluorescent Protein Sensors

In contrast to FRET sensors, constructs which limit their use of fluorescent proteins to one per probe and observe its modulation, are more versatile and easier to design and construct. The need of only one fluorescent protein allows the scientist to be able to choose more freely from the available spectrum of fluorescent proteins. These sensors, generally, exhibit a higher dynamic range, than their FRET-based counterparts, due to lower background fluorescence. Furthermore, the utilization of only one fluorescent probe leads to smaller overall sensors. However, these probes are often intensiometric and thus allow no absolute quantification of the analyte.

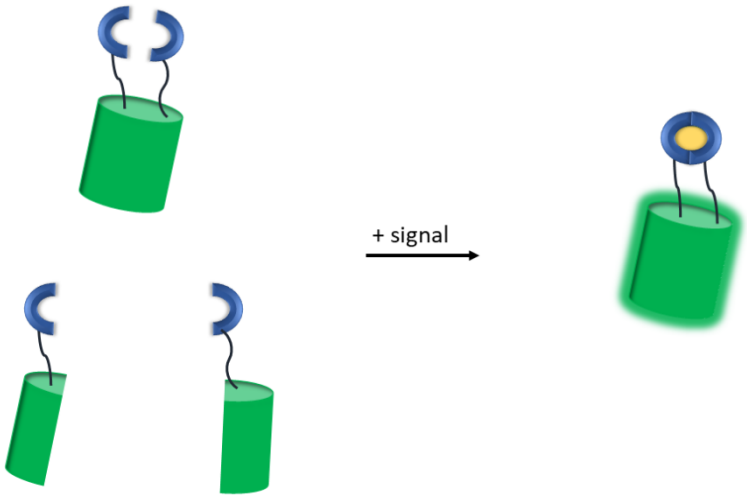

Figure 4 Scheme for the working mode of single fluorescent protein sensors of the conformational (**top**) and complementation (**bottom**) kind. Upon binding an analyte or generally detecting a signal, the subunits binding the analyte transfer the change in conformation to the fluorescent protein, which thus alters its fluorescence (**top**). In the bottom, the separated subunits of the fluorescent proteins are able to interact due to the binding of the analyte and the functional fluorescent protein is generated (**bottom**).

There are various applications of single fluorescent protein (SFP) sensors, where some exploit an intrinsic susceptibility of the chromophore itself (Kneen, Farinas, Li, & Verkman, 1998; Llopis et al., 1998; McAnaney et al., 2005), as in eGFP-pHSens, a derivative of the GFP fluorophore, which acts as a pH sensor (Hanson et al., 2002; Schmitt et al., 2014) and, therefore, these probes need no further sensing unit in combination with the fluorophore. In conformational sensors, the design is built on constructing a chimera of an analyte-specific moiety and a fluorophore, which changes its fluorescence according to the structural changes in the sensing unit (**Figure 4**, top). Complementation sensors are another manifestation of SFPs, in which the fluorescing unit is split and non-fluorescent when no interaction with the analyte is possible. When the analyte is bound to the sensing unit, this induces the complementation of the components of the fluorescing units, generating the desired signal (**Figure 4**, bottom). This effect has recently been exploited in the so-called iSplit, a probe to determine protein-protein interactions. iSplit is based on

the biliverdin-binding iRFP713 (Filonov & Verkhusha, 2013). This protein is a red-to-far-red fluorescent probe, derived from bacterial phytochromes (Filonov et al., 2011). In iSplit, the two chromophore-binding domain subunits, PAS and GAF, are separated and expressed in conjunction with the targeted protein subunits, which are desired to be examined based on their interaction capabilities. When the subunits of the protein are in close proximity and effectively bind to another, the subunits of the fluorescing unit are brought into proximity as well, which leads to assembly of the fluorescent protein subunits and the respective signal.

The approach of single fluorescent protein sensors has also been applied to devise new sensors to report on intracellular NADH and NAD^+ levels.

6 Genetically Encoded NADH Sensors

Due to the high interest in knowledge about the intracellular NADH and NAD^+ concentration and their ratio, efforts have been directed towards designing genetically-encoded fluorescent sensors, in order to spy on these molecules *in vivo* (Bilan & Belousov, 2016; Zhao & Yang, 2015; Zhao, Yang, & Loscalzo, 2014). Genetically encoded fluorescent sensors offer the great advantage of being able to report dynamically in high-throughput measurements on the desired substrate in cells.

Generally, fluorescent NADH sensors contain a bacterial NADH-sensing protein of the so-called Rex protein family, which is fused to a circularly permuted fluorescent protein, therefore combining the specificity of already existing NADH sensing proteins to a fluorescent probe as the output domain. The sensors exploit the high affinity of the Rex proteins for their substrates NADH and to some extent NAD^+ (Bilan & Belousov, 2016; Bilan et al., 2014; Zhao et al., 2015, 2016), and some also utilize the conformational change induced by binding of NADH (Hung et al., 2011; Zhao et al., 2011).

Rex repressors contain a nucleotide binding C-terminal domain, and a DNA binding N-terminal domain (Brekasis & Paget, 2003; Sickmier et al., 2005). While the [NADH]/[NAD^+] ratio is low, the repressor binds one NAD^+ molecule in the

Rossman fold, while also binding to a DNA strand hindering the expression of target genes. Upon binding of two NADH molecules the protein undergoes a structural change and releases the DNA strand.

In the fluorescent NADH probe, these conformational changes induced by binding either the oxidized or reduced nicotinamide can be translated into a differing fluorescence output of the linked circularly permuted fluorescent protein (cpFP). cpFPs are fluorescent proteins, in which the native C and N-termini are fused by a linker, and new termini are generated in close proximity to the chromophore (Baird, Zacharias, & Tsien, 1999). This makes the chromophore more susceptible towards environmental changes.

The sensor's nucleotide sensing moiety binds either of the nicotinamides according to their intracellular concentration, as well as the proteins affinity for each of the molecules. Since the utilized bacterial Rex repressors exhibit affinities towards NADH in the nanomolar range, the affinity needs to be tuned appropriately towards the desired application and cell line in order to circumvent saturation of the sensor.

Many sensors have been developed with this topology, from which one of the first was Peredox.

6.1 Peredox

Peredox has been developed in the laboratory of Loscalzo in 2011. The sensor is constructed by fusing a circularly permuted T-Sapphire between two full subunits of the Rex repressor from *Thermus aquaticus* (*T. aquaticus*) (Hung et al., 2011). The first construct derived this way, P0, showed profound pH dependency of its fluorescence. During various rounds of mutation this pH sensitivity was eliminated and the [NADH]/[NAD^+] sensor Peredox was established.

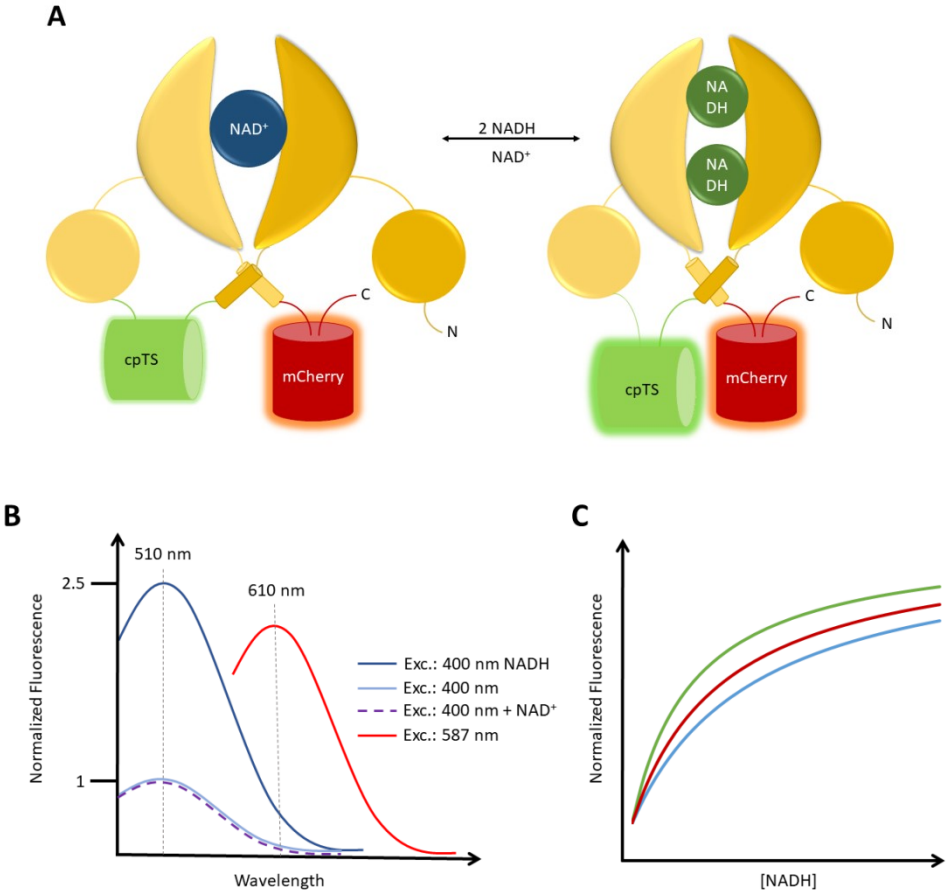

Figure 5 Topology of the Peredox sensor (**A**). The fluorophore (green barrel, cpT-Sapphire, cpTS) is inserted between the two full Rex subunits of *T. aquaticus* (yellow and brown subunits). For normalization of the sensor signal, another fluorophore (red barrel, mCherry) is fused to the sensor C-terminally. The cpTS fluorophore is excited at 400 nm and produces a fluorescence emission spectrum with a peak at 510 nm (**B**, light blue curve). Upon binding two molecules of NADH, the fluorescence in this emission band increases (blue curve). Excitation of the mCherry unit at 587 nm produces an emission spectrum centered at 610 nm (red curve), which is independent from the binding of nucleotides. Binding of NAD^+ does not alter the spectral characteristics of the cpTS fluorophore (dashed purple line). However, the affinity of the sensor towards NADH is decreased in presence of increasing NAD^+. Panel **C** demonstrates schematic affinity curves of the sensor in presence of growing NAD^+ from the green over the red to the blue curve, indicating lowered affinity for NADH when increasing NAD^+.

The sensor demonstrates a high affinity towards the reduced nicotinamide dinucleotide (K_D = 5 nM), while the oxidized form can also bind to the probe, given a sufficiently low [NADH]/[NAD^+] ratio. Therefore, this sensor does not report the

NADH concentration in cells, but rather the NADH concentration compensated for NAD^+ (Hung et al., 2011), and the fluorescence response is usually reported as a marker of the ratio R', which is defined as

$$R' = \frac{[NADH] * 1000}{[NAD^+]} \quad (\mathbf{1})$$

This definition was chosen, since the intracellular NAD^+ concentration is usually about 1000 times larger than the NADH concentration. In order to normalize for different expression levels of the sensor in cells, a mCherry fluorescent protein was fused to Peredox at the C-terminus, hence circumventing the intensiometric drawback of SFPs and generating a ratiometric output, which permits normalization of the sensor signal to sensor concentration. The authors reported the utilization of this sensor in various mammalian cell lines, in which application of external lactate or pyruvate showed a dose-dependent change in fluorescence. This approach of administering different lactate and pyruvate levels exploits the NADH-dependent equilibrium of lactate and pyruvate via the lactate-dehydrogenase (LDH), which has been mentioned above in the established method to determine NADH and NAD^+ levels indirectly.

$$\text{Pyruvate} + \text{NADH} + H^+ \rightarrow \text{Lactate} + NAD^+$$

Administering pyruvate to the cells, therefore, leads to formation of lactate by means of the LDH and, concomitantly, a reduction in cellular NADH levels and increase in $[NAD^+]$, which is represented by reduced fluorescence of Peredox. Conversely, administering lactate leads to an increase in [NADH] and elevated fluorescence. The time courses of these experiments have been reported, and it was shown that Peredox is fast enough to give a dynamic, real time response in cellular environments. The application of Peredox has been tested in the cytosol of the cells, where it delivered robust signals. When applied in mitochondria of the respective cell lines, Peredox, due to its high affinity, was found to be saturated by the present nicotinamides (Hung et al., 2011). Mitochondria, due to their purpose as primary location of cell respiration, exhibit a higher $[NADH]/[NAD^+]$ ratio than

for example the cytosol. Peredox thus proves to be an important tool for estimating the cytosolic [NADH]/[NAD^+] ratio of different cell lines and has been widely applied to determine the nicotinamide ratio in various cells (Bilan et al., 2014; Chang et al., 2017; Marcu, Wiczer, Neeley, & Hawkins, 2014; Mongeon, Venkatachalam, & Yellen, 2016; Steinbeck et al., 2020; Tejwani et al., 2017; Z. Zhang, Cheng, Zhao, & Yang, 2020; Zhao, Zhang, Zou, & Yang, 2018). However, the application of the senor in environments with high NADH content left it saturated and unable to report on changes of the intracellular concentrations (Hung et al., 2011; Tejwani et al., 2017).

6.2 Frex and FrexH

In 2011, another pair of genetically encoded fluorescent NADH sensors was introduced, named Frex and FrexH. In these constructs, the Rex repressor protein from *Bacillus subtilis* (*B. subtilis*) was fused to a circularly permuted YFP. The derived sensors possess a topology in which a full subunit of Rex is fused to a cpYFP, followed by a truncated second Rex subunit, which only contains the nucleotide binding domain. The authors constructed various forms of this topology, altering the linker lengths between the sensing and fluorescent units. In order to enhance the specificity of the utilized Rex protein towards NADH and decrease binding of its congeners, 20 variants with single amino acid exchanges near the NADH binding site were screened for optimized NADH specificity. Upon this series of mutations, two proteins were found exhibiting either a 9-fold increase or 3-fold decrease in fluorescence upon NADH titration after excitation at 500 nm, while showing no response in presence of NAD^+ or other nicotinamide analogues.

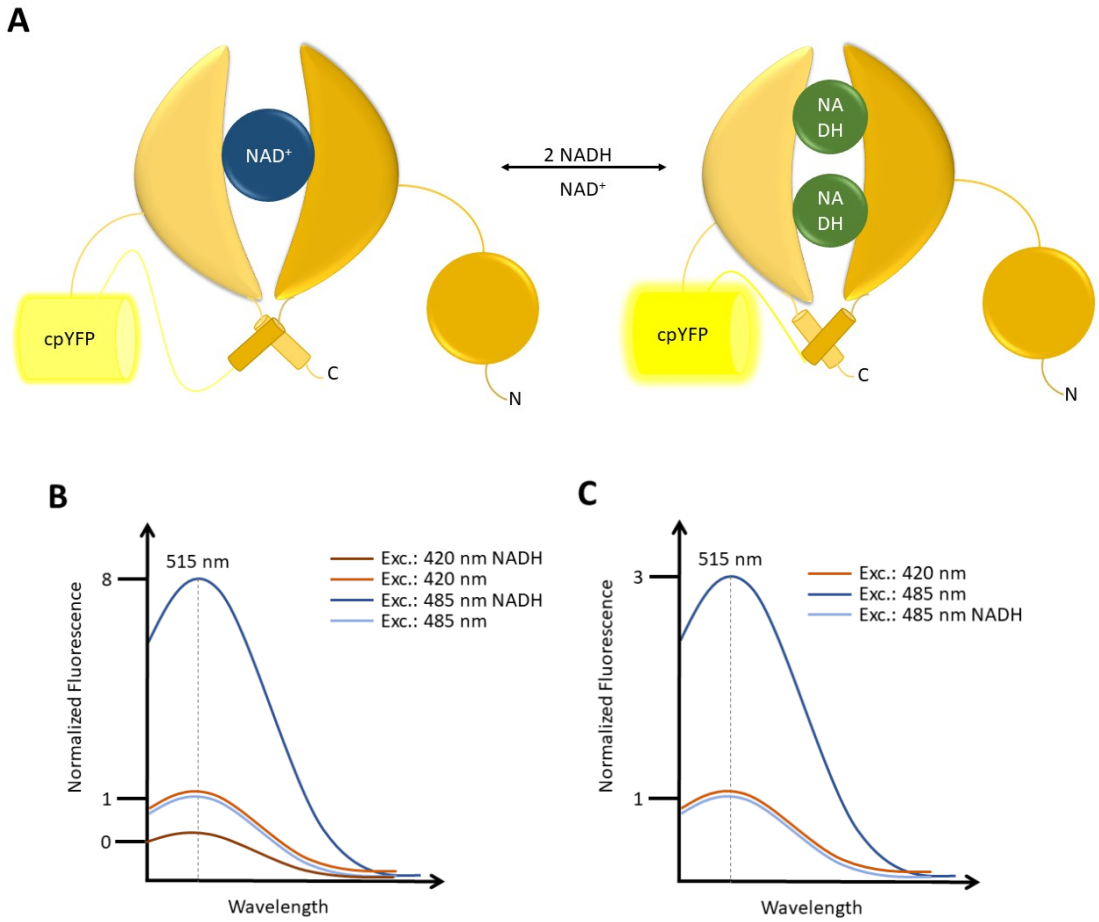

Figure 6 Topology of Frex and FrexH sensor family (**A**). The cpYFP (yellow barrel) is inserted between the two Rex subunits (bright brown and brown subunits), in one of which the DNA binding domain is replaced by the fluorophore. Upon binding of two NADH molecules, the conformation of the sensor changes and the fluorescence of the cpYFP is enhanced. The cpYFP fluorophore effectively shows two excitation peaks at 420 and 485 nm, with an emission maximum at 515 nm. A schematic representation of the resulting fluorescence of the Frex sensor is given in **B**, while the respective schematic spectra for FrexH are given in **C**. Whereas for Frex, the fluorescence after excitation at 485 nm increases according to the present NADH concentration, the opposite is true for the fluorescence after excitation at 420 nm. For FrexH the fluorescence after excitation at 485 nm decreases upon NADH binding, while the fluorescence after excitation at 420 nm remains unchanged.

The proteins are named Frex (fluorescent Rex) and FrexH (Frex of high affinity) respectively. Frex exhibits an affinity for NADH in the low micromolar range (K_D = 3.5 µM), while FrexH shows a K_D of about 40 nM. Due to the utilization of cpYFP as fluorescent probe, these proteins exhibit a profound pH sensitivity, effectively increasing the fluorescence at alkaline pH, and decreasing fluorescence by as much

as 50 % if the pH is slightly altered from 7 to a more acidic 6.5 (Day & Davidson, 2009). Hence, the authors advised to carry out control experiments under the same conditions expressing only the cpYFP. The rationale is that if the cpYFP's fluorescence is altered under the experimental conditions, these alterations are due to changing pH rather than differing NADH concentrations. The Frex family sensors show one emission band around 518 nm and two excitation bands at 400 and 500 nm, typical for GFP-based sensors (Chattoraj, King, Bublitz, & Boxer, 1996; Morise, Shimomura, Johnson, & Winant, 1974). The presence of two excitation wavelengths makes it possible to resolve changes in intracellular media and concomitantly normalize for expression levels, effectively producing a ratiometric value.

With this dual sensor system, the authors described experiments in different cellular locations of mammalian cells, using the high affinity variant FrexH primarily for loci with low NADH concentrations, such as the cytosol, while Frex was used to estimate NADH concentrations in cellular compartments such as the mitochondria. The authors found that the cytosol of 293FT cells exhibits the same fluorescence signature as an *in vitro* sample of FrexH in presence of 130 nM NADH and thus concluded that the intracellular concentration should be of the same order of magnitude. For measurement of [NADH] in the mitochondria, Frex was fused to a mitochondrial targeting sequence. The fluorescence of the protein in this compartment was evaluated to correspond to a NADH concentration of about 30 μM, verifying the notion that mitochondria exhibit higher [NADH] than the cytosol.

These two sensors are hence capable of reporting the intracellular [NADH] in different cellular compartments in 293FT cells, and Frex, specifically, has been employed to monitor lactic acid production in *Lactobacillus paracasei* (Tian et al., 2015). However, these sensors still exhibit drawbacks for streamlined utilization. For one, the sole dependency of Frex and FrexH on NADH is unfortunate, since the readout of the [NADH]/[NAD^+] ratio is physiologically more relevant (Zhao et al., 2011), since it directly reflects the redox state of the cell. Furthermore, the profound pH sensitivity the Frex sensors inherited from its fluorophore complicates its application, making further control experiments with cpYFP necessary to rule out fluorescence responses solely due to pH alterations. The

utilization of excitation wavelengths below 450 nm is challenging, since light of these wavelengths also excites substantial autofluorescence in cells, especially for the readout of values in high [NADH] environments such as the mitochondria. The substantial autofluorescence can confound the results, making further processing of the obtained signal necessary, in order to discriminate between actual sensor signal and fluorescence background noise, and, thus, hindering simple application of the sensors.

6.3 RexYFP

In 2014, another sensor termed RexYFP was established (Bilan et al., 2014). This sensor is based only on one Rex subunit, derived from *T. aquaticus*, in which the fluorophore, cpYFP, is inserted into the loop between the nucleotide- and the DNA-binding domain (**Figure 7 A**). In contrast to the aforementioned sensors, RexYFP needs interaction of two of the expressed sensor subunits, consisting of the Rex domain and the cpYFP fluorophore, in order for a given signal to occur.

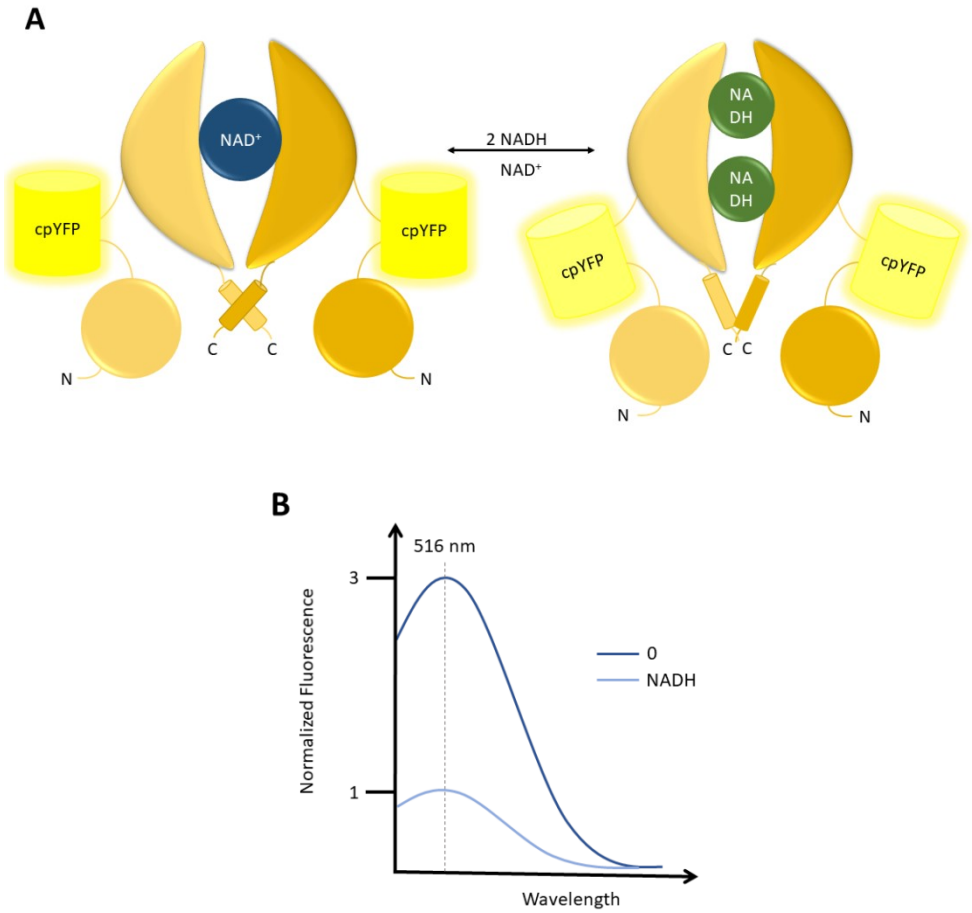

Figure 7 Topology of RexYFP sensor (**A**). The fluorophore (cpYFP, yellow barrels) is inserted between the two Rex subunits (brown subunits). While no NADH molecules are bound, the protein is strongly fluorescent. Upon binding of two NADH molecules in the Rossman fold, structural changes are transmitted to the fluorophore which in turn generates less fluorescence. The resulting spectra are schematized in panel **B**. After excitation at 485 nm the fluorescence at 516 nm is intense in the absence of NADH (dark blue line), while the fluorescence decreases upon binding of NADH (light blue curve).

The utilization of only one subunit greatly reduces the size of the gene construct in comparison to Peredox and Frex(H). Furthermore, the construction of the sensor based on two subunits greatly enhances the brightness of the probe, since the ratio between fluorophore and subunit is one in RexYFP, while it is 0.5 in Peredox and Frex(H). This sensor only allows intensiometric measurements at one wavelength, with the excitation at 490 nm and emission at 516 nm (**Figure 7 B**), as is typical for the cpYFP probe. This utilization of only one excitation mode allows the dynamic monitoring of the NAD(H) status in live cell imaging. However, since no possibility for a ratiometric readout is given, the sensor cannot be used for intercellular

comparison, and can neither quantify the NAD(H) pools, nor their ratio. Upon binding of NADH the fluorescence emission decreases by a factor of about two (**Figure 7 B**). RexYFP exhibits an apparent affinity constant of 180 nM, which thus is between the affinities of Peredox and Frex. The sensor might be susceptible towards binding of NADPH, due to its affinity constant of 6.3 μM for the phosphorylated congener, although it is markedly larger than the affinity constant for NADH. However, the NADPH pool is more reduced and, hence, the intracellular concentration of this nicotinamide might be in the range of the sensor's affinity. Furthermore, due to utilization of the cpYFP probe and its inherent pH sensitivity, the derived sensor also exhibits fluorescence changes due to altered proton concentrations, as was mentioned for the Frex probes. These effects need to be accounted for by carrying out the analogous experiments with a cpYFP-derived peroxide sensor HyPer. In the original publication, it was demonstrated that using a mutant of the H_2O_2 sensor, which lost its peroxide sensing function, was able, even though the sensors showed differing pK_a values, to correct for pH effects in eukaryotic cell lines under different pH levels (Bilan et al., 2014). Due to its intermediate affinity, RexYFP can be used in the cytosol of mammalian cells as well as in mitochondria, facilitating the comparison between these organelles.

6.4 SoNar

In continuing efforts to design a probe optimally attuned for reporting on $[NAD^+]/[NADH]$, a 2015 publication introduced a new sensor, SoNar (Zhao et al., 2015). SoNar is a $[NAD^+]/[NADH]$ sensor based on one subunit of Rex from *T. aquaticus* (as RexYFP, vide supra), in which the fluorophore, cpYFP, is inserted into the surface loop of the nucleotide binding site (**Figure 8 A**). The DNA-binding domain of the subunit is truncated for optimal sensor characteristics.

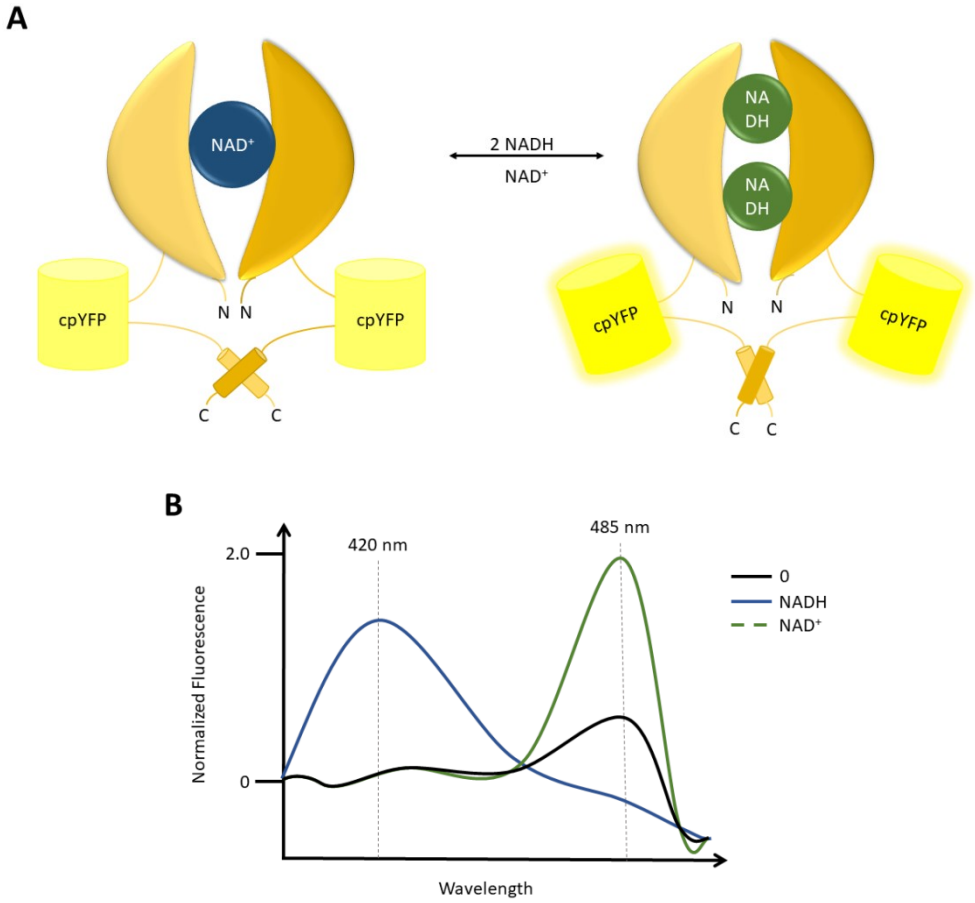

Figure 8 Topology of the SoNar sensor (**A**). The sensor consists of one subunit of *T. aquaticus* Rex (brown subunits), fused to a cpYFP (yellow barrels), and the connection is at a surface loop of the nucleotide binding domain. The cpYFP is fused C-terminally to a truncated DNA-binding domain. The functional sensor consists of two separately expressed units. The cpYFP fluorophore effectively shows two excitation peaks at 420 and 485 nm, with an emission maximum at 515 nm. Panel **B** illustrates a schematic representation of the fluorescence excitation spectra in presence of no nucleotides (0, black curve), NADH (blue curve) and NAD^+ (green curve). The fluorescence after excitation at 420 nm is specifically sensitive for NADH changes, while the fluorescence after excitation at 485 nm is potentially altered by both, present NADH and NAD^+.

Alike the RexYFP probe, SoNar is only completely functional, when two of the Rex-cpYFP monomers interact, and under this condition the probe exhibits fluorescence dependent on the present [NADH], [NAD^+], and their ratio. This also means, that the brightness of SoNar, again alike RexYFP, is superior compared to Peredox and the Frex family probes. Owing to its cpYFP chromophore, the probe demonstrates two excitation maxima, one at 400 nm and one at 500 nm. Upon

exciting the probe at 400 nm, the emission maximum at 515 nm is increasing in a positively correlated manner depending on the present NADH concentration. However, upon exciting the sensor at 500 nm, the sensors fluorescence is dependent on the [NAD^+]/[NADH] ratio, with the emission increasing in the presence of increasing NAD^+ concentrations and decreasing in the presence of increasing NADH. To evaluate the sensor signal, it was advised to utilize the fluorescence readout after excitation at 420 nm divided by the fluorescence emission after excitation at 485 nm, therefore, again normalizing the signal for intercellular deviations in expression levels of the sensor. The ratiometric readout would increase for lower [NAD^+]/[NADH] ratios and vice versa. Even though the 420 nm excitation is prone to variations by deviating pH levels, the [NAD^+]/[NADH] ratio read out was robust over the physiological pH span between 7 – 7.8. The apparent affinity constants of the sensor for NADH and NAD^+ are 200 nM and 5 μM respectively. These affinity constants effectively leave the sensor saturated under physiological conditions, by either NAD^+, NADH or a ratio of them, since the affinities are well below their typical intercellular concentrations, since in mammalian cells the total NAD(H) pool lies between 50 and 400 μM (Patterson et al., 2000; Yamada, Hara, Shibata, Osago, & Tsuchiya, 2006; H. Yang et al., 2007; Yu & Heikal, 2009). Assuming that about 5 % of the total pool represents the free nicotinamide fraction (Q. Zhang et al., 2002), the free NAD pool would be between 2.5 and 20 μM.

SoNar's dynamic range is 1500 % for the ratiometric measurements, a value unprecedented in NADH sensors. With the utility of SoNar sensor the free [NAD^+]/[NADH] ratios of various cell lines have been determined, which was as low as 96 in human lung cancer cells, about 400 in human embryonic kidney cells (HEK293FT), and as high as 650 in primary mouse hepatocytes (Zhao et al., 2015, 2016). The sensor has also been applied in further studies, describing the NADH/NADH level in pathological (Hao et al., 2019; Titov et al., 2016) or non-pathological cells (Zou et al., 2018). The actual quantification of intracellular [NADH] or [NAD^+], however, is not possible with this probe, since the sensor will always be stimulated by a ratio of both nicotinamide species, if they are present.

7 The Soluble Hydrogenase of *R. eutropha*

R. eutropha is a gram-negative proteobacterium, which hosts a very versatile metabolism (Cramm, 2009). It is a facultative aerobic organism, which is capable of utilizing hydrogen and carbon dioxide (lithotrophic) (B. Friedrich & Schwartz, 1993) or various organic carbon compounds (heterotrophic) for growth. While NADH and NAD^+ metabolism in *R. eutropha* depend on the common energy pathways such as aerobic and anaerobic respiration, additionally other metabolic pathways such as the Calvin-Benson-Bassham cycle, which is used to fix CO_2, are deeply intertwined with the cellular [NADH]/[NAD^+] state. In *R. eutropha* the NADH pool is further directly influenced by a cytosolic, soluble, bidirectional, NAD^+ dependent [NiFe] hydrogenase (soluble hydrogenase, SH) (Vignais & Billoud, 2007), which is one of four hydrogenases found in this organism (Burgdorf et al., 2006; Cornelius G. Friedrich, Friedrich, & Bowien, 1981; O. Lenz & Friedrich, 1998; O Lenz, Bernhard, Buhrke, Schwartz, & Friedrich, 2002). The SH is capable of oxidizing molecular hydrogen while concomitantly reducing its other substrate NAD^+.

$$H_2 + NAD^+ \rightarrow H^+ + NADH$$

The soluble hydrogenase is strongly biased towards hydrogen oxidation *in vivo*, supplying the cell with reducing equivalents (Burgdorf et al., 2006; Schneider & Schlegel, 1976). However, given a sufficiently reduced environment, the SH can also act as an electron valve, effectively reducing the cell's redox potential while generating hydrogen (Kuhn, Steinbuchel, & Schlegel, 1984).

7.1 Structure of the Soluble Hydrogenase

The SH is a heteromultimeric protein of about 280 kDa in size, consisting of two modules, termed the diaphorase module and the hydrogenase module (Burgdorf et al., 2006). Both modules are built up of two subunits, where the hydrogenase module is capable of the oxidation or production of hydrogen, while the diaphorase module is responsible for the reduction of NAD^+ (Lauterbach, Idris,

Vincent, & Lenz, 2011)(**Figure 9**). The hydrogenase module consists of the HoxHY heterodimer, while the diaphorase module is made up from the HoxFU heterodimer. In connection with the supposedly regulatory HoxI homodimer (Burgdorf et al., 2005), the full protein is formed.

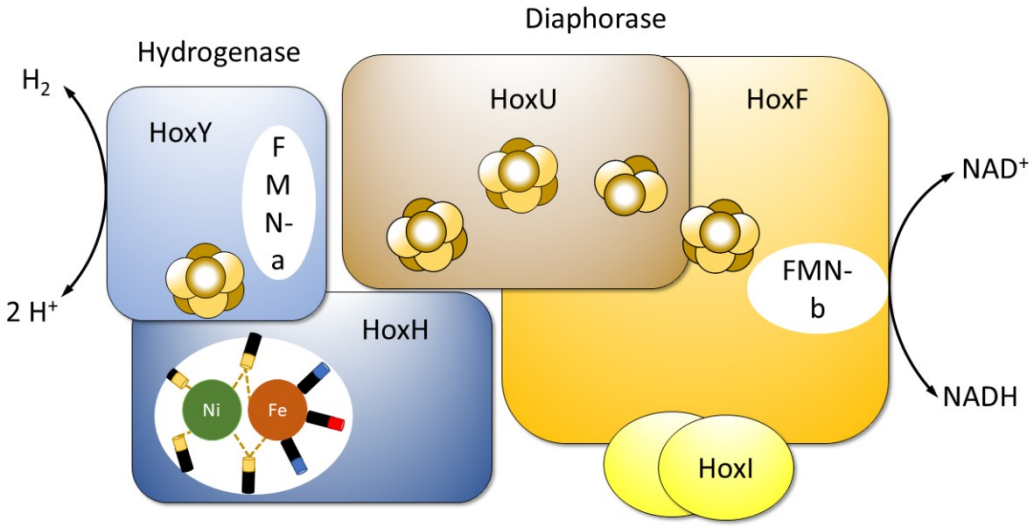

Figure 9 Composition of the soluble hydrogenase from *Ralstonia eutropha*. The hydrogenase module (blue modules) is built up of the two subunits HoxY and HoxH, in which the catalytic [NiFe] center is located. The diaphorase module (brown and yellow modules) consists of the HoxU and HoxF subunits. Furthermore, the SH also contains two HoxI subunits (light yellow). The active center is comprised of a nickel and an iron atom. The ligand set is consisting of sulfur bridges from thiols, of which two are bridging (black = carbon, yellow = sulfur), two cyanide ligands (blue = nitrogen), and one carboxyl ligand (red = oxygen), keeping the iron atom in the low spin state. The [4Fe4S] cluster are depicted as clusters of brown and yellow spheres, one cluster of which can be found in the HoxY subunit, three in the HoxU subunit and one in the HoxF subunit. This figure is based on the depiction of the soluble hydrogenase in (Lauterbach & Lenz, 2013).

The soluble hydrogenase contains two flavin mononucleotide (FMN) binding sites, one in the HoxY subunit of the hydrogenase module (FMN-a), and one is located in the HoxF subunit of the diaphorase module (FMN-b) (Schneider & Schlegel, 1978; Van Der Linden et al., 2004), where the FMN molecule in binding site FMN-b is bound in a non-classical Rossman fold (Lauterbach, Lenz, & Vincent, 2013). These FMN molecules are of vital importance for the electron transduction between

hydrogen and NAD. The electron transport is further facilitated by various [FeS] clusters in the protein, of which four are located within the diaphorase module and one in the hydrogenase module in close proximity to the catalytic center (M. Horch, Lauterbach, Lenz, Hildebrandt, & Zebger, 2012). Since the iron-sulfur clusters are only capable of transferring one electron at a time, and NAD and hydrogen are two electron centers, the FMN molecules, being capable of various redox states, have the further role of mediating between these species. The electron transport between the two reaction partners H_2 and NAD is thus finely regulated by the interplay between the catalytic [NiFe] center, the [FeS] clusters and the FMN molecules.

7.2 The Active Center of the Soluble Hydrogenase

The nickel atom of the catalytic center is coordinated by four cysteinyl thiolate donors originating from the protein backbone, from which two are bridging ligands also interacting with the iron atom. The iron atom is further complexed by non-proteinaceous ligands, namely two cyanide and one carboxyl ligand, which are uncommon ligands in biological systems except hydrogenases (Happe, Roseboom, Pierik, Albracht, & Bagley, 1997; Pierik, Roseboom, Happe, Bagley, & Albracht, 1999; Volbeda et al., 1996).

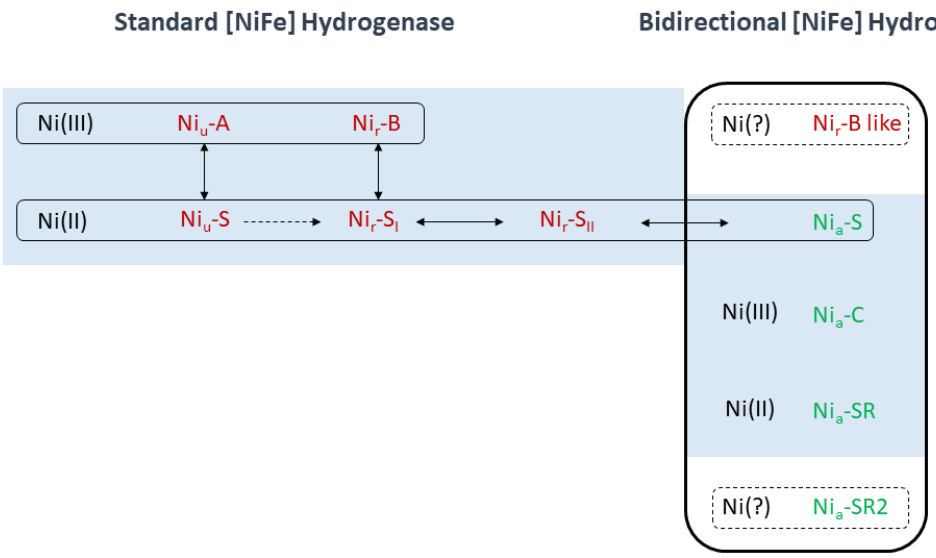

Figure 10 Redox states of standard [NiFe] (blue background) and the bidirectional [NiFe] hydrogenase from *R. eutropha* (box) (Bleijlevens et al., 2004; Lubitz, Reijerse, & van Gastel, 2007). The inactive states are depicted in red, while the active states are depicted in green. The states in the dashed boxes refer to states found specifically in bidirectional [NiFe] hydrogenases (Germer et al., 2009; Marius Horch et al., 2010). Figure adapted from (M. Horch et al., 2012)

During its catalytic cycle the SH transitions between different redox states, in which the iron remains in a Fe(II) low spin state and the nickel is the redox active part. In "standard" [NiFe] hydrogenases, the active center traverses through three different states in this cycle, whereby in one (Ni_C or Ni_a-C depending on the nomenclature) the nickel atom is paramagnetic. Since historically the active site of standard [NiFe] hydrogenases was primarily investigated by EPR spectroscopy, the Ni_a-C state was the only detectable state of the Ni belonging to the catalytic species (S.P.J. Albracht, Graf, & Thauer, 1982; Cammack, Patil, Aguirre, & Hatchikian, 1982). Other states detected by EPR spectroscopy were Ni_u-A and Ni_r-B, in which the Ni is in oxidation state III (S. P.J. Albracht, Van Der Zwaan, & Fontijn, 1984; S.P.J. Albracht et al., 1982; Simon P.J. Albracht, 1994; Cammack et al., 1982). Both of these states are inactive, but can be transformed into active catalytic species, albeit with very different kinetics, whereby the reductive activation by hydrogen in an anaerobic environment of Ni_r-B is achieved in minutes, the same process takes hours for Ni_u-A (Fernandez, Hatchikian, & Cammack, 1985). The different activation kinetics are supposedly due to different

oxygen species bound to the active centre (Van Gastel et al., 2006; Volbeda et al., 2005). Further activation leads to the Ni_a-S (for active (EPR)-silent), which together with the Ni_a-SR (for active silent ready) and the aforementioned Ni_a-C state comprise the active states in standard [NiFe] hydrogenases. The Ni_a-S and Ni_a-SR states are diamagnetic and can be detected by infrared (IR) spectroscopy (De Lacey, Fernández, Rousset, & Cammack, 2007; De Lacey et al., 1997), in which the C-N and C-O stretching vibrations of the inorganic ligand set at the iron atom can be utilized to gather information about the status of the active site of the hydrogenase (Lubitz et al., 2007), therefore providing another experimental tool to understand the processes in the biocatalysts.

In studies carried out on bidirectional hydrogenases, it was found that the obtained states of the catalytic centre are slightly different in comparison to the ones found for standard [NiFe] hydrogenases (Germer et al., 2009; Marius Horch et al., 2010). For one, a prototypic EPR-active Ni_r-B state was not found, but rather a state conferring the same IR characteristics as Ni_r-B, which is EPR silent and was termed "Ni_r-B-like". This may be due to coupling of the paramagnetic Ni centre with other paramagnetic species in the protein, which could potentially arise from the iron-sulfur clusters and the FMN, which are in close proximity, and thus effectively masking the Ni(III) state, or the fact that the nickel centre in the "Ni_r-B-like" state is actually in oxidation state II (Marius Horch et al., 2010). The catalytic active species, Ni_a-S, Ni_a-C and Ni_a-SR have also been found for the SH of *R. eutropha*. However, also a further reduced species, termed Ni-SR2 has been detected by IR spectroscopy on *R. eutropha* cells, expressing only the SH (Marius Horch et al., 2010).

Due to its oxygen tolerance, the SH is a promising candidate for biohydrogen production, for application in fuel cells or for cofactor recycling and, thus, target of many studies, further trying to facilitate utilization of this enzyme in biotechnological applications (Marius Horch et al., 2015; Lauterbach et al., 2013; Mertens & Liese, 2004; Ratzka, Lauterbach, Lenz, & Ansorge-Schumacher, 2011; Shafaat, Rüdiger, Ogata, & Lubitz, 2013). It is hence of great interest to study the activity of the soluble hydrogenase under varying conditions. The activity of the enzyme can be monitored by measuring produced or consumed H_2 via gas chromatography or by produced and consumed NADH (or electrons) in bioassays

in lysed cells. However, in living cells, this undertaking has been impossible, thus, with the advent of the new NADH biosensors, another tool is offered to monitor the NADH-dependent activity of the soluble hydrogenase. In a first study trying to elucidate [NADH]/[NAD^+] levels in *R. eutropha* cells the biosensor Peredox was utilized.

7.3 Peredox as *in vivo* SH Activity Reporter

In a preceding study, Tejwani et al. have introduced the fluorescent reporter Peredox into a *R. eutropha* host strain, which was genetically modified to only synthesize the soluble hydrogenase, thus implementing a tool to monitor the activity of the endogenous, biotechnologically interesting soluble hydrogenase of this organism (Oliver Lenz, Lauterbach, Frielingsdorf, & Friedrich, 2015; Tejwani et al., 2017). The authors utilized a genetically modified strain of the bacterium, that carried in-frame deletions of the genes for the great subunits of other hydrogenases present in this organism, namely the membrane-bound hydrogenase (MBH) and the regulatory hydrogenase (RH) (Marius Horch et al., 2010). Therefore, in this modified strain only the SH is synthesized, besides the recently discovered actinobacterial hydrogenase, which demonstrates about two orders of magnitude lower hydrogen oxidation rates than the MBH or SH (Schäfer, Friedrich, & Lenz, 2013). It can therefore be reasonably assumed that the consumed or produced hydrogen in the experiments stems from the SH (Marius Horch et al., 2010).

Basal expression of the sensor was confirmed by investigating cell suspensions by fluorescence spectroscopy. In these experiments, the fluorescence of the sensor was observable, indicating functionality of the sensor in the desired environment. In order to trigger the activity of the soluble hydrogenase, the cell suspensions were treated with hydrogen, which serves as a substrate for the SH. The SH-catalysed hydrogen oxidation then leads to elevated NADH levels (and concomitantly reduced NAD^+ levels), which should be represented by a different fluorescence signal of Peredox. However, upon triggering the hydrogen oxidation reaction of the SH, the fluorescence did not change much. These findings were

explained by a cellular milieu, in which the Peredox sensor is almost saturated at the physiological NADH levels. When the SH activity is triggered, the NADH pool increases substantially, but since Peredox is already almost saturated by the basal [NADH] level, no further response can be achieved by the actual changes in [NADH]/[NAD^+].

Thus, in order to gain insight into the present NADH and NAD^+ levels in *R. eutropha* cells, an external calibration method was performed. For this method, Peredox-expressing cells were lysed, and the retrieved lysate was treated with different amounts of NADH and NAD^+ to stimulate signal of the Peredox sensor and to clarify whether the sensor was still responding. The obtained fluorescence was plotted against the given R' values, and it was estimated that the R' value *in vivo* must be higher than 15, given a fluorescence intensity of ≥ 90 % of the sensor's dynamic range in whole cells.

Furthermore, the absolute concentrations of NADH and NAD^+ in *R. eutropha* cells were estimated based on the results from the external calibration method. In order to calculate the total NAD the following assumptions were made

1. The lysis produced a 4000-fold dilution of the cellular components
2. Minimum fluorescence of the sensor in the lysed extract
3. A determined $K_{0.5}$ of Peredox for NADH of about 44 nM

Applying these assumptions, the concentration of NADH in the lysate cannot be higher than 7 nM, assuming that the fluorescence signal of Peredox is not higher than 3 % of its full range for the first measurement after lysis. Based on the dilution factor, a 4000-fold higher minimal concentration of NADH, 28 µM, was predicted for the free cytosolic NADH. Given the observed result that the R' value in whole cells must be at least 15, the free NAD^+ concentration was calculated to be 1.9 mM. Furthermore, the total NAD pool was estimated by assuming that the total NADH and NAD^+ is five times greater than the free pool (Blinova et al., 2005) . This yields a total [NADH] of 140 mM and a total [NAD^+] of 9.5 mM, which matches previously determined values for bacteria (Bennett, Kimball, & Gao, 2009; Zhou et al., 2011).

This preceding study gave an insight into the general magnitude of the NAD(H) pool in the β-proteobacterium *R. eutropha*. However, dynamic monitoring of the

activity of the SH was impossible with the utilized sensor, due to its high affinity towards NAD(H), effectively not being able to report the changes triggered by activating the soluble hydrogenase. For further application it is thus desirable to be able to monitor the SH activity by a fluorescent reporter, which is capable of this task, due to its robust expression in the bacterium and its suitable lower affinity for NADH and NAD^+.

II Motivation

While alternative sensors developed for the reporting on intracellular NADH have been created, these constructs were, in all cases, developed for a potential application in mammalian cells (Bilan et al., 2014; Hung et al., 2011; Zhao et al., 2011, 2016). These cells differ from bacterial cells in many ways. Especially, mammalian cells are highly compartmentalized, each cell component possessing its own metabolite concentrations and redox status, that can vary widely. The cytosolic NAD concentrations in mammalian cells are generally smaller than for their bacterial counterparts (Bennett et al., 2009; Zhao et al., 2011; Zhou et al., 2011). Thus, for an application in the bacterial cytosol, the sensor should have a comparatively low affinity for NADH as well as for NAD^+.

In 2011, a set of new biosensors Frex and FrexH were introduced. Frex and FrexH are NADH-dependent biosensors that are generally related but differ in their affinity for NADH, where the K_D for NADH of Frex is 3.7 μM, and 40 nM for FrexH (Zhao et al., 2011). The sensor Frex thus seemed a reasonable candidate to be utilized for *in vivo* studies in bacterial cells and their generally higher NAD environment in the cytosol. Hence, the aim of this thesis was to introduce the fluorescent NADH biosensor Frex into *R. eutropha* in order to report changes in the intracellular NADH, which could be traced back to changes in SH activity.

Furthermore, engineering of a NADH sensor towards the unique conditions in the bacterial cytosol was targeted. An optimal sensor of NAD(H) in bacterial cells would show an affinity constant for NADH in the micromolar range and for NAD^+ in the millimolar range. The range in the intensity readout should be as large as possible, for the greater the dynamic range is, the more subtle changes can be resolved in terms of the intracellular concentrations. Additionally, the signal should be ratiometric in order to read out quantitative values and facilitate comparisons between different samples. The utilization of red-to-far-red-emitting probes for application in tissues is, due to many factors, superior to their counterparts of the UV-Vis region of the light spectrum. For one, cells exhibit a near-infrared window, in which almost no absorption of light takes place and thus

the excitation as well as the emitted light can pass through the sample nearly unhindered (Jobsis, 1977; Weissleder, 2001). Moreover, light of these wavelengths is less prone to scattering and can thus delve deeper into tissue. The utilization of low-energy light for excitation of the probe also reduces the risk of photodamaging the tissue und consequently allows the sampling to be less invasive. The application of fluorescence sensors with excitation peaks between 400-450 nm, as is common for the NADH biosensors available at present is severely limited in bacterial cells due to their high autofluorescence, which is also triggered by employing light of these wavelengths. Thus, it was the aim to design, construct and test a NADH sensor, that would be optimized for the special requirements encountered in bacterial environments.

III Materials & Methods

1 Plasmids & Cell Lines

The utilized plasmids and cell lines are given in **Table 1** & **Table 2**. For DNA production, *E. coli* cell lines XL10 Gold and *E. coli* XL 10 Blue were used. For protein production BL21(DE3)pLysS, Rosetta(DE3)pLysS and NEB Turbo have been used. The *E. coli* strain S17-1 was used for the conjugative plasmid transfer to the recipient strains, which were the two *R. eutropha* strains HF500 and HF798.

Table 1 Overview over the utilized plasmids

Plasmid	Features	Reference
E. coli		
pQE81L-Not	Ampicillin resistance, T5-lac promoter, C-terminal His-tag	Qiagen
pRSETb	Ampicillin resistance, T7-lac promoter, C-terminal His-tag	Invitrogen
pET Duet	Two multiple cloning sites (MCS), ampicillin resistance, T7-lac promoter, C-terminal His-tag in first MCS, N-terminal S-tag in the second MCS	Novagen
pRSF Duet	Two multiple cloning sites (MCS), kanamycin resistance, T7-lac promoter, C-terminal His-tag in first MCS, N-terminal S-tag in the second MCS	Novagen
pJOE 5751.1	Ampicillin resistance, T7-rha promoter, C-terminal His.tag	(Hoffmann, Bóna-Lovász, Beuttler, & Altenbuchner, 2012)

pET27b	Kanamycin resistance, T7-lac promoter, N-terminal His-tag	Novagen
R. eutropha		
pLO13SH	Tetracycline resistance, SH-promoter	Dr. Oliver Lenz

Table 2 Overview over the utilized Cell lines

Cell Line	Genotype	Reference
E. coli		
BL21(DE3)pLysS	*E. coli* str. B F⁻ *ompT gal dcm lon hsdS$_B$*($r_B^-m_B^-$) λ(DE3 [*lacI lacUV5-T7p07 ind1 sam7 nin5*]) [*malB*$^+$]$_{K-12}$(λ^S) pLysS[*T7p20 ori*$_{p15A}$](Cm^R)	Moffat
BL21(DE3)	*E. coli* str. B F⁻ *ompT gal dcm lon hsdS$_B$*($r_B^-m_B^-$) λ(DE3 [*lacI lacUV5-T7p07 ind1 sam7 nin5*]) [*malB*$^+$]$_{K-12}$(λ^S)	Studier, Moffat
Rosetta(DE3)pLysS	*E. coli* str. B F⁻ *ompT gal dcm lon? hsdS$_B$*($r_B^-m_B^-$) λ(DE3 [*lacI lacUV5-T7p07 ind1 sam7 nin5*]) [*malB*$^+$]$_{K-12}$(λ^S) pLysSRARE[*T7p20 ileX argU thrU tyrU glyT thrT argW metT leuW proL ori*$_{p15A}$](Cm^R)	Novagen
NEB Turbo	*glnV44 thi-1 Δ(lac-proAB) galE15 galK16 R*(*zgb-210*::Tn*10*)Tet^S *endA1 fhuA2 Δ(mcrB-hsdSM)5*, ($r_K^-m_K^-$) F′[*traD36 proAB*$^+$ *lacI*^{q} *lacZΔM15*]	New England Biolabs
XL 10 Gold	endA1 glnV44 recA1 thi-1 gyrA96 relA1 lac Hte Δ(mcrA)183 Δ(mcrCB-	Stratagene

	hsdSMR-mrr)173 tet^R F'[proAB $lacI^q$ZΔM15 Tn10(Tet^R Amy Cm^R)]	
XL 1 Blue	endA1 gyrA96(nal^R) thi-1 recA1 relA1 lac glnV44 F'[::Tn10 $proAB^+$ $lacI^q$ Δ(lacZ)M15] hsdR17(r_{K^-} m_{K^+})	Stratagene
S17-1	Strep, Tet^R, thi, pro, hsdR17(r_{K^-} m_{K^+}), hsdM+, recA, RP4-2	Simon et al., 1983
R. eutropha		
HF798	Δ*hoxG*Δ*hoxC* SH^+, MBH^-, RH^-	Marius Horch et al., 2010
HF500	Δ*hoxG*Δ*hoxC*Δ*hoxH* SH^-, MBH^-, RH^-	Kleihues, Lenz, Bernhard, Buhrke, & Friedrich, 2000

2 Media, Buffer and Antibiotics

E. coli

Medium/buffer	**Component**	**Final Concentration**
PBS	NaCl	137 mM
	KCl	2.7 mM
	Na_2HPO_4	10 mM
	KH_2PO_4	1.8 mM
PBST	PBS	
	Tween 20	0.1 % v/v
Ripa lysis buffer	NaCl	150 mM
	Tris base	50 mM
	Triton X-100	1 % v/v
	sodium deoxycholate	0.5 % w/v
	SDS	0.1 % w/v
Laemmli buffer	Tris-HCl	120 mM
	glycerol	20 % v/v
	SDS	4 % w/v
	bromophenol blue	0.02 % w/v
Equilibration buffer	PBS	
	NaCl	300 mM

	$NiCl_2$	1 µM
Washing buffer	PBS	1 x
Elution buffer	PBS	1 x
	imidazole	300 mM
LB medium	NaCl	171 mM
	tryptone	1 % w/v
	yeast extract	0.5 % w/v
TB medium	K_2HPO_4	72 mM
	KH_2PO_4	17 mM
	yeast extract	2.4 % w/v
	tryptone	2 % w/v
	glycerol	4 % v/v
SOB medium	$MgCl_2$	10 mM
	$MgSO_4$	10 mM
	NaCl	10 mM
	KCl	2.5 mM
	tryptone	2 % w/v
	yeast extract	0.5 % w/v
SOC medium	SOB medium	
	glucose	20 mM
YT medium	tryptone	1.6 % w/v
	Yeast extract	1 % w/v
	NaCl	86.6 mM
R. eutropha		
H16	Na_2HPO_4	25.1 mM
	KH_2PO_4	11 mM
AutN	H16 buffer	
	NH_4Cl	37.4 mM
	$MgSO_4$	0.81 mM
	$CaCl_2$	68 µM
	$FeCl_3$	18 µM
	$NiCl_2$	1 µM
FN	AutN medium	
	fructose	0.4 % w/v
FGN	AutN medium	
	fructose	0.2 % w/v
	glycerol	0.2 % w /v
GN	AutN medium	
	glycerol	0.4 % w/v

Antibiotic	Working concentration	Manufacturer
Ampicillin	100 µg/mL	Carl Roth GmbH & Co. KG, Karlsruhe, Germany
Kanamycin	50 µg/mL	Carl Roth GmbH & Co. KG, Karlsruhe, Germany
Chloramphenicol	34 µg/mL	Carl Roth GmbH & Co. KG, Karlsruhe, Germany
Tetracycline	10 µg/mL	Formerly Fluka Chemie GmbH, Buchs, Switzerland Now Sigma-Aldrich Chemie GmbH, Steinheim, Germany

3 DNA Methods and Materials

3.1 Oligonucleotide Primers

For introduction of mutations in already existing DNA constructs the Q5 mutagenesis kit (New England Biolabs) was utilized. Primers were designed according to the online tool NEBaseChanger and are given in **Table 3**. Primers were regularly obtained from MWG Biotech (Ebersberg, Germany).

Table 3 Mutagenesis Primer for the respective mutants

Primer	Sequence
I194E forward	GAACGTTGACGAGCTGGCCGGTC
I194E reverse	TCAACAGCCACTTCCTTG
F194E forward	AAACGTTGATGAGCTGGCCGGCC
F194E reverse	TCAACAGCAACTTCCTTAG
I194Y forward	GAACGTTGACTACCTGGCCGGTC
I194Y reverse	TCAACAGCCACTTCCTTG
I194Q forward	GAACGTTGACCAGCTGGCCGGTC
I194Q reverse	TCAACAGCCACTTCCTTG
F194Y forward	AAACGTTGATTACCTGGCCGGCC
F194Y reverse	TCAACAGCAACTTCCTTAGGAACC
F194Q forward	AAACGTTGATCAACTGGCCGGCC
F194Q reverse	TCAACAGCAACTTCCTTAG

For the DNA generation of the newly designed NADH sensor constructs, recombinant polymerase chain reactions (PCR) were carried out. The primers used for lifting the respective subunits and finally conjoining them to the new constructs are given in **Table 4**.

Table 4 Primer sequences for the design of the newly constructed fluorescent biosensor Bili-Sense and its derivatives.

Primer	Sequence	Characteristics
GAF-for	TATTACAACAGCCCCCCCCAGCGGGACG	Forward primer for the elongation of the GAF subunit, containing an overlap to the Rex(I) subunit
GAF-rev	TGTCATGGTACCCTCTTCCATCACGCCGATCTG	Reverse Primer for the elongation of the GAF subunit, containing an overlap to the Rex(II) subunit
GAF-Rex-for	GTGATGGAAGAGGGTACCATGACAGACGTCATC	Forward primer for the elongation of the Rex(II) subunit, containing an overlap to the GAF subunit
GAF-Rex-rev	GCTGGGGGGGGCTGTTGTAATAATGCTTCAAAAAA	Reverse primer for the elongation of the Rex(I) subunit, containing an overlap to the GAF subunit
PAS-Rex-for	GGAACCCCCCATGAATAAGGATCAATCAAAAATTC	Forward primer for the elongation of the Rex(I) subunit, containing an overlap to the PAS subunit
PAS-Rex-rev	ATCCTTATTCATGGGGGGTTCCAGTTCCAG	Reverse primer for the elongation

of the PAS subunit, containing an overlap to the Rex(I) subunit

3.2. PCR

Recombinant PCR was carried out with Phusion high-fidelity polymerase (Thermo Fisher Scientific GmbH, Darmstadt, Germany). The samples were prepared according to manufacturer's instructions, with annealing temperatures determined by the T_m calculator of Thermo Fisher Scientific. The elongation time was calculated according to the extension rate of 20 seconds per kilobase. The respective PCR products were transferred to an agarose gel and verified for successful reaction by sequencing.

For site-directed mutagenesis, the Q5 mutagenesis kit (New England Biolabs GmbH, Frankfurt am Main, Germany) was used. The procedure followed manufacturer's instructions, and the resulting clones were checked for successful mutation by sequencing.

For colony PCR, 10-20 colonies of the desired product were screened. The PCR was carried out with DreamTaq polymerase (Thermo Fisher Scientific GmbH, Darmstadt, Germany), with the first denaturation step prolonged to 1 minute in order to lyse cells and release DNA. The samples were verified by agarose gel electrophoresis.

4 Conjugation

For transfer of plasmid DNA from *E. coli* into *R. eutropha* strains, the following steps according to an established protocol were carried out (B. Friedrich, Hogrefe, & Schlegel, 1981).

R. eutropha cells of the desired strain were cultivated in glass flasks, in which the liquid phase accounted for one fifth of the total volume. Cells were kept in 10 mL of fructose minimal growth medium at 37 °C and 220 rpm overnight.

The cDNA-bearing pLO13SH plasmid was introduced into the *E. coli* strain S17-1. This strain is genetically modified to allow horizontal gene transfer between donor and recipient cells (Phornphisutthimas, Thamchaipenet, & Panijpan, 2007).

The next day, 10 mL of LB were inoculated from a single colony and grown overnight at 37 °C and 220 rpm. The overnight cultures of both the *E. coli* and *R. eutropha* cells were washed twice and resuspended in 1 mL H16 buffer. 200 µL of both cell suspensions were combined into one spot on a LB agar plate and kept at 37 °C for six hours. The cell material was collected from the plate with a sterile glass pipette, washed in H16 buffer and resuspended in 1 mL of H16 buffer. The resulting mixture was appropriately diluted and plated onto an FN agar plate containing tetracycline for selection of the utilized plasmid. The cells were kept at 37 °C for two days until colonies appeared. The colonies were transferred to a new FN-agar plate containing tetracycline and again incubated for two days at 37 °C. Afterwards, the grown colonies were checked for successful integration of the desired plasmid.

5 Protein Expression

5.1 Expression of Frex

The Frex cDNA-containing plasmid pRSETb was transformed into the *E. coli* cell line BL21(DE3)pLysS. 10 mL of LB medium containing 100 µg/mL ampicillin and 34 µg/mL chloramphenicol were inoculated from a single colony and kept overnight at 37 °C and 220 rpm. The next day the main culture was inoculated 1:100 (10 mL in 1 L). Protein expression was induced at OD_{600} = 0.6 with 0.5 mM IPTG (isopropyl-β-D-1-thiogalactopyranoside, Carl Roth GmbH & Co. KG, Karlsruhe, Germany) and the culture was transferred to 18 °C and kept for 48

hours. The cells were harvested at 5000 x *g*, for 10 minutes at 4 °C and resuspended in lysis buffer containing PBS, Complete® protease inhibitor (Roche Molecular Biochemicals, Mannheim, Germany) and 100 mg/mL lysozyme. The cells were lysed by three subsequent freeze/thaw cycles in freeze ethanol (100 % ethanol containing dry ice). The cell residues were separated from the supernatant containing the protein by centrifugation (18,000 x *g*, 10 minutes, 4 °C). The filtered supernatant was applied to a cobalt affinity column (HiTrap™ Talon® crude 5 mL, GE Healthcare Europe GmbH, Freiburg, Germany), washed three times and eluted with 300 mM imidazole (Carl Roth GmbH & Co. KG, Karlsruhe, Germany). The sample was concentrated to 2.5 mL (Macrosep® Advance Centrifugal Devices 10 K, Pall Corporation) and the imidazole was removed by loading the sample onto a desalting column (PD-10 desalting column, GE Healthcare Europe GmbH, Freiburg, Germany). The purified protein was collected, and aliquots were snap frozen in liquid nitrogen and stored at -80 °C until further use.

5.2 Expression of Peredox-mCherry and its Mutants

The Peredox-mCherry containing pRSETb vector was transformed with *E. coli* BL21(DE3)pLysS cells. A single colony was used to inoculate 10 mL of YT medium containing 100 μg/mL ampicillin and 34 μg/mL chloramphenicol. The liquid culture was cultivated at 37 °C and 220 rpm overnight. The next day the pre-culture was used to inoculate 1 L of YT medium as the main culture. The cells were kept at 37 °C and 220 rpm until an OD_{600} of 0.6 was reached. The culture was induced by 1 mM IPTG and transferred to 18 °C. The culture was kept at room temperature for 21 hours and subsequently harvested. The desired protein was purified from the harvested cells as described above for Frex.

5.3 Expression of Bili-Sense

E. coli Rosetta(DE3)pLysS cells were transformed with the Bili-Sense pJOE5751.1 and hHOX pQE plasmids. A single colony was picked and used to inoculate 10 mL of TB medium containing 100 μg/mL ampicillin and 50 μg/mL kanamycin. The cells were grown overnight at 37 °C and 220 rpm. Cells were induced at OD_{600} = 0.6 with 0.1 mM IPTG (Roth) and 0.02 % rhamnose (Sigma-Aldrich Chemie GmbH, Steinheim, Germany), to induce chromophore and protein production. Cells were kept at 37 °C for 24 hours. The medium was collected, and the volume was reduced 10-fold. The concentrated medium was treated with 80 % $(NH_4)_2SO_4$ (Carl Roth GmbH & Co. KG, Karlsruhe, Germany) at 4 °C and stirred for 1 hour. The solution with the precipitated protein was centrifuged (5000 x *g*, 10 minutes, 4 °C) and the supernatant was discarded. The protein was resuspended in PBS buffer and dialyzed against PBS buffer overnight at 4 °C, to remove remaining $(NH_4)_2SO_4$. The dialyzed solution was applied to a cobalt affinity column (HiTrap TM Talon® crude 5 mL, GE Healthcare Europe GmbH, Freiburg, Germany). The protein was washed three times and eluted with 300 mM imidazole (Carl Roth GmbH & Co. KG, Karlsruhe, Germany). The protein solution was dialyzed against PBS overnight at 4 °C and aliquoted the following day. The protein was frozen in liquid nitrogen and stored at -80 °C until further use.

5.4 Expression of Frex and SH in *R. eutropha*

For expression of the SH and Frex in *R. eutropha*, a pre-culture of 50 mL of FN medium containing 10 μg/mL tetracycline in a 250 mL glass flask were inoculated from a glycerol stock and kept at 37 °C and 220 rpm for two days. The pre-culture was diluted to an OD_{435} of 0.1 in FGN medium containing 10 μg/mL tetracycline and kept at 30 °C and 220 rpm. The cells were continuously monitored by fluorescence spectroscopy for adequate Frex production. Once the biosensor signal was sufficient, the cells were collected and resuspended in fresh GN medium.

6 Protein Analytics

6.1 SDS PAGE

For expression tests, samples of the expression cultures were taken in certain time intervals. For samples, the corresponding volume of 1 mL of cells at OD_{600} 0.8 were harvested by centrifugation (5000 x *g*, 10 min, 4 °C) and stored at -21 °C until further use. The cell pellets were resuspended in 500 µL ddH_2O, amounting to an OD_{600} of 1.6. To 12.5 µL of cells, 2.5 µL RIPA lysis buffer were added and the mixture was incubated at 4 °C for 10 minutes. 15 µL of Laemmli buffer were added to the lysed cells and the samples were heated to 75 °C for 10 minutes. The samples were centrifuged (12,000 rpm, 5 min, RT) and 15 µL of the samples were applied per well, as well as 5 µL of PageRuler™ Prestained Protein Ladder (Thermo Fisher Scientific GmbH, Darmstadt, Germany) for reference.

For analysis of purified proteins, an appropriate volume of the concentrated protein (2-5 µL) was diluted in ddH_20 to 15 µL and mixed with 15 µL Laemmli buffer. Further processing was as described above.

Gels were run in SDS running buffer at a voltage of 50 V until the samples had passed the stacking gel. Afterwards, voltage was increased to 150 V and the gel was run until separation of the desired bands was achieved (2-6 hours).

After running the experiment, the gels were stained in Coomassie staining solution (Roti®-Blue ready to use, Carl Roth GmbH & Co. KG, Karlsruhe, Germany) for about an hour or until bands became visible. The gels were washed until the background was unstained.

6.2 Western Blot

The SDS gels were blotted onto a nitrocellulose membrane following a standard semi-dry western blot protocol at constant current (110 mA, 2-4 hours of blotting,

depending on the protein size). The membrane was blocked by treatment with PBST buffer and 5 % milk powder (AppliChem GmbH, Darmstadt, Germany) for 1 hour at 18 °C. Subsequently, the membrane was incubated with the primary Anti-His-tag antibody (1:2500, MicroMol GmbH, Karlsruhe, Germany) in PBST containing 1 % milk powder overnight at 18 °C. The next day, the membrane was rinsed thrice in PBST, and the membrane was incubated with the secondary antibody (goat anti-rabbit, 1:5000, Carl Roth GmbH & Co. KG, Karlsruhe, Germany) in PBST containing 1 % milk powder for 1 hour at 18 °C. The secondary antibodies were conjugated to horseradish peroxidase, allowing for the visualization of protein bands with ECL reagents (Amersham™ ECL™ start Western blotting detection reagent, GE Healthcare Europe GmbH, Freiburg, Germany). The membrane was washed thrice with PBS and was incubated for 1 minute in a 1:1 mixture of the chemiluminescence solution. The membrane was exposed to an X-ray film, with the duration of the exposure adjusted for optimal visibility of protein bands.

7 Experiments with Frex as SH Activity Sensor

7.1 *In vivo* Experiments on the SH

Cells were grown as described in section 5.4. Harvested Frex- and SH-containing *R. eutropha* cells were washed and resuspended to an OD_{435} of 1 in fresh GN medium without tetracycline. 1 mL of the cell suspension was transferred into a quartz cuvette and sealed with a rubber septum. The cell suspension was aerated with the respective gas via a cannula connected to a gas outlet, until a steady fluorescence signal was reached (10-20 min of bubbling at gas pressure of 1 bar). The fluorescence of the cell suspension was subsequently monitored, under constant stirring, until it reached basal or constant level.

7.2 *Ex vivo* Experiments on the SH

For experiments with lysed Frex- and SH-containing *R. eutropha* cells, these were harvested and resuspended to an OD_{435} of 10 in fresh GN medium. The cell suspension was lysed by three passages in a French press at 250 MPa. The lysed cells were then diluted to an OD_{435} of 1 and monitored by fluorescence spectroscopy. Appropriate concentrations of NADH and NAD^+ were added to the solution and the corresponding fluorescence was recorded.

8 Spectroscopy

8.1 UV-Vis Spectroscopy

UV-Vis spectroscopy was carried out with a Shimadzu UV-1800 spectrophotometer. The samples were diluted in PBS to an OD between 0.1 and 0.5 and were measured in a quartz cuvette.

8.2 Steady-state Fluorescence Spectroscopy

Time-integrated fluorescence spectra were recorded at a Fluoromax-2 spectro-fluorometer (Horiba Jobin Yvon, Bensheim, Germany). For the recording of fluorescence spectra, the slits were set to 4 and 2 nm for excitation and emission, respectively.

For studies on purified protein, the protein was diluted in PBS until signal was nine times the noise level. For measurements on Frex contain *R. eutropha* cells, the cell suspensions were diluted to an OD_{600} of 0.5.

For the automated recording of fluorescence spectra, the batch scan mode of the spectrometer was utilized. For measurements on Frex in *R. eutropha* cells, the

excitation wavelength was set to 490 nm and the recorded wavelength range was set to 490 – 550 nm. With the increment set to 1 nm and an integration time of 1 s, these parameters amounted to a fully recorded spectrum every minute. The following measurements were carried out without pauses inbetween.

For the titration spectra of iRFP713 in presence of NADH, NADPH and NAD^+, background subtraction was carried out with the Origin Peak Analyzer. Anchor points for the background curve were chosen to the left and right of the signal and the program subtracted an interpolated line from the raw spectra, to remove the background.

8.3 Time-resolved Fluorescence Spectroscopy

Time- and wavelength-correlated single photon counting (TWCSPC) was performed using a Hamamatsu R59 16-channel multi-anode photomultiplier tube (PMT) with 16 separate output (anode) elements and a common cathode and dynode system (PML-16C, Becker&Hickl, Berlin, Germany). The polychromator was equipped with a 300 groves/mm grating, resulting in a spectral bandwidth of the PML-16C of 12.5 nm/channel. The excitation of the Frex samples was carried out by a 470 nm pulsed laser diode (LDH-470, Picoquant, Berlin, Germany) delivering 60 ps FWHM pulses, driven at a repetition rate of 20 MHz. The fluorescence was observed via a 488 nm longpass filter (F-76-490, AHF Analysentechnik, Tübingen, Germany). For excitation of the tryptophan samples and the tryptophan residues in the Bili-Sense samples, a 280 nm laser diode (PLS-300, Picoquant, Berlin, Germany), which exhibited a 900 ps FWHM and a repetition rate of 10 MHz, was used, while the S_0 - S_2 transition of the biliverdin chromophore in the Bili-Sense samples was excited with a 405 nm laser diode (LDH-405, Picoquant, Berlin, Germany) with a repetition rate of 20 MHz.

8.4 Determination of Decay-associated Spectra

The fluorescence decays of the time-resolved spectra were analyzed employing a Levenberg-Marquardt algorithm for the minimization of the reduced $\chi r^2(\lambda)$ in each wavelength segment after iterative deconvolution with the instrumental response function (IRF). The value of $\chi r^2(\lambda)$ depends on a parameter set $(p_1, \dots, p_n)$ of the chosen continuous mathematical function $A(t, \lambda, p_1, \dots, p_n)$ for the measured fluorescence intensity $F(t_v, \lambda)$ in each time channel t_v.

The function $\chi r^2(\lambda)$ is evaluated for each time t_v channel (v = 1 ... 4096) after convolution of the function $A(t, \lambda, p_1, \dots, p_n)$ with the IRF, which delivers the fit function

$$F^{fit}(t_v, \lambda) = \int A(t, \lambda, p_1, \dots, p_n) \cdot IRF(t_v - t)dt, \qquad \textbf{(2)}$$

and averaged over all time channels:

$$\chi_r^2(\lambda) = \sum_{v=1}^{4096} \frac{1}{(N-n-1)} \left(\frac{F(t_v, \lambda) - F^{fit}(t_v, \lambda)}{\sqrt{F(t_v, \lambda)}} \right) \qquad \textbf{(3)}$$

Equation (3) is based on the assumption that the number of photons registered in each time channel t_v follows a Poisson distribution, and, therefore, the standard deviation σ in each channel equals the square root of the fluorescence intensity $\sigma(t_v, \lambda) = \sqrt{F(t_v, \lambda)}$. N determines the full number of data points (here 4096 for each wavelength section λ) and n the size of the parameter set for the chosen mathematical function $A(t, \lambda, p_1, \dots, p_n)$, which was, for example, assumed to be a biexponential decay function, here

$$A(t, \lambda) = \sum_{j=1}^{2} a_j(\lambda) e^{-\frac{t}{\tau_j}}, \qquad \textbf{(4)}$$

with the parameters $a_j(\lambda)$ and τ_j denoting the wavelength-dependent amplitude and the time constant of the *j*th exponential decay component for two components (n = 2), respectively. The biexponential fits of all decay curves measured in one

time- and wavelength-resolved fluorescence spectrum were performed as global fits with common values of lifetimes τ_j for all decay curves (linked parameters) and wavelength-dependent pre-exponential factors $a_j(\lambda)$ (non-linked parameters). The quality of the fit was judged by the value of $\chi r^2(\lambda)$, which would be 0 for an optimal fit.

The result of this analysis is usually plotted as a graph of $a_j(\lambda)$ for all wavelength-independent lifetimes τ_j under the constraint that $\alpha_1 + \alpha_2 = 1$ (for $n = 2$), representing so-called normalized decay-associated spectra (DAS) that reveal the spectral distribution of individual decay components. For this calculation, the software of Globals Unlimited® (University of Illinois, Urbana, USA) was used.

IV Results & Discussion

The results section is divided into two parts. In the first, the application of already existing [NADH] and [NADH]/[NAD^+] biosensors as tools to monitor the intracellular [NADH] or [NADH]/[NAD^+] ratio as a representation of the redox status of *R. eutropha* will be described (Part 1). Parts of the results have been published in S. Wilkening et al., 2017 and S. Wilkening et al., 2019, from which some of the figures have been adapted for presentation here. Recording of the time-resolved fluorescence data as well as the analysis of this data, represented in **Figure 14** & **Figure 18**, was carried out by Dr. Franz-Josef Schmitt.

In Part 2, the focus will turn to the optimization of present [NADH]/[NAD^+] sensors for usability in bacterial cells. Finally, the concept of a new sensor, based on an infrared fluorescent probe will be discussed. The data represented in the chapter 5.5 (Time-Resolved Fluorescence Spectroscopy) has been obtained by Dr. Franz-Josef Schmitt.

Part 1 – NADH Sensors for Measurement of the Cellular Redox Status in *R. eutropha*

The NADH dependent soluble hydrogenase (SH) of *R. eutropha* is a potential tool for biohydrogen production. In efforts to facilitate its application, it is fundamental to understand the working mode of the enzyme. Since the enzyme's activity is directly coupled to the intracellular NADH pool, the newly designed [NADH] or [NADH]/[NAD^+] biosensors are optimal tools to monitor the SH activity dynamically *in vivo*. A previous study carried out by Tejwani et al. used the [NADH]/[NAD^+] fluorescence sensor Peredox, the spectroscopic response of which was unfortunately saturated in the bacterial cytosolic environment. However, via an external calibration method the free cytosolic NADH and NAD^+ pool in these cells could be estimated to be 28 μM and 1.9 mM, respectively (Tejwani et al., 2017).

In 2011, an exclusively NADH-sensitive reporter based on a bacterial NADH-binding repressor protein (Rex) was introduced, termed Frex (Zhao et al., 2011). The topology of this sensor allowed to visualize structural changes of the Rex domain, brought upon by binding NADH molecules, via altering the fluorescence output of a circularly permuted yellow fluorescent protein (cpYFP). The designed sensor exhibited a lower affinity towards the reduced form of nicotinamide adenine dinucleotide than other sensors available at that time (Hung et al., 2011; Zhao et al., 2011). The sensor's reduced affinity towards NADH in comparison to the other existing sensor, Peredox-mCherry (Peredox), made it beneficial for application in the high [NADH] environment of the bacterial cytosol. The high concentration of this metabolite ([NADH] ~ 10^{-5} M (Bennett et al., 2009)) was estimated to saturate sensors with high affinity for the nicotinamide, as has been demonstrated in a first study on NADH concentrations in *R. eutropha* carried out with the [NADH]/[NAD^+] sensor Peredox (Tejwani et al., 2017). Therefore, the reported 100-fold lower affinity of Frex towards NADH seemed suitable for application in bacterial cells (Zhao et al., 2011).

1 *in vitro* Characterization of the Frex Sensor

With the intention to utilize the Frex sensor construct, which was developed for a different purpose, in a new setting, the first step was to characterize its behavior in lieu of the new environment. The NADH sensors available to date were all designed with a mammalian cell application in mind (Bilan et al., 2014; Hung et al., 2011; Mongeon et al., 2016; Zhao et al., 2015, 2011, 2016; Zhao & Yang, 2012). The behavior of the Frex sensor was merely tested in presence of up to 100 μM NAD^+ (Zhao et al., 2011). While this concentration is sufficient in mimicking the cytosolic NAD^+ amounts in mammalian cells, bacterial cytosols surpass this value by about an order of magnitude, reaching values in the low millimolar range (Bennett et al., 2009). Thus, higher concentrations of this nicotinamide should be tested *in vitro*, in order to assess the effects of such higher concentrations on the function of the sensor. The sensor's ability to detect the target substrate can be affected, for example by competitive binding events, effectively lowering the affinity of the sensor as well as the specificity. The sensor's affinity is an important factor to consider, needing to be adapted to the particular environment and the issue at hand, desired to be resolved. The high NADH levels in the cytosol of bacterial cells, or also in mitochondria of mammalian cells, saturate the Peredox sensor response under physiological conditions, leaving no room to detect changes towards a more reduced [NADH]/[NAD^+] ratio (Tejwani et al., 2017). While Peredox has been introduced as a [NADH]/[NAD^+] ratiometric sensor, Frex has been described as an exclusively NADH-sensitive reporter. Therefore, after noticing the pitfalls and drawbacks of the Peredox sensor in bacterial cells, the Frex sensor was chosen for this purpose, because Frex seems better suited due to its lower affinity and its specific response towards NADH (Zhao et al., 2011).

1.1 Affinity towards Nucleotides

The Frex sensor, as mentioned in the introduction (vide supra), is a NADH sensor, with two excitation peaks and one emission peak. The UV-Vis spectrum of the protein is shown in **Figure 11 A**.

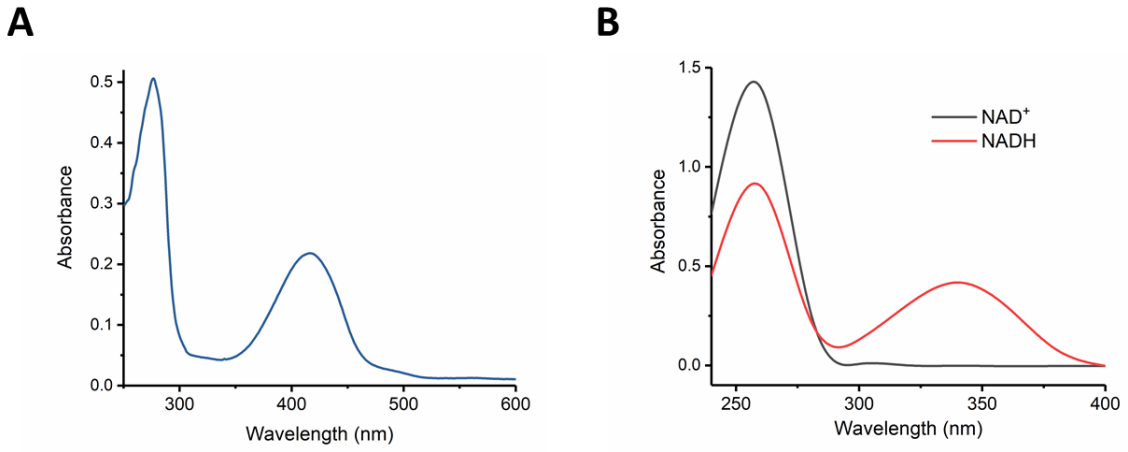

Figure 11 UV-Vis absorption spectrum of a solution of Frex (500 nM) in PBS buffer (**A**). UV-Vis absorption spectrum of NAD^+ and NADH (1 µM) in PBS buffer (**B**).

The absorption spectrum of Frex exhibits the typical protein absorption band at 280 nm, which is mainly due to tryptophan residues. A second broad band centered around 405 nm with a small shoulder at 480 nm is due to the cpYFP chromophore in the Frex protein. Frex fluorescence can be excited at 400 and 480 nm. The excitation of a Frex sample at 400 nm in the presence of NADH could potentially also lead to autofluorescence stemming from NADH, since the absorption spectrum of the reduced nicotinamide shows an absorption band centered around 350 nm, which is non-zero at 400 nm (red line in **Figure 11 B**). Thus, at high [NADH], the excitation of Frex at 400 nm will be superimposed by the autofluorescence of NADH (see also **Figure 12 C** & **D**). The oxidized congener NAD^+ only shows one absorption band around 260 nm, which is not overlapping with the fluorescence excitation spectrum of Frex, which usually is excited at 400-480 nm.

For a general estimation of the applicability in the desired cell host *R. eutropha*, titrations of the purified sensor protein with the target nicotinamide (NADH), as

well as the oxidized congener NAD^+ were carried out *in vitro*. For a first set of experiments, the protein was titrated with NADH, in order to determine its spectral behavior in presence of the nucleotide.

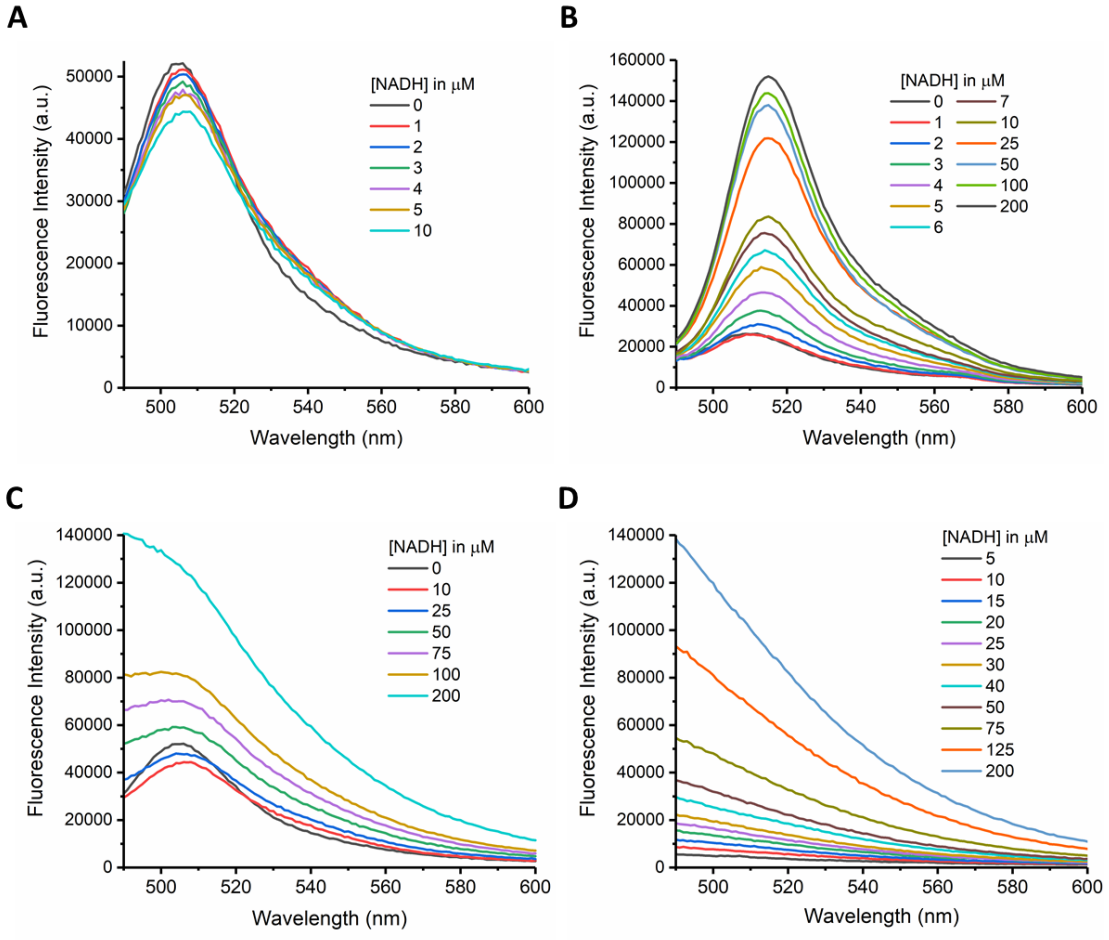

Figure 12 Fluorescence emission spectra of a solution of Frex (500 nM) in PBS buffer excited at 400 nm (**A** + **C**) and 480 nm (**B**). Fluorescence emission spectra of NADH in PBS, with the excitation wavelength set to 400 nm (**D**). The NADH amounts were added sequentially in order to obtain the stated concentrations in the sample.

In order to apply this sensor for measurements of bacterial NADH levels, its response towards nucleotide concentrations anticipated for this environment were tested. The *in vitro* characterization was carried out by titrating 500 nM Frex protein with concentrations of NADH ranging from 1 – 200 µM, covering an order of magnitude below and above the sensor's affinity constant. First, the sensor was excited at 400 nm and the resulting emission spectra were recorded around the maximum of 505 nm (**Figure 12 A** & **C**). **Figure 12A** shows the emission spectra for NADH concentrations up to 10 µM. The fluorescence intensity decreases upon

addition of NADH, just as has been described in the introducing publication (Zhao et al., 2011). The sensor shows a second excitation peak at 480 nm due to its integral fluorescent protein, yellow fluorescent protein (YFP). After exciting the sensor at 480 nm, the fluorescence emission was recorded around the maximum at 515 nm (**Figure 12 B**). The curves show a dose-dependent increase in fluorescence intensity in the emission peak of cpYFP at 515 nm, showing antipodal effects resulting from varying NADH concentrations on the sensor's fluorescence intensity depending on the excitation wavelength. The dynamic range in fluorescence intensity, a factor of about 8, is larger for the long wavelength excitation, while the short wavelength excitation only decreases to 80 % in intensity. Furthermore, upon adding ≥ 10 μM NADH concentrations, the autofluorescence of NADH overlaps with the sensor fluorescence, as can be seen in **Figure 12 C**, making quantitative evaluation difficult. The curve for 25 μM NADH (blue curve) is exhibiting a greater fluorescence intensity than the one recorded in presence of 10 μM (red curve). This is contradictory to the reported sensor's mode of action upon excitation at 400 nm (decreasing fluorescence intensity upon increasing NADH concentrations (Zhao et al., 2011)) and is due to overlapping NADH fluorescence itself. This complicates processing of the spectra, since the signal from the sensor has to be differentiated from the nicotinamide signal. **Figure 12 D** shows the fluorescence spectra of a pure NADH solution in phosphate buffered saline (PBS) upon excitation at 400 nm. Generally, the spectra could be processed by subtracting the equivalent spectra of NADH in PBS from the sensor fluorescence spectra; however, it was observed, that this procedure led to overcompensation of the signal. This is especially cumbersome at high NADH concentrations in the millimolar range, where the sensor signal only contributes about 30 % of the total signal. These findings indicate that the 400 nm excitation wavelength is only reasonably usable up to concentrations of 10 μM NADH. This is, however, detrimental for the designated use in bacterial environments, which contain 10^{-5} to 10^{-4} mol/L of total NADH (as reported for *E. coli*) (Bennett et al., 2009; Zhou et al., 2011), and about 30 μM free NADH as a lower threshold (as reported for *R. eutropha*)(Tejwani et al., 2017), rendering the short excitation wavelength unfeasible for the desired *in vivo* application.

The publication introducing Frex suggested a ratiometric readout scheme to excite the sensor at both wavelengths, and to further process the spectra by dividing the obtained emission amplitude maxima measured for the two excitation wavelengths (F_{480}/F_{400}), in order to generate a normalized value, which is independent from the sensor protein concentration (Zhao et al., 2011). The titration spectra were, hence, processed by the suggested protocol and the obtained values were then scaled to the value in absence of NADH ([NADH] = 0, set to one) and plotted against the administered NADH concentration (**Figure 13 A**).

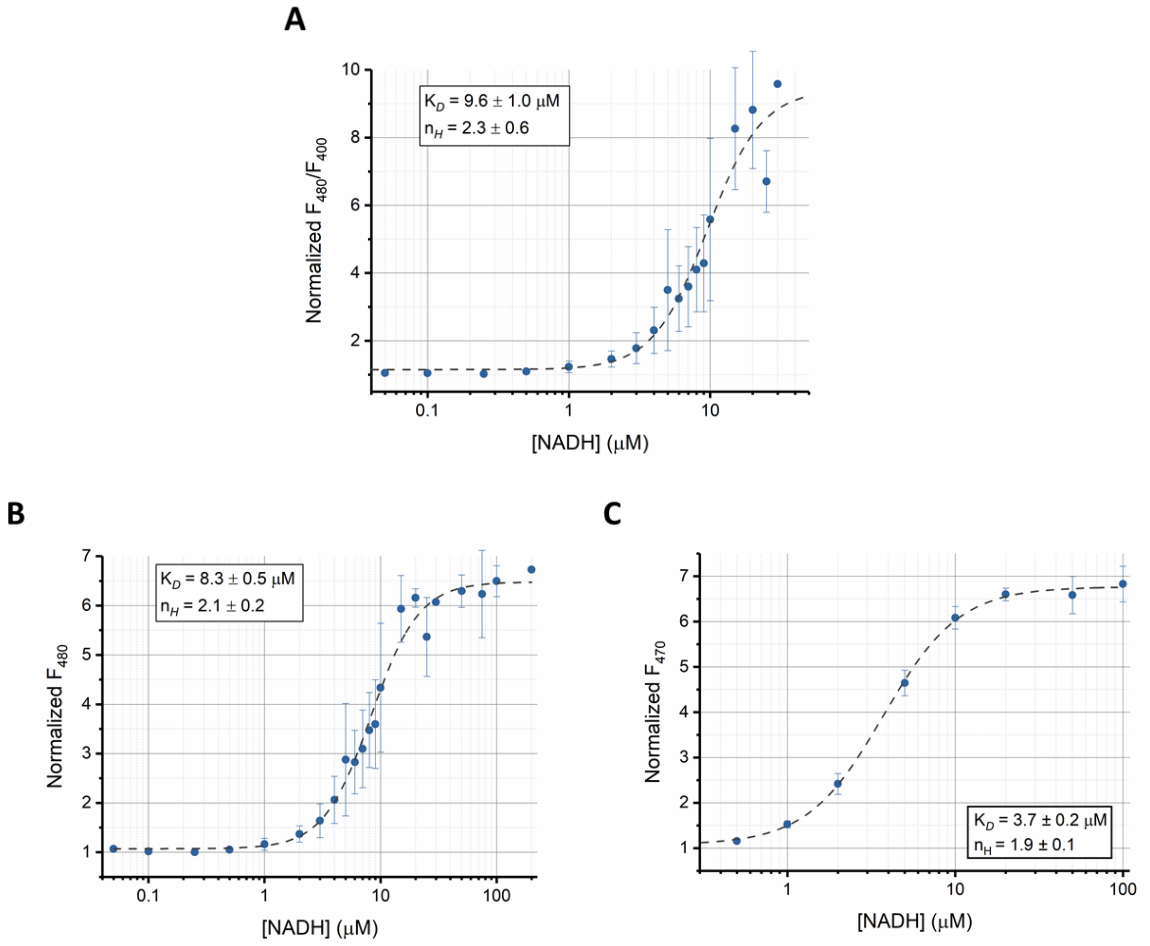

Figure 13 Fluorescence maxima at 515 nm after excitation at 480 nm (F_{480}) divided by fluorescence maxima at 505 nm after excitation at 400 nm (F_{400}) plotted against the administered NADH concentrations (**A**). The value in the absence of NADH was set to one and the remaining values were scaled, accordingly. For comparison, also the fluroescence maxima at 515 nm after excitation at 480 nm without division by the values obtanied after 400 nm excitation are plotted against the administered NADH concentration (**B**). The data set was fit by a Hill equation (dashed curve) and the parametres are given in the inset. Panel **C** shows the fluroscence maxima at 515 nm obatined after excitation at 470 nm (F_{470}), again with non-ratiometric processing, in a tempereature-controlled cuvette (20 °C). The

data are fit by a Hill equation (dashed curve) and the parameters are given in the inset. Protein concentration was set to 500 nM in PBS. Data are mean values ± S.D. of n=3 experiments.

The plot in **Figure 13 A** shows an increase of the amplitude ratio (F_{480}/F_{400}) upon increasing [NADH] up to 30 μM. At higher NADH concentrations the contribution of the nicotinamide's autofluorescence leads to an artificial decrease in the ratio. These values bias the readout of the sensor; hence, these values were neglected for evaluation of the sensor parameters by a Hill fit. The affinity constant derived by this method equates to 9.6 ± 1.0 μM, with a Hill coefficient of 2.3 ± 0.6. The Hill factor represents the amount of equivalent binding sites in the investigated protein, which is two for Frex, representing the two Rex subunits of the protein (Zhao et al., 2011). Thus, the value is compatible with two within error limits. The dynamic range of nine reported for Frex could be successfully reproduced in the titration experiments.

Since the preliminary NADH titration experiments showed that Frex fluorescence readout upon excitation with 400 nm is not adequate for application *in vivo* in bacterial cells, the Frex fluorescence responses were also evaluated solely based upon the fluorescence emission maxima obtained after excitation at 480 nm, which does not excite nicotinamide autofluorescence (**Figure 13 B**). The dissociation constant evaluated from the F_{480} fluorescence amplitudes equates to 8.3 ± 0.5 μM, while the Hill coefficient yields a value of 2.1 ± 0.2. Therefore, the dissociation constants derived by the two modes agree within error limits, as well as the corresponding Hill coefficients, the latter indicating binding cooperativity in both evaluations. The dynamic range of the F_{480} fluorescence amplitude is reduced to about eight, which was also observed in **Figure 12 A** & **B**.

The determined dissociation constants of 9.6 μM from ratiometric evaluation and 8.3 μM from the F_{480} mode were both larger than the value reported in the original publication (3.7 μM (Zhao et al., 2011)). The disparity might be due to different temperatures, while recording the fluorescence spectra. The binding assays in **Figure 13 A** & **B** were conducted at 30 °C, while the original publication specified no temperature for the experiment, presumably the temperature was close to room temperature (20 °C). Binding equilibria, are of course, temperature-

dependent, the relation being disclosed by Gibb's law ($\Delta G° = -RT\ln K_D$). To test the influence of temperature, experiments were carried out in a temperature-controlled setup. In this set of experiments samples were excited with a 470 nm laser at 20 °C, and the emission was recorded solely after 470 nm excitation. The titration data of these experiments are displayed in **Figure 13 C** and the determined dissociation constant of 3.7 ± 0.2 µM exactly reproduced the constant determined in the original publication (Zhao et al., 2011). The dynamic range was determined to be seven in the temperature-controlled setup.

In order to infer if the sensor's change in fluorescence amplitude is due to an effect on the fluorescence quantum yield by a dynamic change of the fluorescence lifetime, time-resolved fluorescence measurements were carried out.

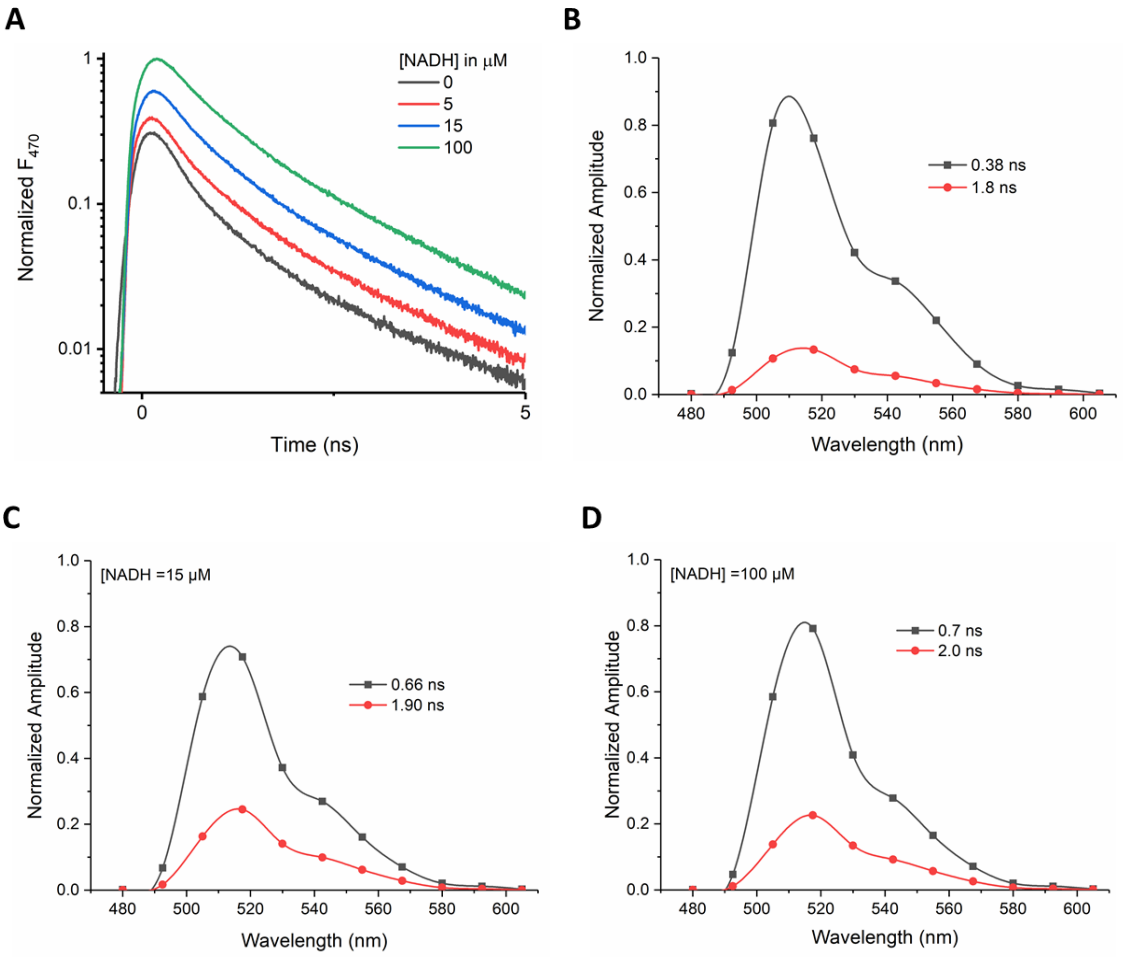

Figure 14 Fluorescence decay curves of Frex monitored at 520 nm (spectra recorded between 480 and 605 nm) in the absence (black curve) or presence

(colored curves) of NADH after excitation with a ps-pulsed laser source at 470 nm (**A**). The decay curves were normalized to the maximal amplitude in the presence of 100 µM NADH. Panels **B** - **D** show the decay-associated spectra (DAS) derived from a global fit of a biexponential function to the decay curves in **A**. The data points were connected by a spline function to guide the eye. The lifetimes of the biexponential fits are given in the insets and the amplitude peaks were normalized according to $\alpha_1 + \alpha_2 = 1$. DAS are shown for zero NADH (**B**), 15 µM NADH (**C**) and 100 µM NADH (**D**). Protein concentration was 500 nM in PBS, and experiments were carried out at 20 °C.

Figure 14 A shows the fluorescence decay curves at 520 nm after excitation with a ps-pulsed laser at 470 nm. The amplitude obtained in the presence of 100 µM NADH (green curve) was set to one and the remaining amplitudes were scaled, accordingly. The difference in amplitudes between zero and 100 µM NADH equates to a factor of about four. A global fit procedure with two exponential functions was carried out for the different decay curves and the resulting decay-associated spectra (DAS) for the spectral range between 480 – 605 nm are shown in panels **B** – **D**. For zero NADH, the short lifetime of about 400 ps has a fractional amplitude of about 0.9, while the long lifetime (1.8 ns) only makes up the remaining 0.1 of the amplitude. The DAS show a clear fluorescence maximum at 515 nm, with a shoulder at 545 nm. Upon addition of NADH, both lifetimes increase slightly, and a change in the ratio of the fractional amplitudes is observed as well, effectively enhancing the long lifetime component (1.9 ns, fractional amplitude = 0.2, **Figure 14 C**). Interestingly, upon further increases of NADH concentration, the lifetimes only change slightly, while also the fractional amplitudes remain relatively constant. These slight variations in fluorescence lifetimes and fractional amplitudes however fail to explain the observed seven- or eightfold increase in fluorescence intensity in the time-integrated experiments. The resulting average lifetime for Frex in absence of NADH equates to $\bar{\tau} = \alpha_1\tau_1 + \alpha_2\tau_2 = 550\,ps$, while the average lifetime increases to 1 ns in presence of 100 µM NADH, leading to a twofold change. However, combined with the fourfold change in fluorescence amplitude, this re-establishes the sensor's dynamic range of 7-8. It thus seems that the elevated fluorescence upon addition of 100 µM NADH does not mostly stem from alteration in the fluorescence lifetime pattern of Frex, but rather from fluorescence activation of sensor molecules. Tis interpretation implies that Frex

molecules are in a "dark" state, when no NADH is bound. Upon binding of NADH the fluorescence is switched on and, once activated, these molecules emit fluorescence with the same characteristic and do not largely alter the lifetimes nor fractional amplitudes, but only the total amplitudes.

Hence, in the absence of NAD^+, the sensor showed the already established apparent affinity for NADH in the lower micromolar range and an eightfold change in fluorescence intensity towards saturating NADH concentrations, when the fluorescence emission upon 480/470 nm excitation is considered (**Figure 13**) (Zhao et al., 2011).

However, bacterial cells exhibit cytosolic concentrations of NAD^+ in the millimolar range, in accordance with the concentrations found for *E. coli* (Bennett et al., 2009; Zhou et al., 2011), or *R. eutropha* (Tejwani et al., 2017). With the application in bacterial cells in mind, it was important to investigate the behavior of the Frex sensor *in vitro* in the presence of 100 µM NAD^+, to compare with literature data, in which no effect of 100 µM NAD^+ on the fluorescence response of Frex was reported (Zhao et al., 2011), as well as 1 mM NAD^+ in order to identify or exclude effects of enhanced NAD^+ concentrations on the sensor's response (**Figure 15**).

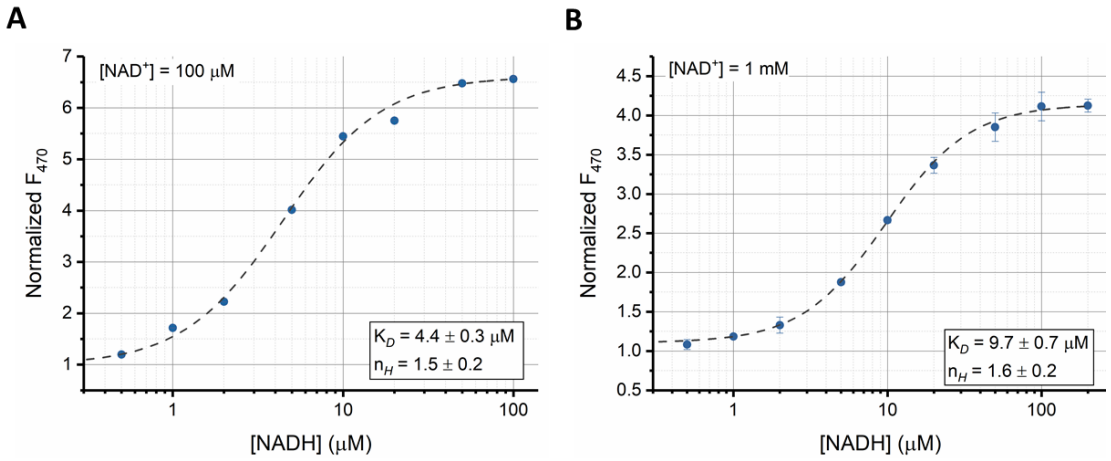

Figure 15 Fluorescence emission amplitude of Frex monitored at 515 nm obtained upon excitation at 470 nm in presence of 100 µM NAD^+ (**A**) or 1 mM NAD^+ (**B**) plotted against the administered NADH concentration. Protein concentration was set to 500 nM in PBS, and experiments were carried out at 20 °C. The value in absence of NADH was set to one and the remaining values were scaled accordingly. The data sets were fit by a Hill equation (dashed curve) and the parameters are given in the insets. Data are mean values ± S.D. of n=3 experiments, while error bars are smaller than the symbol size for **A**.

Figure 15 A shows the Frex fluorescence amplitudes measured at the emission maximum around 515 nm upon excitation at 470 nm (F_{470}) dependent on the NADH concentration in presence of 100 μM NAD^+, a concentration reported to have no effect on Frex sensor properties (Zhao et al., 2011; Zhao & Yang, 2012). However, the apparent dissociation constant for NADH increases from 3.7 μM in absence of NAD^+ slightly to 4.4 ± 0.3 μM in presence of 100 μM NAD^+. This effect might not be dramatic; however, the Hill coefficient is diminished to 1.5 ± 0.2 from 1.9 ± 0.1, indicating a different binding mode in presence of NAD^+. Upon increasing the NAD^+ concentration to 1 mM, a concentration well within bacterial cytosolic ranges for this metabolite, the apparent dissociation constant further increased to 9.7 ± 0.7 μM (**Figure 15 B**), while the Hill coefficient remains at around 1.5, compared to the measurement in presence of 100 μM NAD^+. It is noticeable, that the sensor's dynamic range is diminished: in the case of the 100 μm NAD^+ the reduction is only small, but in the presence of 1 mM NAD^+ it is reduced to about four. These findings indicate that NAD^+ is able to interact with the Frex sensor, a behavior already described for the parental Rex protein (E. Wang et al., 2008). While the Rex repressor protein can bind two molecules of NADH, one per each subunit, Rex allows to only bind one molecule of the oxidized congener, which readily explains the effect of lowered Hill coefficients and reduced dynamic range of the Frex reporter protein in presence of NAD^+ (Gyan, Shiohira, Sato, Takeuchi, & Sato, 2006; Larsson, Rogstam, & von Wachenfeldt, 2005; McLaughlin et al., 2010). NAD^+ alters the affinity of Rex for NADH, a factor that needs to be considered for the intended *in vivo* applications. To further elucidate the effect of NAD^+ on Frex, the titration experiments were carried out with differing amounts of the oxidized nicotinamide while keeping [NADH] constant.

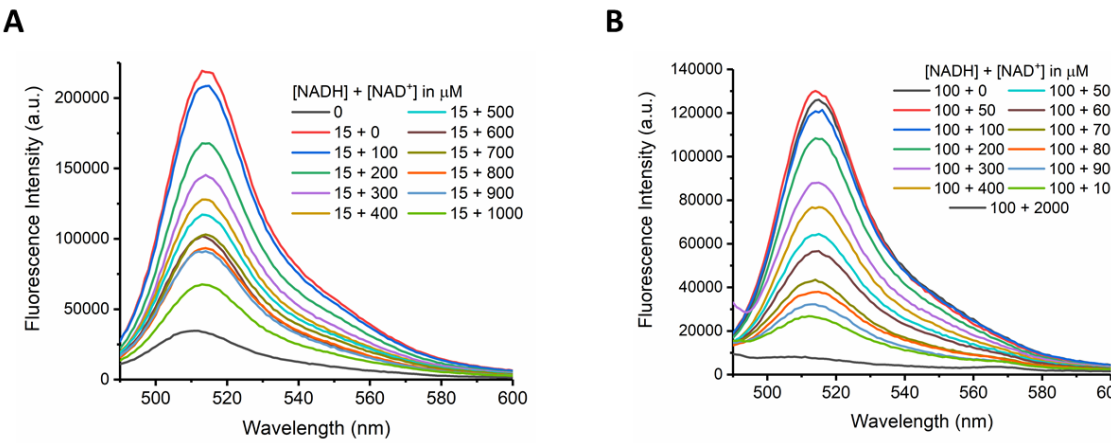

Figure 16 Emission spectra of the Frex sensor in the presence of 15 µM NADH (**A**) or 100 µM NADH (**B**) upon excitation at 480 nm. The sensor concentration was adjusted to 500 nM in PBS and fluorescence was triggered by adding the specified NADH amounts. Subsequently, NAD^+ was added as indicated in the insets. The experiments were carried out at 30 °C.

The fluorescence spectra of Frex from a NAD^+ titration experiment in the presence of 15 µM NADH, a concentration resembling free *in vivo* bacterial concentrations, and a NAD^+ titration in presence of 100 µM NADH, a concentration sufficient to fully saturate the Frex sensor response, are shown in **Figure 16**. The emission spectra upon excitation at 480 nm show the typical increase in fluorescence intensity upon addition of NADH (compare black and red curve in **Figure 16 A**). However, upon addition of increasing [NAD^+], the fluorescence intensity decreases again. The spectra recorded for Frex upon excitation at 480 nm, in the presence of 100 µM NADH exhibit an analogous decrease with increasing [NAD^+] (**Figure 16 B**). The data from both titration experiments were evaluated for the normalized F_{480} maxima and plotted against the applied NAD^+ concentrations (**Figure 17**).

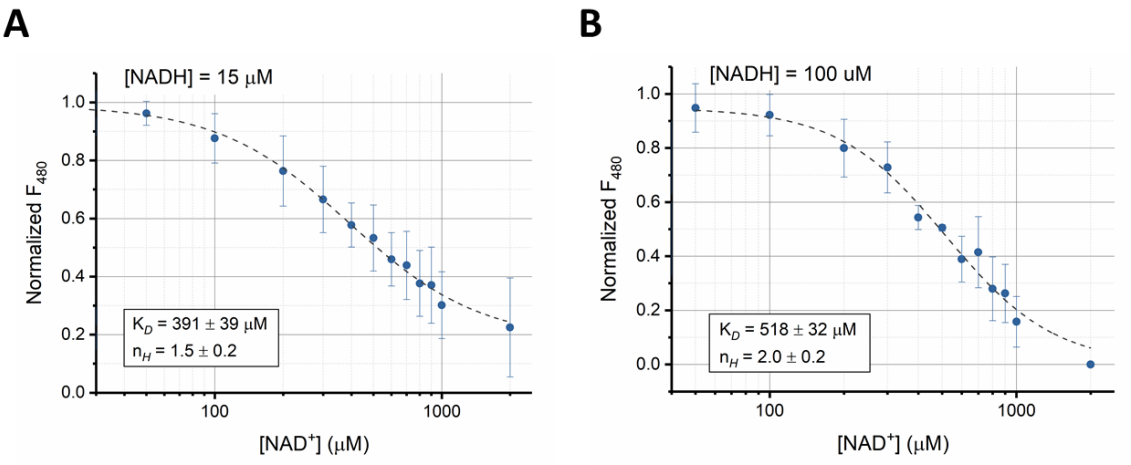

Figure 17 Fluorescence responses of the purified Frex sensor protein, expressed as the fluorescence amplitudes at 515 nm measured upon 480 nm excitation (F_{480}) at different [NAD^+] in the presence of 15 µM NADH (**A**) or 100 µM NADH (**B**). The fluorescence intensity was normalized to F_{480} in the absence of NAD^+. The concentration of the sensor protein was 500 nM in PBS. Data are mean values ± S.D. of n=4 experiments.

The curves for both NADH concentrations show the same general trend. Upon titration of NAD^+, the fluorescence decreases, indicating a "quenching" mechanism, in which NAD^+ can bind to Frex (without inducing a positive response on the sensor's fluorescence, since NAD^+ alone does not affect Frex fluorescence (Wilkening et al., 2017)) and eventually displace or dissociate NADH by some (as yet uncharacterized) competitive interaction mechanism, which, in effect leads to a decrease in sensor fluorescence. The apparent dissociation constants for NAD^+ were determined to 391 ± 39 µM in presence of 15 µM NADH and 518 ± 32 µM in presence of 100 µM NADH, reproducing the K_D value reported for NAD^+ for the parental Rex protein of about 500 µM (E. Wang et al., 2008). The higher NADH concentration of 100 µM seems to positively compete with NAD^+, increasing the dissociation constant for the oxidized congener. In order to infer, if NAD^+ solely influences the fluorescence amplitude (in terms of a "static" fluorescence quenching mechanism), or also exhibits an effect on the fluorescence lifetime (in terms of a "dynamic" or collisional quenching mechanism), a NAD^+ titration experiment was carried out in a time-resolved fluorescence experiment.

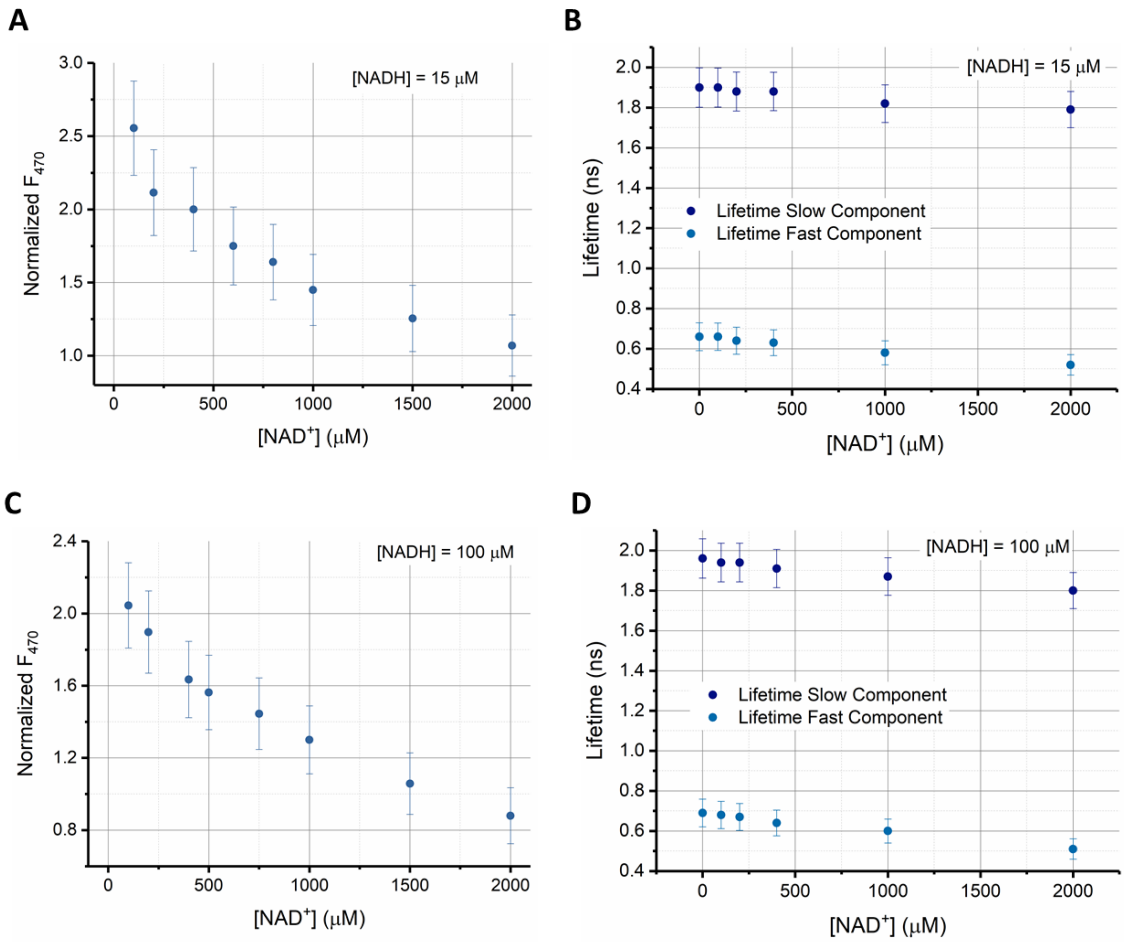

Figure 18 Fluorescence amplitudes of Frex monitored at 520 nm in the presence of either 15 µM NADH (**A**) or 100 µM NADH (**B**) dependent on the applied [NAD+]. Panels **B** & **D** show the alterations of the slow (dark blue) and fast (blue) lifetime components from fits of the fluorescence decay curves with a biexponential function dependent on the applied [NAD+]. In each experiment, the protein concentration was adjusted to 500 nM in PBS. Spectra were recorded at 20 °C. Data are mean values ± S.D. of n=3 experiments.

Figure 18 A & **C** show the decrease of the fluorescence amplitudes upon addition of the oxidized nicotinamide, as already observed in **Figure 17**. However, the lifetimes remain relatively unchanged upon titration with NAD+ (**Figure 18 B** & **D**), maximally decreasing by about 10 % for the fast component over the whole [NAD+] range of the experiment. Since the NAD+-dependent decrease in fluorescence amplitude is much larger, this finding implies that the NAD+-dependent fluorescence decrease can mainly be attributed to a "static" quenching effect on the fluorescence amplitude. Thus, both, NADH binding to Frex as well as its dissociation by competition with NAD+ (which interacts with the sensor without

altering its fluorescence) only affects the fluorescence quantum yield without any influence on the fluorescence lifetime.

For an *in vivo* application in bacteria, the determined sensitivity of Frex towards NAD^+ will complicate the readout of the fluorescence signal. Since bacterial NAD^+ levels are in the millimolar range, one can suspect that NAD^+ will counteract the effects of NADH binding to the sensor. Furthermore, a distinction between elevation of [NADH] and concomitantly enhanced fluorescence versus less interaction with NAD^+ and, therefore, relief from quenching of the sensor fluorescence is not possible. At the nucleotide concentrations typically found in bacteria, it seems more likely that Frex will interact with both, NADH and NAD^+. Upon alterations of the redox state of the cells, e.g. leading to lower NAD^+ levels, the sensor would interact less with the fluorescence "inhibitor" (quencher) NAD^+ and concomitantly be able to bind more NADH, which is present in concentrations sufficient to generate a high fluorescence signal of the sensor even at relatively oxidized conditions. Therefore, the fluorescence signal would likely depend on the competing NAD^+ levels, which determines whether the sensor can "sense" the present [NADH], effectively leading to a competitive effect of NAD^+ on the sensor fluorescence. However, if the NAD^+ concentration in bacteria is about 10-fold larger than [NADH] (e.g. 100 µM to 1 mM), even substantial changes in [NADH] from 10 µM to 100 µM will only change [NAD^+] by about 10 %, i.e. [NAD^+] remains rather constant in terms of its effect on the Frex fluorescence amplitude, while [NADH] changes substantially within the sensor's dynamic range and causes large changes in Frex fluorescence.

Besides non-competitive and uncompetitive inhibition, competitive inhibition is a well-established concept for enzyme-substrate complexes. In this concept, the inhibitor (in this case NAD^+) binds to the enzyme (Frex), mainly at the active site, making it inaccessible for the actual ligand (NADH). This model calls for the binding to be unambiguous, either the ligand is bound or the inhibitor, while simultaneous binding of both, ligand and inhibitor, is not possible in this model (J. M. Berg et al., 2015). This mode of inhibition can be deduced from the analysis of fits of a Hill function, since the affinity constant of the enzyme or sensor is artificially lowered (higher K_D) towards the ligand in presence of the inhibitor. The competitive binding mechanism is a mechanism commonly found in regulatory

feedback loops of enzymes (Bisswanger, 2017). It has been elucidated from X-ray crystal structure data that the Rex protein not only can bind two molecules of NADH but also (and exclusively) one NAD^+ molecule and NADPH (E. Wang et al., 2008). The engineering of Frex towards applications in mammalian cells took this into account, and, due to genetic optimization, the affinity towards competing nicotinamides (NAD^+ and NADPH) was efficiently lowered (Zhao et al., 2011). However, bacterial applications impose different constraints and necessities regarding the actual nucleotide concentrations.

Hence, a model for the interaction of Frex with NADH and NAD^+ was devised, in order to estimate the signal obtained in the presence of NADH and NAD^+, both being able to interact with the sensor. This model incorporates the already established binding modes for the Rex protein and is based on the competitive inhibition model described above. In this model, it is assumed based on X-ray studies of the parental Rex protein that (i) binding of NAD^+ was restricted to one molecule per sensor and would not change the fluorescence output, and (ii) binding of two molecules NADH per sensor is highly cooperative and leads to a change in fluorescence (Sickmier et al., 2005). A scheme of the model is given in **Figure 19**.

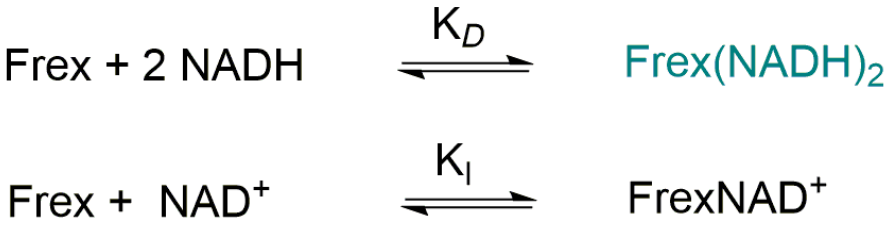

Figure 19 Minimal model of the interaction between Frex and NAD(H). For the binding of two molecules of NADH only one step, with the accompanying equilibrium constant K_D, is assumed due to its high cooperativity. For the binding of the oxidized congener, only one molecule is assumed to bind, with the accompanying equilibrium constant K_I. The complex leading to fluorescence is highlighted in teal color.

The binding between sensor and NADH can be further detailed by a two-step process, in which at first one molecule NADH binds to Frex with the dissociation

constant $K_{D,1}$ subsequently followed by the binding of the second molecule NADH with the associated dissociation constant $K_{D,2}$ (see **eq. (5)**).

$$Frex + 2\,NADH \overset{K_{D,1}}{\rightleftharpoons} FrexN + NADH \overset{K_{D,2}}{\rightleftharpoons} FrexN_2 \tag{5}$$

These two affinity constants ($K_{D,1}$ and $K_{D,2}$) can be combined in one macroscopic affinity constant K_D, which references the one from the spectral *in vitro* characterizations, without NAD^+. For the binding of NAD^+ the equation looks accordingly.

$$Frex + NAD^+ \overset{K_I}{\rightleftharpoons} FrexN^+ \tag{6}$$

For binding of one NAD^+ molecule to Frex the dissociation constant K_I is given, which corresponds to the K_D from the NAD^+ titrations of the in vitro characterizations. If we now assume that only the species $FrexN_2$ contributes to the fluorescence, the total fluorescence can be described as

$$F \sim \frac{[FrexN_2]}{[Frex] + [FrexN_2] + [FrexN^+]} \tag{7}$$

Expanding by 1/[Frex] leads to

$$F \sim \frac{\frac{[FrexN_2]}{[Frex]}}{1 + \frac{[FrexN_2]}{[Frex]} + \frac{[FrexN^+]}{[Frex]}} \tag{8}$$

We now exploit the relationship between equilibrium constant for the binding of NADH and the concentrations of the participative compounds

$$K_d = \frac{[Frex] \cdot [N]^2}{[FrexN_2]} \tag{9}$$

For the binding of NAD^+

$$K_I = \frac{[Frex] \cdot [N^+]}{[FrexN^+]} \tag{10}$$

Substitution of the quotients in **equation (8)** leads to

$$F \sim \frac{\frac{[N]^2}{K_D}}{1 + \frac{[N]^2}{K_D} + \frac{[N^+]}{K_I}} \quad (11)$$

Expansion with K_D yields

$$F \sim \frac{[N]^2}{K_D + [N]^2 + \frac{[N^+]K_D}{K_I}} \quad (12)$$

A normalization constant F_{max}, equal to the maximum fluorescence (high [NADH], no or low [NAD^+]) is included

$$\frac{F}{F_{max}} = \frac{[N]^2}{K_D + [N]^2 + \frac{[N^+]K_D}{K_I}} \quad (13)$$

Inversion of this equation gives

$$\frac{F_{max}}{F} = 1 + \frac{K_D}{[N]^2} + \frac{[N^+]K_D}{K_I[N]^2} \quad (14)$$

Therefore, a plot of the maximal fluorescence (zero [NAD+]) divided by the actual fluorescence in the presence of a certain [NAD^+] against the NAD^+ concentration, should result in a line, for which the y-axis intercept is $1 + K_D/[N]^2$ and the slope is given by $K_D/(K_I * [N]^2)$, and can therefore be exploited to determine the affinity constants for both nucleotides (**Figure 20**).

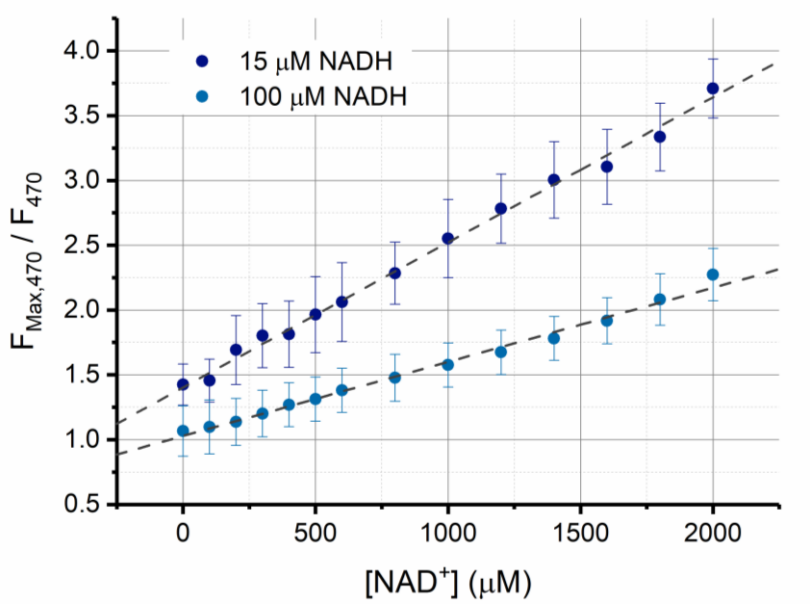

Figure 20 NAD⁺-dependent Frex fluorescence emission plotted as F_{max}/F obtained upon excitation at 470 nm in the presence of 15 µM NADH (dark blue) and 100 µM NADH (light blue) at 20 °C. Data are mean values ± S.D. of n=3 experiments. Protein concentration was adjusted to 500 nM in PBS. Results of a line fit to the data are superimposed (dashed grey lines).

As predicted by the aforementioned model, these plots show a linear dependency of the ratio of maximal fluorescence to measured fluorescence on the concentration of NAD⁺. For 15 µM NADH the F_{max}/F ratio shows larger variations (see error bars), which indicates that in presence of a lower NADH concentration the inhibitor NAD⁺ is more potent, hence the quenching more effective, and therefore the ratio allows values higher than for 100 µM NADH, for which the slope of the curve is smaller. The parameters derived from line fitting (model function $y = m \cdot x + b$) are for 15 µM NADH:

$$m = 1.12 \cdot 10^{-3} \pm 2.16 \cdot 10^{-5}\ \mu M^{-1} \qquad \textbf{(15)}$$
$$b = 1.40 \pm 0.02$$

and for 100 µM NADH:

$$m = 5.72 \cdot 10^{-4} \pm 1.63 \cdot 10^{-5}\ \mu M^{-1} \qquad \textbf{(16)}$$
$$b = 1.03 \pm 0.02.$$

Evaluating the parameters of the fit in the presence of 15 µM NADH and substituting the y-axis intercept for $K_D/[N]^2$ according to **equation (17)** yields

$$1.40 \pm 0.02 = 1 + \frac{K_D}{[N]^2} \quad (17)$$

$$K_D = 315 \pm 4.5\ \mu M.$$

The parameters for the fit of the data obtained in presence of 100 µM NADH lead to a determined dissociation constant of 300 ± 200 µM for NAD^+, which is in line with the direct titration experiment shown in **Figure 17**, from which dissociation constants of 391 ± 40 µM and 496 ± 28 µM in presence of 15 µM NADH or 100 µM NADH were determined, respectively.

1.2 pH Dependence of Frex

The Frex sensor was constructed with a circularly permuted YFP as the chromophore (Zhao et al., 2011). Hence, the sensor inherits its spectral characteristics, like the two excitation wavelengths and a profound pH dependency of the fluorescence spectrum (Elsliger, Wachter, Hanson, Kallio, & Remington, 1999; Schwarzländer et al., 2014; Wachter, Elsliger, Kallio, Hanson, & Remington, 1998; Zhao et al., 2011). This fact was already mentioned in the introducing publication of Frex, and it was advised, in order to validate if a given signal from the sensor is in fact due to altered [NADH] and not due to altered pH, to concomitantly carry out control experiments with the isolated chromophore cpYFP. For a basic idea of the probe's behavior at different pH levels, we chose to investigate Frex fluorescence response towards different pH levels *in vitro*. The F_{480} maxima were plotted against the applied pH value (**Figure 21**).

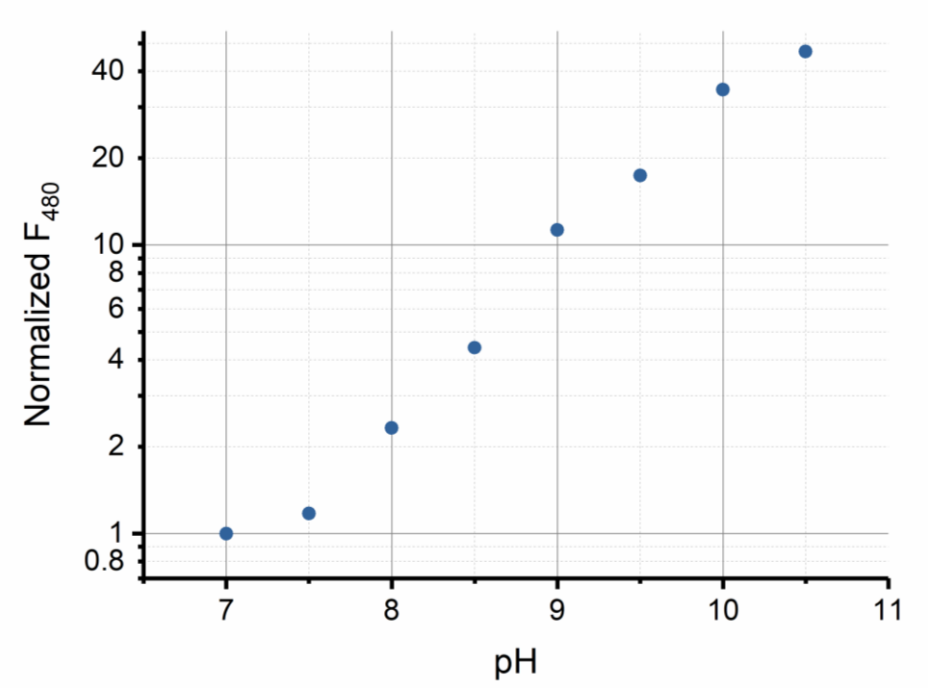

Figure 21 Fluorescence responses of the purified Frex sensor protein measured at 510 nm, expressed as the logarithm of the fluorescence amplitudes measured upon 480 nm excitation (F_{480}), at different pH-values in the absence of NADH and NAD^+. The fluorescence amplitudes were normalized to the maximum of F_{480} at pH 7. The inset shows normalized fluorescence amplitudes for the range between pH 7 and 8.5. The concentration of the sensor protein was 500 nM in PBS. Experiments were carried out at 30 °C.

Within the pH range between 7 and 10.5, the fluorescence emission of the probe enhances dramatically upon alkalization of the sample. Between pH 7 and 10.5 an enhancement factor of the fluorescence amplitude of about 45 is observed, which is about 5.5 times the dynamic range of the sensor due to NADH binding at neutral pH. These findings are supported by the literature, in which also an enormous increase of the fluorophore's dynamic range upon alkalization of the surrounding environment was found, and the pK_a of cpYFP was estimated to lie between 8.6 – 8.9, almost entirely stemming from the long wavelength excitation (Griesbeck, Baird, Campbell, Zacharias, & Tsien, 2001; Schwarzländer, Logan, Fricker, & Sweetlove, 2011). While it is highly unlikely that the intracellular pH deviates as much as one unit from the neutral state, even small aberrations in pH have profound effects on the probe's emission. Specifically, between pH 7 and pH 8 the fluorescence emission was enhanced by a factor of 2.5.

These *in vitro* characterizations indicate several pitfalls regarding the use of Frex *in vivo*. For one, the ideally exclusive NADH sensor does in fact respond to the oxidized congener of NADH, a fact which, if not accounted for, would give ambiguous readouts, especially in the concentration range of NAD^+ which is presumably present in the desired host *R. eutropha*. For another, the experimental conditions need to be inspected closely for alterations in pH, since even small intracellular pH fluctuations can rapidly generate greater changes in the fluorescence signal, than the interaction between the senor and the probe ever could.

2 Frex for Intracellular Application in *R. eutropha*

Frex was aimed to report on NADH levels in *R. eutropha* cells, expressing the soluble hydrogenase (SH). The SH couples the oxidation of hydrogen to the reduction of NAD^+ and the generation of NADH. This elevation of NADH levels upon activity of the SH is supposed to be reported by Frex sensor. In order for the Frex protein to be expressed in the β-proteobacterium, the cDNA was introduced on a plasmid vector under the control of the promotor of the soluble hydrogenase, therefore ensuring coincident expression of the SH and its activity reporter Frex. The cultivation of *R. eutropha* was carried out heterotrophically, hence the cells were kept in fructose-containing growth medium for two days. Afterwards the culture was diluted to an OD_{435} of 0.1 in growth medium containing both fructose and glycerol in equal amounts (0.2 % each). The expression of SH and Frex is dependent on the triggering of the SH promoter. The SH promoter is activated by switching from the preferably metabolized carbon source fructose to glycerol. This switch of growth conditions from utilization of fructose to glycerol mostly occurs about one day after start of cultivation, when cells are kept at 30 °C (B. Friedrich, Heine, Finck, & Friedrich, 1981; C. G. Friedrich, 1982). The cultures are kept at this temperature, since the promoter is temperature-sensitive, repressing expression under control of this promoter at temperatures above 30 °C (C. G. Friedrich & Friedrich, 1983).

Table 5 Characteristics of the utilized *R. eutropha* strains.

strain	characteristics	Origin
H16	Wild-type strain SH$^+$, MBH$^+$, RH$^+$	
HF500	Δ*hoxG*Δ*hoxC*Δ*hoxH* SH$^-$, MBH$^-$, RH$^-$	(Kleihues et al., 2000)
HF798	Δ*hoxG*Δ*hoxC* SH$^+$, MBH$^-$, RH$^-$	(Lauterbach, 2013)

The cDNA for Frex was introduced into two different host strains, namely HF500 and HF798 (**Table 5**)(Kleihues et al., 2000; Lauterbach, 2013). The strain HF500 carries deletions of the genes for the large subunits of the regulatory hydrogenase, as well as the membrane-bound hydrogenase and the soluble hydrogenase and is thus not capable of expressing functional hydrogenases of these kinds. The HF798 strain is derived from the HF500 strain by re-introduction of the genes for the large subunit of the soluble hydrogenase, allowing for the functional expression of this enzyme. The HF798 strain was chosen over the wild-type strain, which expresses all of the aforementioned hydrogenases, in order to be able to connect the metabolization of hydrogen directly with a single hydrogenase, with no other conceivable side reactions. The HF500 strain itself acts as a negative control, in order to determine the effects on Frex fluorescence in response to experimental parameters not related to the SH activity. For the general experimental protocol both strains were exposed to the same stimuli and the differences in the observed behavior should enable us to infer correlations to SH activity.

2.1 Expression of Frex in *R. eutropha*

In order to determine the optimal conditions for SH experiments, the cultures were examined after different intervals of cultivation for expression of Frex. This was carried out by pelleting cells and resuspending them in H16 buffer to obtain an OD_{600} of 0.5. These cell suspensions were analyzed by fluorescence spectroscopy (**Figure 22**).

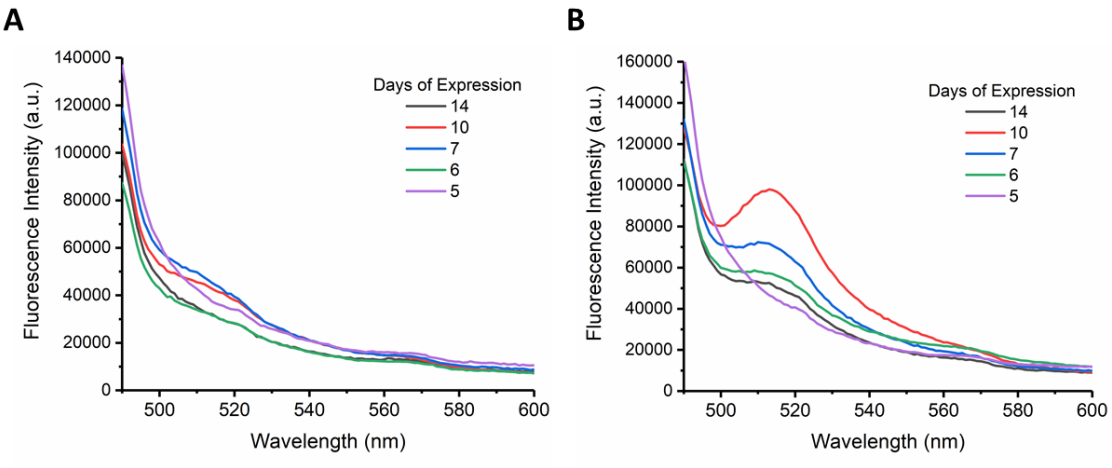

Figure 22 Emission spectra of Frex in *R. eutropha* strain HF798. The excitation was set to 480 nm and the emission spectra for different expression durations are shown (**A**). Note the substantial scattering background superimposed to the spectra. Panel **B** shows the emission after fumigating the cell solution with H_2 gas for ten minutes.

Panel **A** of **Figure 22** shows the signal of Frex after excitation at 480 nm in *R. eutropha* strain HF798 in aerobic atmosphere. The signature emission band of Frex centered around 515 nm is only slightly visible as a band starting around 500 nm and expanding up to 530 nm for expression durations of seven and ten days (blue and red line, respectively). Shorter cultivation periods of up to seven days showed no visible Frex signature in these spectra, as well as cultivation periods longer than 14 days. This indicates that at shorter cultivation times, Frex concentration is not sufficient to give a traceable signal under normal aerobic conditions, after more than 14 days of cultivation, the Frex protein seems to be degraded, effectively yielding low intracellular concentrations. Larger Frex signals are obtained, when the Frex- and SH-expressing cells are treated with pure hydrogen, the substrate of the SH. With the SH generating elevated NADH levels, an increased Frex fluorescence upon excitation at 480 nm is observed (**B**). These experiments show that for 5 days of cultivation (purple line) even H_2 supply does not lead to a recognizable Frex signal, while cultivation durations between 6 and 10 days show steadily increasing Frex fluorescence, indicating concomitant increasing intracellular concentration of the fluorescent protein. For the culture kept for 14 days (black line), however, the signal has already diminished again, further supporting the notion that for these prolonged cultivations Frex protein is

degraded. Hence, for further experiments on *R. eutropha* cultures, these were cultivated for ten days under the aforementioned conditions (vide supra).

In a first set of experiments, the aim was to distinguish response of *R. eutropha* cells to treatment of hydrogen in strains HF798 and HF500. In order to confirm the expression of Frex in these cells, a cell suspension was treated with alkaline buffer, which (i) lysed the cells, and (ii) invoked the pH dependent fluorescence increase of the cpYFP moiety of the sensor protein at alkaline pH (**Figure 23**) (Schwarzländer et al., 2014; Zhao et al., 2011), which readily confirms robust and similar expression of the sensor protein in both cell lines.

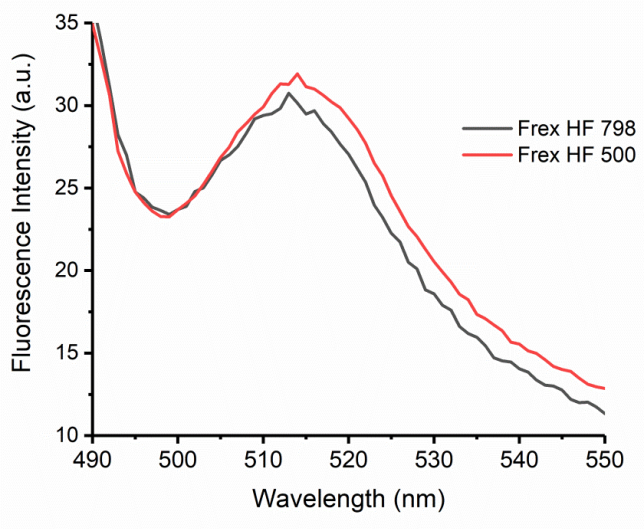

Figure 23 Test experiments for the expression of Frex in the SH-expressing strain HF798 (black curve) and in the SH-deficient strain HF500 (red curve). Cell lysis (and sensor fluorescence) were induced by treatment with pH 11 buffer and subsequent excitation of the Frex sensor at 480 nm. Spectra were normalized at 490 nm for better comparability.

2.2 Effect of Gas Treatment on Frex Fluorescence

It was aimed to infer differences in the Frex fluorescence readout between the strain carrying the genes for SH and the one without, while carrying out the same

general experimental protocol and, therefore, enabling to trace back these differences to the activity of the SH. For this reason, cell suspensions of either *R. eutropha* HF798 or HF500 were treated with molecular hydrogen, the substrate of the SH, which should generate NADH while concomitantly oxidizing H_2 in the SH-expressing strain but not in the SH-deficient strain. In a first set of experiments, cell suspensions were aerated with H_2 for ten minutes, or until a steady maximal fluorescence was achieved. The cells showed robust fluorescence after H_2 treatment when excited at 480 nm in both utilized strains (**Figure 24 A** & **B**, red curves).

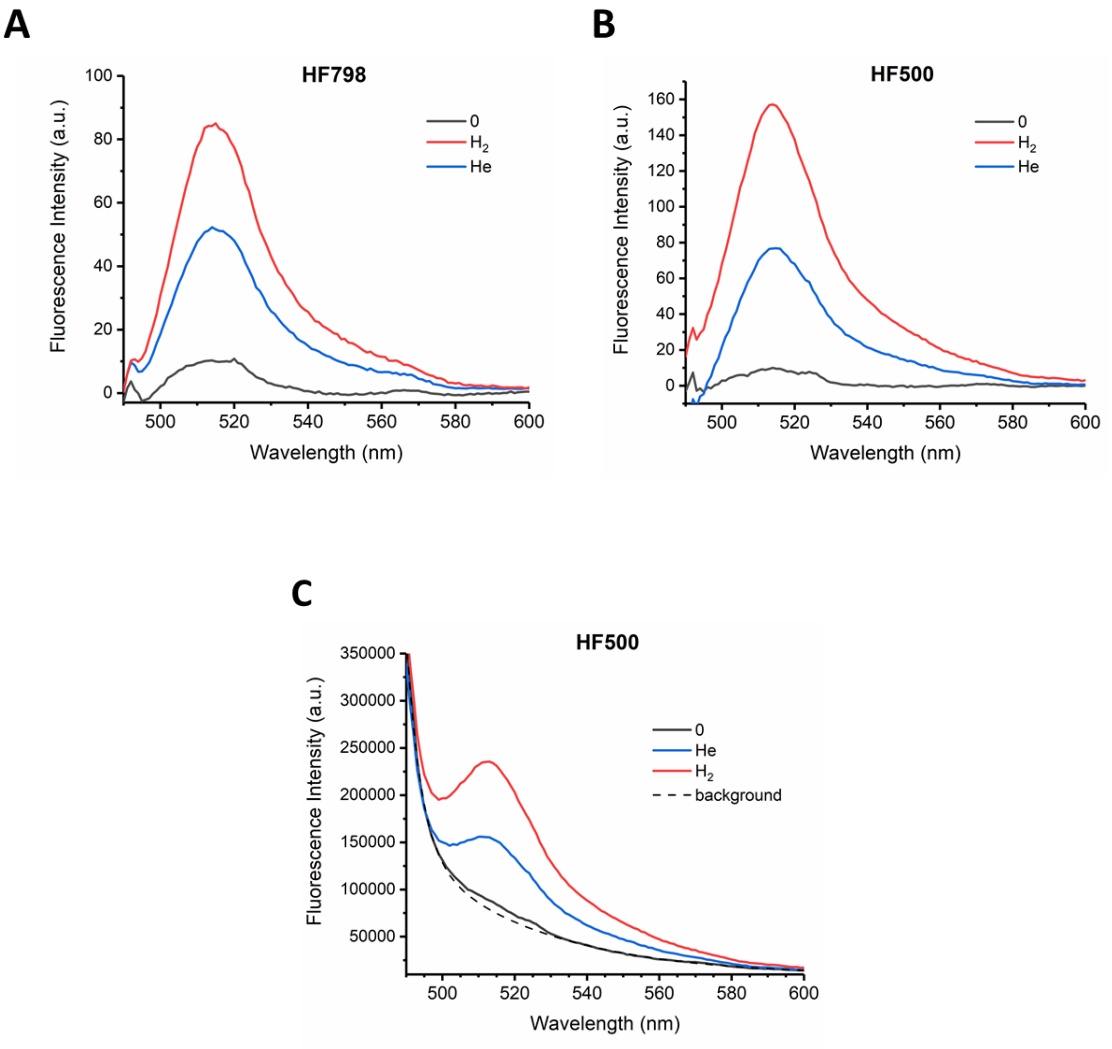

Figure 24 Background-corrected fluorescence emission spectra of Frex-expressing *R. eutropha* cell suspensions of strain HF798 (**A**) and HF500 (**B**). Spectra were recorded prior to treatment (0, black curve) and after treatment with H_2 (red curve) or He (blue curve). Fluorescence spectra of cells show high background noise due to light scattering by cells and their components, as can be seen from the unprocessed spectra in **C**. A biexponential curve was applied in order to

specifically select the Frex signal from the scatter background (**C**, background fit). When this curve is subtracted from the spectra, the curves in **B**, and likewise the curves in **A**, are generated.

The result that both strains behaved similarly in the presence of 100 % hydrogen atmosphere indicated that no specific SH activity could be discriminated under these experimental conditions. The fact that the SH-deficient strain also shows an increase in fluorescence, which should be correlated with an increase in intracellular [NADH], can be explained by the general anaerobization of the sample due to the treatment with hydrogen. Since oxygen is replaced from the environment, the aerobic respiratory chain cannot transfer its reduction equivalents from NADH to the terminal electron acceptor O_2. Hence, an accumulation of NADH is observed, which likewise triggers the Frex fluorescence in both strains. In order to test if anaerobization by a different, in particular metabolically inert gas, which should not serve as a substrate for the SH, would yield the same results for both utilized strains, the cells of the two strains were also treated with helium. Helium treatment, again, led to an increase of Frex fluorescence; however, in both strains the intensity of the fluorescence is only about 50 % of the fluorescence emission of Frex after H_2 treatment. Since this behavior is observed in both strains, the difference between these intensities cannot be due to the presence or absence of SH, but may rather be related to differences in the physicochemical properties of both gases, such as different Henry constants (Sander, 2015), diffusion constants ("Engineering ToolBox," 2008) or water/lipid partition coefficients.

While the fluorescence intensity was similar after 10-minute treatment of cells with hydrogen for both strains, the time course of elevated fluorescence after H_2 treatment was extremely different (**Figure 25**)

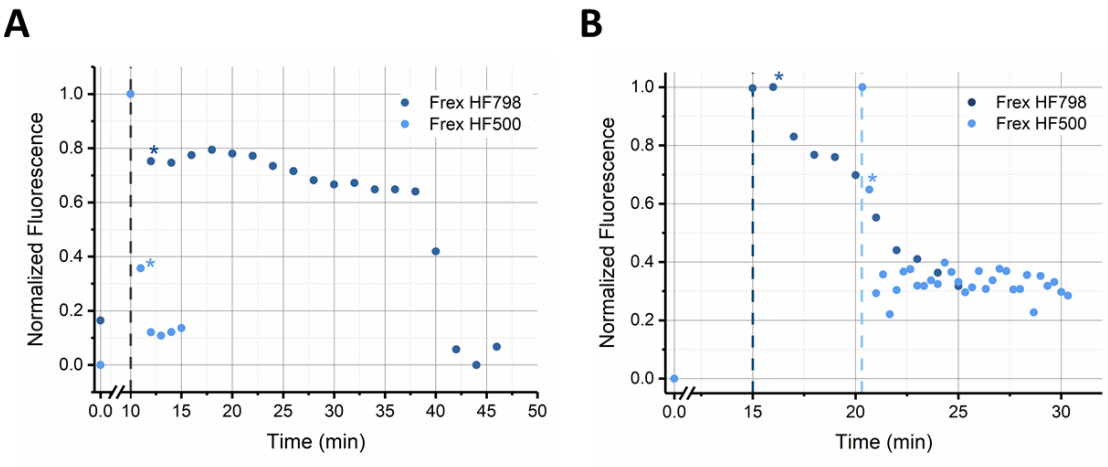

Figure 25 Normalized Frex fluorescence response (excitation 480 nm, plotted are the emission maxima at ~515 nm at various time points during the experiment) of HF798 (dark blue) and HF500 (light blue) cell suspension during and after treatment with hydrogen (**A**) and during and after treatment with helium (**B**). The data points at time zero indicate the measurements before gas treatment. Samples were aerated with hydrogen in a fluorescence cuvette (closed with a rubber septum) until the signal was stable. The first measurement after treatment of the cells with the respective gas is indicated by a line, while the asterisk signifies removal of the septum on the cuvette, consequently re-exposing the cells to the surrounding air.

Figure 25 A shows the effects of hydrogen treatment on the *R. eutropha* strains HF798 (dark blue dots) and HF500 (bright blue dots). Comparison of the time-dependent responses upon hydrogen exposure show that for Frex in *R. eutropha* HF500 (bright blue dots in **Figure 25 A**), the signal has a sharp maximum at the ten-minute mark. This was the first measurement after treatment with hydrogen. After this measurement, the septum, which was previously kept on the cuvette during treatment of the cells with the respective gas, was removed, and the surrounding air was allowed to diffuse into the sample. In the next measurement (indicated by an asterisk), the signal already dropped considerably, and after two minutes, the fluorescence signal had returned to its basal level. Therefore, as soon as the sample is exposed to air, the effects of oxygen limitation are reversed, and the system takes about two minutes to relax to normal aerobic conditions. For the SH-expressing strain (dark blue dots), also a sharp maximum at the ten-minute mark with only a slight drop at the next measurement was observed (indicated by the asterisk). As described, the measurement indicated by an asterisk is the first one after removal of the septum, which for one exposes the sample to air, but also

releases the slight overpressure, that was present during aeration of the septum-sealed cuvette with hydrogen, leading to a higher partial pressure for hydrogen in the septum-sealed cuvette. The time course for the bacterial strain containing the SH (HF798, dark blue dots) showed an almost constant elevated value until the 40-minute mark, at which the fluorescence intensity drops sharply between two measurements back to its original level. So, while in terms of the initial fluorescence intensity no distinction could be made between the two strains, in terms of time traces, a clear difference is observable. The distinctive behavior of both utilized strains in presence of hydrogen can be attributed to the activity of the NADH-generating enzyme, the SH. In the HF500 strain, not expressing the SH, the signal (and hence the intracellular NADH level) rises, when oxygen is removed from the sample, and thus the aerobic respiration is blocked. This effect is rapidly reversed, once the cells are exposed to air, as can be seen by the fast decrease of fluorescence intensity in strain HF500. In the strain expressing the soluble hydrogenase, this effect, of course, also occurs, but is superimposed by the effects due to the activity of the SH, which is able to metabolize the dissolved hydrogen from the fluid medium further until it is consumed or diffused into the environment.

These findings indicate that the intracellular NADH levels are sufficient to saturate the sensor, keeping the fluorescence maximal for about 40 minutes. During this time [NADH] is effectively larger than the sensors K_D, and only after the 40-minute mark the NADH concentration is of the same order of magnitude as the sensors K_D. These concentrations are traversed rather quickly, before the NADH level resumes the value prior to gas treatment. This effect explains, why a simple quantitative comparison of the fluorescence intensities is not suited to discriminate between treatment with either H_2 or He. Aeration with either of these gases saturate the sensor, and thus it appears as if the intensities are equal. Only over time one can discriminate and observe the longer lasting high intensity of Frex fluorescence in presence of H_2.

For a cross validation experiment the behavior of both strains in the presence of 100 % helium atmosphere was monitored as well. This gas cannot serve as substrate for any specific reactions in the cells, and therefore should only lead to displacement of oxygen from the sample. Hence, it is expected that both strains are

indistinguishable by their temporal behavior under helium treatment. The time traces for this experiment are shown in **Figure 25 B**.

The signal, again, reaches a maximum after 15 minutes of helium treatment for HF798 (dark blue dots) and 20 minutes for HF500 (bright blue dots), indicating the period of time the culture was exposed to helium. Afterwards, the septum was removed, and the samples were allowed to re-aerate. For the HF500 strain, the basal level is reached about three minutes after removal of the septum, while the HF798 strain takes about seven minutes to relax back to basal NADH levels. Thus, the time dependency of the NADH levels in both utilized strains after helium treatment is, within the experimental error, the same and comparable to the time course of the HF500 strain under hydrogen atmosphere. It seems, therefore, that the cells show a general anaerobization effect due to gas treatment, when no SH is present.

This difference of the time course of the fluorescence signal of the different strains under hydrogen atmosphere, can, of course, be attributed to the activity of the SH. In the HF500 strain the fluorescence signal purely reflects the oxygenation state of the sample due to treatment of the cells with 100 % hydrogen and the concomitant inhibition of the respiratory chain leading to accumulation of NADH. As soon as oxygen is allowed to diffuse into the sample this process is reversed, and the fluorescence signal follows the decrease in [NADH]. However, in the strain expressing the SH, hydrogen treatment led to a profound prolongation of the elevated fluorescence signal, much longer than the time needed for reversal of inhibition of the respiratory chain. The activity of the reactivated respiratory chain seems not to be sufficient to significantly reduce the NADH level generated by the SH. The conclusion that the intracellular NADH level stays elevated for a certain period of time due to the generation of NADH by the SH activity, and, therefore, a profound influence of the SH on the intracellular [NADH]/[NAD^+] -ratio seems justified.

In order to exclude the effect of the anoxic conditions (and therefore the inhibition of aerobic respiration), and to exclusively monitor the signal component stemming from SH activity, a further set of experiments was carried out, in which cells were treated with hydrogen/air gas mixtures containing certain percentages (vol/vol) of hydrogen, in order to ensure that sufficient oxygen is present in the cell

suspensions for the respiratory chain being fully operational. From such an experiment, the increase in [NADH] monitored by Frex fluorescence can unambiguously be assigned to activity of the SH.

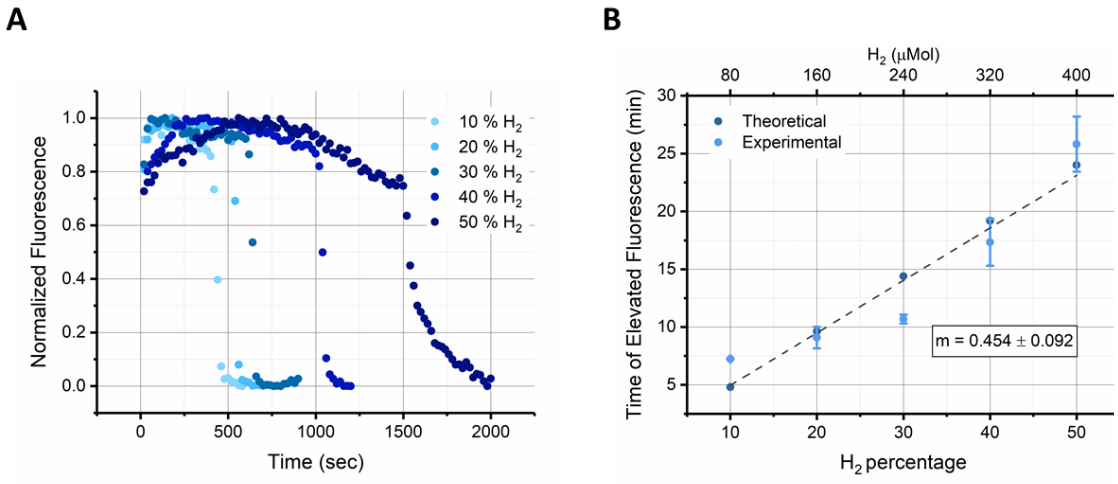

Figure 26 Frex fluorescence in the presence of the specified hydrogen/air mixtures (H_2 content in % v/v as indicated) in the SH-expressing strain HF798 (**A**). Excitation was carried out at 480 nm and fluorescence emission maxima at ~ 515 nm were plotted at various time points. The signals were normalized to peak intensity for better comparability. Plot of the duration of elevated fluorescence against the applied hydrogen percentages (partial pressure) (**B**). The dark blue data points represent the results from calculations based on a simplified reaction model (*vide infra*). The light blue data points represent the evaluated data points from experiments as in (**A**). The experiments were carried out in triplicate and the mean values ± S.D. of these experiments was plotted. The data were fit by linear regression model and the slope of this fit is given in the inset.

The normalized fluorescence signals show a direct relationship between hydrogen percentage (partial pressure) applied and the duration of elevated fluorescence (**Figure 26 A**). For 10 % hydrogen (lightest blue dots) the signal drop occurs after about 480 seconds, while the fluorescence stays elevated for the 50 % hydrogen experiment for up to 25 minutes (1500 seconds, darkest blue dots). The exact times of the signal drops, interpreted as total "reaction times" needed to consume H_2 in the sample, were evaluated by a logistic fit of the data and determination of the time for the signal drop to half maximum. These times were then plotted against the applied hydrogen percentages (partial pressure, or concentration respectively) in **Figure 26 B**. The relationship is not strictly linear but exhibits an

upward curvature indicating a larger increase in reaction time at higher hydrogen partial pressures.

These values for the "reaction times" needed to consume hydrogen in the samples can be compared to an activity assay of the SH that was carried out on permeabilized SH and Frex expressing cells. For this assay, the cells were concentrated to an OD_{435} of 118 and subsequently 2 µL of this concentrated cell pellet was resuspended in H_2-saturated 50 mM Tris pH 8.0 buffer, which was kept at 30 °C. The buffer is kept at 30 °C, being close to the activity optimum of the native enzyme at 33 °C, while the adjusted pH of 8 was determined to be optimal for SH activity (Schneider & Schlegel, 1976). The cells were mildly permeabilized by the means of a detergent, CTAB. Finally, NAD^+, the substrate of the SH, was added to the solution, effectively starting the reaction. The cell suspension was kept in a cuvette and the reaction was monitored spectrophotometrically by evaluating the extinction of the sample at 365 nm. The extinction at this wavelength is mainly dependent on NADH, which should be synthesized by the SH. The kinetics of the reaction gives an idea of the activity of the expressed SH, which can then be calculated by

$$specific\ activity = \frac{\frac{\Delta E}{\Delta t} \cdot V_{tot}}{\varepsilon \cdot V_{cells} \cdot c_{SH} \cdot d} \quad \textbf{(18)}$$

Where $\Delta E/\Delta t$ is the change of the extinction coefficient with time. This value can be evaluated by the spectrometer and was determined to be 0.016 min^{-1}. The total volume (V_{tot}) of the sample was 2 mL. ε is the extinction coefficient of NADH at 365 nm, which equals to 3.4 mL/(cm·µmol) and d represents for the thickness of the utilized cuvette (=1 cm). The concentration of the SH cannot be determined for the *in vivo* experiments, hence, the activity derived from the assay on the CTAB-permeabilized cells will be related by the OD to the measurements on whole cells for the *in vivo* experiments. Evaluation of the equation with these parameters equals to

$$activity = \frac{0.016\ min^{-1} \cdot 2\ mL}{3.4 \frac{mL}{cm \cdot \mu mol} \cdot 1\ cm} = \underline{0.0094\ \mu mol/min.} \quad \textbf{(19)}$$

The activity of the SH in CTAB-permeabilized cells equals to 0.0094 µmol/min (=units or u). This value can be normalized for the applied OD_{435} in the activity measurements, which was 0.3. Therefore, the OD-normalized activity equals to

$$\frac{0.0094\ \mu mol/min}{0.3\ OD} = \underline{0.03\ u/OD}. \qquad (\mathbf{20})$$

This value was used to calculate theoretical reaction times for the supplied hydrogen partial pressures for the experiments according to a zeroth order reaction. Since the utilized OD_{435} in these experiments was set to one, the activity of these cell suspensions was assumed to be 0.03 u. In order to use **equation** (**20**), the applied hydrogen percentages were recalculated as concentrations. In order to convert the utilized partial pressures, the Henry constant for hydrogen in water, which equates to K_H= 1282.05 L·atm·mol^{-1} (Atkins & de Paula, 2014), was used. Thus, a 100 % hydrogen-saturated solution at standard conditions corresponds to a concentration of about 800 µM, or 80 µM for 10 % hydrogen partial pressure. The utilized total volume of the cell suspension was 1.8 mL, resulting in a total of 144 nmol H_2 in the cuvette. Hence, the time needed for the SH to metabolize 144 nmol H_2, under the assumption of the calculated activity of 0.03 u, equates to 4.8 minutes. The resulting values for the other applied hydrogen concentrations are displayed in **Table 6**.

Table 6 Calculated values for the reaction times of SH in presence of differing H_2 amounts.

H_2 percentage	**n H_2 [nmol]**	**Calculated Reaction Time [min]**	**Experimental Reaction Time [min]**	**Activity [u]**
10 %	144	4.8	7.2	0.020 u
20 %	288	9.6	9.1	0.032 u
30 %	432	14.4	10.7	0.040 u
40 %	576	19.2	17.3	0.033 u
50 %	720	24	25.8	0.028 u

The comparison of these values derived from a coarse and simplified reaction model with the experimental ones show remarkable agreement, indicating that the activity determined by the CTAB assay can be transferred to the experimental data. These theoretically derived values were also plotted in **Figure 26 B**. The linear fit of the data points corresponds to an average activity of the cell sample. For the theoretical values the slope equals the derived activity of 0.03 u. For the experimental data the slope corresponds to 0.454 min/percentage H_2. Expressed in terms of concentrations rather than percentages, the value evaluates to 0.032 u and is nearly indistinguishable from the value derived from the activity assay on CTAB-treated cells. The activity values can also be determined for every applied concentration independently and not as a mean of all experiments combined, since the activity can well be dependent on the starting concentration of the substrate. For this method, the concentration of hydrogen in the samples is divided by the experimentally derived reaction times, indicated by the time of elevated fluorescence. The derived values are shown in **Table 6**. The data hint at an activity maximum of the SH for the value obtained in 30 % hydrogen-saturated solution. The average over these values equals to 0.031 u, being almost identical with the value obtained by the fit.

This indicates, that (i) the CTAB-permeabilized cell activity assay provides a good estimate of the actual intracellular activity of the SH and (ii) the derived method is a reasonable tool in order to determine SH activity in whole, living cells.

2.3 Effect of Cell Density on Frex Fluorescence upon H_2 Treatment

Since the variation of the substrate concentration offered interesting insight into the activity of the SH, the other component of the reaction, the total enzyme concentration in the cell suspension was also varied. For this purpose, the optical density (defining the number of cells and therefore indirectly the amount of SH) of the cell suspensions was changed to see whether the duration of the elevated fluorescence signals is coupled to the total amount of SH in the samples. For this

experiment cell suspensions of different ODs were treated with a constant hydrogen partial pressure of 50 % in air (**Figure 27**).

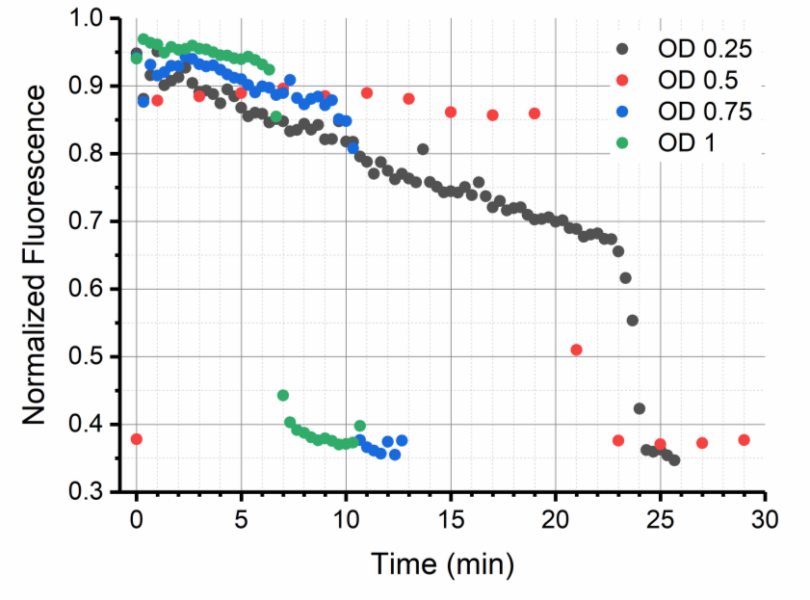

Figure 27 Frex fluorescence in the presence of 50 % H_2 in samples of differing OD. Frex was excited at 480 nm and the fluorescence emission maxima at ~515 nm were plotted at various time points. The more enzyme is present in the samples and, thus, the higher the OD, the faster the substrate is metabolized. The initial fluorescence signal amplitudes were normalized to 1 for better comparability.

It is noticeable that the enzyme concentration (represented by the optical density i.e. cell density of the sample) has an effect on the duration of elevated fluorescence of the Frex sensor protein, as expected. For higher ODs, therefore, more enzyme is available for metabolizing H_2 to NADH, and the signal consequently drops earlier in its characteristic sharp way than for lower ODs (less enzyme), for which a gradual decrease is observed, followed again by a sharp drop.

2.4 pH Effects

In order to exclude that the pH sensitivity of the Frex fluorescence probe (cpYFP used as chromophore) biases the observed signals, experiments were carried out,

in which *R. eutropha* cultures expressing only the fluorescent protein, cpYFP, were exposed to the same gas conditions. cpYFP shows enhanced fluorescence at alkaline pH (Elsliger et al., 1999; Wachter et al., 1998), which has been previously exploited to proof expression of Frex in cells. This pH sensitivity, however, also has its drawbacks, since it is not possible without calibration by cpYFP to infer, if changes in fluorescence result from different intracellular NADH levels, or if pH changes are confounding sensor readout. In order to exclude effects of pH changes, the cpYFP chromophore was tested in *R. eutropha* under the same conditions as the Frex sensor. Given that all experimental parameters are the same, any cpYFP fluorescence change cannot be due to changing NADH concentrations, but rather due to changes in intracellular pH. On the other hand, if Frex gives a signal under the same conditions and cpYFP does not, this signal can be confidently attributed to changing NADH levels.

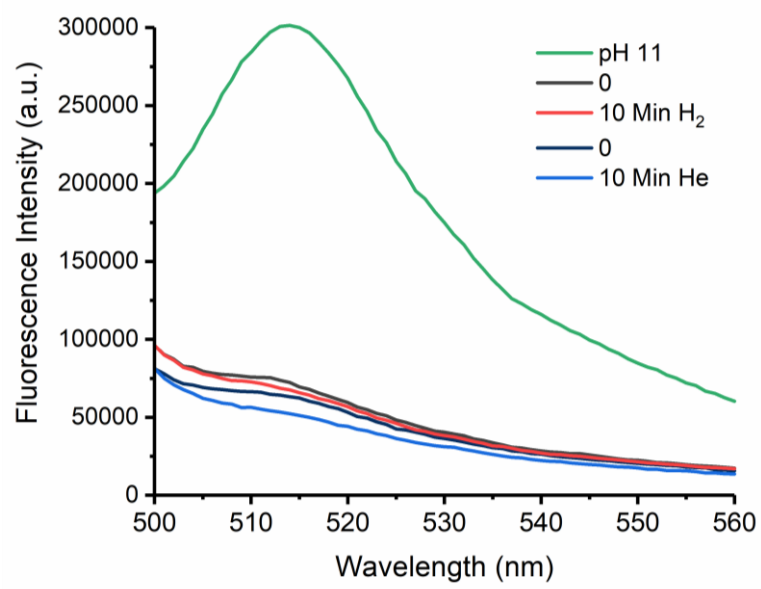

Figure 28 cpYFP fluorescence spectra from *R. eutropha* cells (strain HF798) expressing cpYFP and lysates derived thereof after excitation at 480 nm. The fluorescence before (black) and after alkaline lysis in buffer with pH 11 (green curve) as well as after treatment of intact cells with hydrogen (red curve) or helium (blue curve) are shown.

In order to test, if cpYFP was expressed, the alkaline lysis procedure already described (vide supra) was employed (**Figure 28**, green curve). A stable fluorescence after treatment with pH 11 buffer showed the expression of the

isolated chromophore unit. In subsequent experiments, a cpYFP-expressing *R. eutropha* cell suspension was either treated for ten minutes by aeration with hydrogen (red curve) or ten minutes of aeration with helium gas (blue curve), just as was the procedure for the Frex-expressing cells. Under these conditions the fluorescence of cpYFP does not increase in comparison to the fluorescence intensity recorded before treatment (black, and dark blue curves, respectively). This is in line with expectations, since the SH-catalyzed reaction generates one proton per NADH molecule, hence the cytosol was not expected to alkalize, but rather to undergo a slight acidification (if proton production exceeds the buffer capacity of the cytoplasm). However, since there is no observable difference between the samples after helium or hydrogen treatment, it seems that this effect is either negligible due to the strict pH stabilization by the cell, or due to the fact, that cpYFP does not alter its fluorescence upon lowering the pH substantially.

In conclusion, all changes in fluorescence of Frex during experiments can be unequivocally assigned to changing NADH levels, since control experiments with the cpYFP probe under the same experimental conditions provided no indication for pH-related signal changes.

2.5 *ex vivo* Calibration

Determining absolute NADH levels intracellularly is severely impaired because, as shown above, the use of short-wavelength excitation for signal normalization is not feasible in bacterial cells. This lack of a second excitation wavelength leads to a lack of ability to normalize the spectra according to the amount of protein expressed, a factor confounding the findings, since it is both possible to lead to higher fluorescence due to (i) higher intracellular [NADH] or (ii) higher overall expression of Frex. In order to circumvent this problem, another technique was exploited, previously utilized for Frex by Zhao et al., and also for Peredox by Tejwani et al. (Tejwani et al., 2017; Zhao et al., 2011; Zhao & Yang, 2012). In this method, Frex-expressing cells are lysed, and the cell lysates treated with different NADH and NAD^+ concentrations, in order to determine a titration curve. The signals are then compared to the signals in intact cells, since the fluorescence

should be similar and expression of Frex is kept stable and the background fluorescence of the cells also prevails. The effect of increased light scattering for whole cells in comparison to lysed cells should be considered. However the scattering properties of the lysed cell suspensions should more closely resemble the *in vitro* measurements.

Heterotrophically grown *R. eutropha* cells were harvested and diluted to an OD_{600} of 0.1. The cells were lysed by a French press procedure, in a total volume of 10 mL, leading to a 12,000-fold dilution of cellular components. The fluorescence emission spectra after excitation at 480 nm were recorded for different NADH concentrations and are shown in **Figure 29 A**.

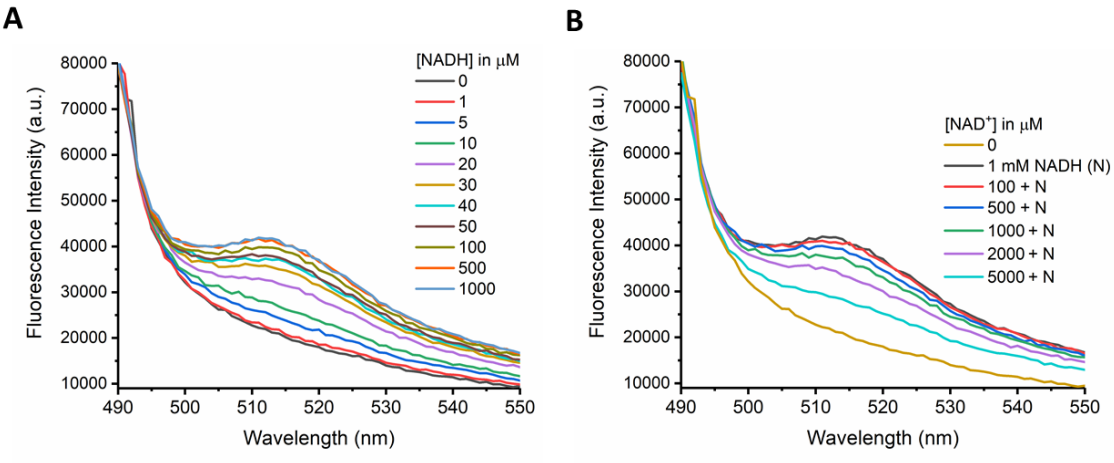

Figure 29 Emission spectra for an ex vivo calibration of Frex in HF798. A cell suspension of OD_{600} = 0.1 was lysed, effectively diluting intracellular components by a factor of 12,000. Spectra for the NADH titration (**A**) and spectra in presence of the denoted NADH amounts titrated with NAD^+ (**B**) were recorded.

The black curve shows the sensor's response after lysis without any nucleotides added. As expected, the sensor's signature is not observable in this spectrum, since upon lysis the nucleotide concentrations are strongly diluted, and fall under the detection threshold of the sensor. The solution of lysed cells is subsequently titrated with increasing amounts of NADH and the fluorescence increased, accordingly. The recorded spectra indicate that the senor is fully saturated at NADH concentrations in the sample of ≥ 500 µM (orange curve), a concentration which is half an order of magnitude larger than for the *in vitro* characterization

(see **Figure 13**). This may be indicative of the sensor's overexpression in cells, since the amount of substrate needed to fully saturate would be enhanced proportionally to the sensor concentration. Another, more likely possibility could be that other NADH-binding cellular components with higher affinity towards NADH reduce the pool of free NADH, making the relevant free NADH concentration essentially unknown.

Panel **B** of **Figure 29** shows the raw spectra of the corresponding NAD^+ titration of the lysed cells. The black curve represents the fluorescence of the sensor in presence of 1 mM NADH, the spectra were recorded subsequently upon titrating this cell suspension with NAD^+. Upon addition of NAD^+, the signal decreases as expected, but, as previously seen for the NADH titration in panel **A**, a rather large NAD^+ concentration was required to reduce the signal back to its basal level (>5 mM), since even the largest concentration of 5 mM NAD^+ was not sufficient to reduce the signal to its original value (turquoise curve).

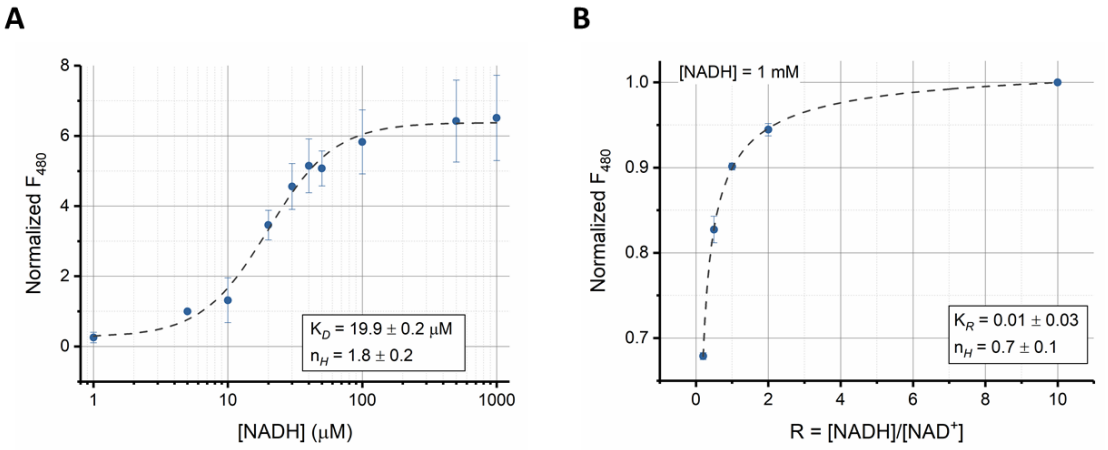

Figure 30 Emission maxima at 515 nm after excitation at 480 nm plotted against the present NADH concentration (**A**), or the NADH/NAD^+ ratio (**B**). The data points are normalized to the value in absence of NADH (**A**) or in presence of 100 µM NAD^+ and 1 mM NADH (R = 10). Data are mean values ± S.D. of n=3 experiments. The data is fitted by a Hill equation (dashed curve) and the fit parameters are given in the inset.

In **Figure 30**, the maxima at 515 nm of the *ex vivo* titrations are plotted against the titrated NADH concentration (**A**) or the existing [NADH]/[NAD^+] ratio (**B**), denoted as R. The values are fitted with a Hill curve and the parameters of the fit are given in the inset. For the NADH titration the dissociation constant (K_D) takes the value

of about 20 μM, a value about six-fold larger than for the *in vitro* characterization, further corroborating the presence of high amounts of Frex in the lysate or the high concentration of other NADH binding proteins in the lysate. The Hill coefficient is comparable to the *in vitro* characterization and shows the already established high cooperativity for NADH binding.

The Hill fit of the NAD^+ titration gives the parameter K_R which is the value at which both NADH and NAD^+ have the same likelihood to bind to Frex. The evaluated factor of 0.01 indicates that Frex shows a 100-fold higher affinity towards NADH than towards NAD^+, which can be verified by comparing the K_D values for NADH and NAD^+ from *in vitro* characterization (3.5 and 500 μM).

In summary, it was demonstrated that Frex is an appropriate tool in order to measure qualitative changes in the [NADH]/[NAD^+] pool of bacterial cells. Since many enzymes and/or metabolic processes interfere with or alter this ratio, Frex is a tool to monitor these activities. Because NAD^+ interacts with the sensor, the reported fluorescence is a value depending on the NADH concentration, corrected by the NAD^+ concentration, especially at values exceeding 100 μM. This value is by itself of great physiological importance; however, quantitative determination of [NADH] or [NADH/[NAD+] values based on utilization of the Frex sensor is limited due to the fact that the short wavelength excitation for signal normalization is not feasible in bacterial cells.

3 SoNar for Intracellular Application in *R. eutropha*

In 2015 another sensor was published, that is capable of sensing NADH and NAD^+ simultaneously (Zhao et al., 2015). This sensor is closely related to the Frex sensor, carrying also the cpYFP chromophore between two truncated subunits of the Rex monomers of *Bacillus subtilis*. The sensor, therefore, also offers two excitation wavelengths. But, in contrast to Frex, the sensor's emission after excitation at 480 nm is dependent on NADH as well as NAD^+, while the emission after excitation at 400 nm is only dependent on NADH. Upon binding of NADH the fluorescence

emission after excitation with 400 nm is increased, while the emission after excitation at 480 nm is decreased, making this sensor very susceptible towards NADH changes. Furthermore, the emission after excitation at 485 nm is increased upon increasing NAD^+ concentrations. This gives the opportunity to solely look at NADH effects on the sensor upon the short wavelength excitation and of the [NADH]/[NAD^+] ratio after long wavelength excitation. In contrast to Frex this sensor shows no pH dependence in the physiologically important pH range between 7.0 and 7.8. The affinity constants for NAD^+ and NADH are 5 µM and 200 nM, respectively (Zhao et al., 2015). These affinities are rather high for application in bacteria *in vivo*, nevertheless the feature of the sensor to discriminate between NADH and NAD^+ effects seemed promising enough.

The cDNA was, as previously described for Frex cDNA, subcloned into the pLO13SH vector and was inserted via spot mating of appropriate *E. coli* and *R. eutropha* strains. The sensor was subsequently excited at both excitation wavelengths of the chromophore in the SH-expressing HF798 strain, in the absence or presence of hydrogen and helium gas in order to determine its fluorescence responses.

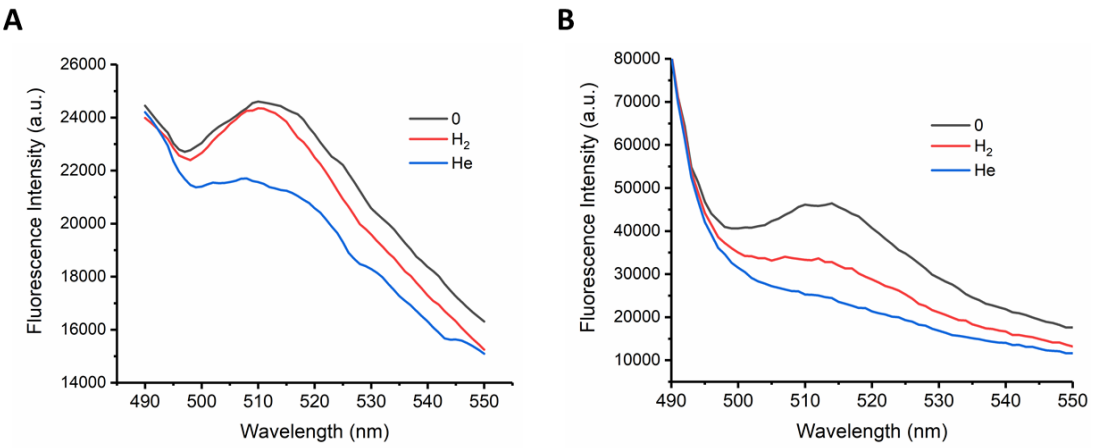

Figure 31 Fluorescence emission spectra of SoNar in *R. eutropha* HF798 after excitation at 400 nm (**A**) or 480 nm (**B**). Emission of the cell suspension was captured before treatment (black curves) in order to determine baseline levels of SoNar fluorescence in the cell host. Fluorescence emission was also recorded either after saturation of the suspension with hydrogen (red curves) or helium (blue curves). Cells were resuspended in H16 buffer to an OD_{600} of 0.5.

For the short wavelength excitation at 400 nm the sensor shows a broad maximum around 515 nm preceding any gas treatment (**Figure 31 A**, black cure). The fluorescence emission stimulated by 400 nm excitation is reportedly only dependent on [NADH], indicating that in this application, the cytosolic NADH concentration is sufficient to trigger fluorescence of SoNar. The long wavelength excitation yields a clear emission band around 515 nm, typical for the cpYFP probe (**Figure 31 B**, black curve). Since the emission after excitation at 480 nm is both dependent on [NAD^+] and [NADH], where an increase in [NAD^+] will lead to an increase in fluorescence and an increase in [NADH] will lead to a decrease in fluorescence emission, it is expected that upon gas treatment, the signal of SoNar should be diminished. Upon treatment with any given gas, [NADH] is supposed to rise, due to anaerobic effects on the cells and thus hindering their respiratory chain to transfer electrons from NADH to oxygen, effectively accumulating NADH. Treatment with hydrogen should also induce the metabolization of the hydrogen by the expressed SH in strain HF798, even further enhancing the intracellular [NADH]. The spectra after gas treatment indicate, that for excitation at 400 nm, the signal does not increase in fluorescence as expected, exhibiting even a decrease in signal for the helium treatment (**Figure 31 A** & **B**, red & blue curves). The fluorescence after excitation at 480 nm does in fact display the expected behavior in decreasing its intensity. However, the intensity decrease upon hydrogen treatment is only half as strong as under helium treatment. This is counterintuitive since hydrogen should for one trigger both aforementioned pathways to reduce the cytosolic milieu, (i) blockage of the respiratory chain and hence accumulating NADH, as well as (ii) SH catalyzed generation of NADH by utilization of hydrogen as substrate. All the while helium only induces the anaerobic blockage of the respiratory chain. Furthermore, hydrogen itself should be more potent at installing an anaerobic cellular milieu, since it is, due to its size, able to diffuse more freely than other gases. This behavior is also in contrast to the findings with the Frex sensor, which showed a higher response towards hydrogen treatment. However, it has been discussed that the SH is not only able to catalyze hydrogen oxidation but also the reverse reaction of proton reduction, given a sufficiently reduced cellular milieu (Kuhn et al., 1984).

The non-observable increase in fluorescence intensity after excitation at 400 nm may be explained by the sensor's affinity towards NADH being high enough, that the sensor is even in normal reduced cytosolic environments sufficiently saturated with NADH and thus unable to report changes towards even higher [NADH]. The same phenomenon was observable in usage of Peredox sensor, which was unsuited with its high affinity (K_D = 5 nM) to report on bacterial cytosolic [NADH] levels (Tejwani et al., 2017). The affinity of SoNar towards NADH was reported to be 200 nM, even though this is two orders of magnitude lower than the affinity of Peredox, compared to Frex, which was also saturated under gas treatment (see **Figure 25 A** & **Figure 26**, **A**) it is an order of magnitude higher. The response of the probe after treatment with helium showed lowered fluorescence in both excitation channels, which is not in accordance with the reported behavior of the sensor. This might indicate that the sensor suffers upon treatment with helium, effectively losing its capability to detect changes in the [NADH]/[NAD^+] pool. The fluorescence emission after excitation at 480 nm seemed, again, to be the only robust response of the sensor, usable for *in vivo* application in *R. eutropha* cells. Hence, the following experiments were carried out by examining the fluorescence emission after excitation at 480 nm. When the time-dependent behavior of the probe is observed after treatment with either hydrogen or helium, a strange phenomenon occurs.

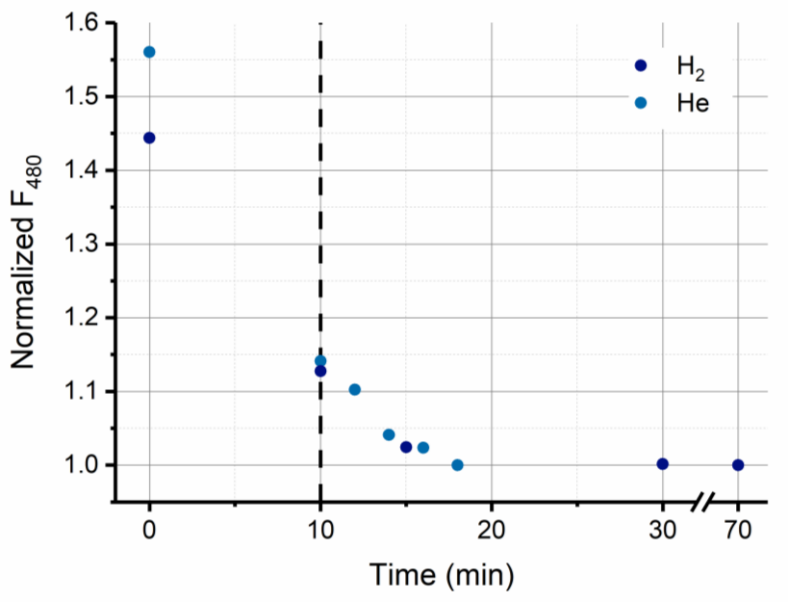

Figure 32 Time courses of the fluorescence emission at 515 nm after excitation at 480 nm. The samples were investigated prior to gas treatment (0) and

subsequently treated with the designated gas until a steady-state fluorescence was reached (dashed vertical line). The fluorescence was measured at the given time intervals. The signal was normalized to the signal after longest exposure and the remaining data points were scaled accordingly.

Figure 32 shows the time courses of the fluorescence maximum at 515 nm after excitation at 480 nm. The samples were measured before treatment with gas (0) and subsequently treated with either hydrogen (dark blue points) or helium (blue points) until a steady-state fluorescence was reached, but mostly for ten minutes (indicated by the dashed vertical line). Upon treatment with either gas, the fluorescence is diminished, as is expected. After the treatment under saturating gas conditions, the samples were allowed to reoxygenate by keeping the cuvettes containing the cell suspension in exchange with the atmosphere. However, while re-exposing the samples to the surrounding air, the signal does not retreat to its original value, as would be expected, but rather gradually decreases even further, no matter if the treatment occurred with hydrogen or helium. Recovery of NADH levels after treatment with helium was, as observed with the Frex probe, rather fast (about one to two minutes until the baseline level was re-established). In comparison, the SoNar probe does not shown recovery to the initial basal fluorescence levels even after eight minutes of re-aeration, even more so, the fluorescence is further decreasing, erroneously indicating on an ever-increasing NADH level. The same trend was observable for experiments carried out in presence of hydrogen. While the Frex probe indicated a restored NADH level after about 40 minutes, the SoNar probe does not exhibit any change towards decreasing [NADH] even after 70 minutes (point after axis break). The observed behavior of the SoNar probe seems to indicate that the sensor does not recover from gas treatment and seems further impaired to respond to intracellular NADH changes.

The high affinity of SoNar towards NADH, made this probe, as already expected, unsuited to report changes in NADH, for at least the excitation at 400 nm. The fluorescence emission after excitation at this wavelength showed no (hydrogen) or a counterintuitive (helium) response after gas treatment, rendering this excitation mode futile. Furthermore, the treatment of cell suspensions with different gases

rendered the probe dysfunctional, since the sensor signal did not change even after prolonged re-exposure to an aerobic atmosphere, indicating a slow degradation of the sample. These findings suggest that the SoNar probe would need a much more detailed pre-characterization, and, at the time being - does not appear suited for reporting intracellular [NADH]/[NAD^+] levels in *R. eutropha*.

The high affinities of SoNar and Peredox towards both nucleotides are reasonable for application in mammalian cell lines or cell lines with a smaller total nucleotide pool compared to bacteria. However, for a good bacterial sensor, these high affinities impaired their applicability for successfully reporting on the existent parameters. While NADH sensors for mammalian cell systems have their own legitimacy for sure, it would be detrimental to ignore the wealth of bacterial cells, which itself display an interesting NADH dependent metabolism, and, furthermore, are an interesting study object, due to the ease of the manipulation of these organisms, especially *E. coli*. Hence, it would be beneficial to design a sensor, equally suited to report on this important metabolite in bacterial cells.

Part 2 -Developing New NADH Sensors

Since the utility of the available NADH sensors for mammalian cells, unfortunately, fell short for applications in bacterial cells, it is desirable to design a sensor attuned to the environmental parameters of these cells. Bacterial cells contain higher cytosolic concentrations of NADH, NAD^+ and other fluorescent compounds such as flavins than their mammalian counterparts, leading to extensive autofluorescence of these species in the spectral region up to 550 nm (Bennett et al., 2009; Croce, Bottiroli & Unit, 2014; Tejwani et al., 2017). As a first idea to generate a NADH sensor for bacterial cells, it was proposed to alter the affinity of the already existing sensor Peredox-mCherry towards NADH, to render it usable in bacterial cytosol. This sensor was chosen, since the integral chromophore is considerably brighter than the cpYFP chromophore utilized in Frex and SoNar (Hung et al., 2011; Zhao et al., 2015, 2011, 2016). Furthermore, the cpT-Sapphire chromophore does not exhibit pH sensitivity and the fused mCherry probe offered the opportunity to normalize the obtained NADH dependent signal to a red-fluorescent chromophore, and, thus, correct for differing expression levels (Hung et al., 2011) between cells or cell batches.

4 Adjusting Peredox-mCherry for Usage in High NADH Concentration Environments

In the original publication introducing Peredox-mCherry, the route of synthesis starting from the parental Rex protein leading to the final sensor product was described, and 18 important amino acid positions for the enhancement of applicability as [NADH]/[NAD^+] sensor were mentioned (Hung et al., 2011) (see **Figure 33**).

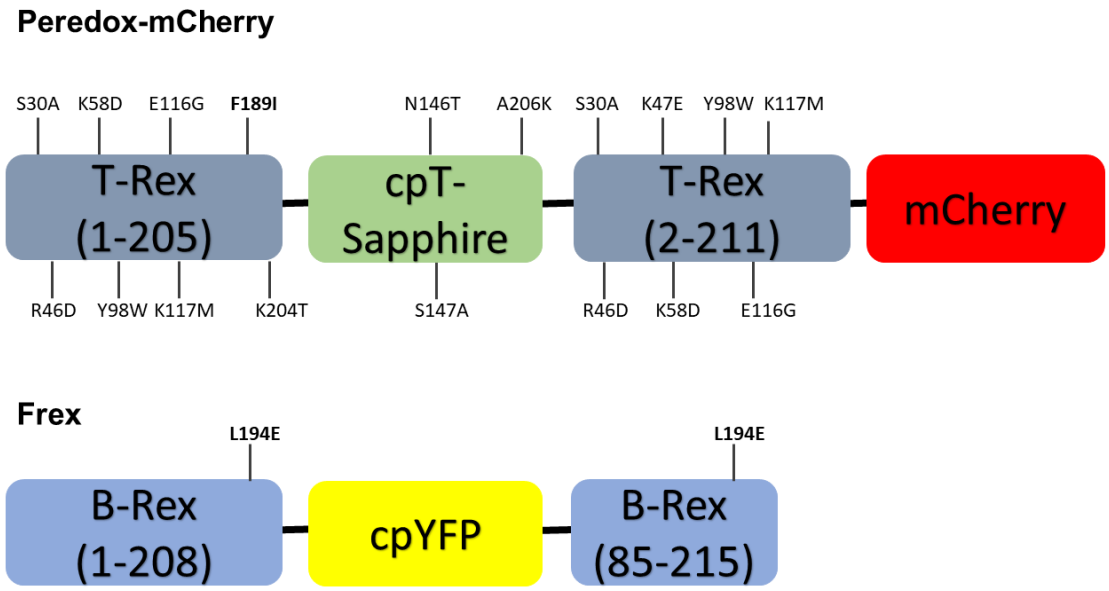

Figure 33 Mutations carried out in the optimization of Peredox-mCherry and Frex. The F189I mutation in the first T-Rex subunit (bold) of Peredox-mCherry was discussed to be of importance for the interaction of the sensor with NAD^+/NADH. In Frex, only one mutation at position 194 (bold) in both subunits was described.

The sensor consists of a T-Rex monomer fused to the cpT-Sapphire fluorophore followed by another truncated T-Rex monomer. In the first subunit, the isoleucine at position 189 (numbering according to the parental Rex) was found to be an important amino acid for tuning the interaction between the protein and the nucleotide (Hung et al., 2011). In comparison with Frex, another potential amino acid to finetune interaction of the sensor with NADH was discovered. In the Frex sensor, the leucine at position 194 in both B-Rex subunits was exchanged for a glutamic acid (Zhao et al., 2018). Since Frex shows a lowered affinity, the rationale was to also alter the corresponding amino acid in homologous position in the second subunit of T-Rex (in this case a phenylalanine) to a glutamic acid. Furthermore, the isoleucine at the homologous position in the first subunit was also to be exchanged for a glutamic acid. Glutamic acid is comparable in size to the isoleucine but carries a negative charge. The negative charge should, in theory, lead to electrostatic repulsion between the inserted amino acid and the negatively charged nicotinamide and thus reduce the likelihood of interaction between the protein and NADH, effectively lowering the sensor's affinity.

4.1. Glutamic Acid Mutants

It was decided to solely replace the isoleucine at position 189 in the first T-Rex subunit of Peredox-mCherry, as well as the phenylalanine at position 194 in the second T-Rex subunit with a glutamic acid, in order to assess how these mutations alter the sensor's NADH sensitivity. Furthermore, a double mutant carrying both mutations, I189E and F194E, was conceptualized.

The cDNA for the single mutants I189E, F194E and the double mutant was constructed by site-directed mutagenesis via PCR utilizing the NEB Q5 Mutagenesis Kit and introduced into *E. coli* cells for expression. The purified protein was investigated by fluorescence spectroscopy and the data for the NADH titration is shown in **Figure 34**.

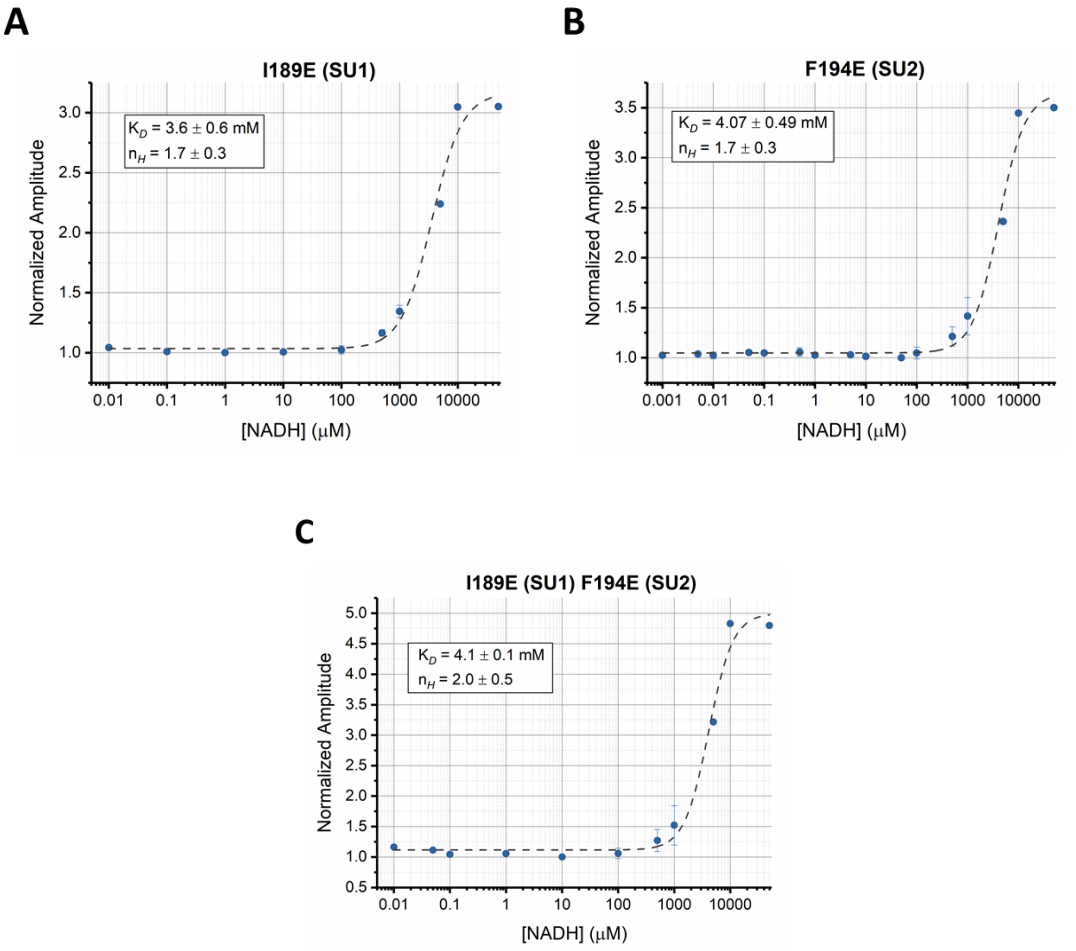

Figure 34 Fluorescence emission maxima at 515 nm after excitation at 490 nm and divided by the fluorescence maximum obtained after 590 nm excitation are plotted against the applied NADH concentrations for the Peredox-mCherry mutants. Panel **A** shows the dependency for the I189E mutation (mutation in the first T-Rex subunit, SU1). Panel **B** shows the titration experiment for the F194E mutation (mutation in the second T-Rex subunit, SU2). Panel **C** shows the titration experiment results for the double mutant I189E F194E. The spectra were normalized to the maximum value in absence of NADH. The plot of relative fluorescence against NADH concentration was fitted by a Hill equation (dashed curves) and the parameters are given in the inset. Data are mean values ± S.D. of n=3 experiments.

In all three mutants of the Peredox sensor generated, the affinity towards NADH was drastically reduced to values in the millimolar range, ranging between 3.5 – 4.1 mM. The dynamic range of the sensor was increased slightly by the mutation(s), since the dynamic range reported for the parental Peredox is 2.5 (Hung et al., 2011), while it varied between 3 – 5 for the mutant proteins. The inserted negative charge at or close to the NADH binding site does in fact exhibit a pronounced effect on the sensor's affinity. The results are independent from the actual location of the mutation, validating the fact that both mutated positions are crucial for interaction of the protein with the nicotinamide, but there is no additive effect induced by the double mutation. The affinity is already so vastly lowered in the single mutants by the negatively charged amino acid, that there is no difference discernible towards the double mutant.

The effect of lowered NADH affinity seems intuitive and was expected since NADH itself carries two negative charges as well, leading to electrostatic repulsion between the nicotinamide and the protein. However, the extent of the reduction of the sensor's affinity was surprising considering that Frex carries similar mutations (L194E in both B-Rex subunits, in which the amino acid residues are also found in the NADH binding pocket), but only exhibits a mildly reduced affinity of 3.7 μM (Zhao et al., 2011). However, these mutations here lowered the affinities towards NADH too drastically, making the constructed sensors unsuitable for the anticipated *in vivo* application in bacterial cells. Since the positions of the mutated amino acids do in fact seem to have profound effects on tuning of the affinity of the

sensor, less disruptive amino acid substitutions were introduced to modify the affinity of the sensor towards NADH more gradually.

4.2 Tyrosine and Glutamine Mutants

In a second set of targeted mutations, it was aimed to replace the aforementioned isoleucine with a tyrosine or glutamine. The mutations were only carried out to replace the isoleucine in the first subunit, since alteration of both positions seemed to have a similar effect. The tyrosine was expected to mimic the phenylalanine in size, while also adding a polar group, which should alter the interaction between the polar nicotinamide molecule and the amino acid residue. A glutamine was introduced, since it is structurally similar to the initially present isoleucine, carrying a polar group but no charge, which also should alleviate the mutation's effect on the sensor's affinity. The cDNA of the isoleucine mutants (I189Y and I189Q) was constructed and the protein was heterologously expressed. The purified protein was investigated by fluorescence spectroscopy. The data for the NADH titrations is shown in **Figure 35**.

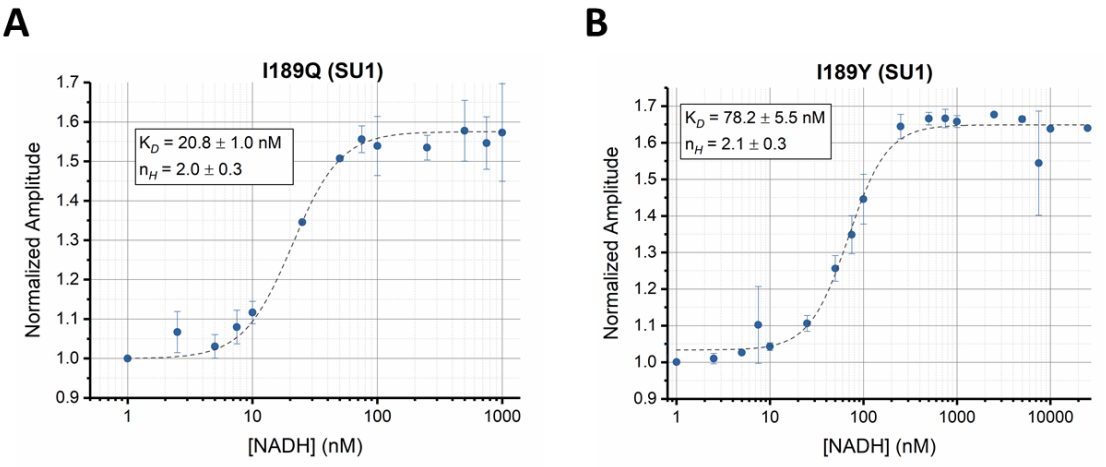

Figure 35 Fluorescence emission maxima at 515 nm after excitation at 490 nm and divided by the fluorescence maximum obtained after excitation at 590 nm are plotted against the applied NADH concentrations for the Peredox-mCherry mutants. Panel **A** shows the titration experiment results for the I189Q mutation (mutation in the first T-Rex subunit, SU1). Panel **B** shows the titration experiment

results for the I189Y mutation (mutation in the first T-Rex subunit, SU1). The spectra were normalized to the maximum value in absence of NADH. The plot of relative fluorescence against NADH concentration was fitted by a Hill equation (dashed curves) and the parameters are given in the inset. Data are mean values ± S.D. of 3 experiments.

The determined affinities for both mutants were decreased compared to the parental Peredox protein (~5 nM) (Hung et al., 2011), since the K_D of the I189Q mutant for NADH was determined to be about 21 nM (**Figure 35 A**), while the affinity for the tyrosine variant was even further lowered to 79 nM (**Figure 35 B**). The Hill factor is close to two for both mutants and therefore in accordance with the determined Hill factor for Peredox-mCherry, showing high cooperativity of NADH binding. The dynamic range of the sensor mutants, however, is slightly reduced from 2.5 for the original Peredox sensor to about 1.5 in both mutants. These mutants, though demonstrating reduced affinities towards NADH, are still not optimally suited for the application in bacterial cells yet. Due to the cytosolic NADH concentrations in the micromolar range (Bennett et al., 2009; Tejwani et al., 2017), a potential sensor should demonstrate an affinity towards the desired analyte in the same order of magnitude.

In summary it was shown that the exchange of either the nonpolar and aliphatic amino acid isoleucine at position 189 in the first subunit of T-Rex, or the exchange of the nonpolar and aromatic amino acid phenylalanine at position 194 in the second subunit of T-Rex by the negatively charged glutamic acid leads to a sharp decrease in the sensor's affinity towards NADH. This indicates that both of these positions are crucial for tuning the sensors affinity towards NADH. The negatively charged amino acid residues in the mutants might lead to too strongly repulsive forces between the protein and the negatively charged nucleotide, and, therefore, reduce the affinity of the mutants towards values in the millimolar range.

Therefore, in a second set of experiments, it was aimed to exchange the nonpolar aliphatic amino acid by tyrosine, a close homologue to phenylalanine, albeit a polar aromatic amino acid, and also by glutamine, a polar but uncharged amino acid. Titration studies with these mutants showed affinities were lowered compared to the parental Peredox-mCherry. However, for an application in bacteria, the

affinities were not lowered sufficiently, indicating that the structural or electrostatic changes in the NADH binding environment are too subtle to change the binding behavior of the sensor into the micromolar range as is desired for application in high NADH concentration environments. Hence, the generated Peredox variants do still not appear appropriate for intracellular NADH sensing in *R. eutropha*.

5 New Sensors Based on NIR Probes

The design of a new NADH-sensor for application in bacterial cells, must meet certain conditions, in order to generate an optimized sensor reporting on the chosen analyte. In case of a quantitative NADH sensor designed for *in vivo* monitoring in bacterial cells based on the experience with previously available NADH sensors, the following points should be fulfilled:

1. Affinity towards NADH in the high micromolar range ($K_D \sim 100$ μM)
2. Negligible affinity towards structurally related molecules such as NAD^+, NADPH, etc.
3. NADH-dependent fluorescence response in the red region of the spectrum
4. Large dynamic range
5. Ability to normalize the fluorescence signal, for better intercellular comparability
6. No pH effects on sensor response
7. Robust expression of the sensor in various prokaryotic, but possibly also, eukaryotic cell hosts

The utilization of a red-fluorescent protein appears as an optimal choice for the fluorescent probe, in order to benefit from the aforementioned advantages. For a NADH-dependent fluorescence response in the red spectral range, a suitable fluorophore with the right spectral characteristics should be incorporated into the sensor. iRFP713 is a far-red emitting protein derived from a bacterial phytochrome of *Rhodopseudomonas palustris* (RpBphP2), which hence binds biliverdin IXα as a cofactor (Filonov et al., 2011). In a 2013 paper, the group around Verkhusha described iSplit, a probe for protein-protein interaction (PPI) derived from this far-red fluorescent protein iRFP713. In this probe, the subdomains of the chromophore-binding domain (PAS and GAF domain) are split and separately expressed, with the remarkable observation that a red fluorescent protein is formed upon recombination of the domains mediated by protein-protein interactions (Filonov & Verkhusha, 2013).

This iSplit probe appears as a good starting point to develop concepts for the construction of new infrared sensor proteins.

5.1 iRFP713

iRFP713 exhibits far-red-shifted fluorescence with a maximum at 713 nm and is comprised only of the chromophore-binding domain (CBD), itself being subdivided into PAS and GAF domains, of the RpBphP2 bacteriophytochrome ancestor. Within the CBD, the PAS domain caries a cysteine residue, at which the chromophore is covalently bound (Lamparter et al., 2004, 2003). The probe was designed by protein engineering to yield far-red-shifted fluorescence emission centered at 713 nm, after excitation of the chromophore at either 680 nm (Q band) or at 405 nm (Soret band). In total, iRFP713 had been genetically optimized by 13 mutations, also to obtain a much higher fluorescence quantum yield than the bacteriophytochrome ancestor.

For a first test, it was investigated, whether the spectral properties of iRFP713 (excitation/emission spectra) exhibited any dependence on NADH. For these experiments, the protein was expressed in *E. coli*, purified, and aqueous buffer solutions of the purified protein were titrated with NADH, NAD^+ and NADPH in order to scrutinize the protein's fluorescence excitation and emission behavior in the presence of these nucleotides.

5.1.1. NADH Titration

The excitation spectrum of iRFP713, with the detection wavelength set to the emission maximum at 713 nm was recorded and is shown in **Figure 36**.

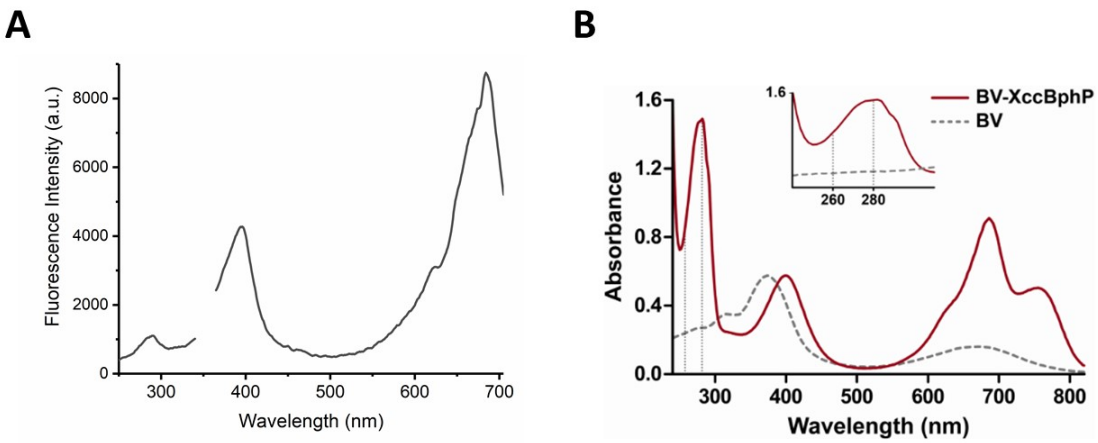

Figure 36 Excitation spectrum of iRFP713 (**A**). The emission wavelength was set to 713 nm and the spectrum was recorded over the shown wavelength range in two different recordings (250 – 350 nm and 370 – 700 nm). The protein concentration was set to 500 nM (OD_{680}) in PBS buffer. (**B**) Absorption spectrum of the bacteriophytochrome from *Xanthomonas campestris* pv. *campestris* containing biliverdin IXα as a chromophore (red line) as well as the one of biliverdin IXα itself (dashed gray line) (Klinke et al., 2014). The spectrum is magnified in the inset, showing that the absorption of biliverdin is non-zero in the protein-specific absorbance range at 280 nm (to which mostly tryptophan residues contribute).

The excitation spectrum was recorded in two intervals, which are depicted together in **Figure 36 A**. The recorded excitation spectrum is prototypical for iRFP713, exhibiting two major excitation peaks, one around 405 nm (Soret band of the chromophore) and one around 680 nm (Q band of the chromophore). In the blue region there is also a peak of lower intensity found at around 280 nm, which requires more detailed considerations. Firstly, the absorption of biliverdin between 260 nm and 300 nm is non-zero (**Figure 36 B**, dashed gray lines), so direct excitation of the iRFP713 chromophore by UV light is also possible. However, there is a clear peak in the action spectrum centered at 280 nm, which is generally not present in absorption spectra of biliverdin. This concerns a wavelength range, for which it is known that tryptophan residues in proteins absorb. If, however, 713 nm emission were due to 280 nm excitation of tryptophan residues in iRFP713, this would suggest that there is fluorescence resonance energy transfer from tryptophan residues in iRFP713 to the biliverdin chromophore. While such an energy transfer has been described in the literature for heme-binding proteins (Janes, Holtom, Ascenzi, Brunori, & Hochstrasser, 1987;

Kamal & Behere, 2001; Joseph R. Lakowicz, 2006; Sebban, Coppey, Alpert, Lindqvist, & Jameson, 1980), this as yet unexplored spectroscopic feature of iRFP713 needs further investigation, and it will be important for a novel principle of fluorescence sensor design. Indeed, iRFP713 carries three tryptophan residues, of which one is found in the PAS domain and two are found in the GAF domain (**Figure 37**).

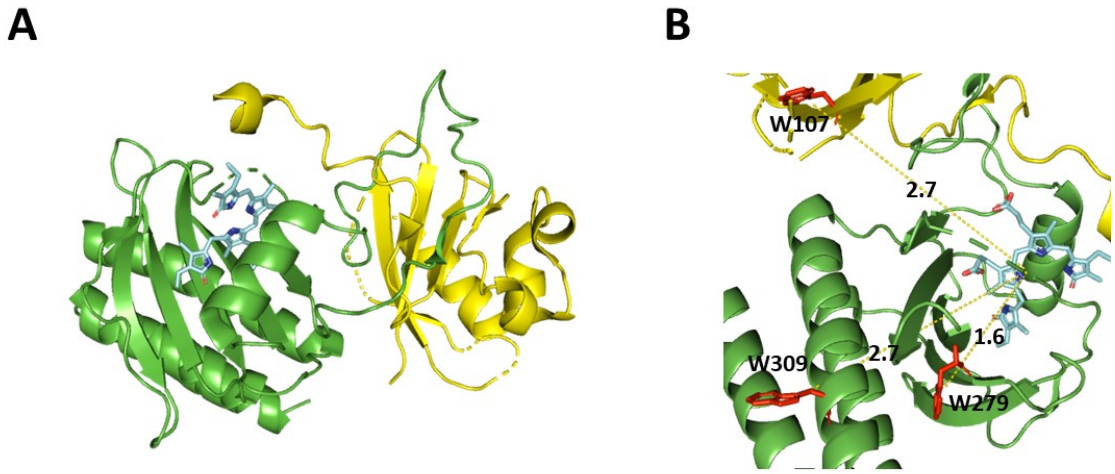

Figure 37 PyMOL model of iRFP713, based on its ancestor BphP2 from *Rhodopseudomonas palustris* (PDB entry 4R6L) (**A**). The PAS domain is depicted in yellow, while the GAF domain is illustrated in green. The chromophore biliverdin IXα is depicted in cyan (nitrogen: blue and oxygen: red). Enhanced view of the chromophore in its binding pocket (**B**). The three tryptophan residues of the protein, which are conserved in iRFP713, and their proximity to the chromophore (center to center) in nanometer are annotated.

Figure 37 A shows the PAS and GAF domains of the parental BphP2 protein of *Rhodopseudomonas palustris*, from which the iRFP713 was created by the exchange of 13 amino acids, however, none of the tryptophan residues are altered between RpBphP2 and iRFP713. The chromophore is embedded in the GAF domain, which carries two tryptophan residues (**Figure 37 B**), while a third tryptophan residue is located in the PAS domain. The three tryptophan residues present in the iRFP713 protein, as highlighted in the model structure in **Figure 37 B,** lie close enough (distances between 1.6 and 2.7 nm) to the chromophore to permit excitation energy transfer, as distances for FRET are usually in the same order of magnitude as the size of proteins (Joseph R. Lakowicz, 2006).

In order to explore, whether the protein's fluorescence response depends on NADH, the nicotinamide was added to the protein solution and the resulting spectra upon excitation at 280 nm were recorded (**Figure 38**). Light of this wavelength – besides exciting the BV chromophore with low probability – targets the fluorescence of endogenous tryptophan residues.

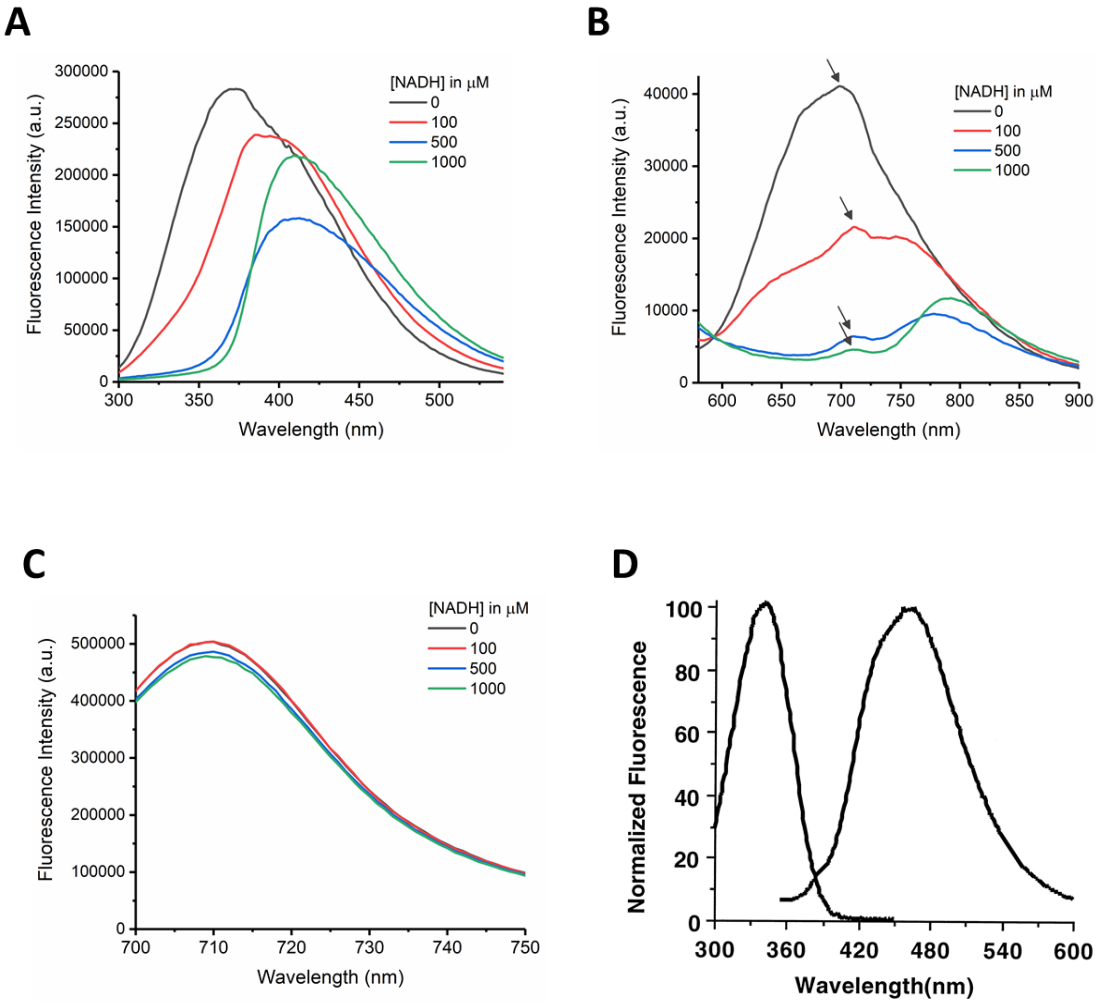

Figure 38 Emission spectra of iRFP713 upon excitation at 280 nm in either the wavelength range between 300 – 560 nm (**A**) and between 590 – 900 nm (**B**). Emission spectrum of iRFP713 after excitation at 680 nm in the wavelength region between 700 – 750 nm (**C**). The protein concentration was set to 500 nM (OD_{680}) in PBS buffer and NADH was added at concentrations given in the insets. The arrow in **B** marks the emission peak stemming from the biliverdin chromophore. Excitation and emission spectra of NADH (**D**). NADH concentration was set to 1 µM in a buffer containing 50 mM NaH_2PO_4, 50 mM sodium acetate, 50 mM glycine at pH 7.0. The excitation spectrum was recorded from 300 – 460 nm, where the emission wavelength was set to 465 nm. The emission spectrum was recorded upon excitation at 340 nm for the wavelength range between 350 – 600 nm, as

described in Patterson, Knobel, Arkhammar, Thastrup, & Piston, 2000.

Figure 38 A shows the emission spectrum of iRFP713 in the absence and in the presence of different NADH concentrations upon excitation at 280 nm in the wavelength range between 300 – 560 nm. The spectrum (black curve in **Figure 38 A**) represents the emission of the endogenous tryptophan residues of the protein in the absence of NADH. Obviously, the fluorescence emission of the three tryptophan residues is inhomogeneous, as the black curve in **Figure 38 A** exhibits a peak at around 370 nm and a shoulder at around 400 nm, indicating that the tryptophan residues encounter different microenvironments, for which it is known that a more polar (e.g. water-exposed) environment causes red-shifted tryptophan emission. Importantly, upon addition of NADH (colored lines in **Figure 38 A**) the intensity of the 360 nm fluorescence band decreases monotonously with increasing [NADH], and almost vanishes already at 500 µM NADH. In contrast, the spectral response above 400 nm is more complex, which is due to the overlap of red-shifted tryptophan emission and the inevitable fluorescence emission of NADH, which is also excited at 280 nm with a fluorescence maximum around 470 nm (**Figure 38 D**). For 100 µM NADH, the 400 nm band intensity is almost unchanged and is reduced to about 50-60 % at 500 µM NADH (red and blue lines in **Figure 38 A**). However, at 1 mM NADH, the fluorescence intensity increases (green line), which is due to the increasing contribution of NADH fluorescence that exhibits a maximum around 470 nm. Altogether, these observations indicate that the addition of NADH quenches the fluorescence of the present tryptophan residues in iRFP713 differentially: The fluorescence of blue-shifted tryptophan residues is quenched in a dose-dependent manner almost absolutely, whereas the emission of (a) red-shifted tryptophan(s) is not fully quenched by NADH. As a drawback, the overlap with NADH fluorescence complicates quantitative analysis of the red-shifted tryptophan emission band. Nevertheless, these spectra demonstrate that the fluorescence of the tryptophan residues in iRFP713 is dependent on NADH, so the question remains, whether or not tryptophan excitation has an impact on the fluorescence of the biliverdin cofactor of iRFP713, e.g., by FRET, since such a process should transfer the [NADH] dependence of tryptophan fluorescence to the fluorescence properties of iRFP713 fluorescence.

To test this hypothesis, the emission spectra of iRFP713 in the wavelength region between 590 – 900 nm upon excitation at 280 nm and in presence of various amounts of NADH were recorded, as shown in **Figure 38 B**. However, these spectra show the limitations for using conventional fluorescence spectrometers such as the Fluoromax-2 instrument, if largely divergent spectral ranges are covered (here: excitation at 280 nm and emission detection above 700 nm). Conventional spectrometers use a diffraction grating to split the light spectrally, and usually one uses only the first order diffraction for spectral measurements. If the detection range is set to far red-shifted wavelengths (here: above 700 nm, which is about twice the wavelength of the tryptophan emission maximum), superposition with second order diffraction from wavelengths of about half the detection value (here: around 350 nm) occurs, if no technical measures such as blaze grating or filters are introduced, which is not available in the Fluoromax-2 instrument. Thus, the second order diffraction of tryptophan emission (with maxima of the two populations at 360 nm and 400 nm) at around 720 nm and 800 nm, respectively, is expected, whereas the second order diffraction of NADH fluorescence (with maximum around 470 nm) around 940 nm is off the detection range. The "emission spectra" shown in **Figure 38 B** clearly indicate second order diffraction of the two tryptophan populations, and the dependence of these signal components on the NADH concentration follows the same trend as seen in direct (first order) fluorescence detection of tryptophan emission, namely that the 2nd order diffraction of the blue-shifted tryptophan emission (around 720 nm) vanishes almost completely at 1 mM NADH, whereas the red-shifted component at around 800 nm only ceases to about 50-60 %. However, the signals, particularly visible at an intermediate NADH concentration of 500 µM (arrows in **Figure 38 B**), clearly exhibit a peak at 713 nm, which can be attributed to the (first order of diffraction) direct iRFP713 emission. Evidently, this iRFP713 fluorescence component, which is observed upon 280 nm excitation of the endogenous tryptophan residues, is due to fluorescence resonance energy transfer (FRET) to the biliverdin chromophore, as can be crudely inferred from the [NADH] dependence of the 713 nm peak amplitude. Hence, this type of sensitized emission of iRFP713 obviously also shows a dependence on NADH concentration.

For direct excitation of the biliverdin chromophore, the protein was also excited at 680 nm and the resulting emission spectra are shown in **Figure 38 C**. These spectra exhibit the typical emission band of the biliverdin chromophore in iRFP713 centered around 713 nm upon excitation into the Q band by 680 nm light. The figure shows spectra recorded in the absence (grey line) and presence of various concentrations of NADH (colored lines). Upon addition of NADH, the spectrum of iRFP713 neither changes its intensity, nor its shape, indicating that the presence of NADH does not alter the chromophore fluorescence when excited directly via the Q band. Thus, excitation of the biliverdin chromophore via the Q band does not show any dependence on the NADH concentration, and it can be assumed that chromophore excitation via the Soret band would produce similar [NADH]-independent spectra as seen in **Figure 38 C**, albeit of lower intensity.

Though the spectra recorded with the Fluoromax-2 spectrometer are inevitably biased by second order diffraction signals at the used settings, these experiments show the crucial property that iRFP713 could – in principle – be utilized as a FRET-based sensor of NADH-dependent tryptophan fluorescence. Fluorescence emission of endogenous tryptophan residues is evidently dependent on [NADH], as shown directly in **Figure 38 A.** The endogenous tryptophan residues also transfer excitation energy to the biliverdin cofactor by FRET, as seen from the overlapping characteristic iRFP713 emission at 713 nm, which is also dependent on [NADH]. This would endow a biliverdin-based FRET sensor of NADH-dependent tryptophan fluorescence in a protein-specific manner with the ability to sense tryptophan fluorescence quenching by NADH. The huge spectral red shift of the fluorescence emission by the FRET process also separates the signal from the inevitable background fluorescence in the blue spectral region in the case of measurements in cells, which contain numerous sources of near-UV-induced blue fluorescence species. It should be emphasized here that excitation of fluorescence in cells by 280 nm, which (among other sources) targets essentially all tryptophan residues within the cell, would never result in a viable sensing strategy for [NADH] based on the concept of concentration-dependent quenching of tryptophan fluorescence by NADH alone. However, the fact that the endogenous tryptophan residues in iRFP713 particularly transfer excitation energy to the biliverdin chromophore,

discriminates the specific response of particularly these residues to [NADH] within a vast "bath" of cellular tryptophan fluorescence.

In further experiments we focused on the emission in the red region of the spectrum. Since the fluorescence spectra recorded by the Fluoromax-2 instrument comprise three signal components (2nd order diffraction of two species of tryptophan emission, sensitized emission of biliverdin via FRET, and possibly minor contributions from 2nd order diffraction of NADH fluorescence far above 800 nm), we aimed to reduce the complexity of the spectra by applying different excitation wavelengths. We chose excitation at 320 nm, in order to target the most red-shifted tryptophan residues, while at the same time minimizing the contribution of 2nd order diffraction signals from the blue-shifted tryptophan residues, which overlaps with the biliverdin cofactor's emission around 713 nm. The 320 nm wavelength, however, would lead to substantially enhanced NADH excitation, for which the 2nd order diffraction of its fluorescence emission would blur the far-red detection range. With this excitation wavelength, promising spectra could be recorded, since the background due to 2nd order diffraction signal from blue-shifted tryptophan residues was greatly reduced and the biliverdin emission band could clearly be discriminated (**Figure 39 B**).

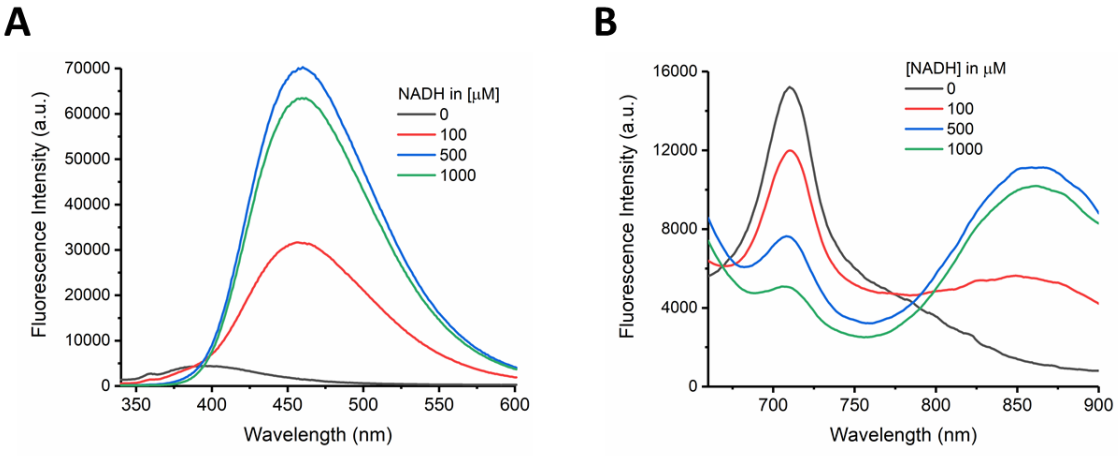

Figure 39 Emission spectra of iRFP713 after excitation at 320 nm in the wavelength range between 340 – 600 nm (**A**) and the wavelength region between 670 – 900 nm (**B**) recorded with the Fluoromax-2 instrument. Protein concentration was adjusted to 500 nM (OD_{680}) in PBS buffer and NADH was added at concentrations as given in the insets.

Figure 39 A shows the iRFP713 emission spectra after excitation at 320 nm in the wavelength region between 340 – 600 nm. The spectrum recorded in absence of NADH (grey line) shows a small peak at 360 nm and a broad band centered around 390 nm reflecting the dominant emission of the red-shifted tryptophan residue(s). Upon addition of the nucleotide, however, the autofluorescence of NADH quickly overshadows the actual iRFP713 tryptophan signal, due to the nearly optimal excitation of NADH at 320 nm. The long wavelength range, however, shows a behavior, that offers a suitable read-out as potential NADH sensor (**Figure 39 B**). Two distinct bands appear in the spectra, one around 713 nm clearly standing out, which stems from the biliverdin chromophore of iRFP713 and decreases upon increasing NADH concentrations, in accordance with the hypothesis that this band is due to sensitized biliverdin emission by resonance energy transfer from red-shifted tryptophan residues conferring their [NADH] sensitivity. A second band around 850 nm, which only appears upon addition of NADH and increases with increasing nicotinamide concentrations, again represents the 2nd order diffraction signal of the NADH autofluorescence. The reduction of the fluorescence intensity in the 713 nm band of the biliverdin chromophore according to [NADH], however, represents the read-out of the FRET-based NADH sensor. The data in **Figure 39 B** also show that the 713 nm emission upon 320 nm excitation is not (or only to a minor extent) due to direct excitation of biliverdin by near-UV light, since in this case, the 713 nm emission should not show a NADH dependence (compare fluorescence in presence of NADH after direct biliverdin excitation via the Q band in **Figure 38 C**).

Since the spectra in the long-wavelength range upon excitation at 320 nm show a dose-dependent decrease of fluorescence, another set of spectra with a more incremental addition of the nucleotide in a smaller wavelength window, not covering the distracting 2nd order diffraction of NADH autofluorescence, were recorded by setting the excitation wavelength to 320 nm and the emission range around the 713 nm band of iRFP713 emission to use it as read out for the NADH concentration (**Figure 40**).

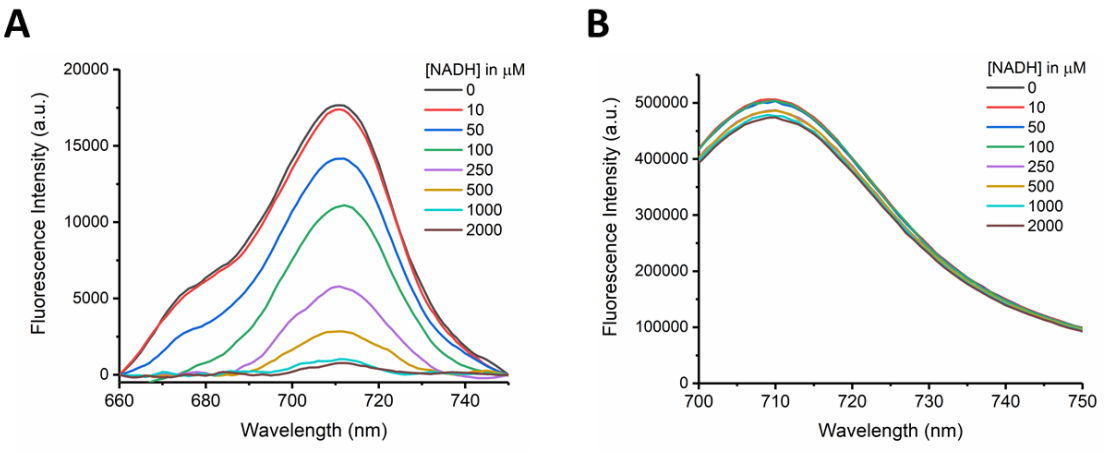

Figure 40 Background-corrected (see Methods & Materials **8.2**) emission spectra of iRFP713 upon excitation at 320 nm. Sensitized emission due to FRET from endogenous, red-shifted tryptophan residues (**A**) and raw emission spectra upon excitation at 680 nm, directly exciting the biliverdin chromophore (**B**). Protein concentration was adjusted to 500 nM (OD_{680}) in PBS buffer and NADH was administered in the designated amounts.

Figure 40 A shows the background-corrected emission spectra upon excitation at 320 nm. As was already observed in the preliminary titration spectra, the fluorescence band with a maximum at 713 nm decreases gradually, due to the sensitized emission, upon addition of increasing NADH concentrations up to 2 mM (**Figure 40 A**). As previously shown, the biliverdin fluorescence emission can also be directly excited at 680 nm, but the spectra obtained upon direct excitation do not change depending on the nucleotide concentration as mentioned above, making them a suitable tool for signal normalization (**Figure 40 B**), because the amplitude is only dependent on the concentration of the fluorescence protein.

This mode of normalization would be especially useful for the application of an iRFP713-based ratiometric fluorescence sensor *in vivo*, since variations of fluorescence intensity due to different expression levels, or chromophore bleaching during the experiment can be accounted for by this method. Thus, we investigated an evaluation mode, in which the fluorescence amplitude at the emission maximum (713 nm) upon excitation at 320 nm was divided by the fluorescence amplitude at 713 nm upon 680 nm excitation. The obtained values were plotted against the added NADH concentration and evaluated by fitting a Hill function to the data to determine specific apparent affinity parameters of iRFP713

towards the interaction with NADH, such as the apparent dissociation constant and the corresponding Hill coefficient (**Figure 41**).

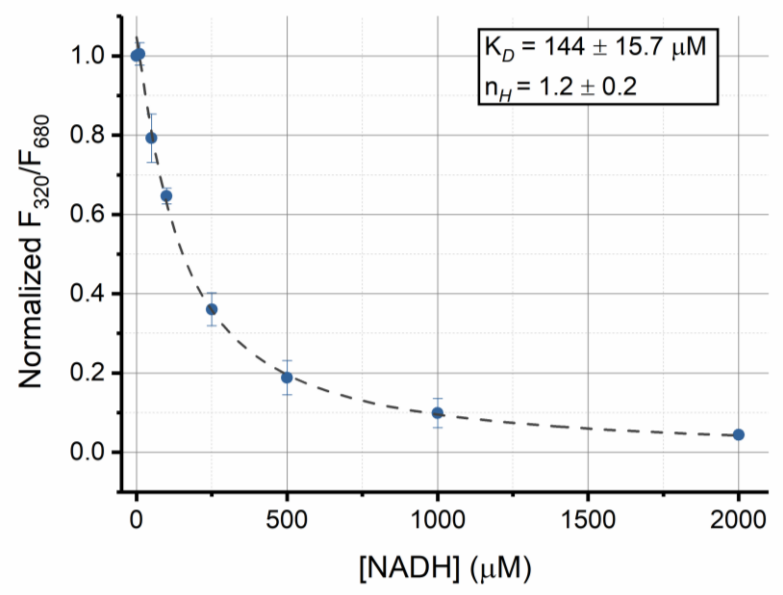

Figure 41 Plot of the ratio of the fluorescence emission amplitudes at 713 nm obtained upon excitation at 320 nm and at 680 nm (F_{320}/F_{680} ratio). The fluorescence ratio in the absence of NADH was set to one and the remaining data points were scaled accordingly. Data are mean ± S.D. of n=3 experiments. The data points were approximated by a Hill equation and the parameters of the fit are given in the inset.

Approximation of the data points by a Hill equation yields information about the interaction between the protein (and its tryptophan residues in particular) and the nicotinamide. The Hill equation has two independent parameters, K_D the dissociation constant, representing the concentration at which the ratiometric fluorescence signal is half maximal. The other parameter is the so-called Hill parameter as a marker for the cooperativity of the interaction, predominantly in multi-domain or multi-subunit proteins harboring several binding sites (Cornish-Bowden & Cardenas, 1987; Hill, 1910; Porter & Miller, 2012). In case of no cooperativity this value is one. Since iRFP713 is a monomeric protein, without a distinct NADH binding site, and presumably without a response towards [NADH] in terms of conformational changes, one could expect that the Hill factor for this interaction is around one, which is indeed the outcome of the fit (1.2 ± 0.2). The

dissociation constant evaluated by the fit corresponds to 144 ± 15.7 µM. This value is several orders of magnitudes larger than the K_D values of other NADH sensors (5 nM – 3.5 µM) described in the literature (Bilan et al., 2014; Hung et al., 2011; Zhao et al., 2015, 2011). However, for the application in bacteria, the value of this parameter is very well suited, since the concentrations of this nicotinamide in bacteria are in the micromolar range (Bennett et al., 2009; Tejwani et al., 2017).

These first experiments on iRFP713 itself showed the promising feature of a dose-dependent signal of the protein upon excitation at 320 nm, while the fluorescence emission was stable upon 680 nm excitation.

The obtained data allow to formulate a hypothesis about the sensing mechanism at work here. The proposed hypothesis is outlined in **Figure 42**.

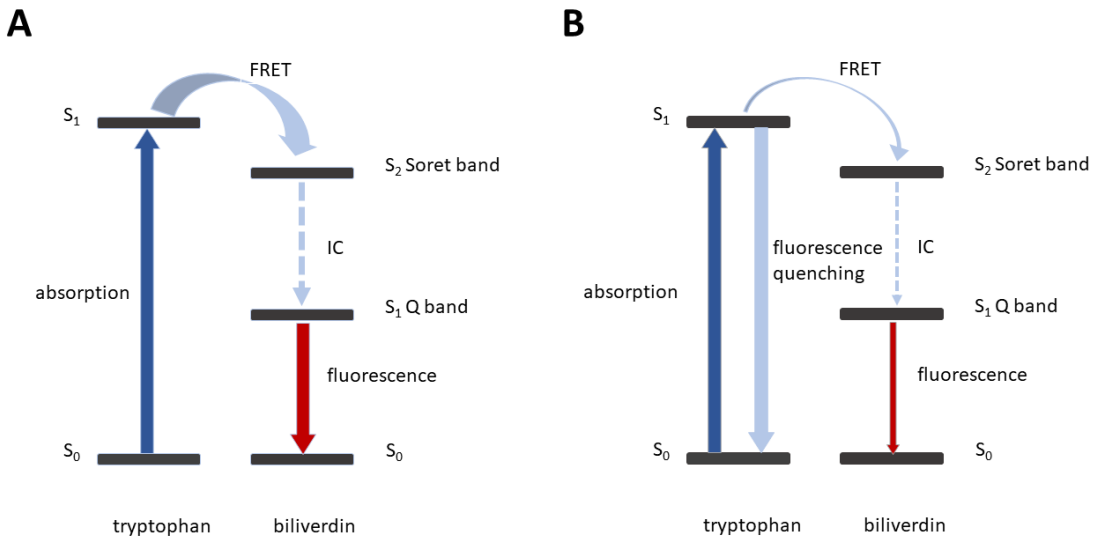

Figure 42 Schematic representation of excitation and emission in iRFP713 in absence (**A**) or presence of NADH (**B**). In absence of NADH the absorption of 320 nm light excites one or more tryptophan residue(s) and the excitation energy is transferred on to the Soret band of the biliverdin chromophore, presumably via Förster resonance energy transfer (FRET). The energy is then dissipated by internal conversion (IC) and the emission occurs from the Q band of the chromophore. In presence of NADH the excited state energy of tryptophan is quenched by NADH (fluorescence quenching), therefore, less energy can be transferred via FRET to the biliverdin chromophore and its emission decreases, accordingly (as indicated by smaller arrows).

According to this hypothesis, the 320 nm light excites a red-shifted tryptophan, which is able to transfer its excitation energy to the biliverdin chromophore via the Soret band, and after subsequent internal conversion to the level of the Q band fluorescence is finally emitted from the Q band of the biliverdin chromophore (**A**). Addition of NADH directly quenches tryptophan fluorescence, hence, less excitation energy can be transferred to biliverdin leading to reduced fluorescence from the chromophore's Q band (**B**). The direct excitation into the Q band at 680 nm circumvents the FRET mechanism, and the resulting fluorescence signal is only dependent on the amount of holoprotein present, therefore no change in intensity of this fluorescence mode should be observable in the presence of NADH, which coincides with the experimental data. This emission upon direct chromophore excitation thus can be used to normalize the spectra obtained after 320 nm excitation.

The NADH dependence of intrinsic protein tryptophan fluorescence has been reported before (e.g. the early accounts of the effect as determined for pig heart lactase and cytoplasmic malate dehydrogenase (Torikata, Forster, Johnson, & Rupley, 1979; Torikata, Forster, Neal, & Rupley, 1979) as well as horse liver alcohol dehydrogenase (Luisi & Favilla, 1970). Even the usefulness of cellular tryptophan fluorescence for NADH sensing by three photon excitation has been explored previously (Jyothikumar, Sun, & Periasamy, 2013). Furthermore the energy transfer between tryptophan and heme in proteins has been widely reported in the literature (Fontaine, Jameson, & Alpert, 1980; Monni, Haddad, Mourik, Auböck, & Chergui, 2015), but also the quenching of tryptophan fluorescence in bovine serum albumin (BSA) by added biliverdin has been reported (Wei et al., 2006). Since the biliverdin IXα chromophore is spectrally similar to heme, and also exhibits the Soret absorption band, the assumption, that energy transfer might also be possible between tryptophan and biliverdin seems justified.

However, quenching of tryptophan fluorescence might be a property, which is not exclusive to NADH, therefore, related nucleotide species need to be investigated as well. In order to evaluate the applicability of iRFP713 as NADH sensor further, iRFP713 was examined in presence of NADH analogues such as NADPH and NAD^+.

5.1.2. NAD⁺ Titration

For the evaluation of iRFP713 in the presence of NAD⁺, spectra were recorded in the wavelength region between 660 – 750 nm upon excitation at 320 nm, in order to monitor the response of the fluorescence from the biliverdin Q band by indirect excitation (**Figure 43 A**) as well as the emission in this wavelength range after excitation at 680 nm for direct excitation into the Q band of the BV chromophore (**Figure 43 B**).

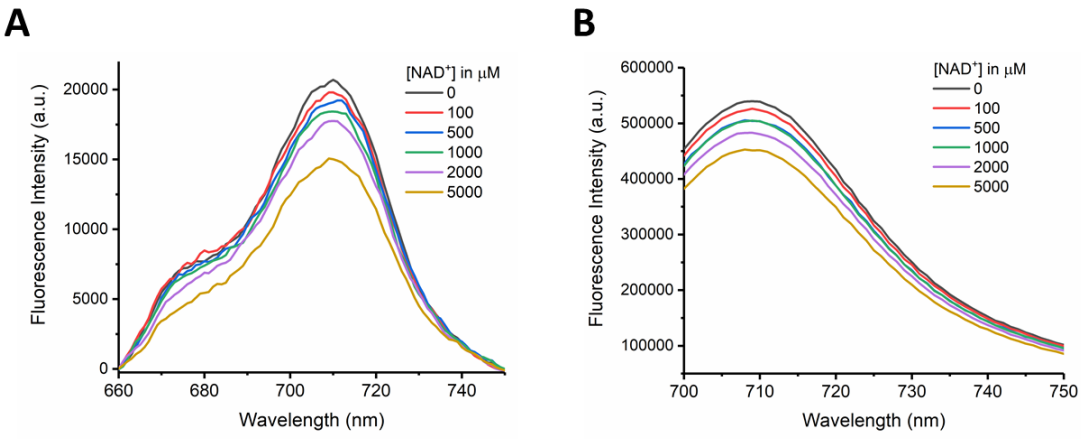

Figure 43 Background-corrected (see Methods & Materials **8.2**) emission spectra of iRFP713 after excitation at 320 nm (**A**) and raw emission spectra upon excitation at 680 nm (**B**). The protein concentration was adjusted to 500 nM (OD_{680}) in PBS and the denoted amounts of NAD⁺ were administered sequentially to the protein solution**.**

The background-corrected emission spectra in **Figure 43 A** exhibit a decrease of the fluorescence intensity with increasing NAD⁺ concentrations. Since NAD⁺ absorption at 320 nm is zero, there is no fluorescence component due to 2nd order diffraction signals to be seen in the spectra. A dilution artefact can be largely excluded, because the total dilution for the largest concentration of 5 mM NAD⁺ is 5 %, while the total intensity loss referenced to the 710 nm maximum is about 30 %, surpassing the dilution factor by far. The fluorescence decrease due to

dilution is clearly reflected by the spectra recorded after excitation at 680 nm. The decrease in intensity for panel **B** is about 10 %, thus only slightly larger than the calculated dilution of 5 % and may reflect photodestruction of the chromophore or protein degradation during the experiment. This also implies that about 20 % of the reduction of the fluorescence intensity in panel **A** is caused by interaction of NAD^+ with the iRFP713. Analogous to the preceding chapter the emission maxima at 713 nm after excitation at 320 nm are divided by the emission maxima at 713 nm after excitation at 680 nm and plotted against the added nucleotide concentration (**Figure 44**).

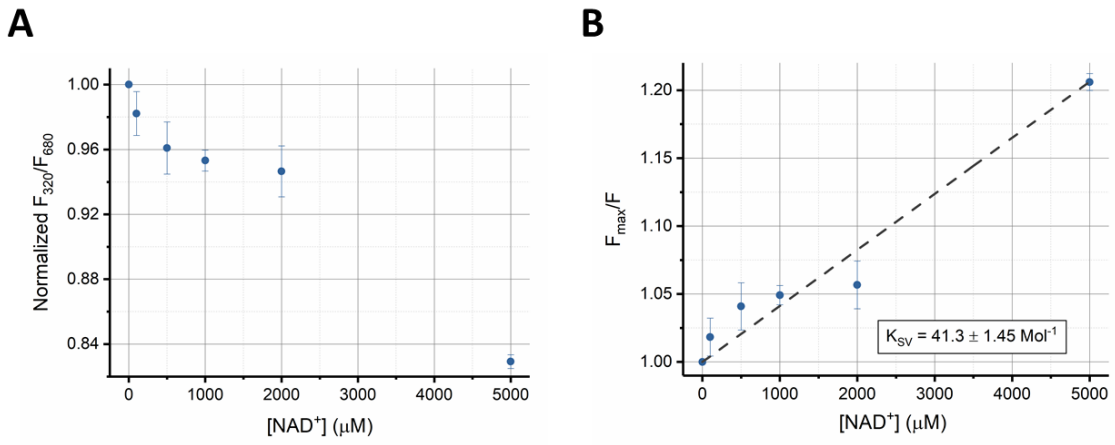

Figure 44 Plot of the ratio of fluorescence emission at 713 nm obtained upon excitation at 320 nm and 680 nm (**A**). The values were normalized to the fluorescence response obtained in the absence of NAD^+ and the remaining data points were scaled accordingly. Plot of F_{max}/F against the applied NAD^+ concentration (**B**). F_{max} is the F_{320}/F_{680} ratio in absence of the nicotinamide, while F represents this ratio in presence of the different amounts of NAD^+. The data were fit by a linear regression model, representing the Stern-Volmer equation (dashed line). Data are means ± S.D. of 3 experiments.

In **Figure 44** the normalized emission maxima after excitation with 320 nm and 680 nm are plotted against the NAD^+ concentration. The course of these data points is different from the data obtained for the NADH titration and does not clearly exhibit a sigmoidal shape, although this could be an artefact of the chosen NAD^+ concentration window. The represented data, however, rather seems to follow a linear course. This would indicate that quenching of NAD^+ occurs due to a different mechanism. Due to the apparent linearity of the data, we chose an evaluation procedure according to the Stern-Volmer equation (**Figure 44 B**). The

fluorescence data was plotted as the ratio of the maximal fluorescence in absence of NAD^+ (F_{max}), divided by the fluorescence measured in presence of the administered [NAD^+] (F), against the quencher concentration. The data points were fitted by a linear regression model. This fit defines the slope of the fit as the Stern-Volmer constant, which was examined to be about 41.3 ± 1.45 M^{-1}. Of note, quenching of the iRFP713 fluorescence by NAD^+ is only about 4 % at 1 mM NAD^+ and about 8 % at 2 mM NAD^+, therefore, NAD^+ concentrations in the low millimolar range would not interfere too much with the protein's response to NADH with the determined K_D of about 140 µM. But, quenching is not completed even at 5 mM NAD^+ so that care must be taken in the case of high millimolar NAD^+ concentrations.

5.1.3. NADPH Titration

The protein's fluorescence was subsequently also examined in presence of the phosphorylated form of NADH, in order to see if the spectra are more relatable to the NADH or NAD^+ titration (**Figure 45**).

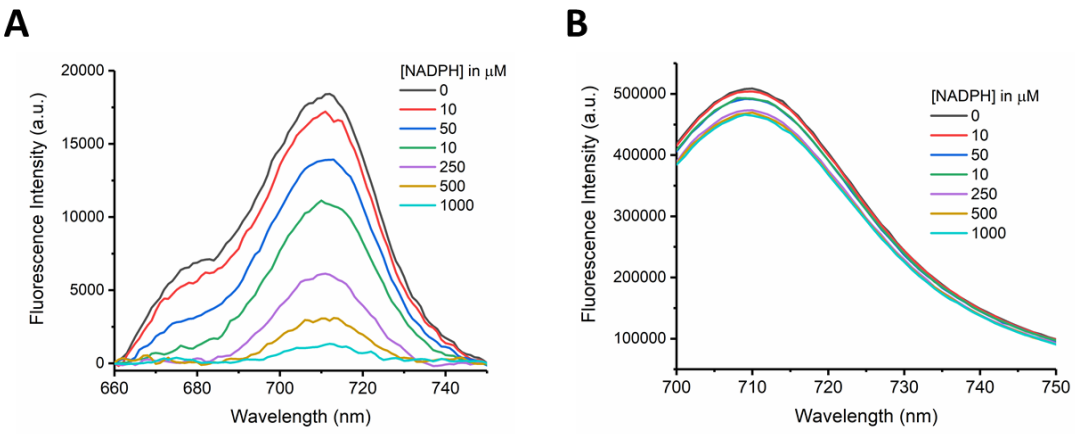

Figure 45 Background-corrected (see Methods & Materials **8.2**) emission spectra of iRFP713 upon excitation at 320 nm (**A**) and raw emission spectra upon excitation at 680 nm (**B**). Protein concentration was adjusted to 500 nM (OD_{680}) in PBS and NADPH was added in the denoted amounts.

The background-corrected titration data of iRFP713 in presence of NADPH (**Figure 45 A**) is essentially indistinguishable from the titration data with NADH in **Figure 40**. The direct excitation into the chromophore Q band gives the familiar spectra, showing no dependence on NADPH concentration (**Figure 45 B**). The data was processed as described above and the ratio of the fluorescence maxima were plotted against the administered NADPH concentration (**Figure 46**).

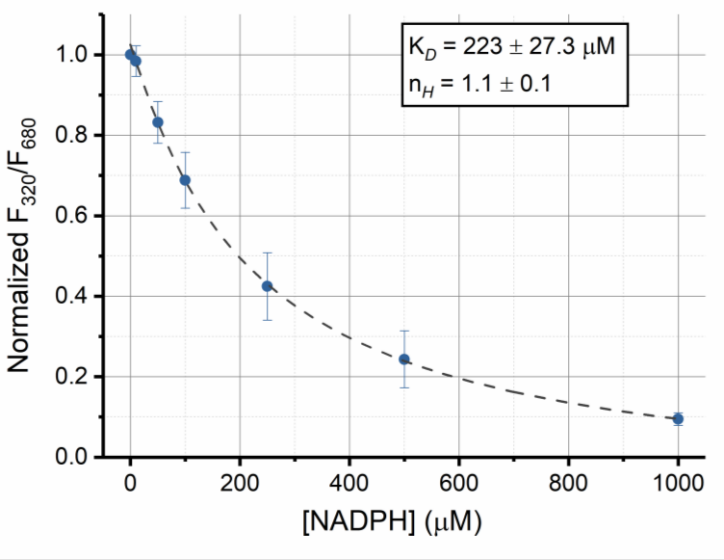

Figure 46 Plot of the ratio of the fluorescence emission amplitudes at 713 nm obtained upon excitation at 320 nm and at 680 nm (F_{320}/F_{680} ratio). The fluorescence ratio in the absence of NADPH was set to one and the remaining data points were scaled accordingly. Data are mean ± S.D of n=3 experiments. The data points were approximated by a Hill equation and the parameters of the fit are given in the inset.

Approximation by a Hill equation yielded a dissociation constant of 223 ± 27.3 µM. The obtained value is lightly elevated compared to the dissociation constant for the NADH interaction with iRFP713 (about 140 µM). Even though the values are not distinct enough in order to delineate that the interaction of iRFP713 with NADH and NADPH must be different. This means, for a potential *in vivo* application, that effects of quenching due to NADH or NADPH might not be discriminated. The Hill coefficient is 1.1 ± 0.1 corresponding to a non-cooperative interaction process, as above.

Since these preliminary experiments on iRFP713 indicate a promising NAD(P)H detection tool, we aimed at further identifying the components of the sensing mechanism. As hypothesized the characteristic band around 713 nm stems from biliverdin emission of iRFP713, which was investigated in this chapter. To further confirm the hypotheses and clarify the contribution of the 2nd order diffraction signal of tryptophan and NADH emission, we investigated solutions of these substances in the same set-up (Fluoromax-2 instrument).

5.2 Tryptophan

The aforementioned preliminary results concerning the spectral characteristics of the sensor seemed to hint at a tryptophan-based sensing mechanism, which is involved in an excitation energy transfer (EET) process. To confirm the quenching mechanism on tryptophan, we investigated the quenching of tryptophan fluorescence by nucleotides, recorded in two wavelength ranges, first, to monitor tryptophan and NADH fluorescence between 300 nm and 500 nm directly and then setting the detection range to 700 nm to cover the contribution of the 2nd order diffraction of the fluorescence signals.

To investigate the mode of NADH-dependent quenching of tryptophan fluorescence, tryptophan solutions were spectrally analyzed. For this, 10 μM tryptophan was dissolved in PBS buffer and titrated with different nucleotides. For a first experiment and in order to generate data for comparability with iRFP713, tryptophan solutions were titrated with NADH.

5.2.1 NADH Titration

Tryptophan was either excited at 280 nm, which is the excitation maximum in aqueous solution or, for comparison with the iRFP713 data, at 320 nm and the corresponding emission profiles were recorded (**Figure 47**).

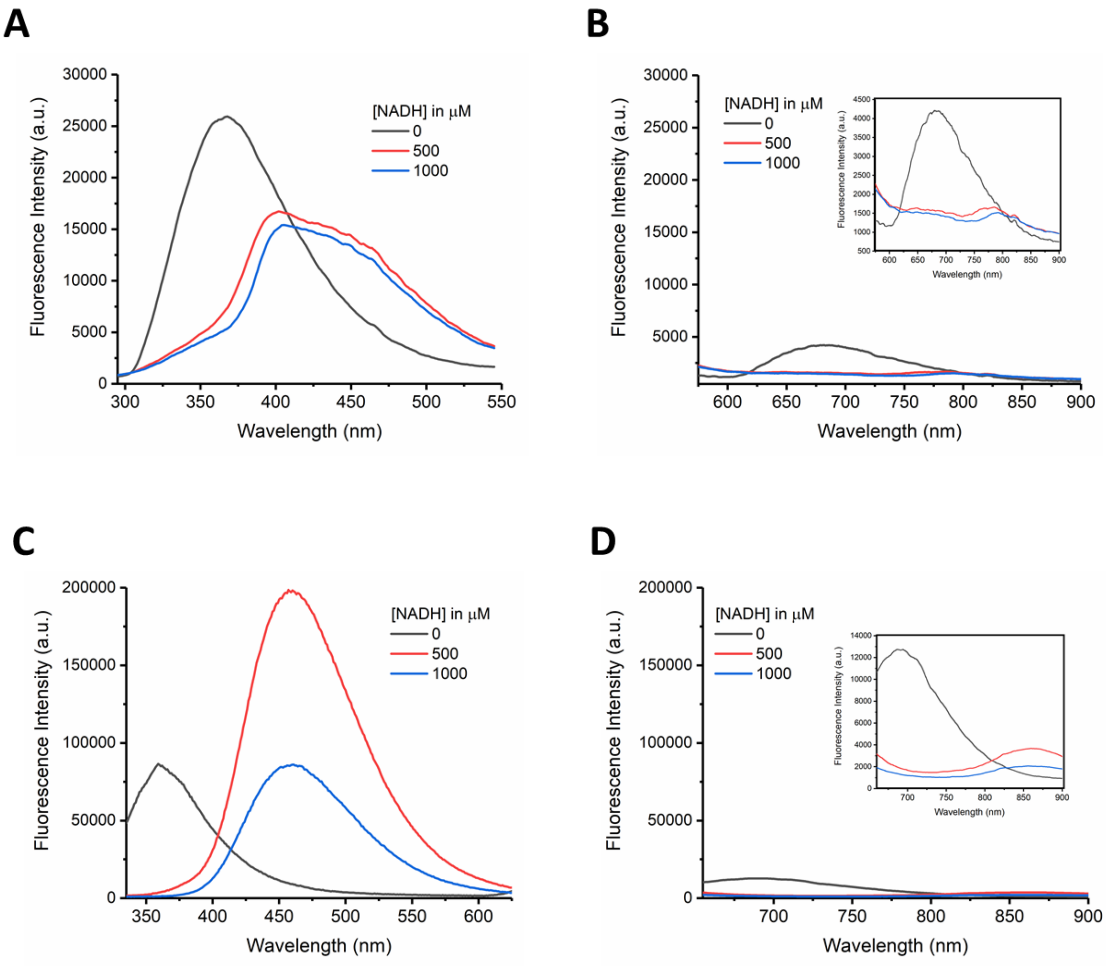

Figure 47 Emission spectra of tryptophan (10 µM) in PBS in the presence of the denoted NADH concentrations. The top row shows the emission spectra upon excitation at 280 nm in the short (300 – 500 nm) (**A**) and long (600 – 900 nm) (**B**) wavelength region using the same scale for the y-axis. The inset in **B** shows the same spectrum rescaled to its maximum. The bottom row shows the emission spectra after 320 nm excitation in the short (340 – 625 nm) (**C**) and long (650 – 900 nm) (**D**) wavelength region using the same scale for the y-axis. The inset in **D** shows the same spectrum rescaled to its maximum.

For a first general assessment, the tryptophan solutions were titrated with NADH in large increments, in order to examine if the signal in both the short (300 – 500 nm) and long (600 – 900 nm) wavelength regimen were correlated. The comparison of both excitation wavelengths (280 nm as standard for tryptophan excitation) and 320 nm (for comparison with the sensor data) shows essentially similar emission spectra of tryptophan in the absence of NADH (**Figure 47 A** & **C**,

respectively) with larger amplitude due to 280 nm excitation in accordance with the absorption maximum of tryptophan. With both excitation wavelengths, the emission spectrum is asymmetric with a pronounced red flange. Upon 280 nm excitation, the signal decreases with increasing [NADH] in the region of the main peak at 360 nm, while the flange at 400 nm is less responsive, with the result that the maximum shifts to longer wavelengths with a maximum at 400 nm (**Figure 47 A**). Also, a broad background appears due to NADH fluorescence (vide infra). The spectrum shown in **Figure 47 B** for the long wavelength regime shows the corresponding 2nd order diffraction signals, which essentially follow the same behavior. There is no observable difference in the spectra for the 500 µM and 1 mM NADH measurement (red and blue curve, respectively), indicating that the NADH effect is saturated at above 500 µM. The emission spectra upon excitation at 320 nm shown in **Figure 47 C** show that the characteristic tryptophan emission band vanishes almost completely at 500 – 1000 µM NADH, with no tryptophan fluorescence signature remaining at the red flange at high [NADH], but the strong NADH autofluorescence peaking at 470 nm dominates the spectra at high [NADH] due to more optimal NADH excitation at 320 nm. Also, here the signals recorded in the long-wavelength regime (**Figure 47 D**) reflecting the 2nd order of diffraction correspond to the short-wavelength spectra, again with roughly 1/7 of the amplitude of the "true" emission spectra.

Since the fluorescence signal of the tryptophan solution was most robust upon excitation at 280 nm and emission detection around 400 nm, these settings were chosen to carry out a more detailed titration study (**Figure 48**).

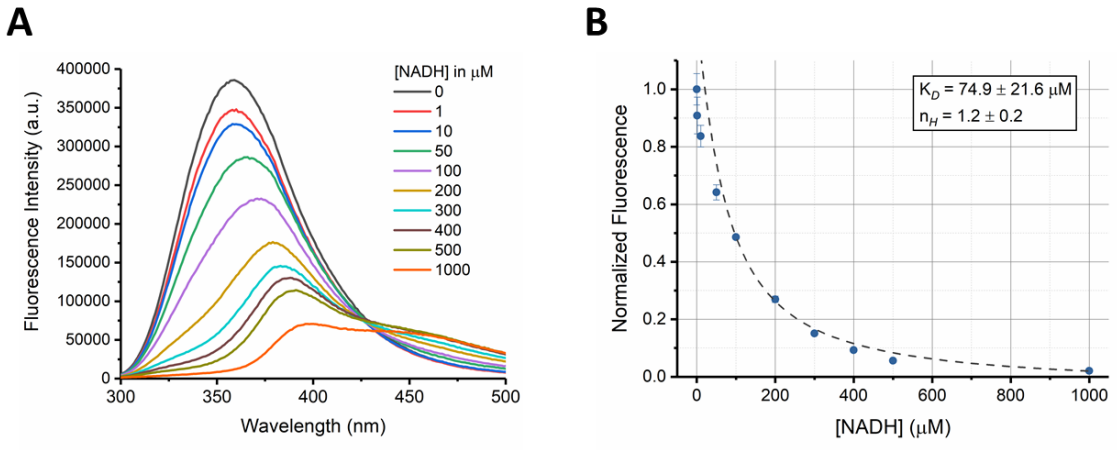

Figure 48 Emission spectra of tryptophan in solution (10 µM) in PBS after

excitation at 280 nm (**A**), upon addition of the designated NADH amounts. Fluorescence maxima at 350 nm plotted against the administered NADH concentration (**B**). The data point in absence of NADH was set to one and the rest were scaled accordingly. The data points were fitted by a Hill equation (dashed line) and the parameters are given in the inset. Data are mean ± S.D. of n = 3 experiments.

The fluorescence data shows that, analogous to iRFP713, tryptophan fluorescence especially in the blue flange of the emission spectrum is quenched almost completely by the added nicotinamide (**Figure 48 A**), with a signature at 400 nm that is less sensitive to [NADH]. Alongside the decrease of fluorescence upon addition of NADH, also the familiar spectral shift of the maximum is observed, and for higher nucleotide concentrations (≥ 200 μM) a new band around 460 nm appears (NADH fluorescence). These findings replicate the shifting of iRFP713's fluorescence emission after addition of NADH (compare **Figure 38 A**).

Plotting the emission maxima at 350 nm against the added nucleotide concentration gives **Figure 48 B**. The data points are approximated by a Hill equation. Tryptophan exhibits a higher affinity towards NADH, as its K_D was evaluated to 74.9 ± 21.6 μM, as compared to the value found for iRFP713 (about 140 μM). The Hill factor is evaluated to about one according to non-cooperativity. These experiments support the idea that a tryptophan residue is important in the mechanism for detecting NADH in iRFP713, as indicated by the closely related dissociation constants and similar general spectral behavior. Thus, it can be concluded that with high probability a tryptophan in the iRFP713's polypeptide structure is responsible for at least part of the sensing mechanism. In order to further substantiate the hypothesis, analogous experiments with tryptophan were undertaken with NAD^+ and NADPH.

5.2.2 NAD^+ Titration

In another set of experiments, studies with the oxidized congener NAD^+ were carried out (**Figure 49**).

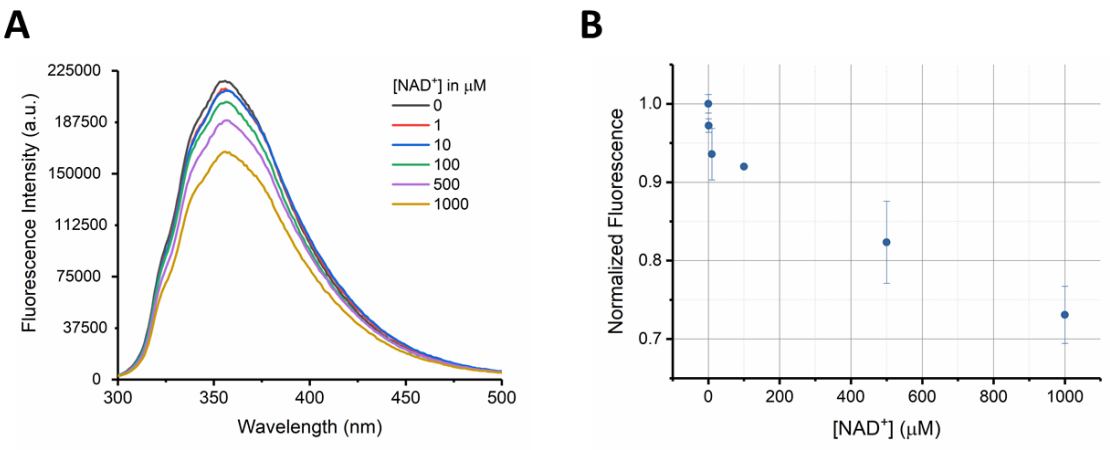

Figure 49 Titration spectra of tryptophan in the presence of the denoted NAD^+ amounts after excitation at 280 nm (**A**). Plot of normalized fluorescence maxima against the administered NAD^+ concentration (**B**). The data point generated in absence of NAD^+ was set to one and the remaining data points were scaled accordingly. Data are mean ± S.D. of n = 3 experiments.

Figure 49 A shows the emission spectra of tryptophan in presence of NAD^+ after excitation at 280 nm. The curves obtained, show a dose-dependent decrease of the fluorescence intensity at 355 nm. The decrease between the curve prior to NAD^+ addition (black curve) and the curve in presence of maximum applied NAD^+ corresponds to a decrease of about 30 % in intensity. This outcome is greater than a simple effect of dilution upon addition of the NAD^+ solution, which would correspond to about 3 %. The signals do not show contributions of fluorescence other than tryptophan emission (NAD^+ is non-fluorescent), thus the increase of the 470 nm emission band in NADH titration experiments (and shifting of the wavelength of the maximum) is validated as an artefact from NADH autofluorescence, mixing into the tryptophan emission band. The fluorescence of tryptophan seems to be quenched by NAD^+, albeit with a different sensitivity to the NADH quenching, just as has been observed for iRFP713. Tryptophan fluorescence has been described, as well as utilized, to be quenched by many ions or molecules, such as CN^-, I^-, or Cl^- for example (Joseph R. Lakowicz, 2006; Möller & Denicola, 2002). Importantly, it is notable that NAD^+ concentrations in the millimolar range are needed to induce substantial quenching of tryptophan fluorescence (**Figure 49 B**). All these properties are reflected by the iRFP713 fluorescence responses that

we attribute to FRET from NADH-sensitive tryptophan residues to the biliverdin chromophore.

5.2.3 NADPH Titration

The effect of the phosphorylated congener NADPH was indistinguishable from NADH in the case of iRFP713, and spectrally, these molecules are also essentially identical. Thus, the effect of NADPH on tryptophan was investigated (**Figure 50**).

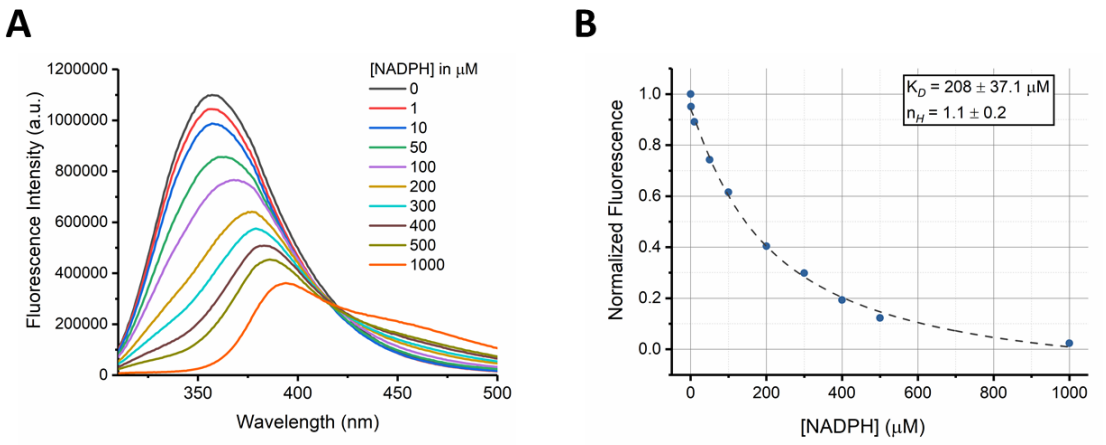

Figure 50 Titration spectra of tryptophan fluorescence in the presence of the denoted NADPH concentrations upon excitation at 280 nm (**A**). Plot of the normalized fluorescence maxima at 350 nm against the administered NADPH concentration (**B**). The intensity of the data point in absence of NADPH was set to one and the remaining data points were scaled accordingly. The data points were fit by a Hill equation and the parameters of the fit are given in the inset. Data are mean ± S.D. of n = 3 experiments.

Figure 50 A shows the emission spectra of a tryptophan solution titrated with varying amounts of NADPH. These spectra are practically indistinguishable from the spectra recorded for the NADH titration (**Figure 48 A**). It seems rather intuitive that NADPH produces the same signal with a tryptophan solution as NADH, since they are chemically very similar and spectrally indistinguishable and the quenching effect on tryptophan fluorescence does not differ between these two compounds. The maxima are plotted against the applied NADPH concentration and the resulting data was fit by a Hill equation (**Figure 50 B**). The determined

dissociation constant (K_D = 208 ± 37.1 μM) is, however, about twice as high as the constant obtained from the NADH titration (K_D = ~80 μM), indicating that the interaction between tryptophan and NADH is of higher affinity than the interaction with NADPH. The Hill parameter is again in the order of magnitude of one, indicating no cooperativity.

The experiments carried out on the tryptophan solutions, further substantiated the assumption, that a tryptophan residue is responsible for the interaction of the nucleotides and the iRFP713 protein, as these solutions showed a similar behavior in presence of the various nicotinamides as the full protein. For NADH and NADPH both iRFP713 as well as the amino acid solution showed a behavior that seems to stem from an energy transfer between tryptophan and NADH (Cao, Wallrabe, Siller, Rehman Alam, & Periasamy, 2019), while the oxidized congener NAD^+ also quenches iRFP713 and tryptophan in solution, with the notable difference that 10- to 20-fold larger concentrations of NAD^+ are required to produce a significant effect.

5.3 NADH in PBS

To ascertain that the signal that was detected upon 320 nm excitation around 850 nm did indeed portray the 2nd order diffraction of NADH fluorescence, a solution of NADH in PBS buffer was examined (**Figure 51**).

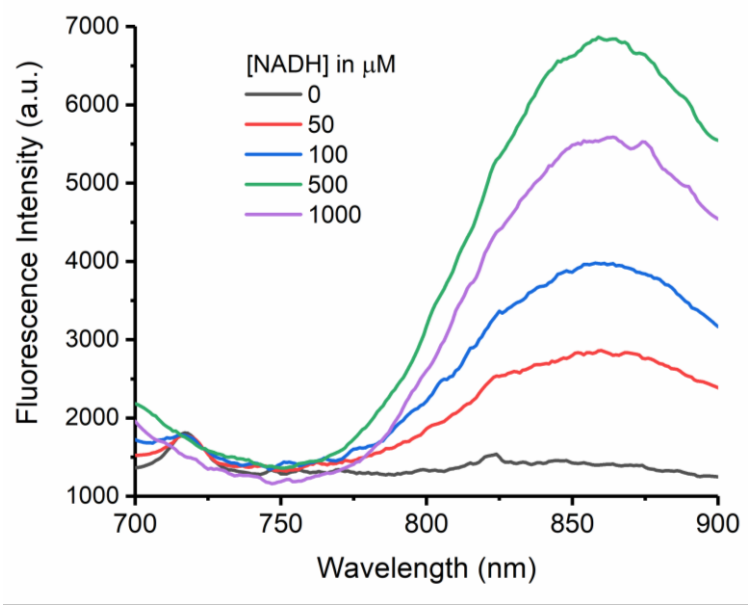

Figure 51 Fluorescence emission spectra of PBS buffer (pH 7.4) containing the denoted amounts of NADH. Excitation wavelength was set to 320 nm.

The fluorescence spectra of NADH in PBS buffer show a broad peak around 850 nm after excitation at 320 nm (**Figure 51**). The intensity is increasing until the concentration of 500 µM NADH (red curve), while the intensity for 1 mM NADH (purple curve) has already declined again. This is the second order diffraction of the intrinsic NADH fluorescence, which occurs around 460 nm in the first order (Joseph R. Lakowicz, 2006). In contrast to the observed emission of iRFP713 in the presence of NADH, the NADH fluorescence increases with increasing concentration of the nucleotide. Noticeably, the arising band in the 850 nm region of the iRFP713 emission profile can be explained by the second order diffraction signal of the autofluorescence of NADH in the Fluoromax-2 instrument, showing the same spectral characteristics.

For a good NADH sensor, the protein should be able to exclusively react to its target molecule while showing no dependence on similar nucleotides, to achieve a specific, reliable signal. iRFP713 itself, however, due to the lack of a unique binding site is not capable of discriminating sharply between NADH, NAD^+ and NADPH, with only the oxidized congener NAD^+ requiring higher concentrations to be effective, as the data above have shown. However, the different concentration ranges, in which the partners of the NADH/NAD^+ redox couple exert their effect,

represent a good starting point to develop more sophisticated constructs based on the "FRET-augmented tryptophan sensor" concept. If it were possible to engineer a more specific sensor response, e.g., based on the transmission of conformational changes of a specific binding domain upon binding of a compound to the conformation of the tryptophan-based FRET augmentation sensor, a novel and attractive sensor concept could be established. In order to facilitate the specificity of the response of the sensor, a domain, which would introduce NADH binding sites in close proximity to the chromophore, should be utilized for the design of a specific NADH sensor. Borrowing the idea from the already established NADH sensors, we hypothesized that a protein constructed from the iSplit variant of iRFP713 (Filonov & Verkhusha, 2013), fused with bacterial Rex domains, which would confer the sensitivity for NADH, would exploit the sensing mechanism as seen in the parental iRFP713, but hopefully with an exclusively specific response to NADH. We thus undertook the task of designing a new NADH sensor, based on a far-red fluorescent protein.

5.4 Bili-Sense

For a new far-red fluorescent NADH sensor a similar design to the existing sensors described above, in which a Rex tandem dimer is interspersed with the fluorescent reporter protein (Bilan et al., 2014; Hung et al., 2011; Zhao et al., 2015, 2011) was chosen. For the new sensor, the fluorescent probe is also composed of two domains instead of one cyclically permuted FP in the existing [NADH] or [NADH]/[NAD^+] sensors (Buhrke et al., 2016; Chiang, Li, & Truong, 2006). These two domains, PAS and GAF comprise the chromophore-binding domain of the iRFP713, in which the chromophore biliverdin is bound to the PAS domain and embedded in the GAF domain, therefore, substantial fluorescence will only occur, when both domains interact (Filonov & Verkhusha, 2013; Lamparter et al., 2004). The splitting of the PAS and GAF domains was supposed to reduce background fluorescence and thus enhance the dynamic range of the sensor. The resulting structure of the sensor, therefore, was designed to exhibit alternating fluorophore-

associated and Rex domains, leading to the final PAS-Rex-GAF-Rex construct (**Figure 52 C**).

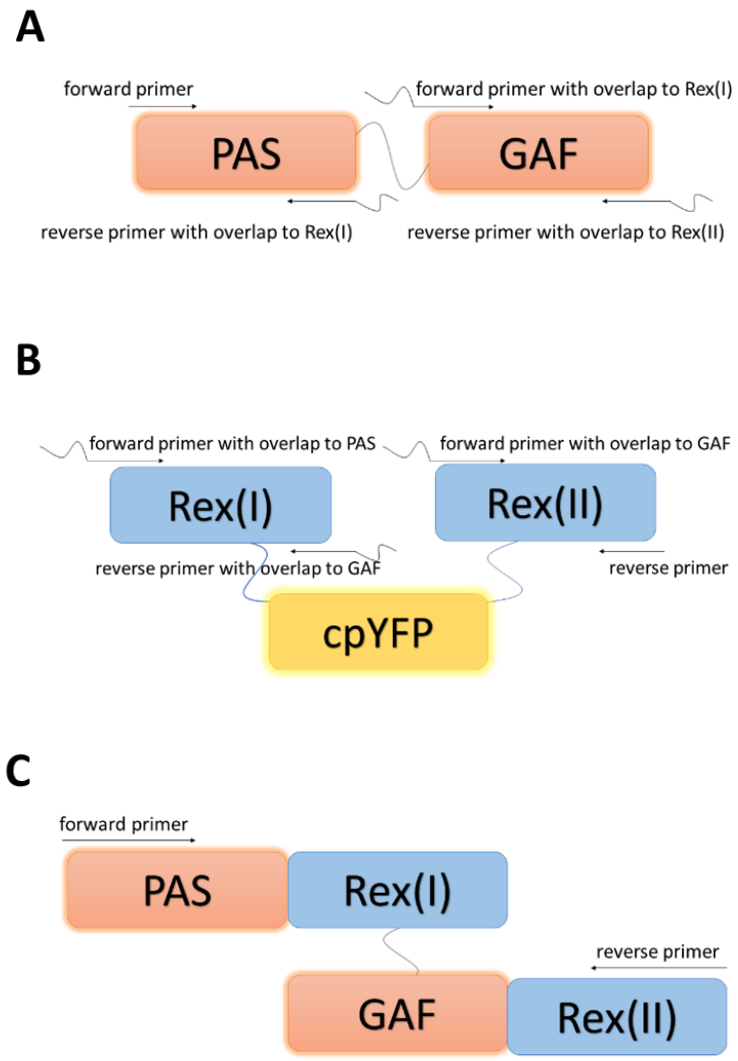

Figure 52 Scheme of the construction of Bili-Sense. The cDNA sequences of PAS and GAF domains were replicated by PCR using appropriate primers, which share an overlap to the next domain to be inserted for design of the sensor (**A**). Linkers between domains are represented by curved lines. Analogous PCR schemes were carried out with the Rex subdomains using the Frex cDNA as a template (**B**). In further PCR experiments, the cDNAs of two or more domains were added to a reaction mixture to generate the full-length cDNA sequence of the PAS-Rec-GAF-Rex or Bili-Sense sensor by recombinant PCR using the appropriate flanking primers, in order to generate the final construct (**C**).

The sensor's cDNA was constructed via recombinant PCR based upon the iRFP713 PAS and GAF domains, as well as the Rex subdomains of Frex, of which the general scheme is outlined in **Figure 52**. In a first set of PCR experiments the cDNAs of the PAS and GAF domain were replicated by primers that carried an overlap to the first Rex subunit for PAS and an overlap to both the first and second Rex subunit for the GAF domain cDNAs, respectively (**Figure 52 A**). The sequences of the NADH-binding domains were lifted using the Frex cDNA as a template. Here, the cDNA of the first Rex subunit was elongated with primers generating an N-terminal overlap to the PAS subunit and a C-terminal overlap to the GAF subunit. The second cDNA of a truncated Rex subunit was generated with primers generating an N-terminal overlap to the GAF domain cDNA (**B**). The final construct was generated by recombinant PCR of the whole sequence with the appropriate flanking primers (**C**). The generated construct was verified by sequencing and subcloned into various expression vectors. The sensor was termed Bili-Sense.

5.4.1 Expression of Bili-Sense

Bili-Sense was expressed in different *E. coli* cell lines optimized for recombinant protein expression. For one, an expression system based on the *E. coli* endogenous T5 RNA-polymerase was chosen, based on good previous experience with recombinant expression of iRFP713 and mutants thereof (Buhrke et al., 2016; Velázquez Escobar et al., 2017). The plasmid carrying the cDNA of the Bili-Sense sensor (pQE81L with an ampicillin resistance) was cotransformed with a plasmid (pQE81L with a kanamycin resistance) harboring the gene for the human heme oxygenase 2 (hHOX2), which is necessary for chromophore (biliverdin) generation in *E. coli* from the readily available precursor heme, in order to effectively form the desired holoprotein *in vivo*. For another approach, the cDNA of the sensor was subcloned into various vectors carrying a T7 promoter. The T7 RNA polymerase recognizing this promoter is not endogenous to *E. coli*, though there are multiple expression strains commercially available, which were genetically modified to produce said polymerase. For holoprotein production with T7 promoter vectors, there were two general approaches. For one, the cDNA was subcloned into the first

multiple cloning site of a bicistronic vector, while the gene for the heme oxygenase was cloned into the second multiple cloning site (pDuet vector constructs, Novagen/Merck Millipore, U.S.A./Germany). For the other approach, again a co-transformation was carried out, in which the cDNA of the heme oxygenase was introduced to the cell host by a separate plasmid vector (pQE81L). This vector was firstly combined with a vector carrying the Bili-Sense cDNA under a rhamnose-inducible promoter (pJOE, (Stumpp, Wilms, & Altenbuchner, 2000)), offering the advantage of separate induction of the expression of the sensor and the heme oxygenase. In order to test the effect of the location of the His-tag (N- or C-terminal) on expression and folding of the target protein, the cDNA was introduced into a T7 promoter-based vector with the His-tag fused to the C-terminus of the target protein rather than the N-terminus, as in the other utilized vector constructs (pET27b). These constructs were introduced into various *E. coli* cell strains and the combinations of plasmids and constructs are given in **Table 7**.

Table 7 Conditions for expression of Bili-Sense. Given are the various vectors, cell lines, media and expression temperatures tested. Specific features of the expression systems are denoted.

Vectors	Cell Line	Medium	Expression Temperature	Feature
Bili-Sense pQE + hHOX2 pQE	NEB Turbo	Luria-Bertani (LB)	37 °C 30 °C 21 °C	endogenous T5 RNA-polymerase
		Terrific broth (TB)	37 °C 30 °C 21 °C	
Bili-Sense pQE + hHOX2 pQE	BL21(DE3)pLysS	LB	37 °C 30 °C 22 °C 18 °C	endogenous T5 RNA-polymerase
		TB	37 °C 21 °C	
Bili-Sense pQE + hHOX2 pQE	Rosetta(DE3)pLysS	LB	37 °C 30 °C 21 °C	endogenous T5 RNA-polymerase
		TB	37 °C 30 °C 21 °C	
Bili-Sense pRSF(1) hHOX2 pRSF (2)	BL21(DE3)pLysS	LB	37 °C 30 °C 21 °C	bicistronic vector
		TB	37 °C 30 °C 21 °C	
			37 °C	

Bili-Sense pJOE + hHOX2 pQE	BL21(DE3)pLysS	LB	30 °C 21 °C 37 °C	rhamnose-inducible promoter
		TB	30 °C 21 °C	
Bili-Sense pJOE + hHOX2 pQE	Rosetta(DE3)pLysS	LB	37 °C 30 °C 21 °C 37 °C	rhamnose-inducible promoter
		TB	30 °C 21 °C	
Bili-Sense pET27b + hHOX2 pQE	BL21(DE3)pLysS	LB	37 °C 30 °C 21 °C 37 °C	C-terminal His-Tag
		TB	30 °C 21 °C	
Bili-Sense pET27b + hHOX2 pQE	Rosetta(DE3)pLysS	LB	37 °C 30 °C 21 °C 37 °C	C-terminal His-Tag
		TB	30 °C 21 °C	

In a first set of test expressions, the cDNA for the Bili-Sense sensor was cloned into the pQE81L vector, co-transformed with the hHOX2 pQE81L vector and expressed in two different host strains, BL21(DE3)pLysS and Rosetta(DE3)pLysS. The expressions were carried out in terrific broth (TB) medium either at 37 °C or 18 °C. These specific expression temperatures were chosen, since 37 °C is an optimal growth temperature for *E. coli* as well as the temperature optimum for generation of the human heme oxygenase, while lower temperatures are advantageous for protein folding, leading to more functional target protein and less misfolding. The experiments showed brightly green cultures for the 37 °C cultures, while the ones kept at lower temperature were only slightly green, indicating differing chromophore synthesis between cultures as predicted. However, purification attempts to obtain the target protein from the cell pellets of these cultures resulted in very low yields pointing at almost no expression of the target protein.

Since, judged from the green color of the cultures, the production of biliverdin did not appear to be the bottleneck of the expression experiments, it seemed likely that the inducer IPTG may have disproportionately triggered chromophore synthesis, but only insufficiently the synthesis of the sensor protein. Therefore, it seemed reasonable to establish a system in which the expression of the chromophore-generating hHOX2 and the expression of the sensor itself could be targeted independently. For this, the cDNA of Bili-Sense was subcloned into a plasmid carrying a rhamnose-inducible promoter (pJOE). The expression was, again, carried out at different temperatures and the obtained cultures showed a bright green color 24 hours after induction. The cultures at 37 °C showed the greatest coloration and the pellets from these cultures were investigated for the desired protein.

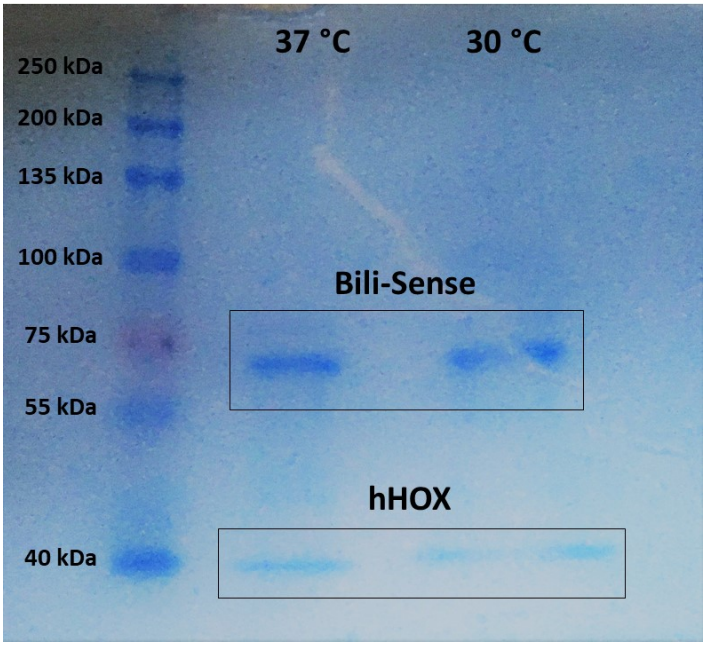

Figure 53 Coomassie-stained SDS-PAGE gel of expression cultures kept either at 37 °C or 30 °C for Bili-Sense pJOE & hHox2 pQE81L in Rosetta(DE3)pLysS. The pellets derived from the cultures were lysed and the lysate directly loaded into the gel. The cultures were evaluated for target protein expression 24 hours after induction of expression. The gel was stained and de-stained as described in the Materials & Methods section. The successful expression of Bili-Sense is indicated by a strong protein band at circa the same height as the marker band corresponding to 75 kDa (Protein Marker VI, *Applichem*). The second strong band corresponds to the 40 kDa band of the utilized marker and represents the likewise overexpressed heme oxygenase 2, which has a molecular weight of 41 kDa.

SDS-PAGE analysis of the pellets of cell cultures kept at 37 °C and 30 °C, induced and after 24 hours of expression exhibit a strong band at around 75 kDa, corresponding to the Bili-Sense protein (**Figure 53**). Another band slightly of lower intensity is found around 40 kDa, corresponding to hHOX2. The high intensity of these target bands over the very low background signal from endogenous *E. coli* proteins indicated sufficient protein production, and hence purification from cultures kept at these optimized conditions was carried out. However, the IMAC (immobilized metal ion affinity chromatography) purification of the protein from the cell pellet only yielded low amounts of holoprotein (with the BV cofactor integrated properly), as indicated by low coloration of the purified protein. Hence, the brightly green appearing culture medium was also examined

for target protein after 24 hours of expression at 37 °C. By fluorescence spectroscopy, characteristic spectral traces of the Bili-Sense protein and a purification procedure for the protein from the medium were obtained.

The culture medium was separated from the cell pellet by centrifugation at 5,000 x *g* for 10 minutes at 4 °C. The supernatant, which was supposed to be analyzed for protein content, was retrieved, and treated with ammonium sulfate to a final concentration of 80 %, while the pellet as contrary to the first purification was discarded. The treatment of the supernatant with ammonium sulfate leads to the precipitation of the protein. In order for the precipitation of the target protein to be complete, the solution was kept at 4 °C for an hour. The solution was again centrifuged (5,000 x *g*, 10 minutes, 4 °C) and resuspended in PBS buffer. The solution was dialyzed against PBS buffer overnight, in order to remove remaining $(NH_4)_2SO_4$ and thus allowing the protein to resolve in the buffer. The dialyzed solution was then purified via Cobalt affinity chromatography as described in the Materials & Methods section. The protein was eluted with 300 mM imidazole buffer, desalted by dialysis, aliquoted and kept frozen at 4 °C.

This protein purified from the expression system with the rhamnose-inducible promoter for the sensor and the IPTG-inducible promoter for the hHox2 was the starting point for the spectroscopic characterization of the sensor.

5.4.2 UV-Vis Spectroscopy of Bili-Sense

The purified sensor protein was characterized by UV-Vis absorption spectroscopy. In order to identify which part of the absorption signal is reliably stemming from the holoprotein, the spectrum of apoprotein was also recorded. To generate the apoprotein, the sensor was expressed as described previously; however, the chromophore-generating heme oxygenase (hHOX2) was not present in these experiments, leading to non-chromophorylated protein.

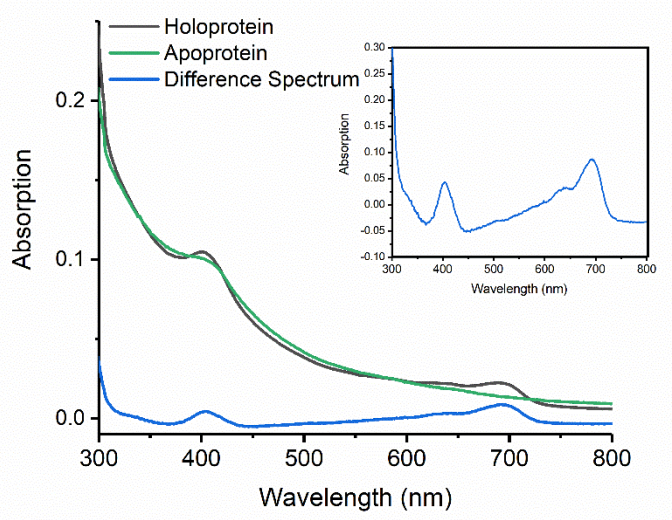

Figure 54 UV-Vis spectra of the Bili-Sense holo- (black curve) and apoprotein (green curve), and the respective difference spectrum (blue curve). Shown in the inset is the difference spectrum enhanced by a factor of ten.

The UV-Vis spectra show the absorption of the Q band of the biliverdin chromophore around 700 nm in the holoprotein (black curve), while it is missing in the apoprotein (green curve) (**Figure 54**). The absorption in the 400 nm region is also more intense for the chromophore-containing protein, in line with the Soret band of the chromophore. The absorption of the apoprotein is non-zero, likely since the protein is co-purified with a certain amount of NADH bound, which also absorbs in that wavelength region. For a better visualization, the difference spectrum is depicted (blue curve), which clearly exhibits the common biliverdin bands, with a band around 405 nm and a slightly more intense band around 600 – 700 nm. These bands are characteristic for porphyrins (Gouterman, 1978). The band in the near ultraviolet represents a strong $S_0 \rightarrow S_2$ transition, the so-called Soret band (Soret, 1883). The $S_0 \rightarrow S_1$ transition is mostly weak in porphyrins and is located between 550 and 700 nm. It is represented by the so-called Q bands (Gouterman, 1978; Weiss, 1972). Biliverdin is an open-chain tetrapyrrole break-down product of heme metabolism and thus structurally related to the family of porphyrins. In prototypical biliproteins, such as iRFP713, the parental protein to the sensor, both of these bands occur, however, the intensity of the Q band is normally higher than the intensity of the Soret band. Furthermore, the absorption maximum of iRFP713 is located at 692 nm (Filonov et al., 2011).

This pattern can also be found in the Bili-Sense absorption spectra, where the Q band absorption is broad, with a peak at 695 nm. The absorption band at 280 nm indicates the presence of protein, since it stems from absorption of particular amino acids, mainly tryptophan. The total protein concentration can also be estimated from the absorption at 280 nm and a calculated extinction coefficient based on the amino acid sequence (48,040 M^{-1} cm^{-1}, ProtParam). This approach yields a total protein concentration of 2.3 μM. For comparison, the holoprotein concentration was also estimated by the absorption maximum at 695 nm. For reference, the extinction coefficient of iRFP713 was used (85,000 M^{-1} cm^{-1}) (Filonov et al., 2011), assuming similar spectral properties of the biliverdin chromophore in both, iRFP713 and Bili-Sense, the holoprotein concentration can be estimated to 120 nM, indicating that only 5 % of the total protein is carrying a chromophore. This value is further supported by analysis of the absorption maximum in the Soret Band and the corresponding extinction coefficient of free biliverdin (39,900 M^{-1} cm^{-1}) (Shu et al., 2009), since this approach yields a concentration of 130 nM.

The intensity of the 280 nm band is greatly enhanced in comparison to the biliverdin bands, further corroborating the presence of high amounts of protein from which only a low percentage carries the chromophore.

5.4.3 Fluorescence Spectroscopy

For further characterization of the Bili-sense protein, the sensor's fluorescence excitation and emission spectra were recorded (**Figure 55**). For the recording of the spectra the samples were concentrated to a total protein concentration of 4 μM, corresponding to 220 nM holoprotein.

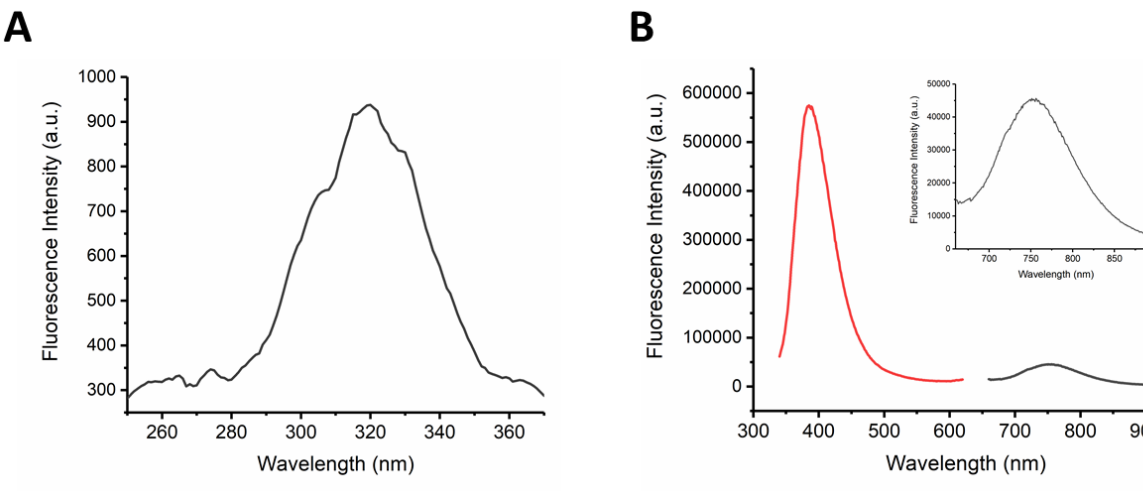

Figure 55 Excitation spectrum of the designed sensor Bili-sense (**A**). The emission wavelength was set to 750 nm and the spectrum was recorded over the shown wavelength range. Emission spectrum of Bili-Sense after excitation at 320 nm in the short (340 – 630 nm) and long (660- 900 nm) wavelength region (**B**). Comparison of the emission spectra after excitation with 320 nm in the short (red curve) and long (black curve, corresponding to 2nd order diffraction signal of tryptophan fluorescence) wavelength region of the spectrum show an about 12 times higher fluorescence intensity in the short wavelength region. Shown in the inset is the emission spectrum in the long wavelength region on an enlarged scale. Concentration of Bili-Sense was adjusted to 4 μM (OD_{280}) in PBS buffer.

In a first set of experiments, excitation spectra with emission detection set to 750 nm were recorded, since the biliverdin chromophore is known (from properties of iRFP713) to emit in this region (**Figure 55 A**). These spectra indicated an excitation maximum of the protein around 320 nm, the wavelength that was previously used as excitation of iRFP713 for the NADH titrations. When 320 nm light was used for excitation, the spectrum shown in **Figure 55 B** was recorded, which exhibits a very broad emission band centered around 750 nm. This band seems to be only composed of the 2nd order diffraction of the tryptophan fluorescence in the used Fluoromax-2 instrument, which was already observed in the iRFP713 spectra. In contrast to the iRFP713 fluorescence spectra, no distinct chromophore peak at 713 nm was observed, and recording of the emission spectra in the wavelength region between 300 and 500 nm (**Figure 55 B**) showed clear characteristics of tryptophan fluorescence, which verified that the spectral features in the red region are merely due to the 2nd order diffraction of tryptophan

fluorescence. The intensity of the spectra in the first order diffraction (around 380 nm) and second order diffraction (around 750 nm) varies about 12-fold.

In order to determine whether the sensor carried the biliverdin chromophore, the protein was also investigated by excitation at 660 and 680 nm, which should excite an embedded biliverdin chromophore via the Q band (**Figure 56**).

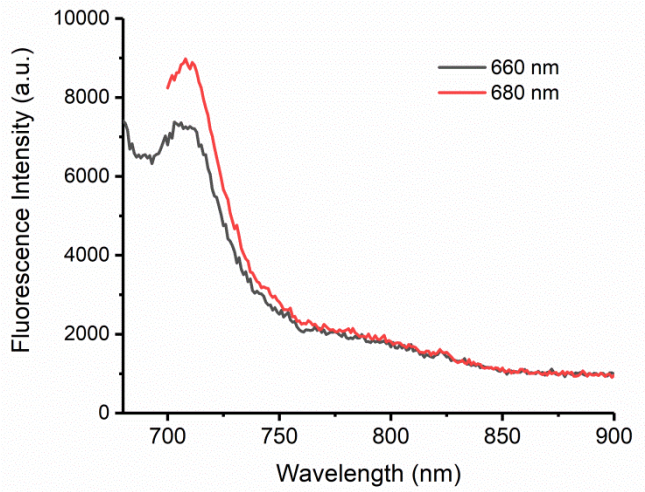

Figure 56 Emission spectra after excitation with 660 nm (black curve) and 680 nm (red curve). Concentration of Bili-Sense was adjusted to 4 µM (OD_{280}) in PBS buffer.

The emission spectra shown in **Figure 56** exhibit the specific biliverdin emission peak for both excitation wavelengths positioned at 710 nm, very close to the emission peak of the parental iRFP713 (Filonov et al., 2011). This indicates that the purified sensor is at least partially chromophorylated in order to detect biliverdin-specific fluorescent traces.

In order to improve chromophorylation of the protein and thereby enhancing the contribution of the biliverdin fluorescence within the broad background of 2nd order diffraction around 750 nm of Bili-Sense holoprotein, the expression was carried out at lower temperatures as well (compare **Table 7**). The corresponding proteins were purified from these cultures and they were analyzed by fluorescence spectroscopy (**Figure 57**).

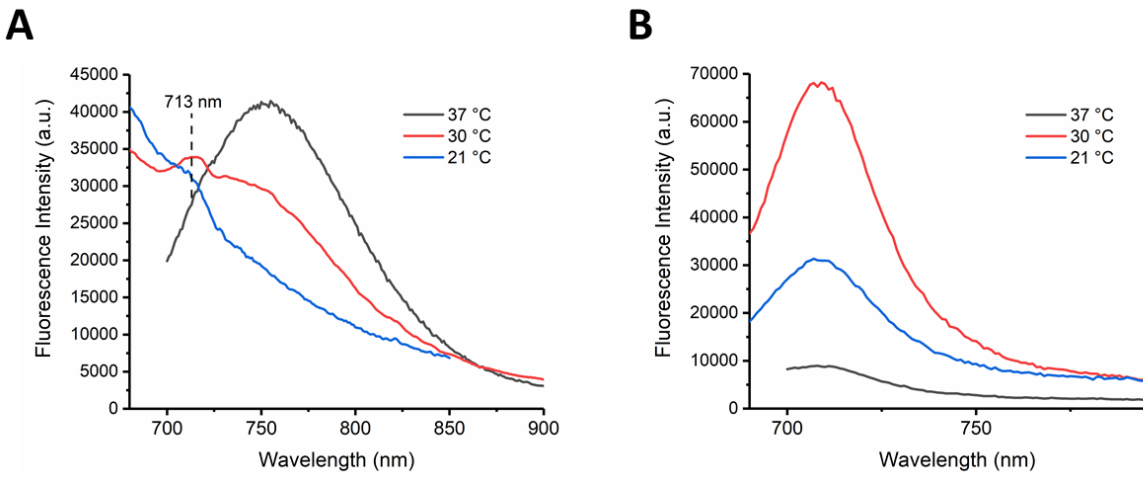

Figure 57 Emission spectra in the wavelength region between 690 – 900 nm after excitation at 320 nm for Bili-Sense purified from cultures kept either at 37 °C (black curve), 30 °C (red curve) or 21 °C (blue curve) (**A**). Emission spectra in the wavelength range between 690 – 800 nm after excitation at 680 nm for the three different expression temperatures, 37 °C (black curve), 30 °C (red curve) and 21 °C (blue curve) (**B**). Protein concentration was adjusted to 4 µM (OD_{280}) in PBS.

When the protein purified from cultures grown at 21 °C or 30 °C was investigated, apparent differences appeared in the respective spectra, most noticeably upon excitation with 320 nm and 660 nm (**Figure 57**). In **Figure 57 A** the emission spectra upon excitation at 320 nm for proteins obtained from three different expression temperatures are shown. The spectrum for the protein expressed at 37 °C shows the already discussed broad 2nd order diffraction of tryptophan fluorescence centered around 750 nm. The broad fluorescence emission is also observable for protein purified from expression cultures grown at 30 °C; however, the intensity of the fluorescence is slightly weaker. The protein purified from an expression culture grown at 21 °C exhibits the lowest contribution of the 2nd order diffraction signal. Notably, both spectra of the protein expressed at 21 °C and 30 °C show a pronounced shoulder or even a small peak at 713 nm, indicative of the biliverdin chromophore. This indicates that the emission in the red spectral range can at least partially be attributed to the biliverdin chromophore and not just to the spectrometer artefact.

In **Figure 57 B** the emission spectra of the corresponding proteins are plotted after excitation at 680 nm. All three spectra show the characteristic 710 nm band resulting from the direct excitation of the chromophore. However, notably, the

spectrum of the protein from 30 °C expression exhibits an intensity about seven times higher than the protein sample retrieved from cultures kept at 37 °C. The protein retrieved from the 21 °C expression shows a medium intensity upon excitation at 680 nm. These findings suggest that the protein sample retrieved from cultures kept at 37 °C is only marginally consisting of holoprotein, with the majority being made up of apoprotein. The 2nd order diffraction signal of tryptophan fluorescence dominates the spectrum after excitation at 320 nm, while in the spectra of the other two expression conditions a discernible shoulder at 713 nm is observable. The spectra obtained upon 680 nm excitation support these findings and show that the protein obtained from the culture grown at 30 °C incorporated the highest amount of chromophore and exhibited the largest holoprotein fraction.

However, even with the slightly optimized chromophorylation in the samples from the 30 °C cultures, the signal in the red wavelength region upon 320 nm excitation will mainly be comprised of the 2nd order diffraction of tryptophan fluorescence.

In order to test if the newly designed sensor showed a specific answer towards NADH that was detectable as a change in fluorescence lifetime, the protein was examined in a different spectrometer for time-resolved fluorescence detection. This setup is equipped with a blazed grating that suppresses the 2nd order diffraction of tryptophan fluorescence emission. The time-resolved spectra obtained with this spectrometer showed a biliverdin-specific signal at 713 nm upon 320 nm excitation (vide infra), which thus confirmed that some part of the signal around 750 nm in the spectrometer without blazed grating must contain signatures of a biliverdin-specific signal.

5.5 Time-Resolved Fluorescence Spectroscopy

Time-resolved fluorescence spectroscopy was utilized in order to clarify the interaction between the three components of the energy transfer mechanism initially noticed in iRFP713, which might also be present in Bili-Sense considering that it contains the tryptophan residues and the chromophore biliverdin as well.

The time-resolved measurements consisted of three data sets. First the sensor was excited directly at 405 nm by a pulsed laser source. This experimental scheme excludes the effects of an energy transfer process from tryptophan residues to the chromophore, since this leads to a direct excitation of the biliverdin chromophore via the Soret band. By observing the corresponding fluorescence in the wavelength region between 640 and 800 nm, it can be observed if addition of NADH still exhibits an effect on the apparent lifetime of the biliverdin fluorescence.

The second scheme used excitation at 280 nm to excite the tryptophan residues of the protein. Capturing the resulting fluorescence, again, in the biliverdin emission range between 640 and 800 nm should reveal, if sensitized emission of the chromophore by excitation energy transfer from tryptophan occurs. Furthermore, the effect of added NADH on the time-dependent fluorescence is investigated.

Third, as a control, tryptophan in aqueous solution is excited at 280 nm and the fluorescence is monitored between 340 and 460 nm, and the effects of added NADH on the fluorescence intensity and lifetimes are observed.

5.5.1 Fluorescence of Bili-Sense

Bili-Sense was excited with a 405 nm pulsed laser source (PLS-300, Picoquant, Berlin, Germany) and the fluorescence decay curves were recorded from 640 – 800 nm with a multi-channel detector (PML-16C, 16 spectral channels). In these experiments the time-resolved fluorescence of the biliverdin chromophore by direct excitation via the Soret band (S_0-S_2 excitation) was captured (**Figure 58**).

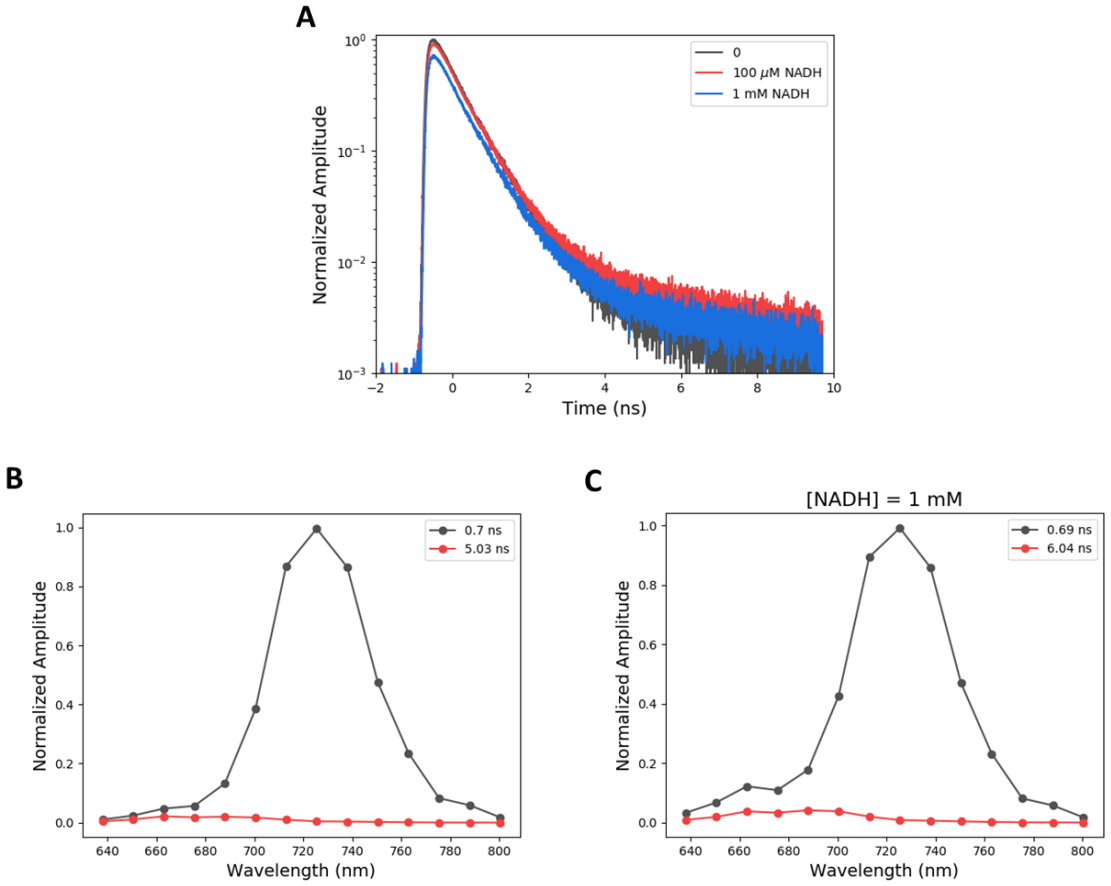

Figure 58 Fluorescence decay curves at the 710 nm emission maximum of Bili-Sense after excitation with a pulsed 405 nm laser in the absence (black curve) or presence (colored curves) of NADH (**A**). Decay associated spectra (DAS) of the sensor in the absence (**B**) or presence (**C**) of 1 mM NADH. The total amplitude for both components of each DAS was normalized to one ($\alpha_1 + \alpha_2 = 1$).

Figure 58 A shows the fluorescence decay curves obtained in this experiment. The difference in amplitude for 100 µM NADH is rather small and about 20 % reduction is seen in the presence of 1 mM NADH. **Figure 58 B** & **C** exhibit the DAS for the whole spectral range from 640 to 800 nm, and indicate that biliverdin fluorescence decays nearly monoexponentially with a lifetime of 700 ps (black curve), irrespective of whether NADH is present or not. This indicates that the about 20 % reduction of the fluorescence amplitude by 1 mM NADH is due to e.g. static quenching, but without an effect on fluorescence lifetime. A small contribution of a long decay component with about 5 ns (see red curve in **Figure 58 B** & **C**) is present in both DAS shown, which only shows an increase from 5.03 to 6 ns in the presence of 1 mM NADH. The peak of the fast component in the DAS lies at around 720 nm, corresponding to the fluorescence maximum of the biliverdin

chromophore in iRFP-like proteins. The observed differences, taken together, indicate that NADH dos not influence the lifetime of the biliverdin chromophore and the reduced amplitude may either be due to static quenching, or the effect could be explained by chromophore bleaching during the long-lasting single photon counting experiment (30 minutes per measurement).

In order to test the hypothesis, whether there is excitation energy transfer from tryptophan residues to the embedded biliverdin chromophore, and whether the emission of tryptophan residue(s) rather than that of biliverdin itself is affected by certain nicotinamides, time-resolved experiments were conducted with a 280 nm pulsed diode as excitation light source, and the fluorescence decay curves were recorded from 650 – 820 nm. The decay-associated spectra from these decay curves are shown in **Figure 59**.

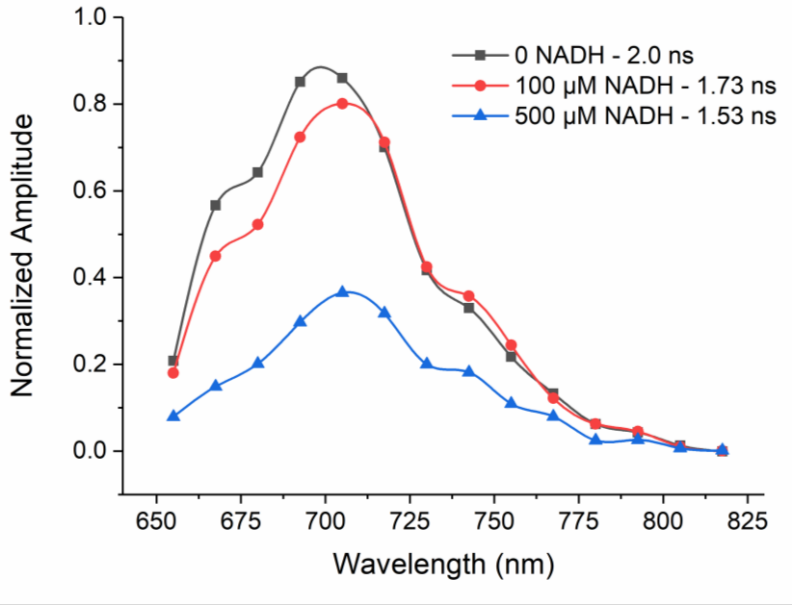

Figure 59 DAS derived from a global fit of the fluorescence of the Bili-Sense sensor with a monoexponential model in the absence (black curve) or presence (colored curves) of NADH. Pulsed excitation was performed with a 280 nm diode laser. The DAS amplitudes were set to zero at the highest wavelength.

The DAS shown in **Figure 59** verify the presence of an excitation energy transfer from tryptophan residues (directly excited by the pulsed 280 nm laser) to the biliverdin chromophore (sensitized emission recorded between 650 and 820 nm). The black curve depicts the long wavelength emission in the absence of NADH. Compared to 405 nm excitation, the DAS are markedly different. The maximum of

the spectrum lies at around 713 nm with two shoulders, one at 675 nm and one at 750 nm. The spectrum is of course different from the time-integrated experiments done with the Fluoromax-2 spectrometer, as the 2nd order diffraction signal from tryptophan fluorescence is suppressed by the utilized detector (by blazed gratings), and only the true emission bands contribute to the recorded signal. Also, the lifetimes are different from those measured with 405 nm excitation, starting with 2 ns, which is markedly different from the ~700 ps fluorescence lifetime of iRFP-like proteins (seen with direct 405 nm excitation, Figure 59), and rather approximates to the characteristic lifetime of tryptophan fluorescence in aqueous solution (2.8 nm, see below) (Cao et al., 2019). If FRET occurs, the characteristics of tryptophan fluorescence (donor) would be transferred to the lifetime of the FRET acceptor (biliverdin) and determine the lifetime of the overall ET. The observation of a clear biliverdin emission band in the DAS also further clarify that the sensor signal and response is not just a spectrometer artefact, but clearly the biliverdin signal contributes to the NADH-dependent response. The band structure of the emission is conserved upon addition of NADH, while the total amplitude decreases as does the fluorescence lifetime. Concomitant with the decrease in the amplitude, the time-constant of the observed process is reduced from 2 ns in the absence of NADH to 1.53 ns in the presence of 500 μM NADH, leading to a further decrease in observable fluorescence. This indicates that quenching of tryptophan fluorescence in the Bili-sense protein by NADH is due to a superposition of static and dynamic quenching (red and blue curve). The time constant observed in this experiment is theoretically constituted of the whole excitation energy transfer from the excited tryptophan to the biliverdin chromophore and subsequent emission from the chromophore. In the previously proposed model of interaction of the sensor with NADH, it was hypothesized that light excites tryptophan residue(s) in the protein backbone, which transfer their excitation energy towards the biliverdin chromophore. The chromophore accepts the energy via transfer into the Soret band, and finally emission of fluorescence from the Q band of the chromophore occurs. When NADH is present, the nicotinamide competes for this energy transfer process and offers an alternative relaxation pathway, thereby reducing the efficiency and likelihood of resonance energy transfer. Here, it is critical to determine, by which process (static or dynamic) the fluorescence of tryptophan is quenched by NADH. If the quenching process were purely static, the

lifetime of tryptophan fluorescence would remain unchanged and only the amplitude would decrease. Thus, the fluorescence lifetime observed in the Bili-Sense experiments shown in **Figure 59** hints at a superposition of these two different quenching mechanisms.

5.5.2 Fluorescence of Tryptophan

In order to scrutinize the mechanism by which the fluorescence of tryptophan in aqueous solution is quenched by NADH, time-resolved fluorescence measurements of tryptophan solutions titrated with NADH were carried out (**Figure 60**).

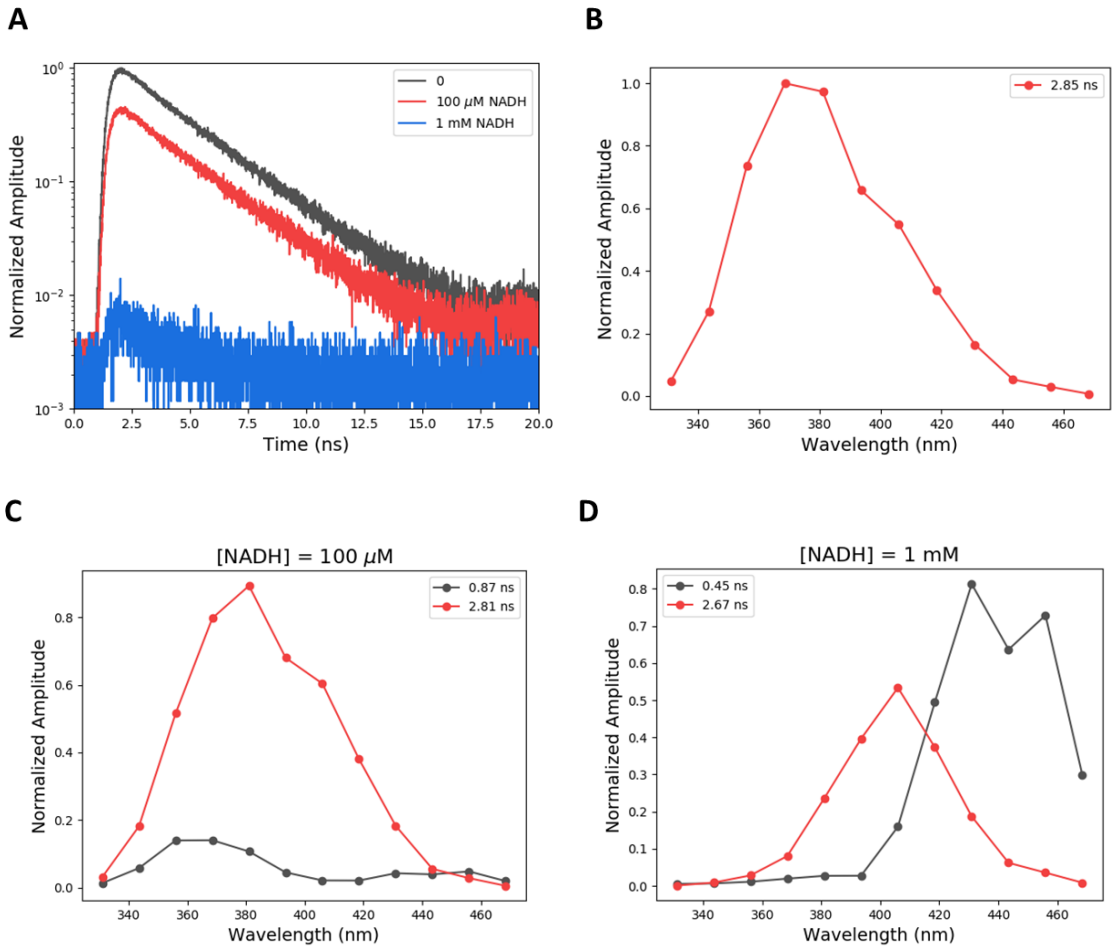

Figure 60 Fluorescence decay curves of a tryptophan solution after excitation with a pulsed 300 nm diode in the absence (black curve) or presence (colored curves) of NADH (**A**). The fluorescence amplitudes are normalized to the maximal value in absence of NADH. DAS spectra of the sensor in the absence (**B**) and presence of 100 µM (**C**) or 1 mM NADH (**D**). The amplitude for the

monoexponential fit (**B**) was normalized to one, for the biexponential fits (**C** & **D**) the sum of the amplitudes was normalized to one ($\alpha_1 + \alpha_2 = 1$).

The fluorescence decay curves in **Figure 60 A** clearly show that the quenching process by increasing NADH concentrations does not affect the dominant fluorescence lifetime of tryptophan, only a decrease of the fluorescence amplitude of tryptophan emission upon addition of increasing amounts of NADH can be seen, and tryptophan fluorescence drops to almost zero in the presence of 1 mM NADH (blue curve) making determination of the lifetime at 1 mM NADH difficult. The DAS in the absence of NADH were approximated well by a monoexponential fit of the respective fluorescence decay curve (**Figure 60 B**), corroborating that only one fluorescent species with a 2.9 ns time constant is present, which is in agreement with documented fluorescence lifetimes of tryptophan in aqueous solution (Joseph R. Lakowicz, 2006). Upon addition of NADH the decay curves show a minor second component, with a time constant of 0.9 ns in presence of 100 μm NADH and 0.5 ns in presence of 1 mM NADH (**Figure 60 C** & **D**), which, as already indicated, is difficult to resolve accurately. The fluorescence component with a time constant of about 0.5 ns is either caused by strongly quenched tryptophan, or a rotamer of tryptophan with a typical time constant of 500 ps (expected in the spectral range between 340 nm and 400 nm), or represents autofluorescence of NADH (expected between 400 – 470 nm), since the latter one is especially clearly visible from its characteristic spectral location in **Figure 60 D**. In the presence of 1 mM NADH, the autofluorescence of the NADH even shows a higher fractional amplitude than tryptophan. With differing amounts of NADH, the time constant of tryptophan fluorescence decay was stable, indicating that the quenching mechanism of NADH on tryptophan in solution is almost exclusively static. Therefore, the NADH-dependent effect on the fluorescence lifetime of the Bili-sense protein is most likely due to a different quenching mechanism. We hypothesize that the sensor protein, which carries two Rex subunits that rearrange upon NADH binding, alters its conformation upon binding NADH also within the split PAS-GAF part of the protein, in which the sensing tryptophan residues are located (McLaughlin et al., 2010; Sickmier et al., 2005; E. Wang et al., 2008). In effect, the rearrangement of the Rex subunits alters the spatial arrangement between the tryptophan residues

and the chromophore, with the distance change making the energy transfer more or less efficient and thus exerting a direct effect on the fluorescence lifetime.

Summarizing these experiments, it was confirmed that NADH does not exhibit any direct dynamic quenching effect on biliverdin fluorescence, as shown by direct fluorescence excitation via the Soret band of the chromophore. Therefore, the chromophore fluorescence is not dynamically quenched by the nicotinamide. The experiments on tryptophan in solution showed that the quenching of tryptophan fluorescence by NADH in solution is of static nature, since the lifetime remains constant upon addition of the nicotinamide. Thus, the decrease in lifetime recorded for the fluorescence of the sensor cannot be explained by the interaction of NADH and tryptophan alone. Though the tryptophan residue(s) of the sensor, however, do(es) interact with the applied NADH and their fluorescence is statically quenched, the binding of NADH to the Rex subunits is supposed to exert an additional effect: interaction of the sensor with NADH leads to structural changes, since Rex domains are known to induce conformational shifts in the associated protein (McLaughlin et al., 2010; Sickmier et al., 2005; E. Wang et al., 2008). These conformational shifts might alter the tryptophan-chromophore distance and/or the relative orientation of the two energy transfer partners, effectively leading to a NADH-dependent efficiency for the energy transfer process with an effect on the fluorescence lifetime.

The time-resolved measurements further corroborated the complexity of the sensor system, showing that the quenching mechanism is dependent on multiple components. The quenching process appears to be constituted of static quenching of tryptophan fluorescence (the sensor harbors three tryptophan residues, which might be differentially exposed to the solvent) and a dynamic effect on the biliverdin chromophore fluorescence exerted by NADH due to a structural effect which changes the energy transfer process in the protein. With this in mind, a sensor construct is at hand, which utilizes conformational sensitivity towards a specific compound to interfere with the FRET-augmented tryptophan sensing concept in terms of a specific signal: a change in fluorescence lifetime.

V Summary & Conclusion

Summary Part 1

The findings of the in-depth characterization of Frex showed that the sensor, in contrast to previously published data, is not solely reporting on NADH (Zhao et al., 2011). Given that concentrations are larger than 100 µM, NAD^+ is able to bind to Frex in a competitive fashion to NADH. Hence, the obtained signal of the Frex reporter is not exclusively tied to the present NADH concentration, but the concentration of the oxidized congener has to be taken into consideration for comprehensive evaluation of the signal. This is of great importance for the application of the sensor in bacterial cells, since the NAD^+ levels are generally in the millimolar range in these types of cells, which surpasses the 100 µM threshold at which the sensor is not significantly influenced by the NAD^+ concentration (Bennett et al., 2009; Tejwani et al., 2017; Zhou et al., 2011). Furthermore, the dynamic range of Frex is diminished in relation to the present NAD^+ concentration in an inversely proportional manner, which is intuitive, since Frex molecules with bound NAD^+ cannot interact with NADH, which effectively lowers the available sensor concentration, as is usual for competitive inhibitors (Wilkening et al., 2017; Zhao et al., 2011). Time-resolved experiments revealed that the fluorescence lifetimes decreased only marginally upon NAD^+ binding, indicating that the quenching mechanism is of static nature.

With these drawbacks and the need for corrections in mind, the application *in vivo* in *R. eutropha* cells made it possible to monitor the activity of the soluble hydrogenase qualitatively. Treatment of cell suspensions, either expressing the SH (strain HF798) or not (strain HF500), with hydrogen, the substrate of the SH, or helium, a blind control for gas treatment, which should induce no specific changes, showed the same initial response, an increase in fluorescence from the reporter protein. This increase corresponds to an increase in cellular NADH levels, which occurred in both utilized *R. eutropha* strains after treatment with either gas. Thus, this initial response did not allow for a discrimination between both cell strains,

since an increase in [NADH] can – first of all – be attributed to the disruption of the aerobic respiratory chain. Treatment of the cells with saturating hydrogen or helium removed all oxygen from the samples. In the respiratory chain, oxygen is reduced by NADH, which acts as electron donor. The loss of oxygen leads to an accumulation of NADH and concomitantly an increase in Frex fluorescence. This result of anaerobization contributes to the Frex signal, so the fluorescence intensity readout cannot be unambiguously attributed to the activity of the SH. This effect proved to be reversible as soon as the gas treated cells were exposed to air again.

However, a discrimination between the effects of general anaerobization and SH activity is possible, if the fluorescence intensity of Frex in a hydrogen treatment experiment is monitored over time. Here, it becomes apparent that the SH-expressing strain exhibits elevated fluorescence, and thus NADH levels, for a much longer time than the SH-deficient HF500 strain. The duration of elevated fluorescence stemming from Frex was directly linked to the presence and activation of SH in those cells. The duration of fluorescence was also proportional to the concentration of the H_2 substrate administered to the cells. Thus, a 10 % hydrogen-saturated cell suspension gave a shorter elevated fluorescence signal than a 50 % H_2-saturated cell suspension. Control experiments with *R. eutropha* cells devoid of SH, showed only a short increase in fluorescence upon treatment of these cells with saturating hydrogen as well as helium gas, which decreased almost instantly after re-exposure of the samples to the surrounding air (1 to 5 minutes) (Wilkening et al., 2019).

The experiments investigating possible pH deviations in the cells showed that the intracellular pH is kept very stable, and the signal cannot be explained by variations of this parameter. The Frex sensor thus proves a useful tool to monitor the SH activity in *R. eutropha* qualitatively.

Summary Part 2

The previously developed fluorescent NADH sensors, which were constructed for application in mammalian cells (Bilan et al., 2014; Hung et al., 2011; Zhao et al., 2015, 2011), are only partially suitable for implementation in bacteria due to their comparably higher intracellular NAD concentrations (Bennett et al., 2009; Tejwani et al., 2017; Zhao & Yang, 2012; Zhou et al., 2011). In an effort to tune the affinity of Peredox-mCherry, amino acid residues, which were considered important for the interaction of the sensor and the nicotinamide, were substituted by mutagenesis (Hung et al., 2011; Zhao et al., 2011). Mutation of these residues to glutamic acid lowered the affinity of the sensor substantially to values between 3.5 – 4.1 mM. Unfortunately, such affinities are too low for an application in bacterial cells. In another set of experiments, the selected amino acid residue from the first T-Rex subunit was exchanged for glutamine or tyrosine, which lowered the affinity slightly from 5 nM to about 20 or 80 nM respectively. These experiments indicated that the exchange of the chosen amino acids indeed alters the sensor's affinity, however none of the produced mutants exhibited a favorable affinity in the high micromolar range ($K_D \sim 100$ μM) (Bennett et al., 2009; Tejwani et al., 2017; Zhou et al., 2011).

For the generation of a new fluorescent NADH sensor for bacteria, it seemed advantageous to use a red to far-red fluorescent unit, due to their favorable properties, such as low scattering of the excitation/emission light and thus generally higher penetration depth, utilization of low cellular background absorption in the NIR window, and low excitation energy, leading to less photodamage in the tissue (Jobsis, 1977; Weissleder, 2001). Thus, we investigated the near-infrared fluorescent protein iRFP713, which was derived from bacteriophytochrome P2 from *Rhodopseudomonas palustris* (Filonov et al., 2011; Shcherbakova, Shemetov, Kaberniuk, Andrii, & Verkhusha, 2015). Titration of this fluorescent probe indicated the presence of an energy transfer process between (a) red-shifted tryptophan residue(s) and the biliverdin chromophore of the protein. Excitation of the protein's tryptophan residues at 320 nm leads to fluorescence emission at 713 nm, the emission maximum of the protein's biliverdin chromophore. Thus, it was hypothesized that the excitation energy is transferred

from the tryptophan residues of the protein to the biliverdin via the Soret band. After further internal conversion, light is emitted from the Q band of the chromophore at 713 nm. An energy transfer process between tryptophan and heme in proteins has previously been described in the literature. In fact, heme proteins seem to display almost no tryptophan fluorescence, since the EET between tryptophan and heme is so efficient (Fontaine et al., 1980; Kamal & Behere, 2001; Monni et al., 2015), indicating that an energy transfer between tryptophan and biliverdin is also plausible.

Remarkably, this EET process is disrupted upon addition of NADH to the protein. Quenching of tryptophan fluorescence by NADH has been described before (Jyothikumar et al., 2013; Luisi & Favilla, 1970; Torikata, Forster, Johnson, et al., 1979; Torikata, Forster, Neal, et al., 1979). This allows for a new sensor type, in which the florescence at 713 nm is recorded after excitation at 320 nm as a marker of the feasibility of the EET process, which is gradually decreased upon increasing NADH. The apparent affinity of iRFP713 for NADH as determined by Hill fits of the titration data (K_D = 144 ± 15.7 µM) is in the optimal range for application in bacterial cells. Furthermore, direct excitation of the biliverdin chromophore leads to emission spectra, which are not influenced by the present NADH concentration, but only dependent on the protein concentration itself. This would allow for a normalization of the fluorescence signal according to sensor concentration. Unfortunately, since iRFP713 does harbor specific NADH binding sites, this response of the protein is not unique to NADH, but also analogues such as NADPH alter the EET process.

In an effort to convert this FRET-augmented tryptophan fluorescence sensing concept into an exclusive response towards NADH, a new sensor construct was designed. In this sensor, the chromophore binding domains of iRFP713 (PAS & GAF) have been separated, as it was demonstrated that separate expression of these domains still can lead to functional fluorescent protein (iSplit) (Filonov & Verkhusha, 2013; Zlobovskaya et al., 2016). The PAS and GAF domains were interspersed with the NADH-binding Rex domains from *B. subtilis*, in order to generate the desired specificity for NADH. The corresponding sensor was expressed in *E. coli* and purified, albeit with low amounts of holoprotein. The

sensor was investigated by fluorescence spectroscopy and it was confirmed that the EET process determined for iRFP713 was conserved in Bili-Sense.

Further analysis of Bili-Sense by time-resolved fluorescence spectroscopy disclosed that NADH did not exert any dynamic quenching effect on biliverdin fluorescence, as indicated by the direct excitation of the chromophore via the Soret band. However, the quenching process of the sensor itself by NADH was found to consist of both, static and dynamic quenching, as the fluorescence lifetime is decreased upon addition of NADH to Bili-Sense, from 2 ns in the absence of NADH to 1.5 ns in the presence of 500 μM NADH. In comparison, time-resolved fluorescent experiments on tryptophan in solution showed that quenching of its fluorescence by NADH is only of static nature, thus the decreased lifetime observed in experiments with Bili-Sense and NADH cannot be explained solely by the interaction of the protein's tryptophan residues with NADH. The finding of the decreased lifetime suggests that Bili-Sense, upon interaction with NADH, adopts an altered conformation, as is common for fluorescent NADH sensors (Hung et al., 2011; Zhao et al., 2015, 2011), in which the distances between the tryptophan residues and biliverdin are altered, effectively also altering the fluorescence lifetime.

However, at present, only low amounts of holoprotein could be retrieved. Thus, further optimization strategies are required to enhance expression and holoprotein formation in cellular systems in order to permit further experiments regarding the affinity of the sensor towards structurally related molecules and to further develop the concept of FRET-augmented NADH fluorescence sensors.

VI Outlook

While the qualitative tracking of the SH activity by the NADH sensor Frex is a promising feature, it would be of even greater interest to be able to use a [NADH] or [NADH]/[NAD^+] sensor to infer the actual concentration of the NADH pool, and thus being able to indirectly measure the activity of the hydrogenase. This is in theory possible with the Frex sensor, by employing both excitation wavelengths of the fluorophore cpYFP (400 & 480 nm) (Zhao et al., 2011). By generating the ratio of fluorescence emission after excitation with both wavelengths, the signal is normalized for protein expression, and comparable to *in vitro* titration curves. However, since the usage of the 400 nm excitation triggers an immense amount of cellular autofluorescence as well, and since the fluorescence intensity of cpYFP's emission at this excitation is very low, the sensor signal cannot be discriminated from the cellular background. Hence the application of a sensor with two fluorescence emission profiles, which can be readout in order to normalize the signal would be advantageous. This could either be carried out by modifying the Frex sensor with an N-terminal mCherry probe as has been done in the Peredox sensor (Hung et al., 2011), or the application of a completely new sensor, which exhibits two excitation and emission profiles sufficiently in the red region of the spectrum so as to not trigger autofluorescence of the cells.

This optimized, quantitative NADH sensor could be further applied in combination with *in situ* IR spectroscopy and/or EPR spectroscopy. Preceding studies employing these techniques helped to clarify the various active states of the [NiFe] center and their involvement during the catalytic cycle (Marius Horch et al., 2010; Marius Horch, Rippers, Mroginski, Hildebrandt, & Zebger, 2013). The contemporaneous utilization of a NADH sensor with the aforementioned techniques would allow to check the activity status of the SH in the samples, while also determining the predominant [NiFe] states. This would help to elucidate the reaction and action mechanism and facilitate the application of the SH or other derived model systems for biotechnological processes.

For a new bacterial far-red fluorescent NADH sensor, iRFP713 has been proven an interesting starting point. The sensor concept of tryptophan sensitized biliverdin emission, has many practical advantages. However, for an applicable sensor, either the expression of Bili-Sense and sufficient generation of holoprotein have to be increased or another topology of Rex subunits and iRFP713 fluorescent units with more favorable expression characteristics have to be designed. Suitable tactics could be to express the protein at lower temperatures under the control of weaker promoters than the T7 promoter, fusing the target protein to a highly expressed proteins such as GFP or trying to optimize apoprotein production and completing holoprotein formation by *in vitro* protein-chromophore assembly (Kapust & Waugh, 1999; Sørensen & Mortensen, 2005; Vasina & Baneyx, 1997). The current construct also lacks linkers between the PAS and Rex subunits, as well as the GAF and Rex subunits. Implementation of short (5-6 aa linkers) could offer larger conformational freedom for proper folding and thus confer greater stability to the construct (Amet, Lee, & Shen, 2009; Chen, Zaro, & Shen, 2013; Gokhale & Khosla, 2000; G. G. Yang et al., 2015). This could also lead to enhanced chromophore integration, which seems to be the bottleneck of holoprotein formation.

Furthermore, smaller constructs could possibly facilitate expression. Thus, an idea would be to separately express PAS-Rex and GAF-Rex constructs as in the iSplit system and combine them *in vitro* to give the fully functional NADH sensor.

Potentially obtaining more functional protein, the nature of the sensing mechanism can be characterized more in depth, maybe even offering the potential to transfer this particular sensing mechanism based on tryptophan-to-chromophore FRET to other sensors.

For future experiments on the nature of the sensing mechanism, the tryptophan residues of the sensor could be substituted or removed, in order to describe the mode of interaction, which each tryptophan residues contributes separately to the postulated energy transfer mechanism.

VII List of Figures

VIII References

Agledal, L., Niere, M., & Ziegler, M. (2010). The phosphate makes a difference : cellular functions of NADP. *Redox Report*, *15(1)*, 2–10. https://doi.org/10.1179/174329210X12650506623122

Albracht, S. P.J., Van Der Zwaan, J. W., & Fontijn, R. D. (1984). EPR Spectrum at 4, 9 and 35 GHz of hydrogenase from *Chromatium vinosum*. Direct evidence for spin-spin interaction between Ni(III) and the ironsulphur cluster. *BBA - Bioenergetics*, *766*(1), 245–258. https://doi.org/10.1016/0005-2728(84)90238-X

Albracht, S.P.J., Graf, E.-G., & Thauer, R. K. (1982). The EPR properties of nickel in hydrogenase from *Methanobacterium thermoautotrophicum* . *FEBS Letters*, *140*(2), 311–313. https://doi.org/10.1016/0014-5793(82)80921-6

Albracht, Simon P.J. (1994). Nickel hydrogenases: in search of the active site. *Biochimica et Biophysica Acta (BBA) - Bioenergetics*, *1188*(3), 167–204. https://doi.org/10.1016/0005-2728(94)90036-1

Amet, N., Lee, H. F., & Shen, W. C. (2009). Insertion of the designed helical linker led to increased expression of Tf-based fusion proteins. *Pharmaceutical Research*, *26*(3), 523–528. https://doi.org/10.1007/s11095-008-9767-0

Anderson, K. A., Madsen, A. S., Olsen, C. A., & Hirschey, M. D. (2017). Metabolic control by sirtuins and other enzymes that sense NAD^+, NADH, or their ratio. *Biochimica et Biophysica Acta - Bioenergetics*, *1858*(12), 991–998. https://doi.org/10.1016/j.bbabio.2017.09.005

Atkins, P. W., & de Paula, J. (2014). *Physical Chemistry*. *Journal of The Electrochemical Society* (10th Editi, Vol. 104). Oxford: Oxford University Press.

Baird, G. S., Zacharias, D. A., & Tsien, R. Y. (1999). Circular permutation and receptor insertion within green fluorescent proteins. *Proceedings of the National Academy of Sciences of the United States of America*, *96*(20), 11241–11246. https://doi.org/10.1073/pnas.96.20.11241

Beg, Q. K., Vazquez, A., Ernst, J., de Menezes, M. A., Bar-Joseph, Z., Barabasi, A.-L., & Oltvai, Z. N. (2007). Intracellular crowding defines the mode and sequence of substrate uptake by *Escherichia coli* and constrains its metabolic activity.

Proceedings of the National Academy of Sciences, *104*(31), 12663–12668. https://doi.org/10.1093/nq/s7-I.13.249-a

Belenky, P., Bogan, K. L., & Brenner, C. (2006). NAD^+ metabolism in health and disease. *Trends in Biochemical Sciences*, *32*(1), 12–19. https://doi.org/10.1016/j.tibs.2006.11.006

Bennett, B., Kimball, E., & Gao, M. (2009). Absolute metabolite concentrations and implied enzyme active site occupancy in *Escherichia coli*. *Nature Chemical Biology*, *5*(8), 593–599. https://doi.org/10.1038/nchembio.186

Berg, J., Hung, Y. P., & Yellen, G. (2009). A genetically encoded fluorescenct reporter of ATP/ADP ratio. *Nature Methods*, *6*(2), 161–166. https://doi.org/10.1038/nmeth.1288.A

Berg, J. M., Tymoczko, J. L., Gatto, G. J., & Stryer, L. (2015). *Biochemistry* (8th ed.). New York: W. H. Freeman & Company.

Berger, F., Ramirez-Hernandez, M. H., & Ziegler, M. (2004). The new life of a centenarian : signalling functions of NAD(P). *Trends in Biochemical Sciences*, *29*(3), 111–118. https://doi.org/10.1016/j.tibs.2004.01.007

Bilan, D. S., & Belousov, V. V. (2016). Genetically encoded probes for NAD^+/NADH monitoring. *Free Radical Biology and Medicine*, *100*(11), 32–42. https://doi.org/10.1016/j.freeradbiomed.2016.06.018

Bilan, D. S., Matlashov, M. E., Schultz, C., Enikolopov, G., Belousov, V. V., Gorokhovatsky, A. Y., … Belousov, V. V. (2014). Genetically encoded fluorescent indicator for imaging NAD^+/NADH ratio changes in different cellular compartments. *Biochimica et Biophysica Acta - General Subjects*, *1840*(3), 951–957. https://doi.org/10.1016/j.bbagen.2013.11.018

Bisswanger, H. (2017). *Enzyme Kinetics: Principles and Methods* (3rd ed.). Wiley-VCH Verlag GmbH & Co. KGaA. https://doi.org/10.1002/9783527806461

Blacker, T. S., & Duchen, M. R. (2016). Investigating mitochondrial redox state using NADH and NADPH autofluorescence. *Free Radical Biology and Medicine*, *100*, 53–65. https://doi.org/10.1016/j.freeradbiomed.2016.08.010

Blacker, T. S., Mann, Z. F., Gale, J. E., Ziegler, M., Bain, A. J., Szabadkai, G., & Duchen, M. R. (2014). Separating NADH and NADPH fluorescence in live cells and tissues using FLIM. *Nature Communications*, *5*(1), 3936. https://doi.org/10.1038/ncomms4936

Blasco, M. A. (2005). Telomers and Human Disease : Ageing, Cancer and Beyond.

Nature Reviews Genetics, *6*(August), 611–622. https://doi.org/10.1038/nrg1656

Bleijlevens, B., Van Broekhuizen, F. A., De Lacey, A. L., Roseboom, W., Fernandez, V. M., & Albracht, S. P. J. (2004). The activation of the [NiFe]-hydrogenase from *Allochromatium vinosum*. An infrared spectro-electrochemical study. *Journal of Biological Inorganic Chemistry*, *9*(6), 743–752. https://doi.org/10.1007/s00775-004-0570-z

Blinova, K., Carroll, S., Bose, S., Smirnov, A. V., Harvey, J. J., Knutson, J. R., & Balaban, R. S. (2005). Distribution of mitochondrial NADH fluorescence lifetimes: Steady-state kinetics of matrix NADH interactions. *Biochemistry*, *44*(7), 2585–2594. https://doi.org/10.1021/bi0485124

Bordone, L., Motta, M. C., Picard, F., Robinson, A., Jhala, U. S., Apfeld, J., … Guarente, L. (2006). Sirt1 regulates insulin secretion by repressing UCP2 in pancreatic β cells. *PLoS Biology*, *4*(2), 210–220. https://doi.org/10.1371/journal.pbio.0040031

Brekasis, D., & Paget, M. S. B. (2003). A novel sensor of NADH/NAD+ redox poise in Streptomyces coelicolor A3(2). *EMBO Journal*, *22*(18). https://doi.org/10.1093/emboj/cdg453

Buhrke, D., Escobar, F. V., Sauthof, L., Wilkening, S., Herder, N., Tavraz, N. N., … Friedrich, T. (2016). The role of local and remote amino acid substitutions for optimizing fluorescence in bacteriophytochromes : A case study on iRFP. *Nature Publishing Group*, (March), 1–12. https://doi.org/10.1038/srep28444

Burgdorf, T., Lenz, O., Buhrke, T., Van Der Linden, E., Jones, A. K., Albracht, S. P. J., & Friedrich, B. (2006). [NiFe]-hydrogenases of *Ralstonia eutropha* H16: Modular enzymes for oxygen-tolerant biological hydrogen oxidation. *Journal of Molecular Microbiology and Biotechnology*, *10*(2–4), 181–196. https://doi.org/10.1159/000091564

Burgdorf, T., Linden, E. Van Der, Bernhard, M., Yin, Q. Y., Back, J. W., Hartog, A. F., … Muijsers, A. O. (2005). The Soluble NAD+-Reducing [NiFe]-Hydrogenase from *Ralstonia eutropha* H16 Consists of Six Subunits and Can Be Specifically Activated by NADPH. *Journal of Bacteriology*, *187*(9), 3122–3132. https://doi.org/10.1128/JB.187.9.3122

Cameron, W. D., Bui, C. V., Hutchinson, A., Loppnau, P., Gräslund, S., & Rocheleau, J. V. (2016). Apollo-NADP$^+$: A spectrally tunable family of genetically encoded

sensors for NADP+. *Nature Methods*, *13*(4), 352–358. https://doi.org/10.1038/nmeth.3764

Cammack, R., Patil, D., Aguirre, R., & Hatchikian, E. C. (1982). Redox properties of the ESR-detectable nickel in hydrogenase from *Desulfovibrio gigas*. *FEBS Letters*, *142*(2), 289–292. https://doi.org/https://doi.org/10.1016/0014-5793(82)80154-3

Cao, R., Wallrabe, H., Siller, K., Rehman Alam, S., & Periasamy, A. (2019). Single-cell redox states analyzed by fluorescence lifetime metrics and tryptophan FRET interaction with NAD(P)H. *Cytometry Part A*, *95*(1), 110–121. https://doi.org/10.1002/cyto.a.23711

Chalfie, M., Tu, Y., Euskirchen, G., Ward, W. W., & Prasher, D. C. (1994). Green fluorescent protein as a marker for gene expression. *Science*, *263*, 802–805. https://doi.org/10.1126/science.8303295

Chang, M., Li, L., Hu, H., Hu, Q., Wang, A., Cao, X., … Xu, J. (2017). Using Fractional Intensities of Time-resolved Fluorescence to Sensitively Quantify NADH/NAD+ with Genetically Encoded Fluorescent Biosensors. *Scientific Reports*, *7*(1), 1–9. https://doi.org/10.1038/s41598-017-04051-7

Chattoraj, M., King, B. A., Bublitz, G. U., & Boxer, S. G. (1996). Ultra-fast excited state dynamics in green fluorescent protein: multiple states and proton transfer. *Proceedings of the National Academy of Sciences*, *93*(16), 8362–8367. https://doi.org/10.1073/pnas.93.16.8362

Chen, X., Zaro, J. L., & Shen, W.-C. (2013). Fusion protein linkers: Property, design and functionality. *Advanced Drug Delivery Reviews*, *65*(10), 1357–1369. https://doi.org/10.1016/j.addr.2012.09.039

Chiang, J. J. H., Li, I., & Truong, K. (2006). Creation of circularly permutated yellow fluorescent proteins using fluorescence screening and a tandem fusion template. *Biotechnology Letters*, *28*(7), 471–475. https://doi.org/10.1007/s10529-006-0007-6

Clapper, D. L., Walseth, T. F., Dargie, P. J., & Hon Cheung Lee. (1987). Pyridine nucleotide metabolites stimulate calcium release from sea urchin egg microsomes desensitized to inositol trisphosphate. *Journal of Biological Chemistry*, *262*(20), 9561–9568. https://doi.org/https://doi.org/10.1016/S0021-9258(18)47970-7

Conley, J. M., Radhakrishnan, S., Valentino, S. A., & Tantama, M. (2017). Imaging

extracellular ATP with a genetically-encoded, ratiometric fluorescent sensor. *PLoS ONE*, *12*(11), 1–24. https://doi.org/10.1371/journal.pone.0187481

Cornish-Bowden, A., & Cardenas, M. L. (1987). Co-operativity in Monomeric Enzymes. *Journal of Theoretical Biology*, *124*, 1–23. https://doi.org/10.1016/j.bioorg.2011.11.001

Cramm, R. (2009). Genomic View of Energy Metabolism in *Ralstonia eutropha* H16. *Journal of Molecular Microbiology and Biotechnology*, *16*(1–2), 38–52. https://doi.org/10.1159/000142893

Croce, A. C., Bottiroli, G., & Unit, C. (2014). Autofluorescence spectroscopy and imaging : a tool for biomedical research and diagnosis. *European Journal of Histochemistry*, *58*, 320–337. https://doi.org/10.4081/ejh.2014.2461

D'Amours, D., Desnoyers, S., D'Silva, I., & Poirier, G. G. (1999). Poly(ADP-ribosyl)ation reactions in the regulation of nuclear functions. *Biochemical Journal*, *342*(2), 249–268. https://doi.org/10.1042/bj3420249

Day, R. N., & Davidson, M. W. (2009). The fluorescent protein palette: Tools for cellular imaging. *Chemical Society Reviews*, *38*(10), 2887–2921. https://doi.org/10.1039/b901966a

De Lacey, A. L., Fernández, V. M., Rousset, M., & Cammack, R. (2007). Activation and inactivation of hydrogenase function and the catalytic cycle: Spectroelectrochemical studies. *Chemical Reviews*, *107*(10), 4304–4330. https://doi.org/10.1021/cr0501947

De Lacey, A. L., Hatchikian, E. C., Volbeda, A., Frey, M., Fontecilla-Camps, J. C., & Fernandez, V. M. (1997). Infrared-spectroelectrochemical characterization of the [NiFe] hydrogenase of *Desulfovibrio gigas*. *Journal of the American Chemical Society*, *119*(31), 7181–7189. https://doi.org/10.1021/ja963802w

De Ruyck, J., Famerée, M., Wouters, J., Perpète, E. A., Preat, J., & Jacquemin, D. (2007). Towards the understanding of the absorption spectra of NAD(P)H/NAD(P)$^+$ as a common indicator of dehydrogenase enzymatic activity. *Chemical Physics Letters*, *450*(1–3), 119–122. https://doi.org/10.1016/j.cplett.2007.10.092

Direnberger, S., Mues, M., Micale, V., Wotjak, C. T., Dietzel, S., Schubert, M., … Griesbeck, O. (2012). Biocompatibility of a genetically encoded calcium indicator in a transgenic mouse model. *Nature Communications*, *3*, 1031. https://doi.org/10.1038/ncomms2035

Elsliger, M. A., Wachter, R. M., Hanson, G. T., Kallio, K., & Remington, S. J. (1999). Structural and spectral response of green fluorescent protein variants to changes in pH. *Biochemistry*, *38*(17), 5296–5301. https://doi.org/10.1021/bi9902182

Engineering ToolBox. (2008). Retrieved from https://www.engineeringtoolbox.com/diffusion-coefficients-d_1404.

Esposito, A., Gralle, M., Dani, M. A. C., Lange, D., & Wouters, F. S. (2008). pHlameleons: A family of FRET-based protein sensors for quantitative pH imaging. *Biochemistry*, *47*(49), 13115–13126. https://doi.org/10.1021/bi8009482

Fernandez, V. M., Hatchikian, E. C., & Cammack, R. (1985). Properties and reactivation of two different deactivated forms of Desulfovibrio gigas hydrogenase. *Biochimica et Biophysica Acta*, *832*, 69–79. https://doi.org/https://doi.org/10.1016/0167-4838(85)90175-X

Filonov, G. S., Piatkevich, K. D., Ting, L., Zhang, J., Kim, K., & Verkhusha, V. V. (2011). Bright and stable near infra-red fluorescent protein for *in vivo* imaging. *Nature Biotechnology*, *29*(8), 757–761. https://doi.org/10.1038/nbt.1918.

Filonov, G. S., & Verkhusha, V. V. (2013). A near-infrared bifc reporter for *in vivo* imaging of protein-protein interactions. *Chemistry and Biology*, *20*(8), 1078–1086. https://doi.org/10.1016/j.chembiol.2013.06.009

Fontaine, M. P., Jameson, D. M., & Alpert, B. (1980). Tryptophan-Heme Energy Transfer in Human Hemoglobin: Dependence Upon the State of the Iron. *FEBS Letters*, *116*(2), 310–314. https://doi.org/10.1016/0014-5793(80)80670-3

Förster, T. (1948). Zwischenmolekulare Energiewanderung und Fluoreszenz. *Annalen Der Physik*, *437*(1–2), 55–75. https://doi.org/10.1002/andp.19614630112

Friedrich, B., Heine, E., Finck, A., & Friedrich, C. G. (1981). Nickel requirement for active hydrogenase formation in *Alcaligenes eutrophus*. *Journal of Bacteriology*, *145*(3), 1144–1149.

Friedrich, B., Hogrefe, C., & Schlegel, H. G. (1981). Naturally occurring genetic transfer of hydrogen-oxidizing ability between strains of *Alcaligenes eutrophus*. *Journal of Bacteriology*, *147*(1), 198–205.

Friedrich, B., & Schwartz, E. (1993). Molecular Biology of Hydrogen Utilization in Aerobic Chemolithotrophs. *Annu. Rev. Microbiol.*, *47*, 351–383.

https://doi.org/https://doi.org/10.1146/annurev.mi.47.100193.002031

Friedrich, C. G. (1982). Derepression of hydrogenase during limitation of electron donors and derepression of ribulosebisphosphate carboxylase during carbon limitation of *Alcaligenes eutrophus*. *Journal of Bacteriology*, *149*(1), 203–210. https://doi.org/10.1128/JB.149.1.203-210.1982

Friedrich, C. G., & Friedrich, B. (1983). Regulation of hydrogenase formation is temperature sensitive and plasmid coded in *Alcaligenes eutrophus*. *Journal of Bacteriology*, *153*(1), 176–181. https://doi.org/10.1002/ajp.20766

Friedrich, Cornelius G., Friedrich, B., & Bowien, B. (1981). Formation of Enzymes of Autotrophic Metabolism During Heterotrophic Growth of *Alcaligenes eutrophus*. *Journal of General Microbiology*, *16*(1981), 69–78. https://doi.org/10.1099/00221287-122-1-69

Gaikwad, A., Long, D. J., Stringer, J. L., & Jaiswal, A. K. (2001). *In Vivo* Role of NAD(P)H:Quinone Oxidoreductase 1 (NQO1) in the Regulation of Intracellular Redox State and Accumulation of Abdominal Adipose Tissue. *Journal of Biological Chemistry*, *276*(25), 22559–22564. https://doi.org/10.1074/jbc.M101053200

Germer, F., Zebger, I., Saggu, M., Lendzian, F., Schulz, R., & Appel, J. (2009). Overexpression, isolation, and spectroscopic characterization of the bidirectional [NiFe] hydrogenase from Synechocystis sp. PCC 6803. *Journal of Biological Chemistry*, *284*(52), 36462–36472. https://doi.org/10.1074/jbc.M109.028795

Gokhale, R. S., & Khosla, C. (2000). Role of linkers in communication between protein modules. *Current Opinion in Chemical Biology*, *4*(1), 22–27. https://doi.org/10.1016/S1367-5931(99)00046-0

Gouterman, M. (1978). *The Porphyrins Vol. III*. (D. Dolphin, Ed.). New York: Academic Press New York.

Griesbeck, O., Baird, G. S., Campbell, R. E., Zacharias, D. A., & Tsien, R. Y. (2001). Reducing the environmental sensitivity of yellow fluorescent protein. Mechanism and applications. *Journal of Biological Chemistry*, *276*(31), 29188–29194. https://doi.org/10.1074/jbc.M102815200

Gyan, S., Shiohira, Y., Sato, I., Takeuchi, M., & Sato, T. (2006). Regulatory loop between redox sensing of the NADH/NAD+ ratio by Rex (YdiH) and oxidation of NADH by NADH dehydrogenase Ndh in *Bacillus subtilis*. *Journal of*

Bacteriology, *188*(20), 7062–7071. https://doi.org/10.1128/JB.00601-06

Haggie, P. M., & Verkman, A. S. (2005). Gfp sensors. In *Advanced Concepts in Fluorescence Sensing* (pp. 21–41).

Hanson, G. T., Aggeler, R., Oglesbee, D., Cannon, M., Capaldi, R. A., Tsien, R. Y., & Remington, S. J. (2004). Investigating Mitochondrial Redox Potential with Redox-sensitive Green Fluorescent Protein Indicators. *Journal of Biological Chemistry*, *279*(13), 13044–13053. https://doi.org/10.1074/jbc.M312846200

Hanson, G. T., McAnaney, T. B., Park, E. S., Rendell, M. E. P., Yarbrough, D. K., Chu, S., … Remington, S. J. (2002). Green fluorescent protein variants as ratiometric dual emission ph sensors. 1. Structural characterization and preliminary application. *Biochemistry*, *41*(52), 15477–15488. https://doi.org/10.1021/bi026609p

Hao, X., Gu, H., Chen, C., Huang, D., Zhao, Y., Xie, L., … Shu, H. S. (2019). Metabolic Imaging Reveals a Unique Preference of Symmetric Cell Division and Homing of Leukemia- Initiating Cells in an Endosteal Niche Article Metabolic Imaging Reveals a Unique Preference of Symmetric Cell Division and Homing of Leukemia-Initiating Cell. *Cell Metabolism*, *29*(4), 950–965. https://doi.org/10.1016/j.cmet.2018.11.013

Happe, R. P., Roseboom, W., Pierik, A. J., Albracht, S. P. J., & Bagley, K. A. (1997). Biological activition of hydrogen. *Nature*, *385*, 126. https://doi.org/10.1038/385126a0

Hasmann, M., & Schemainda, I. (2003). FK866, a Highly Specific Noncompetitive Inhibitor of Nicotinamide Phosphoribosyltransferase, Represents a Novel Mechanism for Induction of Tumor Cell Apoptosis. *Cancer Research*, *63*(21), 7436–7442.

Haugh, J. M. (2012). Live-cell fluorescence microscopy with molecular biosensors: What are we really measuring? *Biophysical Journal*, *102*(9), 2003–2011. https://doi.org/10.1016/j.bpj.2012.03.055

Hill, A. V. (1910). The Possible Effects of the Aggregation of the Molecules of Haemoglobin on its Dissociation Curves. *The Journal of Physiology*, *40*, 4–7.

Hoffmann, J., Bóna-Lovász, J., Beuttler, H., & Altenbuchner, J. (2012). In vivo and in vitro studies on the carotenoid cleavage oxygenases from Sphingopyxis alaskensis RB2256 and *Plesiocystis pacifica* SIR-1 revealed their substrate specificities and non-retinal-forming cleavage activities. *FEBS Journal*,

279(20), 3911–3924. https://doi.org/10.1111/j.1742-4658.2012.08751.x

Horch, M., Lauterbach, L., Lenz, O., Hildebrandt, P., & Zebger, I. (2012). NAD(H)-coupled hydrogen cycling - Structure-function relationships of bidirectional [NiFe] hydrogenases. *FEBS Letters*, *586*(5), 545–556. https://doi.org/10.1016/j.febslet.2011.10.010

Horch, Marius, Lauterbach, L., Mroginski, M. A., Hildebrandt, P., Lenz, O., & Zebger, I. (2015). Reversible active site sulfoxygenation can explain the oxygen tolerance of a NAD^+-reducing [NiFe] hydrogenase and its unusual infrared spectroscopic properties. *Journal of the American Chemical Society*, *137*(7), 2555–2564. https://doi.org/10.1021/ja511154y

Horch, Marius, Lauterbach, L., Saggu, M., Hildebrandt, P., Lendzian, F., Bittl, R., … Zebger, I. (2010). Probing the active site of an O_2-Tolerant NAD+-reducing [NiFe]-Hydrogenase from *Ralstonia eutropha* H16 by in situ EPR and FTIR spectroscopy. *Angewandte Chemie - International Edition*, *49*(43), 8026–8029. https://doi.org/10.1002/anie.201002197

Horch, Marius, Rippers, Y., Mroginski, M. A., Hildebrandt, P., & Zebger, I. (2013). Combining spectroscopy and theory to evaluate structural models of metalloenzymes: A case study on the soluble [NiFe] hydrogenase from *Ralstonia eutropha*. *ChemPhysChem*, *14*(1), 185–191. https://doi.org/10.1002/cphc.201200853

Houtkooper, R. H., Cantó, C., Wanders, R. J., & Auwerx, J. (2010). The secret life of NAD^+: An old metabolite controlling new metabolic signaling pathways. *Endocrine Reviews*, *31*(2), 194–223. https://doi.org/10.1210/er.2009-0026

Hung, Y. P., Albeck, J. G., Tantama, M., & Yellen, G. (2011). Imaging Cytosolic NADH-NAD^+ Redox State with a Genetically Encoded Fluorescent Biosensor. *Cell Metabolism*, *14*(4), 545–554. https://doi.org/10.1016/j.cmet.2011.08.012

Ibraheem, A., & Campbell, R. E. (2010). Designs and applications of fluorescent protein-based biosensors. *Current Opinion in Chemical Biology*, *14*(1), 30–36. https://doi.org/10.1016/j.cbpa.2009.09.033

Janes, S. M., Holtom, G., Ascenzi, P., Brunori, M., & Hochstrasser, R. M. (1987). Fluorescence and Energy Transfer of Tryptophans in *Aplysia* Myoglobin. *Biophysical Journal*, *51*(4), 653–660. https://doi.org/10.1016/S0006-3495(87)83390-8

Jobsis, F. F. (1977). Noninvasive, infrared monitoring of cerebral and myocardial

oxygen sufficiency and circulatory parameters. *Science*, *198*, 1264–1267.

Johnson, S., & Imai, S. (2018). NAD^+ biosynthesis, aging, and disease. *F1000Research*, *7*(0), 132. https://doi.org/10.12688/f1000research.12120.1

Jyothikumar, V., Sun, Y., & Periasamy, A. (2013). Investigation of tryptophan–NADH interactions in live human cells using three-photon fluorescence lifetime imaging and Förster resonance energy transfer microscopy. *Journal of Biomedical Optics*, *18*(6), 060501. https://doi.org/10.1117/1.jbo.18.6.060501

Kamal, J. K. A., & Behere, D. V. (2001). Steady-State and Picosecond Time-Resolved Fluorescence Studies on Native and Apo Seed Coat Soybean Peroxidase. *Biochemical and Biophysical Research Communications*, *289*(2), 427–433. https://doi.org/10.1006/bbrc.2001.6018

Kapust, R. B., & Waugh, D. S. (1999). *Escherichia coli* maltose-binding protein is uncommonly effective in promoting the solubility of polypeptides to which it is fused. *Protein Science*, (8), 1668–1674. https://doi.org/10.1110/ps.8.8.1668

Katoh, A., Uenohara, K., Akita, M., & Hashimoto, T. (2006). Early Steps in the Biosynthesis of NAD in Arabidopsis Start with Aspartate and Occur in the Plastid. *Plant Physiology*, *141*(3), 851–857. https://doi.org/10.1104/pp.106.081091

Kelly, R. A., Leedale, J., Harrell, A., Beard, D. A., Randle, L. E., Chadwick, A. E., & Webb, S. D. (2018). Modelling the impact of changes in the extracellular environment on the cytosolic free NAD^+/NADH ratio during cell culture. *PLoS ONE*, *13*(11), 1–21. https://doi.org/10.1371/journal.pone.0207803

Klaidmann, L. K., Leung, A. C., & Adams Jr., J. D. (1995). High-Performance Liquid Chromatography Analysis of Oxidized and Reduced Pyridine Dinucleotides in Specific Brain Regions. *Analytical Biochemistry*, *228*, 312–317. https://doi.org/10.1006/abio.1995.1356

Kleihues, L., Lenz, O., Bernhard, M., Buhrke, T., & Friedrich, B. (2000). The H_2 sensor of *Ralstonia eutropha* is a member of the subclass of regulatory [NiFe] hydrogenases. *Journal of Bacteriology*, *182*(10), 2716–2724. https://doi.org/10.1128/JB.182.10.2716-2724.2000

Klinke, S., Otero, L. H., Rinaldi, J., Sosa, S., Guimarães, B. G., Shepard, W. E., … Bonomi, H. R. (2014). Crystallization and preliminary X-ray characterization of the full-length bacteriophytochrome from the plant pathogen *Xanthomonas*

campestris pv. *campestris*. *Acta Crystallographica Section F:Structural Biology Communications*, *70*, 1636–1639. https://doi.org/10.1107/S2053230X14023243

Kneen, M., Farinas, J., Li, Y., & Verkman, A. S. (1998). Green fluorescent protein as a noninvasive intracellular pH indicator. *Biophysical Journal*, *74*(3), 1591–1599. https://doi.org/10.1016/S0006-3495(98)77870-1

Kuhn, M., Steinbuchel, A., & Schlegel, H. G. (1984). Hydrogen Evolution by Strictly Aerobic Hydrogen Bacteria Under Anaerobic Conditions. *Journal of Bacteriology*, *159*(2), 633–639.

Lakowicz, J. R., Szmacinski, H., Nowaczyk, K., & Johnson, M. L. (1992). Fluorescence lifetime imaging of free and protein-bound NADH. *Proceedings of the National Academy of Sciences of the United States of America*, *89*(4), 1271–1275.

Lakowicz, Joseph R. (2006). *Principles of Fluorescence Spectroscopy*. (Joseph R. Lakowicz, Ed.) (3rd ed., Vol. 7). Boston, MA: Springer US. https://doi.org/10.1007/978-0-387-46312-4

Lamparter, T., Carrascal, M., Michael, N., Martinez, E., Rottwinkel, G., & Abian, J. (2004). The Biliverdin Chromophore Binds Covalently to a Conserved Cysteine Residue in the N-Terminus of Agrobacterium Phytochrome Agp1. *Biochemistry*, *43*, 3659–3669. https://doi.org/10.1021/bi035693l

Lamparter, T., Michael, N., Caspani, O., Miyata, T., Shirai, K., & Inomata, K. (2003). Biliverdin Binds Covalently to *Agrobacterium* Phytochrome Agp1 via Its Ring A Vinyl Side Chain. *Journal of Biological Chemistry*, *278(36)*(5), 33786–33792. https://doi.org/10.1074/jbc.M305563200

Larsson, J. T., Rogstam, A., & von Wachenfeldt, C. (2005). Coordinated patterns of cytochrome *bd* and lactate dehydrogenase expression in *Bacillus subtilis*. *Microbiology*, *151*(10), 3323–3335. https://doi.org/10.1099/mic.0.28124-0

Lauterbach, L. (2013). *Die Analyse der Sauerstofftoleranz und biotechnologische Anwendung der NAD⁺-reduzierenden Hydrogenase aus Ralstonia eutropha H16*. Humboldt Universität Berlin. https://doi.org/10.3109/10242422.2011.615393

Lauterbach, L., Idris, Z., Vincent, K. A., & Lenz, O. (2011). Catalytic properties of the isolated diaphorase fragment of the NAD+-reducing [NiFe]-hydrogenase from *Ralstonia eutropha*. *PLoS ONE*, *6*(10). https://doi.org/10.1371/journal.pone.0025939

Lauterbach, L., & Lenz, O. (2013). Catalytic production of hydrogen peroxide and water by oxygen-tolerant [NiFe]-hydrogenase during H_2 cycling in the presence of O_2. *Journal of the American Chemical Society*, *135*(47), 17897–17905. https://doi.org/10.1021/ja408420d

Lauterbach, L., Lenz, O., & Vincent, K. A. (2013). H_2-driven cofactor regeneration with NAD(P)+-reducing hydrogenases. *FEBS Journal*, *280*(13), 3058–3068. https://doi.org/10.1111/febs.12245

Lee, H. C. (2001). Physiological Functions of Cyclic ADP-Ribose and NAADP as Calcium Messengers. *Annu. Rev. Pharmacol. Toxicol.*, *41*(3), 317–345. https://doi.org/10.1146/annurev.pharmtox.41.1.317

Lenz, O., & Friedrich, B. (1998). A novel multicomponent regulatory system mediates H_2 sensing in *Alcaligenes eutrophus*. *Proceedings of the National Academy of Sciences*, *95*(21), 12474–12479. https://doi.org/10.1073/pnas.95.21.12474

Lenz, O, Bernhard, M., Buhrke, T., Schwartz, E., & Friedrich, B. (2002). The hydrogen-sensing apparatus in *Ralstonia eutropha*. *Journal Of Molecular Microbiology And Biotechnology*, *4*(3), 255–262.

Lenz, Oliver, Lauterbach, L., Frielingsdorf, S., & Friedrich, B. (2015). Oxygen-tolerant hydrogenases and their biotechnological potential. *Biohydrogen*, 61–96. https://doi.org/10.1515/9783110336733.61

Leonardo, M. R., Dailly, Y., & Clark, D. P. (1996). Role of NAD in regulating the *adhE* gene of *Escherichia coli*. *Journal of Bacteriology*, *178*(20), 6013–6018. https://doi.org/10.1128/jb.178.20.6013-6018.1996

Lin, S. J., Ford, E., Haigis, M., Liszt, G., & Guarente, L. (2004). Calorie restriction extends yeast life span by lowering the level of NADH. *Genes and Development*, *18*(1), 12–16. https://doi.org/10.1101/gad.1164804

Lin, S. J., & Guarente, L. (2003). Nicotinamide adenine dinucleotide, a metabolic regulator of transcription, longevity and disease. *Current Opinion in Cell Biology*, *15*(2), 241–246. https://doi.org/10.1016/S0955-0674(03)00006-1

Lippincott-Schwartz, J., & Patterson, G. H. (2003). Development and use of fluorescent protein markers in living cells. *Science*, *300*(5616), 87–91. https://doi.org/10.1126/science.1082520

Llopis, J., McCaffery, J. M., Miyawaki, A., Farquhar, M. G., Tsien, R. Y., & Biology, C. (1998). Measurement of cytosolic, mitochondrial, and Golgi pH in single living

cells with green fluorescent proteins. *Proceedings of the National Academy of Sciences* , *95*(12), 6803–6808. https://doi.org/10.1073/pnas.95.12.6803

Love, N. R., Pollak, N., Dölle, C., Niere, M., Chen, Y., Oliveri, P., … Ziegler, M. (2015). NAD kinase controls animal NADP biosynthesis and is modulated via evolutionarily divergent calmodulin-dependent mechanisms. *Proceedings of the National Academy of Sciences*, *112*(5), 1386–1391. https://doi.org/10.1073/pnas.1417290112

Lowry, O. H., Passonneau, J. V., Schulz, D. W., & Rock, M. K. (1961). Measurement of Pyridine Nucleotides by Enzymatic Cycling. *Journal of Biological Chemistry*, *236*(10), 2746–2755.

Lubitz, W., Reijerse, E., & van Gastel, M. (2007). [NiFe] and [FeFe] Hydrogenases Studied by Advanced Magnetic Resonance Techniques. *Chemical Reviews*, *107*(10), 4331–4365. https://doi.org/10.1021/cr050186q

Luisi, P. L., & Favilla, R. (1970). Tryptophan Fluorescence Quenching in Horse Liver Alcohol Dehydrogenase. *European Journal of Biochemistry*, *17*(1), 91–94. https://doi.org/10.1111/j.1432-1033.1970.tb01139.x

MacDonald, M. J., & Marshall, L. K. (2000). Mouse lacking NAD^+-linked glycerol phosphate dehydrogenase has normal pancreatic beta cell function but abnormal metabolite pattern in skeletal muscle. *Archives of Biochemistry and Biophysics*, *384*(1), 143–153. https://doi.org/10.1006/abbi.2000.2107

Magni, G., Amici, A., Emanuelli, M., Orsomando, G., Raffaelli, N., & Ruggieri, S. (2004). Enzymology of NAD^+ homeostasis in man. *Cellular and Molecular Life Sciences*, *61*(1), 19–34. https://doi.org/10.1007/s00018-003-3161-1

Magni, G., Amici, A., Emanuelli, M., & Raffaelli, N. (1999). Enzymology of NAD+ Biosynthesis. *Advances in Enzymology and Related Areas of Molecular Biology, Volume 73*, *73*, 135–182. https://doi.org/10.1002/9780470123195.ch5

Mank, M., Santos, A. F., Direnberger, S., Mrsic-Flogel, T. D., Hofer, S. B., Stein, V., … Griesbeck, O. (2008). A genetically encoded calcium indicator for chronic *in vivo* two-photon imaging. *Nature Methods*, *5*(9), 805–811. https://doi.org/10.1038/nmeth.1243

Marcaggi, P., Mutoh, H., Dimitrov, D., Beato, M., & Knopfel, T. (2009). Optical measurement of mGluR1 conformational changes reveals fast activation, slow deactivation, and sensitization. *Proceedings of the National Academy of Sciences*, *106*(27), 11388–11393. https://doi.org/10.1073/pnas.0901290106

Marcu, R., Wiczer, B. M., Neeley, C. K., & Hawkins, B. J. (2014). Mitochondrial Matrix Ca^{2+} Accumulation Regulates Cytosolic NAD^{+}/NADH Metabolism, Protein Acetylation, and Sirtuin Expression. *Molecular and Cellular Biology*, *34*(15), 2890–2902. https://doi.org/10.1128/mcb.00068-14

McAnaney, T. B., Zeng, W., Doe, C. F. E., Bhanji, N., Wakelin, S., Pearson, D. S., … Bagshaw, C. R. (2005). Protonation, photobleaching, and photoactivation of yellow fluorescent protein (YFP 10C): A unifying mechanism. *Biochemistry*, *44*(14), 5510–5524. https://doi.org/10.1021/bi047581f

McLaughlin, K. J., Strain-Damerell, C. M., Xie, K., Brekasis, D., Soares, A. S., Paget, M. S. B., & Kielkopf, C. L. (2010). Structural Basis for NADH/NAD^{+} Redox Sensing by a Rex Family Repressor. *Molecular Cell*, *38*(4), 563–575. https://doi.org/10.1016/j.molcel.2010.05.006

Mertens, R., & Liese, A. (2004). Biotechnological applications of hydrogenases. *Current Opinion in Biotechnology*, *15*(4), 343–348. https://doi.org/10.1016/j.copbio.2004.06.010

Miesenböck, G., De Angelis, D. A., & Rothman, J. E. (1998). Visualizing Secretion and Synaptic Transmission with pH-sensitive Green Fluorescent Proteins. *Nature*, *394*(July), 192–195.

Miyawaki, A., Llopis, J., Heim, R., McCaffery, J. M., Adams, J. A., Ikura, M., & Tsien, R. Y. (1997). Fluorescent indicators for Ca^{2+} based on green fluorescent proteins and calmodulin. *Nature*, *388*(6645), 882–887. https://doi.org/10.1038/42264

Möller, M., & Denicola, A. (2002). Protein Tryptophan Accessibility Studied by Fluorescence Quenching. *Biochemistry and Molecular Biology Education*, *30*(3), 175–178. https://doi.org/https://doi.org/10.1002/bmb.2002.494030030035

Mongan, P. D., Capacchione, J., West, S., Karaian, J., Dubois, D., Keneally, R., & Sharma, P. (2002). Pyruvate improves redox status and decreases indicators of hepatic apoptosis during hemorrhagic shock in swine. *American Journal of Physiology-Heart and Circulatory Physiology*, *283*(4), H1634–H1644. https://doi.org/10.1152/ajpheart.01073.2001

Mongeon, R., Venkatachalam, V., & Yellen, G. (2016). Cytosolic NADH-NAD+ Redox Visualized in Brain Slices by Two-Photon Fluorescence Lifetime Biosensor Imaging. *Antioxidants & Redox Signaling*, *25*(10), 553–563. https://doi.org/10.1089/ars.2015.6593

Monni, R., Haddad, A. Al, Mourik, F. Van, Auböck, G., & Chergui, M. (2015).

Tryptophan-to-Heme Electron Transfer in Ferrous Myoglobins. *Proceedings of the National Academy of Sciences*, *112*(18), 5602–5606. https://doi.org/10.1073/pnas.1423186112

Morise, H., Shimomura, O., Johnson, F. H., & Winant, J. (1974). Intermolecular energy transfer in the bioluminescent system of aequorea. *Biochemistry*, *13*(12), 2656–2662. https://doi.org/10.1021/bi00709a028

Morris, M. C., & Blondel, M. (2014). Editorial: Fluorescent biosensors. *Biotechnology Journal*, *9*(2), 171–173. https://doi.org/10.1002/biot.201400008

Nagai, T., Sawano, A., Park, E. S., & Miyawaki, A. (2001). Circularly permuted green fluorescent proteins engineered to sense Ca2+. *Proceedings of the National Academy of Sciences of the United States of America*, *98*(6), 3197–3202. https://doi.org/10.1073/pnas.051636098

Oewierczyński, J., Somińska, E., Smoleński, R. T., & Mayer, D. (2001). Increase in NAD but not ATP and GTP concentrations in rat liver by dehydroepiandrosterone feeding. *Polish Journal of Pharmacology Pol. J. Pharmacol*, *53*, 125–130.

Olsen, K. N., Budde, B. B., Siegumfeldt, H., & Bjo, K. (2002). Noninvasive Measurement of Bacterial Intracellular pH on a Single-Cell Level with Green Fluorescent Protein and Fluorescence Ratio Imaging Microscopy Noninvasive Measurement of Bacterial Intracellular pH on a Single-Cell Level with Green Fluorescent Prote. *Applied and Environmental Microbiology*, *68*(8), 11–14. https://doi.org/10.1128/AEM.68.8.4145

Patterson, G. H., Knobel, S. M., Arkhammar, P., Thastrup, O., & Piston, D. W. (2000). Separation of the glucose-stimulated cytoplasmic and mitochondrial NAD(P)H responses in pancreatic islet beta cells. *Proceedings of the National Academy of Sciences of the United States of America*, *97*(10), 5203–5207. https://doi.org/10.1073/pnas.090098797

Phornphisutthimas, S., Thamchaipenet, A., & Panijpan, B. (2007). Conjugation in *E. coli*. *Biochemistry and Molecular Biology Education*, *35*(6), 440–445. https://doi.org/10.1002/bambed.113

Pierik, A. J., Roseboom, W., Happe, R. P., Bagley, K. A., & Albracht, S. P. J. (1999). Carbon Monoxide and Cyanide as Intrinsic Ligands to Iron in the Active Site of [NiFe]-Hydrogenases. *Journal of Biological Chemistry*, *274*(6), 3331–3337.

https://doi.org/10.1074/jbc.274.6.3331

Pollak, N., Dölle, C., & Ziegler, M. (2007). The power to reduce: pyridine nucleotides – small molecules with a multitude of functions. *Biochemical Journal*, *402*(2), 205–218. https://doi.org/10.1042/bj20061638

Porter, C. M., & Miller, B. G. (2012). Cooperativity in Monomeric Enzymes with Single Ligand- Binding Sites. *Bioorganic Chemistry*, *43*, 44–50. https://doi.org/10.1016/j.bioorg.2011.11.001.

Ratzka, J., Lauterbach, L., Lenz, O., & Ansorge-Schumacher, M. B. (2011). Systematic evaluation of the dihydrogen-oxidising and NAD+-reducing soluble [NiFe]-hydrogenase from *Ralstonia eutropha* H16 as a cofactor regeneration catalyst. *Biocatalysis and Biotransformation*, *29*(6), 246–252. https://doi.org/10.3109/10242422.2011.615393

Robey, R. B., Ruiz, O., Santos, A. V. P., Ma, J., Kear, F., Wang, L. J., … Arruda, J. A. L. (1998). pH-dependent fluorescence of a heterologously expressed *Aequorea* green fluorescent protein mutant: In situ spectral characteristics and applicability to intracellular pH estimation. *Biochemistry*, *37*(28), 9894–9901. https://doi.org/10.1021/bi980857x

Rodgers, J. T., Lerin, C., Haas, W., Gygi, S. P., Spiegelman, B. M., & Puigserver, P. (2005). Nutrient control of glucose homeostasis through a complex of PGC-1 a and SIRT1. *Nature*, *434*(March), 3–8. https://doi.org/10.1038/nature03314.

Sabariegos, R., Picazo, F., Domingo, B., Franco, S., Martinez, M. A., & Llopis, J. (2009). Fluorescence resonance energy transfer-based assay for characterization of hepatitis C virus NS3-4A protease activity in live cells. *Antimicrobial Agents and Chemotherapy*, *53*(2), 728–734. https://doi.org/10.1128/AAC.01029-08

Sallin, O., Reymond, L., Gondrand, C., Raith, F., Koch, B., & Johnsson, K. (2018). Semisynthetic biosensors for mapping cellular concentrations of nicotinamide adenine dinucleotides. *ELife*, *7*, 1–32. https://doi.org/10.7554/eLife.32638

Sander, R. (2015). Compilation of Henry's law constants (version 4.0) for water as solvent. *Atmospheric Chemistry and Physics*, *15*(8), 4399–4981. https://doi.org/10.5194/acp-15-4399-2015

Sanford, L., & Palmer, A. (2017). Recent Advances in Development of Genetically Encoded Fluorescent Sensors. *Methods in Enzymology*, *589*, 1–49. https://doi.org/10.1016/bs.mie.2017.01.019

Sanni, L. A., Rae, C., Maitland, A., Stocker, R., & Hunt, N. H. (2001). Is ischemia

involved in the pathogenesis of murine cerebral malaria? *American Journal of Pathology*, *159*(3), 1105–1112. https://doi.org/10.1016/S0002-9440(10)61786-5

Schäfer, C., Friedrich, B., & Lenz, O. (2013). Novel, oxygen-insensitive group 5 [NiFe]-hydrogenase in *Ralstonia eutropha*. *Applied and Environmental Microbiology*, *79*(17), 5137–5145. https://doi.org/10.1128/AEM.01576-13

Schmitt, F. J., Thaa, B., Junghans, C., Vitali, M., Veit, M., & Friedrich, T. (2014). EGFP-pHsens as a highly sensitive fluorophore for cellular pH determination by fluorescence lifetime imaging microscopy (FLIM). *Biochimica et Biophysica Acta - Bioenergetics*, *1837*(9), 1581–1593. https://doi.org/10.1016/j.bbabio.2014.04.003

Schneider, K., & Schlegel, H. G. (1976). Purification and properties of soluble hydrogenase from Alcaligenes eutrophus H 16. *Biochimica et Biophysica Acta (BBA) - Enzymology*, *452*(1), 66–80. https://doi.org/10.1016/0005-2744(76)90058-9

Schneider, K., & Schlegel, H. G. (1978). Identification and Quantitative Determination of the Flavin Component of Soluble Hydrogenase from *Alcaligenes eutrophus*. *Biochem. Biophys. Res. Commun.*, *84*(3), 564–571.

Schwarzländer, M., Logan, D. C., Fricker, M. D., & Sweetlove, L. J. (2011). The circularly permuted yellow fluorescent protein cpYFP that has been used as a superoxide probe is highly responsive to pH but not superoxide in mitochondria: implications for the existence of superoxide 'flashes.' *Biochemical Journal*, *437*(3), 381–387. https://doi.org/10.1042/BJ20110883

Schwarzländer, M., Wagner, S., Ermakova, Y. G., Belousov, V. V., Radi, R., Beckman, J. S., … Murphy, M. P. (2014). The 'mitoflash' probe cpYFP does not respond to superoxide. *Nature*, *514*(7523), E12–E14. https://doi.org/10.1038/nature13858

Sebban, P., Coppey, M., Alpert, B., Lindqvist, L., & Jameson, D. M. (1980). Fluorescence Properties of Porphyrin-Globin from human Hemoglobin. *Photochemistry and Photobiology*, *32*, 727–731. https://doi.org/10.1111/j.1751-1097.1980.tb04049.x

Shafaat, H. S., Rüdiger, O., Ogata, H., & Lubitz, W. (2013). [NiFe] hydrogenases: A common active site for hydrogen metabolism under diverse conditions. *Biochimica et Biophysica Acta - Bioenergetics*, *1827*(8–9), 986–1002.

https://doi.org/10.1016/j.bbabio.2013.01.015

Shcherbakova, D. M., Shemetov, A. A., Kaberniuk, Andrii, A., & Verkhusha, V. V. (2015). Natural Photoreceptors as a Source of Fluorescent Proteins, Biosensors, and Optogenetic Tools. *Annual Review of Biochemistry*, *84*, 519–550. https://doi.org/10.1146/annurev-biochem-060614-034411.Natural

Shu, X., Royant, A., Lin, M. Z., Aguilera, T. A., Lev-Ram, V., Steinbach, P. A., & Tsien, R. Y. (2009). Mammalian Expression of Infrared Fluorescent Proteins Engineered from a Bacterial Phytochrome. *Science*, *324*(5928), 804–807. https://doi.org/10.1126/science.1168683

Sickmier, E. A., Brekasis, D., Paranawithana, S., Bonanno, J. B., Paget, M. S. B., Burley, S. K., & Kielkopf, C. L. (2005). X-Ray Structure of a Rex-Family Repressor/NADH Complex Insights into the Mechanism of Redox Sensing. *Structure*, *13*(1), 43–54. https://doi.org/10.1016/j.str.2004.10.012

Sohal, R. S., & Weindruch, R. (1996). Oxidative Stress, Caloric restriction, and Aging. *Science*, *273*, 59–63. https://doi.org/10.1126/science.273.5271.59

Sørensen, H. P., & Mortensen, K. K. (2005). Soluble expression of recombinant proteins in the cytoplasm of *Escherichia coli*. *Microbial Cell Factories*, *4*(1), 1–8. https://doi.org/10.1186/1475-2859-4-1

Soret, J.-L. (1883). *Analyse Spectrale. - Sur le spectre d'absorption du sang dans la partie violette et ultra-violette*. *Comptes rendus hebdomadaires des séances de l'Académie des sciences*.

Starai, V. J., Celic, I., Cole, R. N., Boeke, J. D., & Escalante-Semerena, J. C. (2002). Sir2-dependent activation of acetyl-CoA synthetase by deacetylation of active lysine. *Science*, *298*(5602), 2390–2392. https://doi.org/10.1126/science.1077650

Steinbeck, J., Fuchs, P., Negroni, Y. L., Elsässer, M., Lichtenauer, S., Stockdreher, Y., … Schwarzländer, M. (2020). *In vivo* NADH/NAD^+ biosensing reveals the dynamics of cytosolic redox metabolism in plants. *Plant Cell*, *32*(10), 3324–3345. https://doi.org/10.1105/tpc.20.00241

Stryer, L. (1978). Fluorescence Energy Transfer as a Spectroscopic Ruler. *Annual Review of Biochemistry*, *47*(1), 819–846. https://doi.org/10.1146/annurev.bi.47.070178.004131

Stumpp, T., Wilms, B., & Altenbuchner, J. (2000). Ein neues, L-Rhamnose-induzierbares Expressionssystem für *Escherichia coli*. *Biospektrum*, 33–36.

Retrieved from http://www.biospektrum.de/blatt/d_bs_pdf&_id=933504

Sun, F., Dai, C., Xie, J., & Hu, X. (2012). Biochemical issues in estimation of cytosolic free NAD/NADH ratio. *PLoS ONE*, *7*(5), 31–36. https://doi.org/10.1371/journal.pone.0034525

Tao, R., Zhao, Y., Chu, H., Wang, A., Zhu, J., Chen, X., … Yang, Y. (2017). Genetically encoded fluorescent sensors reveal dynamic regulation of NADPH metabolism. *Nature Methods*, *14*(7), 720–728. https://doi.org/10.1038/nmeth.4306

Tejwani, V., Schmitt, F.-J., Wilkening, S., Zebger, I., Horch, M., Lenz, O., & Friedrich, T. (2017). Investigation of the NADH/NAD+ ratio in *Ralstonia eutropha* using the fluorescence reporter protein Peredox. *Biochimica et Biophysica Acta - Bioenergetics*, *1858*(1), 86–94. https://doi.org/10.1016/j.bbabio.2016.11.001

Teruel, M. N., & Meyer, T. (2000). Translocation and reversible localization of signaling proteins: A dynamic future for signal transduction. *Cell*, *103*(2), 181–184. https://doi.org/10.1016/S0092-8674(00)00109-4

Tian, X., Zhang, N., Yang, Y., Wang, Y., Chu, J., Zhuang, Y., & Zhang, S. (2015). The effect of redox environment on l-lactic acid production by *Lactobacillus paracasei* - A proof by genetically encoded in vivo NADH biosensor. *Process Biochemistry*, *50*(12), 2029–2034. https://doi.org/10.1016/j.procbio.2015.10.001

Titov, D. V, Cracan, V., Goodman, R. P., Peng, J., Grabarek, Z., & Mootha, V. K. (2016). Complementation of mitochondrial electron transport chain by manipulation of the NAD+/NADH ratio. *Science*, *352*(6282), 231–235. https://doi.org/10.1126/science.aad4017

Torikata, T., Forster, L. S., Johnson, R. E., & Rupley, J. A. (1979). Lifetimes and NADH Quenching of tryptophan Fluorescence in Pig Heart Cytoplasmic Malate Dehydrogenase. *Journal of Biological Chemistry*, *265(9)*(10), 3516–3520.

Torikata, T., Forster, L. S., Neal, C. C. O., & Rupley, J. A. (1979). Lifetimes and NADH quenching of tryptophan fluorescence in pig heart lactate dehydrogenase. *Biochemistry*, *18*(2), 385–390. https://doi.org/10.1021/bi00569a024

Trammell, S. A. J., & Brenner, C. (2013). Targeted, LCMS-based Metabolomics for Quantitative Measurement of NAD⁺ Metabolites. *Computational and Structural Biotechnology Journal*, *4*(5), 1–9. https://doi.org/10.5936/csbj.201301012

Tsai, M. T., Cheng, Y. H., Liu, Y. N., Liao, N. C., Lu, W. W., & Kung, S. H. (2009). Real-

time monitoring of human enterovirus (HEV)-infected cells and anti-HEV 3C protease potency by fluorescence resonance energy transfer. *Antimicrobial Agents and Chemotherapy*, *53*(2), 748–755. https://doi.org/10.1128/AAC.00841-08

Tsien, R. Y. (2005). Building and breeding molecules to spy on cells and tumors. *FEBS Letters*, *579*(4 SPEC. ISS.), 927–932. https://doi.org/10.1016/j.febslet.2004.11.025

Van Der Linden, E., Faber, B. W., Bleijlevens, B., Burgdorf, T., Bernhard, M., Friedrich, B., & Albracht, S. P. J. (2004). Selective release and function of one of the two FMN groups in the cytoplasmic NAD+-reducing [NiFe]-hydrogenase from *Ralstonia eutropha*. *European Journal of Biochemistry*, *271*(4), 801–808. https://doi.org/10.1111/j.1432-1033.2004.03984.x

Van Gastel, M., Stein, M., Brecht, M., Schröder, O., Lendzian, F., Bittl, R., … Lubitz, W. (2006). A single-crystal ENDOR and density functional theory study of the oxidized states of the [NiFe] hydrogenase from <i<Desulfovibrio vulgaris</i> Miyazaki F. *Journal of Biological Inorganic Chemistry*, *11*(1), 41–51. https://doi.org/10.1007/s00775-005-0048-7

van Unen, J., Stumpf, A. D., Schmid, B., Reinhard, N. R., Hordijk, P. L., Hoffmann, C., … Goedhart, J. (2016). A New Generation of FRET Sensors for Robust Measurement of $G\alpha_{i1}$, $G\alpha_{i2}$ and $G\alpha_{i3}$ Activation Kinetics in Single Cells. *PLOS ONE*, *11*(1), e0146789. https://doi.org/10.1371/journal.pone.0146789

Várnai, P., & Balla, T. (2006). Live cell imaging of phosphoinositide dynamics with fluorescent protein domains. *Biochimica et Biophysica Acta - Molecular and Cell Biology of Lipids*, *1761*(8), 957–967. https://doi.org/10.1016/j.bbalip.2006.03.019

Vasina, J. A., & Baneyx, F. (1997). Expression of aggregation-prone recombinant proteins at low temperatures: A comparative study of the *Escherichia coli* cspA and tac promoter systems. *Protein Expression and Purification*, *9*(2), 211–218. https://doi.org/10.1006/prep.1996.0678

Velázquez Escobar, F., Buhrke, D., Michael, N., Sauthof, L., Wilkening, S., Tavraz, N. N., … Hildebrandt, P. (2017). Common Structural Elements in the Chromophore Binding Pocket of the Pfr State of Bathy Phytochromes. *Photochemistry and Photobiology*, *93*(3), 724–732. https://doi.org/10.1111/php.12742

Vignais, P. M., & Billoud, B. (2007). Occurrence, classification, and biological function of hydrogenases: An overview. *Chemical Reviews*, *107*(10), 4206–4272. https://doi.org/10.1021/cr050196r

Virag, L., & Szabo, C. (2002). The Therapeutic Potential of Poly(ADP-Ribose) Polymerase Inhibitors. *Pharmocological Reviews*, *54*(3), 375–429. https://doi.org/10.1124/pr.54.3.375

Vishwasrao, H. D., Heikal, A. A., Kasischke, K. A., & Webb, W. W. (2005). Conformational Dependence of Intracellular NADH on Metabolic State Revealed by Associated Fluorescence Anisotropy. *Journal of Biological Chemistry*, *280*(26(1)), 25119–25126. https://doi.org/10.1074/jbc.M502475200

Volbeda, A., Garcin, E., Piras, C., De Lacey, A. L., Fernandez, V. M., Hatchikian, E. C., … Fontecilla-Camps, J. C. (1996). Structure of the [NiFe] hydrogenase active site: Evidence for biologically uncommon Fe ligands. *Journal of the American Chemical Society*, *118*(51), 12989–12996. https://doi.org/10.1021/ja962270g

Volbeda, A., Martin, L., Cavazza, C., Matho, M., Faber, B. W., Roseboom, W., … Fontecilla-Camps, J. C. (2005). Structural differences between the ready and unready oxidized states of [NiFe] hydrogenases. *Journal of Biological Inorganic Chemistry*, *10*(3), 239–249. https://doi.org/10.1007/s00775-005-0632-x

Wachter, R. M., Elsliger, M. A., Kallio, K., Hanson, G. T., & Remington, S. J. (1998). Structural basis of spectral shifts in the yellow-emission variants of green fluorescent protein. *Structure*, *6*(10), 1267–1277. https://doi.org/10.1016/S0969-2126(98)00127-0

Wang, E., Bauer, M. C., Rogstam, A., Linse, S., Logan, D. T., & Von Wachenfeldt, C. (2008). Structure and functional properties of the *Bacillus subtilis* transcriptional repressor Rex. *Molecular Microbiology*, *69*(2), 466–478. https://doi.org/10.1111/j.1365-2958.2008.06295.x

Wang, Z. Q., Stingl, L., Morrison, C., Jantsch, M., Los, M., Schulze-Osthoff, K., & Wagner, E. F. (1997). PARP is important for genomic stability but dispensable in apoptosis. *Genes and Development*, *11*(18), 2347–2358. https://doi.org/10.1101/gad.11.18.2347

Wei, Y., Li, J., Dong, C., Shuang, S., Liu, D., & Huie, C. W. (2006). Investigation of the Association Behaviors Between Biliverdin and Bovine Serum Albumin by Fluorescence Spectroscopy. *Talanta*, *70*, 377–382.

https://doi.org/10.1016/j.talanta.2006.02.052

Weiss, C. (1972). The Pi Electron Structure and Absorption Spectra of Chlorophylls in Solution. *Journal of Molecular Spectroscopy*, (44), 37–80. Retrieved from http://escholarship.org/uc/item/2rj0w00t

Weissleder, R. (2001). A clearer vision for in vivo imaging. *Nature Biotechnology*, *19*, 316–317. https://doi.org/https://doi.org/10.1038/86684

Wilkening, S., Schmitt, F., Horch, M., Zebger, I., Lenz, O., & Friedrich, T. (2017). Characterization of Frex as an NADH sensor for in vivo applications in the presence of NAD^+ and at various pH values. *Photosynthesis Research*, *133*(1–3), 305–315. https://doi.org/10.1007/s11120-017-0348-0

Wilkening, S., Schmitt, F. J., Lenz, O., Zebger, I., Horch, M., & Friedrich, T. (2019). Discriminating changes in intracellular NADH/NAD+ levels due to anoxicity and H_2 supply in *R. eutropha* cells using the Frex fluorescence sensor. *Biochimica et Biophysica Acta - Bioenergetics*, *1860*(10), 148062. https://doi.org/10.1016/j.bbabio.2019.148062

Wilks, J. C., & Slonczewski, J. L. (2007). pH of the cytoplasm and periplasm of *Escherichia coli*: Rapid measurement by green fluorescent protein fluorimetry. *Journal of Bacteriology*, *189*(15), 5601–5607. https://doi.org/10.1128/JB.00615-07

Williamson, B. D. H., Lund, P., & Krebs, H. A. (1967). The Redox State of Free Nicotinamide-Adenine Dinucleotide in the Cytoplasm and Mitochondria of Rat Liver. *Biochemical Journal*, 514–527.

Wimpenny, J. W., & Firth, A. (1972). Levels of nicotinamide adenine dinucleotide and reduced nicotinamide adenine dinucleotide in facultative bacteria and the effect of oxygen. *Journal of Bacteriology*, *111*(1), 24–32.

Winkler, U., & Hirrlinger, J. (2015). Crosstalk of Signaling and Metabolism Mediated by the NAD^+/NADH Redox State in Brain Cells. *Neurochemical Research*, *40*(12), 2394–2401. https://doi.org/10.1007/s11064-015-1526-0

Xie, N., Zhang, L., Gao, W., Huang, C., Huber, P. E., Zhou, X., … Zou, B. (2020). NAD^+ metabolism: pathophysiologic mechanisms and therapeutic potential. *Signal Transduction and Targeted Therapy*, *5*(1). https://doi.org/10.1038/s41392-020-00311-7

Xie, W., Xu, A., & Yeung, E. S. (2009). Determination of NAD+ and NADH in a Single Cell Electrophoresis. *Analytical Chemistry*, *81*(3), 1280–1284.

https://doi.org/https://doi.org/10.1021/ac802249m

Yamada, K., Hara, N., Shibata, T., Osago, H., & Tsuchiya, M. (2006). The simultaneous measurement of nicotinamide adenine dinucleotide and related compounds by liquid chromatography / electrospray ionization tandem mass spectrometry. *Analytical Biochemistry*, *352*, 282–285. https://doi.org/10.1016/j.ab.2006.02.017

Yang, G. G., Xu, X. Y., Ding, Y., Cui, Q. Q., Wang, Z., Zhang, Q. Y., … Xu, C. S. (2015). Linker length affects expression and bioactivity of the onconase fusion protein in Pichia pastoris. *Genetics and Molecular Research*, *14*(4), 19360–19370. https://doi.org/10.4238/2015.December.29.46

Yang, H., Yang, T., Baur, J. A., Perez, E., Matsui, T., Carmona, J. J., … Sinclair, D. A. (2007). Nutrient-Sensitive Mitochondrial NAD^+ Levels Dictate Cell Survival. *Cell*, *130*, 1095–1107. https://doi.org/10.1016/j.cell.2007.07.035

Ying, W. (2006). NAD+ and NADH in cellular functions and cell death. *Frontiers in Bioscience*, *11*, 3129–3148. https://doi.org/10.2741/2038

Ying, W. (2007). NAD^+ and NADH in brain functions, brain diseases and brain aging. *Frontiers in Bioscience*, *12*, 1863–1888.

Ying, W. (2008). NAD $^+$/NADH and $NADP^+$/NADPH in Cellular Functions and Cell Death: Regulation and Biological Consequences. *Antioxidants & Redox Signaling*, *10*(2), 179–206. https://doi.org/10.1089/ars.2007.1672

Yoshida, T., Kakizuka, A., & Imamura, H. (2016). BTeam , a Novel BRET-based Biosensor for the Accurate Quantification of ATP Concentration within Living Cells. *Nature Publishing Group*, (November), 1–9. https://doi.org/10.1038/srep39618

Yu, Q., & Heikal, A. A. (2009). Two-photon autofluorescence dynamics imaging reveals sensitivity of intracellular NADH concentration and conformation to cell physiology at the single-cell level. *Journal of Photochemistry and Photobiology B: Biology*, *95*(1), 46–57. https://doi.org/10.1016/j.jphotobiol.2008.12.010

Zhang, J., Campbell, R. E., Ting, A. Y., & Tsien, R. Y. (2002). Creating new fluorescent probes for cell biology. *Nature Reviews Molecular Cell Biology*, *3*(12), 906–918. https://doi.org/10.1038/nrm976

Zhang, Q., Piston, D. W., & Goodman, R. H. (2002). Regulation of Corepressor Function by Nuclear NADH. *Science*, *295*(March), 1895–1898.

Zhang, Z., Chen, W., Zhao, Y., & Yang, Y. (2018). Spatiotemporal Imaging of Cellular Energy Metabolism with Genetically-Encoded Fluorescent Sensors in Brain. *Neuroscience Bulletin*, *34*(5), 875–886. https://doi.org/10.1007/s12264-018-0229-3

Zhang, Z., Cheng, X., Zhao, Y., & Yang, Y. (2020). Lighting Up Live-Cell and *in Vivo* Central Carbon Metabolism with Genetically Encoded Fluorescent Sensors. *Annual Review of Analytical Chemistry*, *13*, 293–314. https://doi.org/10.1146/annurev-anchem-091619-091306

Zhao, Y., Hu, Q., Cheng, F., Su, N., Wang, A., Zou, Y., … Yang, Y. (2015). SoNar, a Highly Responsive NAD^+/NADH Sensor, Allows High-Throughput Metabolic Screening of Anti-tumor Agents. *Cell Metabolism*, *21*(5), 777–789. https://doi.org/10.1016/j.cmet.2015.04.009

Zhao, Y., Jin, J., Hu, Q., Zhou, H.-M., Yi, J., Yu, Z., … Loscalzo, J. (2011). Genetically encoded fluorescent sensors for intracellular NADH detection. *Cell Metabolism*, *14*(4), 555–566. https://doi.org/10.1016/j.cmet.2011.09.004

Zhao, Y., Wang, A., Zou, Y., Su, N., Loscalzo, J., & Yang, Y. (2016). In vivo monitoring of cellular energy metabolism using SoNar, a highly responsive sensor for NAD^+/NADH redox state. *Nature Protocols*, *11*(8), 1345–1359. https://doi.org/10.1038/nprot.2016.074

Zhao, Y., & Yang, Y. (2012). Frex and FrexH: Indicators of metabolic states in living cells. *Bioengineered Bugs*, *3*(3), 181–188. https://doi.org/10.4161/bbug.19769

Zhao, Y., & Yang, Y. (2015). Profiling metabolic states with genetically encoded fluorescent biosensors for NADH. *Current Opinion in Biotechnology*, *31*, 86–92. https://doi.org/10.1016/j.copbio.2014.08.007

Zhao, Y., Yang, Y., & Loscalzo, J. (2014). Real time Measurement of Metabolic States in Living Cells using Genetically-encoded NADH Sensors. *Methods in Enzymology*, *542*, 349–367. https://doi.org/10.1097/MPG.0b013e3181a15ae8.Screening

Zhao, Y., Zhang, Z., Zou, Y., & Yang, Y. (2018). Visualization of Nicotine Adenine Dinucleotide Redox Homeostasis with Genetically Encoded Fluorescent Sensors. *Antioxidants & Redox Signaling*, *28*(3), 213–229. https://doi.org/10.1089/ars.2017.7226

Zheng, W., Li, D., & Qu, J. Y. (2010). Monitoring changes of cellular metabolism and

microviscosity *in vitro* based on time-resolved endogenous fluorescence and its anisotropy decay dynamics. *Journal of Biomedical Optics*, *15*(3), 37011–37013. https://doi.org/10.1117/1.3449577

Zhou, Y., Wang, L., Yang, F., Lin, X., Zhang, S., & Zhao, Z. K. (2011). Determining the extremes of the cellular NAD(H) level by using an *Escherichia coli* NAD^+-auxotrophic mutant. *Applied and Environmental Microbiology*, *77*(17), 6133–6140. https://doi.org/10.1128/AEM.00630-11

Zlobovskaya, O. A., Sergeeva, T. F., Shirmanova, M. V., Dudenkova, V. V., Sharonov, G. V., Zagaynova, E. V., & Lukyanov, K. A. (2016). Genetically Encoded Far-Red Fluorescent Sensors for Caspase-3 Activity. *BioTechniques*, *60*(2), 62–68. https://doi.org/10.2144/000114377

Zou, Y., Wang, A., Shi, M., Chen, X., Liu, R., Li, T., … Zhao, Y. (2018). Analysis of redox landscapes and dynamics in living cells and *in vivo* using genetically encoded fluorescent sensors. *Nature Protocols*, *13*(10), 2362–2386. https://doi.org/10.1038/s41596-018-0042-5

IX Acknowledgments

I would like to thank all the people who supported me during this work, the coworkers and colleagues at the Max-Volmer Institute for biophysical chemistry, especially

Prof. Dr. Thomas Friedrich for offering me the opportunity to generate this thesis in his group. I would like to thank him for the support, the understanding, and the trust I was given while working on the assigned projects,

Dr. Oliver Lenz not only for the provision of various strains of *R. eutropha* and for the instruction on how to cultivate and handle those cells. But also, for the constant help and eagerness to improve the experiments,

Dr. Ingo Zebger for the discussions and his input regarding the analysis of the experiments, as well as for the constructive criticism during writing of publications,

Dr. Franz-Josef Schmitt for introducing me to various spectroscopic methods regarding fluorescence spectroscopy, such as steady-state and time-resolved fluorescence spectroscopy as well as handling of the fluorescence microscope. Also, I would like to thank him for his contagious curiosity and many entertaining conversations,

Dr. Marius Horch for the introduction to IR spectroscopy and his thoughtful contribution and careful analysis of the results. His way of thorough thinking improved our collaborative work enormously,

Dr. Neslihan Tavraz for the introduction to basically anything considering the biochemical laboratory. I would like to thank her for the tireless support, for the constant availability in case of questions and her commitment to finding a solution no matter what,

Marcus Moldenhauer for a supportive and extremely nice atmosphere in the lab, for the help, that was offered without hesitation and for many great discussions about science or else, as well as many great new songs written,

Anna Koczula for many stimulating discussions in our shared office and the pickles,

Monika Weß & **Sabine Kussin** for keeping a well-maintained lab and helping out with daily laboratory tasks,

Dr. Jana Staffa, Catharina Kulka & Dr. Sven Hartmann for many well needed coffee-breaks and support in every way imaginable, helping me keep my sanity,

My **family** for the ever-constant support,

And **Simon** who always knew what to say and what to do.